TU Delft

Delft University of Technology

Form Follows Force

A theoretical framework for Structural Morphology, and Form-Finding research on shell structures

Li, Qingpeng

DOI
10.7480/abe.2018.2

Publication date
2018

Document Version
Final published version

Citation (APA)
Li, Q. (2018). *Form Follows Force: A theoretical framework for Structural Morphology, and Form-Finding research on shell structures*. [Dissertation (TU Delft), Delft University of Technology]. A+BE | Architecture and the Built Environment. https://doi.org/10.7480/abe.2018.2

Important note
To cite this publication, please use the final published version (if applicable).
Please check the document version above.

Copyright
Other than for strictly personal use, it is not permitted to download, forward or distribute the text or part of it, without the consent of the author(s) and/or copyright holder(s), unless the work is under an open content license such as Creative Commons.

Takedown policy
Please contact us and provide details if you believe this document breaches copyrights.
We will remove access to the work immediately and investigate your claim.

This work is downloaded from Delft University of Technology.
For technical reasons the number of authors shown on this cover page is limited to a maximum of 10.



Architecture and the Built environment

#02
2018

Form Follows Force

A theoretical framework for Structural Morphology, and Form-Finding research on shell structures

Qingpeng Li

Form Follows Force

A theoretical framework for Structural Morphology, and Form-Finding research on shell structures

Qingpeng Li
Delft University of Technology, Faculty of Architecture and the Built Environment, Department of Architectural Engineering and Technology

Architecture and the Built environment

abe.tudelft.nl

Design: Sirene Ontwerpers, Rotterdam

ISBN 978-94-6366-012-9
ISSN 2212-3202

© 2018 Qingpeng Li

All rights reserved. No part of the material protected by this copyright notice may be reproduced or utilized in any form or by any means, electronic or mechanical, including photocopying, recording or by any information storage and retrieval system, without written permission from the author.

Unless otherwise specified, all the photographs in this thesis were taken by the author. For the use of illustrations effort has been made to ask permission for the legal owners as far as possible. We apologize for those cases in which we did not succeed. These legal owners are kindly requested to contact the publisher.

Form Follows Force

A theoretical framework for Structural Morphology, and Form-Finding research on shell structures

Dissertation

for the purpose of obtaining the degree of doctor
at Delft University of Technology
by the authority of the Rector Magnificus, prof.dr.ir. T.H.J.J. van der Hagen,
Chair of the Board for Doctorates
to be defended publicly on
Monday 12 March 2018 at 10:00 o'clock

by

Qingpeng LI
Master of Engineering in Architectural and Civil Engineering,
Harbin Institute of Technology, P.R. China
born in Binzhou, Shandong, P.R. China

This dissertation has been approved by the promotor.

Composition of the doctoral committee:

Rector Magnificus,	chairperson
Prof.dr.ir. J.G. Rots	Delft University of Technology, promotor

Independent members:

Prof.ir. R. Nijsse	Delft University of Technology
Prof.dr.ir.arch. I.S. Sariyildiz	Delft University of Technology
Prof.dr.-ing. P.M. Teuffel	Eindhoven University of Technology
Prof.dr.ir.arch. N. De Temmerman	Vrije Universiteit Brussel
Dr.ir. P.C.J. Hoogenboom	Delft University of Technology

Other members:

Ir. A. Borgart	Delft University of Technology

This research was funded by Prof. Y. (Yue) Wu from Harbin Institute of Technology, P.R. China, which is gratefully acknowledged.

Dedicated to my beloved grandparents, Bingtai Li & Fengying Lu:
May you rest in peace, you will not be forgotten!

献给我敬爱的爷爷、奶奶，思念依然无尽！

Preface

Since 2010, I began to study at the Space Structures Research Centre (SSRC) of Harbin Institute of Technology (HIT). The first project I participated in was the famous Five-hundred-meter Aperture Spherical Telescope (FAST) project shown in Figure 0.1, whose main structural system is an integrated cable-net structure. It was the first time that I encountered the Form-Finding problem, which inspired my great interest in the relationship between form and force.



FIGURE 0.1 FAST project (https://apod.nasa.gov/apod/ap160929.html).

In the following years, I was involved in the design and analysis of several structures of terminal buildings or stadiums, shown in Figure 0.2. From these practices, I found that effectively cooperative work between architects and structural engineers is of vital importance during the design of the structural geometry. A bad design may lead to a waste of material and energy, and a structurally optimal solution without architectural appearance is not sustainable either. From these experiences it was felt that the role of structural engineers is rather limited in this process.

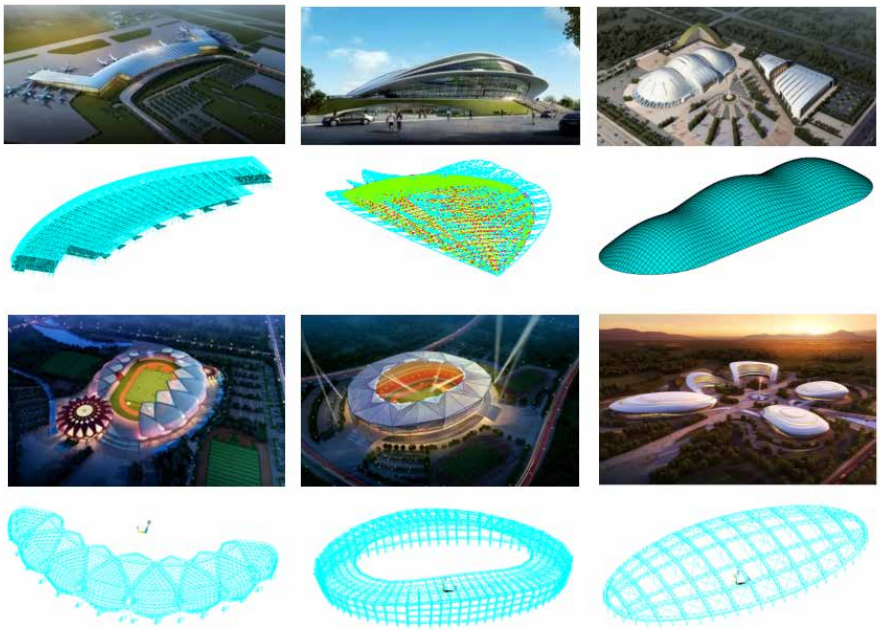


FIGURE 0.2 Several roof-structures of terminal buildings or stadiums.

The reasons for this are multiple. Primarily, in China, with such a high development speed, the professional difference between architecture and structure is huge, and the design time of a project is always limited, which deprives the architects and structural engineers of cooperation time. However, from a worldwide perspective, especially in developed countries, the situation seems better than what I experienced.

Moreover, from a perspective of science, the relation between form and forces has been studied for a prolonged period, especially from the foundation of the International Association for Shell and Spatial Structures (IASS) in 1959. During the 1991 IASS Symposium, the NO.15 IASS Working Group - Structural Morphology Group (SMG) was founded. Generally, 'Structural Morphology' is a term used to describe the study of form and force, while it still does not get a clear definition due to its extensive research content, even though lots of attempts have been made.

The above forms the motivation of this work.

A shell structure is a type of structure in which the structural efficiency strongly depends on its three-dimensional (3D) shape. This means that it has typical and representative problems towards the relationship between form and force. Especially

for freeform shells, the geometry of which is always irregularly shaped, the relationship between form and force becomes more complicated, which introduces more complex but interesting problems. Therefore, to conduct this research, shells are selected as the research subject.

To concentrate on this topic, the focus is on systematic Form-Finding research on shell structures. For example, in Figure 0.3, a mortar shell model was fabricated by hanging a piece of rubber with immature mortar. Using a similar manufacturing method, a workshop in the course Bend and Break Tensegrity (CT3270-15) was organized at Delft University of Technology (TU Delft) in 2017, shown in Figure 0.4. During this workshop, 11 reinforced gypsum shell models were manufactured and tested.

As a further research and application, pushed by me, a cooperation between Professor Yue Wu from HIT and Professor Arno Pronk from Eindhoven University of Technology (TU/e) was formulated, in which three ice composite shells were designed and constructed on the architectural campus of HIT by spraying a cellulose-water mixture on inflatable moulds (Figure 0.5) in the winter of 2016/2017.

In the winter of 2017/2018, the 30.54-meter-high ice composite tower (Flamenco Ice Tower) was built in Harbin using the same construction method, and I was involved in the design, analysis, construction work, and also served as the coordinator during this cooperation between China and the Netherlands (Figure 0.6). This ice tower has become the highest ice shell structure in the world.

This research serves as the fundamental research of three National Natural Science Foundation of China (NSFC) research projects led by Professor Yue Wu, which are:

- Key Problems of Structural Morphology and New-form Space Structures (Grant NO. 51378150, from 01/01/2014 to 31/12/2017),
- Innovative Structural Systems and Optimisation of Super Long-span City Dome (Grant NO. 51578186, from 01/01/2016 to 31/12/2019), and
- Innovative High Performance Ice Composites and Ice Structures (Grant NO. 51778182, from 01/01/2018 to 31/12/2021).

I was involved in the application processes with Professor Wu, and have been serving as the first main member for all of them. The primary aim of this thesis is to establish a feasible basis and research framework for these three ongoing projects.



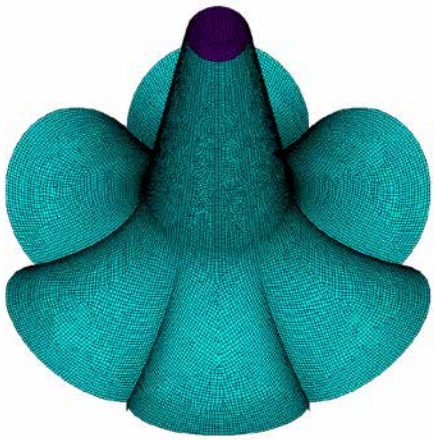
FIGURE 0.3 One mortar shell model manufactured at TU Delft, 2017.



FIGURE 0.4 Workshop of the course Bend and Break Tensegrity at TU Delft, 2017.



FIGURE 0.5 Three ice composite shells built at HIT, 2016



(a) The finite element model of the ice tower.



(b) The ice tower after construction (photo by Maple Village).

FIGURE 0.6 The Flamenco Ice Tower in Harbin of China, 2018.

Contents

Summary 21
Samenvatting 25

PART 1 Introduction

1 Introduction 31

1.1 Background and Motivation 31

1.1.1 Freeform architectures: A trend in modern architecture 31
1.1.2 Freeform structures: New challenges for structural engineers 33
1.1.3 Structural Morphology: A study of the relation between form and force 33

1.2 Research Problem 34

1.3 Scope of This Research 35

1.3.1 Structural systems: Force-Active and Force-Passive 35
1.3.2 Shell structures: The research object of this thesis 36
1.3.3 Form-Finding of shells: From Force-Active to Force-Passive 37

1.4 Research Status and Objectives 38

1.4.1 Research status 38
1.4.2 Research objectives 40

1.5 Outline of This Thesis 40

1.6 References 43

PART 2 Theoretical Framework for Structural Morphology

2 Theoretical Framework for Structural Morphology 47

2.1 Introduction 47

2.2 Numerical Analysis Methods for Structural Systems 49

2.2.1 Conceptual model of numerical analysis methods 49
2.2.2 Numerical examples 52

2.3 Theoretical Framework for Structural Morphology 55

2.4 Conclusions 57

2.5 References 58

3 Form-Finding and Structural Optimisation 61

3.1 Introduction 61

3.2 Form-Finding of Force-Active Structural Systems 62

3.2.1 Form-Finding of hanging structural systems 64
3.2.2 Form-Finding of tension structural systems 65
3.2.3 Form-Finding of pneumatic structural systems 66

3.3 Structural Optimisation of Force-Passive Structural Systems 68

3.3.1 Optimisation of geometry 69
3.3.2 Optimisation of material distribution 71
3.3.3 Optimisation of combined parameters 74

3.4 Conclusions 75

3.5 References 76

PART 3 Form-Finding of Shell Structures

4 Introduction to Shell Structures 81

4.1 Introduction 81

4.2 Structural Forms of Shells 81

4.3 Mechanical Behaviour of Shells 85

4.3.1 Mechanical behaviour assessment of shells in the conceptual design phase 85
4.3.2 Factors to represent linear static analysis results of shells 86

4.4 Form-Finding of Shells 95

4.4.1 Physical Form-Finding methods 95
4.4.2 Numerical Form-Finding methods 98

4.5 Conclusions 100

4.6 References 101

5 VFIFE for Generating Equilibrium Structural Forms of Force-Active Structural Systems 103

5.1 Introduction 103

5.2 The VFIFE Method 103

5.2.1 Basic concepts of the VFIFE method 103
5.2.2 Basic procedure of the VFIFE method 105
5.2.3 Numerical example of a hanging cable net 110

5.3 The Constant Strain Triangle Element 112

5.3.1 Calculation of pure deformation of the triangular membrane element 112
5.3.2 Calculation of the internal force increment of the triangular membrane element 114

5.4 Numerical Examples 117

5.4.1 Equilibrium of one hanging model 118
5.4.2 Equilibrium of one tension model 128
5.4.3 Equilibrium of one pneumatic model 137

5.5 Conclusions 146

6 Controlling Equilibrium Structural Forms with Target Heights 149

6.1 Introduction 149

6.2 Form-Control of the Equilibrium Structural Form with One Target Point 149

6.2.1 Proposal of the problem 149
6.2.2 Form-Control strategy based on the Newton-Raphson method 151
6.2.3 Numerical example 152

6.3 Form-Control of Equilibrium Structural Form with Multiple Target Points 158

6.3.1 Proposal of the problem 158
6.3.2 Form-Control strategy based on the inverse iteration method 158
6.3.3 Numerical example 160

6.4 Form-Finding Plug-in in Rhino-Grasshopper 168

6.5 Conclusions 170

7 Demonstration Towards Diverse Structural Forms 171

7.1 Introduction 171

7.2 Adjusting Strategies for Diverse Structural Forms 171

7.2.1 Strategy by adjusting the parameters of 'geometry' 172
7.2.2 Strategy by adjusting the parameters of 'material properties' 172
7.2.3 Strategy by adjusting the parameters of 'forces' 172
7.2.4 Strategy by adjusting the parameters of 'material distribution' 173
7.2.5 Strategy by adjusting the parameters of 'boundary conditions' 173

7.3 Conclusions 188

PART 4 Influence of Support Shapes on Form-found Shells

8 Influence of Support Shapes: Numerical Research 191

8.1 Introduction 191

8.2 Comparison of Structural Forms of Form-found Shells 196

8.2.1 Introduction of the form-found shells 196
8.2.2 Comparison of structural forms of the form-found shells 200

8.3 Comparison of Structural Behaviour of Form-found Shells Under Symmetrical Loads 203

8.3.1 Linear static analysis 203
8.3.2 Linear buckling analysis 212
8.3.3 Nonlinear static analysis 215

8.4 Comparison of Structural Behaviour of Form-found Shells Under Non-symmetrical Loads 218

8.4.1 Linear static analysis 219
8.4.2 Linear buckling analysis 221
8.4.3 Nonlinear static analysis 224

8.5 Conclusions 224

8.6 References 225

9 Influence of Support Shapes: Experimental Research 227

9.1 Introduction 227

9.2 Manufacture of the Shell Models 227

9.3 Setup and Tests of Shell Models 233

9.4 Analyses of the Test Results 236

9.5 Buckling Analysis of the Shell Models 243

9.6 Conclusions 246

9.7 References 247

PART 5 Conclusions

10 Conclusions 251

10.1 Conclusions Related to the Theoretical Framework of Structural Morphology 251

10.2 Conclusions Related to Form-Finding of Shells 252

10.3 Conclusions Related to the Influence of Support Shapes on Form-found Shells 254

10.4 Limitations of the Current Work 255

10.5 Final Remarks 257

List of Figures 259
List of Tables 265
Acknowledgements 267
Curriculum vitae 271
List of Publications 273

TOC

Summary

The springing up of freeform architecture and structures introduces many challenges to structural engineers. The main challenge is to generate structural forms with high structural efficiency subject to the architectural space constraints during the conceptual structural design process.

Structural Morphology is the study of the relation between form and force, which can be considered the guiding theory for this challenge. The relation between form and force is important for all types of structures during the entire structural design process. Thus, Structural Morphology has a wide range of related research subjects and multiple research approaches. Therefore, Structural Morphology has gained neither a clear definition nor a unified methodology.

In the present research, a theoretical framework for Structural Morphology has been proposed, that provides an effective solution to the challenge mentioned above. To enrich the proposed framework of Structural Morphology, systematic Form-Finding research on shell structures is conducted. Shell structures, the structural efficiency of which depends strongly on their 3D shape, have particular problems regarding the relationship between form and force. To obtain a structurally efficient shell, the form should follow the flow of forces, and a process of Form-Finding can achieve this. In this thesis, Form-Finding of shells indicates a process of generating the equilibrium structural forms of hanging, tent or pneumatic physical models.

In Chapters 2 and 3, a theoretical framework for Structural Morphology is established.

- Structural systems are divided into two categories based on their responses under the loads: 'Force-Active' and 'Force-Passive'. A 'Force-Active' structural system can significantly and actively adjust its shape due to the loads, while a 'Force-Passive' system cannot. A generic conceptual model of the numerical analysis process of structural systems is presented, which is suitable to both categories of structural systems. This conceptual model includes three parts: (1) the initial system described by five categories of parameters: geometry, material distribution, material properties, boundary conditions and forces; (2) the setup of equations and calculation methods to handle the above parameters; and

(3) the structural performance described by two categories of parameters: the structural form and its mechanical behaviour (Chapter 2).

- A conceptual model of Structural Morphology is proposed by adding further requirements of the structural form or the mechanical behaviour and an optimisation process into the above conceptual model of the numerical analysis process of structural systems. Then, a corresponding conceptual formula of Structural Morphology is concluded. Thus, a theoretical framework of Structural Morphology is established. Subsequently, its feasibility is validated by a comprehensive discussion of the two main aspects of Structural Morphology, including 'Form-Finding' and 'Structural Optimisation'. In this research, Form-Finding relates to Force-Active structural systems, which means the generation of multiple equilibrium shapes subject to architectural space constraints. Structural Optimisation relates to Force-Passive structural systems, which indicates the adjustment of relevant parameters of the initial structural system with the aim of improving its mechanical behaviour. The methodology of both aspects is presented. Research achievements completed by the author's research groups from Harbin Institute of Technology (HIT) and Delft University of Technology (TU Delft) are presented to validate the feasibility. These achievements cover the research on Form-Finding of cable-nets and membrane structures, and on the Structural Optimisation of shells and gridshells (Chapter 3).

In Chapters 4 to 7, the proposed theoretical framework for Structural Morphology is enriched by systemic Form-Finding research on shell structures.

- To study the form of shell structures, the curvature analysis of the surface is displayed. To study the mechanical behaviour of shell structures during the conceptual structural design process, an assessment strategy based on its linear static behaviour and buckling behaviour under two different load cases is proposed. To comprehensively study the linear static behaviour of a shell structure where bending moments may or may not be dominant in this shell, the membrane over the total stress ratios and strain-energy ratio are introduced (Chapter 4).

- The Vector Form Intrinsic Finite Element (VFIFE) method is a recently developed numerical analysis method. At the beginning of this research, few studies on the Form-Finding of shell structures using the VFIFE method were found in the literature. The VFIFE method is applied to generate equilibrium shapes of Force-Active structural systems and thus the structural geometries of shells. A MATLAB script and a plug-in in the Rhino-Grasshopper platform are developed (Chapter 5).

– Form-Control of Force-Active structural systems aims to generate form-found structural forms subject to the required architectural space constraints. Two Form-Control strategies are developed by combining two simple optimisation algorithms (the Newton-Raphson method and the inverse iteration method) with the VFIFE method. These strategies can help designers determine the structurally efficient forms more easily and more efficiently than some relatively complicated and time-consuming optimisation algorithms (Chapter 6).

– Based on the proposed theoretical framework of Structural Morphology, multiple structural forms of form-found shell structures are obtained by adjusting the five categories of parameters of the initial structural systems. This work can efficiently and effectively provide multiple structural forms with reasonable mechanical behaviour for designers from the perspective of structural engineers (Chapter 7).

In Chapters 8 and 9, the specific influence of curved supports on the structural forms and the mechanical behaviour of these shells is studied. Intuitively and qualitatively, designers may be able to select the correct shapes for the supports of shells. However, there was a need to quantify the consequences of designing particular shell supports. In this work, form-found shells with slightly different support shapes are analysed numerically and experimentally.

– Four hexagonal form-found shells generated from hanging models with different support shapes but with the same target point are generated. The following four support shapes are considered: straight supports, outward-curved supports, inward-curved supports and strongly inward-curved supports. From the numerical comparison, slight changes of the support shapes have a relatively small influence on the equilibrium structural forms but have a considerable influence on the mechanical behaviour of these form-found shells. It is concluded that we can improve structural efficiency by slightly curving the supports during the Form-Finding process, which would not significantly change the architect's design scheme (Chapter 8).

– In the experimental research, three scaled plastic shell models (with straight supports, outward-curved supports, and inward-curved supports) are tested, and the shadow Moiré method is used in the observation of the deformation of the shells. Form these tests, the influence of the support shapes on form-found shells is studied visually by these obtained Moiré patterns, which represent the

buckling modes of these shell models influenced by the curvature distribution near the supports as well as thickness distribution (Chapter 9).

There are still issues that need to be solved in future research. For instance, the theoretical framework for Structural Morphology needs to be enriched with Structural Optimisation work, more complicated design constraints need to be considered in the Form-Finding process of shell structures (for example, the stress level or distribution in the shell), and more influence factors of the form-found shells need to be researched (for example, the number or length of the supports, and edge beams).

Samenvatting

De opkomst van vrije-vorm-architectuur en -constructies introduceert vele uitdagingen voor constructieve ingenieurs. De grootste uitdaging is het genereren van constructieve vormen met een hoge constructieve efficiëntie, rekening houdend met architectonische ruimtebeperkingen tijdens het conceptuele ontwerpproces. 'Structural Morphology' is de studie van de relatie tussen vorm en kracht, wat de leidende theorie is voor deze uitdaging. De relatie tussen vorm en kracht is belangrijk voor allerlei types van constructies, dus 'Structural Morphology' heeft een breed scala aan verwante onderzoeksonderwerpen en meerdere opvattingen. Daarom heeft 'Structural Morphology' noch een duidelijke definitie, noch een uniforme methodiek.

In het huidige onderzoek wordt een theoretisch kader voor 'Structural Morphology' voorgesteld, dat een effectieve oplossing biedt voor de hierboven genoemde uitdaging. Om het voorgestelde kader van 'Structural Morphology' te verrijken, wordt systematisch onderzoek gedaan naar 'Form-Finding' van schaalconstructies. Schaalconstructies, waarvan de constructieve efficiëntie sterk afhankelijk is van hun 3-dimensionale vorm, hebben specifieke problemen met betrekking tot de relatie tussen vorm en kracht. Om een constructief efficiënte schaal te verkrijgen, moet de vorm van de schaalconstructie de stroom van de krachten volgen. Met behulp van 'Form-Finding' kan dit worden bereikt. In dit proefschrift betekent 'Form-Finding' van schaalconstructies het proces van het genereren van de evenwichtsvorm van de constructie van hangende modellen, tentmodellen of pneumatische modellen.

In hoofdstukken 2 en 3 wordt een theoretisch kader van 'Structural Morphology' vastgesteld.

- Constructieve systemen zijn onderverdeeld in twee categorieën op basis van hun reactie op belastingen: 'Force-Active' en 'Force-Passive'. Een 'Force-Active' constructief systeem kan door de belastingen aanzienlijk en actief zijn vorm aanpassen, terwijl een 'Force-Passive' constructief systeem dat niet kan. Een generiek conceptueel schema van het numerieke analyseproces van constructieve systemen wordt gepresenteerd, dat geschikt is voor beide categorieën van constructieve systemen. Dit conceptuele schema bevat drie delen: (1) het beginsysteem beschreven door parameters die zijn te verdelen in vijf categorieën: geometrie, materiaalverdeling, materiaaleigenschappen, randvoorwaarden en krachten; (2) de opstelling van vergelijkingen en berekeningsmethoden om de bovengenoemde parameters te verwerken; en (3)

de constructieve prestaties beschreven door twee categorieën van parameters: de vorm van de constructie en het mechanisch gedrag daarvan. (Hoofdstuk 2).

– Een conceptueel schema van 'Structural Morphology' wordt voorgesteld door (1) het toevoegen van verdere vereisten aan de vorm van de constructie of het mechanische gedrag daarvan, en (2) een optimalisatieproces van het bovenstaande conceptuele schema van het numerieke analyseproces van constructieve systemen. Er wordt met een overeenkomstige conceptuele formule van 'Structural Morphology' afgesloten. Zo wordt het theoretisch kader van 'Structural Morphology' vastgesteld. Vervolgens wordt de haalbaarheid ervan gevalideerd door een uitvoerige bespreking van de twee hoofdaspecten van de 'Structural Morphology', 'Form-Finding' en 'constructieve optimalisatie'. In dit onderzoek heeft 'Form-Finding' betrekking op 'Force-Active' constructieve systemen, wat betekent dat er evenwichtsvormen worden gegenereerd die onderhevig zijn aan architectonische ruimtebeperkingen. Constructieve optimalisatie heeft betrekking op 'Force-Passive' constructieve systemen, waarbij het aanpassen van relevante parameters van het oorspronkelijke constructieve systeem tot doel heeft om het mechanische gedrag te verbeteren. De methodiek van beide aspecten wordt gepresenteerd. Resultaten van onderzoeken voltooid door de onderzoeksgroepen van de auteur in het Harbin Institute of Technology en de TU Delft worden gepresenteerd om de haalbaarheid te valideren. Deze prestaties hebben betrekking op (1) het onderzoek naar 'Form-Finding' van kabelnetten en membraanstructuren en (2) op het onderzoek naar constructieve optimalisatie van schalen en gridschalen. (Hoofdstuk 3).

In de hoofdstukken 4 tot en met 7 wordt het voorgestelde theoretische kader van 'Structural Morphology' verrijkt met systematisch onderzoek naar 'Form-Finding' van schaalconstructies.

– Om de vorm van schaalconstructies te bestuderen wordt een krommingsanalyse van het oppervlak uitgevoerd. Om het mechanische gedrag van schaalconstructies tijdens het conceptuele constructieve ontwerpproces te bestuderen, wordt een beoordelingsstrategie voorgesteld. Deze is gebaseerd op het lineaire statische gedrag en het knikgedrag bij twee verschillende belastinggevallen. Om het lineaire statische gedrag van een schaalconstructie waarin buigingsmomenten al dan niet dominant zijn te bestuderen, worden de membraan-totale spanningsverhouding en de spanning-energieverhouding geïntroduceerd. (Hoofdstuk 4).

– De Vector Form Intrinsic Finite Element methode (VFIFE-methode) is een recent ontwikkelde numerieke analysemethode. Aan het begin van dit onderzoek werden in de literatuur weinig studies gevonden met betrekking tot het 'Form-Finding' van schaalconstructies met behulp van de VFIFE-methode. De VFIFE-methode wordt toegepast om evenwichtsvormen te genereren van 'Force-Active' constructieve systemen, zoals de geometrie van schaalconstructies. Een MATLAB-script en een plug-in in het platform Rhino-Grasshopper zijn ontwikkeld. (Hoofdstuk 5).

– 'Form-Control' van 'Force-Active' constructieve systemen is gericht op het vinden van vormen, gegenereerd door middel van 'Form-Finding', die voldoen aan de gestelde architectonische ruimtebeperkingen. Twee 'Form-Control'-strategieën zijn ontwikkeld door twee eenvoudige optimalisatie-algoritmen (de Newton-Raphson-methode en de inverse iteratiemethode) te combineren met de VFIFE-methode. Deze strategieën kunnen ontwerpers helpen om de constructief efficiënte vormen gemakkelijker en efficiënter te bepalen dan sommige relatief ingewikkelde en tijdrovende optimalisatie-algoritmen. (Hoofdstuk 6).

– Op basis van het voorgestelde theoretische kader van 'Structural Morphology' worden meerdere constructieve vormen van schaalstructuren verkregen met behulp van 'Form-Finding' door de vijf categorieën parameters van de oorspronkelijke constructieve systemen aan te passen. Zo kunnen door constructieve ingenieurs efficiënt en effectief meerdere constructieve vormen gegenereerd worden met redelijk mechanische gedrag. (Hoofdstuk 7).

In de hoofdstukken 8 en 9 wordt de specifieke invloed van gebogen steunpunten op de constructieve vorm en het mechanische gedrag van deze schaalconstructies bestudeerd. Intuïtief en kwalitatief kunnen constructief ontwerpers de juiste vormen kiezen voor steunpunten van schaalconstructies. Er was echter behoefte om de consequenties van verschillende steunpunten van schaalconstructies in kaart te brengen. In dit onderzoek worden verschillende schaalconstructies, waarvan de vorm is bepaald door middel van 'Form-Finding' en waarbij de steunpunten enigszins verschillen, numeriek en experimenteel geanalyseerd.

– Vier hexagonale vormvaste schaalconstructies zijn gegenereerd met behulp van ophangmodellen met verschillende ondersteuningsvormen maar met hetzelfde richtpunt. Beschouwd worden vier ondersteuningsvormen: (1) rechte ondersteuningen, (2) naar buiten gekromde ondersteuningen, (3) naar binnen gekromde ondersteuningen en (4) sterk naar binnen gekromde ondersteuningen. Uit de numerieke vergelijking tussen de

verschillende schaalconstructies volgt dat kleine veranderingen van de ondersteuningsvormen slechts een relatief kleine invloed hebben op de vorm van de evenwichtsconstructie, terwijl deze een aanzienlijke invloed hebben op het mechanische gedrag van deze schaalconstructies. Er wordt geconcludeerd dat de constructieve efficiëntie verbeterd kan worden door de ondersteuningen lichtjes te krommen tijdens het 'Form-Finding' proces, wat het ontwerp van de architect niet significant zou veranderen. (Hoofdstuk 8).

– In het experimentele onderzoek zijn drie kunststof schaalmodellen (met rechte ondersteuningen, naar buiten gekromde ondersteuningen en naar binnen gekromde ondersteuningen) getest en wordt de Moiré schaduwmethode gebruikt om de vervorming van de schaalmodellen waar te nemen. Bij deze tests wordt de invloed van de ondersteuningsvormen op de schaalconstructies visueel bestudeerd door de verkregen Moiré-patronen, die de knikvormen van deze schaalmodellen representeren. De knikvormen worden beïnvloed door de krommingsverdeling nabij de ondersteuningen en door de dikteverdeling. (Hoofdstuk 9).

Er zijn nog uitdagingen over die moeten worden beschouwd in toekomstig onderzoek. Het theoretische kader van 'Structural Morphology' moet bijvoorbeeld worden verrijkt met constructieve optimalisatie. Ingewikkeldere ontwerpbeperkingen moeten worden meegenomen in het 'Form-Finding'-proces van schaalconstructies (bijvoorbeeld het spanningsniveau en de spanningsverdeling in de schaalconstructies), en meer factoren die invloed hebben op de vorm van schaalconstructies moeten worden onderzocht (bijvoorbeeld het aantal of de lengte van de ondersteuningen en randbalken).

PART 1 Introduction

TOC

TOC

1 Introduction

§ 1.1 Background and Motivation

§ 1.1.1 Freeform architectures: A trend in modern architecture

In recent years, with the increasing living and spiritual requirements of people, freeform shapes are gaining increasing popularity in architecture due to the development of design theory and construction techniques. Freeform geometry has an aesthetic appearance and excellent visual permeability. Examples are shown in Figures 1.1 to 1.4 relating to freeform facades, freeform support structures, freeform roofs, and freeform interior spaces. Freeform architecture has become one of the most important trends in modern architecture. Apart from these engineering practices, a considerable body of literature demonstrates this trend (see [1] - [6]).



(a) Freeform facade.



(b) Freeform support structures.

FIGURE 1.1 Himalayas Centre Shanghai [7].

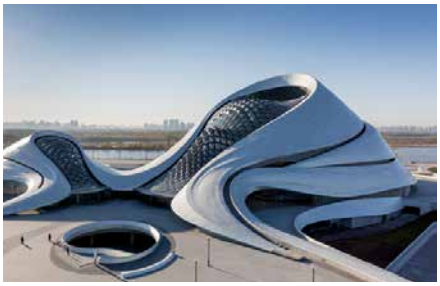


(a) Freeform roof.



(b) Freeform interior spaces.

FIGURE 1.2 Heydar Aliyev Centre [8][9].

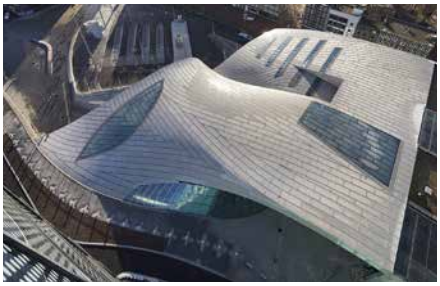


(a) Freeform roof.

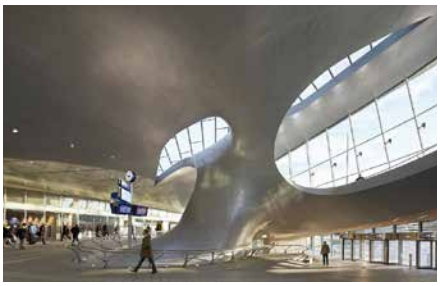


(b) Freeform interior spaces.

FIGURE 1.3 Harbin Opera House [10][11].



(a) Freeform roof.



(b) Freeform support structures or interior spaces.

FIGURE 1.4 Arnhem Centraal station [12].

§ 1.1.2 Freeform structures: New challenges for structural engineers

Structure can be considered the skeleton of architecture, which is used to support the architectural space or surface. Freeform architecture always has irregular shapes, and this introduces great difficulties in both the structural design and construction phases. For example, some complex architectural shapes may lead to unreasonable distribution of internal forces in their structures, which results in a waste of material and energy.

During the conceptual structural design phase [13], which is the first and decisive phase of design, cooperative work between architects and structural engineers is needed to determine an overall architecturally and structurally sound integrated system. As for the conceptual design of freeform structures, many problems arise from the perspective of structural engineers. For instance:

- how to generate architecturally permitted structural geometries with high structural efficiency,
- how to provide architects with novel and diverse structural forms subject to their constraints,
- how to determine the structural types, etc.

The structural modelling and analysis of freeform structures is also much more complicated than for normal structures. For example, the 3D insight, curvatures, and interaction between extension and bending play a role compared to standard orthogonal beams, frames, and plates. Moreover, in the construction phase, the manufacturing of irregular shapes creates great difficulty and thus prohibitive costs in formwork and falsework. Thus, freeform structures lead to new challenges for structural engineers.

§ 1.1.3 Structural Morphology: A study of the relation between form and force

In general, Structural Morphology is a term used to describe the study of the relation between form and force in a structure. However, the problem of the relation between form and force occurs for all types of structures and during the entire structural design process, thus Structural Morphology has a wide range of related research subjects and multiple approaches (see [6], [14]-[17]). Therefore, Structural Morphology does not have a clear definition or a unified methodology. Problems of the relationship

between 'form' and 'force' exist in any type of structure, especially for shell and spatial structures, where form plays a key role to bear force.

In 1991, the Structural Morphology Group (SMG) of the International Association for Shells and Spatial Structures (IASS) was founded. Since then, scholars, designers or engineers over many years have increasingly taken the relationship between forms and forces as one of the key issues to be elaborated. Nowadays, 'structural geometry', the 'form-force relationship', the 'form-mobility relationship', 'technology transfer', 'computation' and 'prototyping' have become the focuses of research for Structural Morphology, and new challenges continuously emerge.

§ 1.2 Research Problem

The research problem of this thesis is:

How to generate structural forms with high structural efficiency subject to architectural space constraints during the conceptual structural design process?

Generally, 'structural form' means the final appearance of the structure, including its geometry (or shape), topology, and cross sections. 'High structural efficiency' indicates the efficient use of structural materials and optimal structural performance under multiple load combinations. It should be noted that architects maintain the decisive role in the architectural form and thus the structural form, so that only the 'architectural space constraints' of structural forms are considered from the perspective of a structural engineer.

However, in the second half of this thesis on Form-Finding research on shell structures, 'structural form' primarily denotes the structural geometry or shape of the shell, and 'high structural efficiency' primarily indicates that the membrane action is dominant in a shell structure and that the optimal stability behaviour is also considered.

As mentioned in the previous section, Structural Morphology can serve as an effective solution to the research problem. However, it is a huge topic. To deal with this topic, the scope of this research must be narrowed. Therefore, solely the theoretical framework rather than a complete theory of Structural Morphology has been developed based on a suitable classification of structural systems. To validate the feasibility of the proposed theoretical framework, systematic Form-Finding research on shell structures has been conducted. The scope of this research will be explained in detail in the next section.

§ 1.3 Scope of This Research

§ 1.3.1 Structural systems: Force-Active and Force-Passive

Problems regarding the relation between form and force may occur in every type of structural system. To develop a feasible theoretical framework of Structural Morphology, a suitable classification of structural systems is needed. However, structural systems can be classified in many ways, such as according to their shape, their function, and the materials from which they are made.

In this thesis, structural systems are divided into two categories based on their responses under load conditions: 'Force-Active' and 'Force-Passive'. A structural system that significantly and actively adjusts its shape due to the loads is called a Force-Active structural system, while a structural system that does not significantly and actively change its shape under loads is called a Force-Passive structural system.



(a) Hanging structural system [18].



(b) Tension structural system [19].



(c) Pneumatic structural system [20].

FIGURE 1.5 'Force-Active' structural systems.

Cable or membrane structures are typical 'Force-Active' structural systems; they are tension structures. As shown in Figure 1.5, Force-Active structural systems can be divided into the following three basic categories: hanging structural systems, tension structural systems, and pneumatic structural systems. These kinds of structural systems follow the 'Form follows Force' principle. The most important problem during their design or analysis process is to generate a stable equilibrium state subject to the architectural space constraints or mechanical constraints, such as the requirements of the distribution of stresses, which is generally called 'Form-Finding'. Strong nonlinearity due to large deformations during the Form-Finding or analysis process is the typical feature of this kind of structural system. In this thesis, Form-Finding

research on Force-Active structural systems is considered one of the two predominant aspects of the proposed theoretical framework of Structural Morphology.

Compared with Force-Active structural systems, 'Force-Passive' structural systems are much more commonly used in standard engineering practices. This kind of structural system is often made from concrete, steel, or other rigid materials. Therefore, during their design or analysis processes, the assumption of small deformations can be applied to meet the accuracy requirements. Due to its stressing feature, unreasonable stress distributions may occur inside the structures. To improve its mechanical behaviour, some optimisation processes can be introduced to adjust the integration of the structural system subject to architectural space constraints. In this thesis, Structural Optimisation of Force-Passive structural systems is considered the other primary aspect of the proposed theoretical framework of 'Structural Morphology'.

In addition, it should be mentioned that Adriaenssens et al. [21] classified the structural systems based on the same principle (their response due to load conditions) but using the terms "Form-Active" and "Form-Passive". In their description, Form-Passive structural systems do not significantly and actively change their shapes under varying load conditions, and shell structures are form-passive structural systems. However, Engel [21] distinguished the structural systems into four categories: Form-Active, Vector-Active, Section-Active and Surface-Active. In his definition, Form-Active structural systems are systems of flexible, non-rigid matter, in which the redirection of forces is affected by a self-found form design and characteristic form stabilisation. He emphasised the function of the structural form on the load transfer mechanism, and counted arch and shell structures among the Form-Active structural systems. In China, scholars use the terms "Flexible Structure" and "Rigid Structure" to distinguish the structural systems; however, these are without clear definitions (see [23]).To avoid confusion, the author follows the classification by Adriaenssens et al. [21], but prefers to refer to them as Force-Active and Force-Passive.

§ 1.3.2 Shell structures: The research object of this thesis

Shell structures are 'Force-Passive' structural systems whose geometric shape plays a significant role in their structural efficiency. A shell can be defined by a curved surface whose thickness is much smaller than the other two dimensions of the surface, as shown in *Figure 1.6*. Shells can be curved in one or two directions.



(a) Deitingen Service Station [24].



(b) Kitagata Community Centre [25].

FIGURE 1.6 Shell structures.

Compared with traditional shells with mathematical shapes or their combination, for freeform shells with irregular shapes, the classical theories of shells based on mathematical shapes lose their applicability to some extent. The relationship between the irregular structural form and its mechanical behaviour becomes unclear, and much more complicated structural behaviour may occur. In this case, shells have a much more complex relation between the structural form and its mechanical behaviour than other types of structures, especially for freeform shells. Therefore, herein, shell structures are selected as the research objective.

§ 1.3.3 Form-Finding of shells: From Force-Active to Force-Passive

Both Form-Finding and Structural Optimisation techniques can be used to generate novel and diverse structural forms of shells with high structural efficiency [21]. Form-Finding is originally used to describe the process of generating the equilibrium state of a Force-Active structural system under the required architectural space constraints. It is a forward process in which parameters are explicitly or directly controlled to find an optimal geometry of a structure that is in static equilibrium with a design load [21]. However, the final equilibrium structural form can also be used as the geometry of a Force-Passive structural system, for example, inverting the hanging chain to obtain the structurally efficient form of an arch. In this case, Form-Finding can also be used to describe the form generation process of Force-Passive structural systems. In this thesis, systematic research on the Form-Finding of shell structures is conducted, which means processes for going from Force-Active structural systems to Force-Passive structural systems.

§ 1.4 Research Status and Objectives

From the perspective of a structural engineer, positioned in the conceptual structural design phase, the primary goal of this research is to reduce the gap between freeform architectures and structures by proposing a theoretical framework for Structural Morphology and enriching it with systematic Form-Finding research on shell structures.

§ 1.4.1 Research status

Based on the introduction in the above sections, the research status of relevant issues is as follows (a detailed literature review will be provided in each relevant chapter):

- Structural Morphology is such a huge topic with a wide range of related research content and diverse approaches. Many scholars have provided their own definition or understanding for this term, but everybody uses his or her personal version, and no unified methodology can be concluded [15][16][17]. In the author's research group, the Space Structures Research Centre of Harbin Institute of Technology, professors and students have done research on tension structures and gridshells for several decades. Based on a generalisation of some achievements in research and practices achieved mainly by our group and a comprehensive literature review, Professor Shen and Professor Wu have provided a definition of Structural Morphology [26]. In this definition, Structural Morphology means a discipline that studies the interaction between the structural form and its mechanical behaviour from an integral perspective, aiming to realise the rationality and efficiency of the structures.

- Form-Finding of shell structures is a relatively mature field [21][27][28]. Four sub-issues are considered as follows:

  - For the quantitative and qualitative assessment of the structural behaviour of shell structures, the finite element method (FEM) is commonly and easily used in many computer programs to analyse the mechanical behaviour of shell structures nowadays. Although finite element analysis provides good insight into the quantitative behaviour of shell structures during loading, it provides very little qualitative insight into their structural behaviour.

  - Regarding equilibrium problems of Force-Active structural systems, many numerical methods have been established and are being developed [21][27].

The VFIFE method is a recently developed numerical analysis method, which has demonstrated a great benefit in these fields on complicated behaviour analysis of structures [29]. At the beginning of this research, few studies on the Form-Finding of shell structures using the VFIFE method were found in the literature.

- Form-Control problems of Force-Active structural systems, which aim to generate form-found structural forms subject to required architectural space constraints, are also a developed area. However, for Form-Control problems with multiple constrained points, some optimisation algorithms are always introduced that are relatively complicated and time-consuming (see [30] [31]). Therefore, simpler and more effective Form-Control strategies need to be researched.

- During the design process of the current situation, the diversity of the architectural geometry primarily depends on architects. However, structural engineers can also contribute to diverse structural forms, which can also consider their structural behaviour. Some scholars have done relevant work for this (see [21][32] and the author's former work [33][34][35]). However, based on the theoretical framework of Structural Morphology with the combination of the VFIFE method, systematic strategies towards diverse structural forms need to be researched.

- During the generation of multiple structural forms, it is found that slightly curved supports only provide small visual differences in the overall appearance of the form-found shells. The specific influence of the curved supports on the structural form and mechanical behaviour of these shells is not clear. On the other hand, to improve the structural efficiency of shell structures, the overall or partial structural geometry and material distribution are always selected to adjust during the Form-Finding or Structural Optimisation (see [21][36][37]). Scarce literature has considered support shapes or conditions to be the optimisation variable, even though it is clear that the most important parts of a shell structure are close to the supports, and designers may be able to select the right shape or condition for the supports during the design process. However, there is a need to quantify the consequences of designing particular shell supports.

§ 1.4.2 Research objectives

Based on the introduction above, this research aims to achieve the following objectives:

- To develop a theoretical framework of Structural Morphology based on the definition given by Shen and Wu;
- To conduct systematic Form-Finding research on shell structures. The sub-objectives are as follows:
  - To quantitatively and qualitatively assess the mechanical behaviour of the shell structure in its conceptual structural design phase;
  - To introduce the VFIFE method to generate equilibrium shapes of membrane structures and thus structural geometries of shells;
  - To establish efficient and effective Form-Control strategies to generate form-found structural forms with a single and multiple target heights;
  - To develop strategies for generating diverse structural forms with reasonable mechanical behaviour based on the theoretical framework of Structural Morphology;
- To quantify the influence of support shapes on the structural form and mechanical behaviour of form-found shells.

§ 1.5 Outline of This Thesis

The logical structure of this thesis is shown in Figure 1.7. This thesis is divided into five parts. The present introduction is the first part. The subsequent four parts are as follows:

– Proposal of a theoretical framework for Structural Morphology and discussions of its basic main contents;

– From-Finding problems of shell structures, including a review of relevant research, equilibrium problems of Force-Active structural systems, Form-Control of form-found shells, and demonstration of multiple form-found shells;

– Influence of support shapes on form-found shells, which are studied numerically and experimentally; and

– Conclusions.

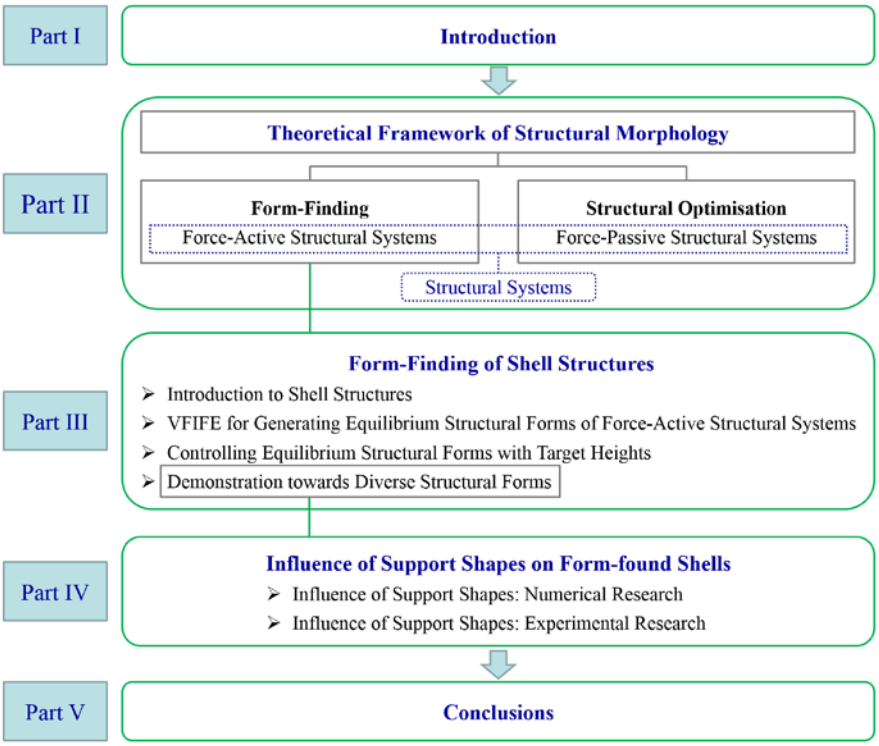


FIGURE 1.7 Logical structure of this thesis.

The main content of each chapter is introduced as follows:

- Chapter 2 introduces the background of Structural Morphology and one common conceptual model of the numerical analysis process of structural systems. According to these, a conceptual formula of Structural Morphology is proposed, which covers its goal and methodology.

- Chapter 3 presents the two main aspects of Structural Morphology. One is Form-Finding, which refers to generating equilibrium forms of Force-Active structural systems subject to the required architectural space constraints. The other one is Structural Optimisation, which refers to an optimisation process to improve structural properties of Force-Passive structural systems under specified constraints. A methodology of either aspect is presented based on the theoretical framework of Structural Morphology. Relevant research achievements completed by the author's research groups are discussed to validate the feasibility. These achievements cover the research on Form-Finding of cable nets and membrane structures, and on the Structural Optimisation of shells and gridshells.

- Chapter 4 introduces the structural form and behaviour of shell structures, and then proposes a strategy and several factors to assess the mechanical behaviour of shell structures. Subsequently, it provides a review of Form-Finding research on shells, including three types of physical Form-Finding methods (hanging models, tent models, and pneumatic models) and several numerical Form-Finding techniques.

- Chapter 5 applies the VFIFE method to generate equilibrium shapes of three types of Force-Active structural systems. The framework of the VFIFE method is established by taking the cable-link element as an example. In addition, a constant-strain triangle element is introduced, and four numerical examples are presented.

- Chapter 6 proposes highly efficient Form-Control strategies during the Form-Finding process. Taking hanging Force-Active structural systems as examples, these strategies aim to generate equilibrium structural forms of Force-Active structural systems under required architectural space constraints.

- Chapter 7 focuses on diverse structural forms of form-found shell structures by adjusting the five categories of parameters of the initial structural systems. These strategies can efficiently and effectively provide diverse structural forms

with reasonable mechanical behaviour for designers from the perspective of structural engineers.

– Chapter 8 analyses the influence of support shapes on the structural form and that of support shapes and conditions on the structural behaviour of shell structures, which takes shell structures generated from hanging models as examples. The research results achieved in this chapter can provide not only qualitative but also quantitative strategies to improve the structural behaviour of shell structures by only slightly adjusting the structural form.

– Chapter 9 introduces experimental research on the same problem solved in the last chapter. Three scaled polyester shell models with different support shapes are manufactured and tested, and the shadow Moiré method is used in the observation of the deformation of the shells. From these tests, the influence of the support shapes on form-found shells are studied visually, and some qualitative conclusions are drawn from the observation and comparison of these Moiré patterns.

– Chapter 10 presents the conclusions, limitations of the current work, and final remarks.

§ 1.6 References

[01] Eekhout A.J.C.M., editor. (2016). Free Form Technology from Delft. IOS Press - Delft University Press, Delft, The Netherlands.
[02] Adriaenssens S., Gramazio F., Kohler M., Menges A., Pauly M., editors. (2016). Advances in Architectural Geometry 2016. VDF Hochschulverlag AG an der ETH Zürich, Switzerland.
[03] Paulo J. S. Cruz, editor. (2016). Structures and architecture beyond their limits : proceedings of the third International Conference on Structures and Architecture (ICSA2016). Taylor & Francis Group, London.
[04] Thomsen M.R., Tamke M., Gengnagel C., Faircloth B., Scheurer F., editors. (2015). Modelling Behaviour: Design Modelling Symposium 2015. Springer International Publishing, Switzerland.
[05] Vambersky J.N.J.A., Schipper H.R., editors. (2010). Precast 2010: Assembling Freeform Buildings in Precast Concrete. Delft University of Technology.
[06] Mungan I., Abel J.F., editors. (2009). Fifty years of progress for shell and spatial structures. Multi-Science Publishing Co. Ltd, Essex.
[07] http://www.designboom.com/architecture/arata-isozaki-himalayas-Centre-zendai-08-11-2015/
[08] http://www.archdaily.com/448774/heydar-aliyev-Centre-zaha-hadid-architects
[09] https://en.wikiarquitectura.com/building/heydar-aliyev-cultural-Centre/
[10] https://www.iconeye.com/architecture/features/item/12384-harbin-opera-house
[11] http://www.archdaily.com/778933/harbin-opera-house-mad-architects
[12] http://www.gebouwvanhetjaar.nl/entry/station-arnhem-centraal/
[13] Horikx M.P. (2017). A Methodical Approach on Conceptual Structural Design. PhD thesis, Delft University of Technology.

[14] Shen S., Wu Y. (2014). Structural morphology and modern space structures. Journal of Building Structures, 35(4): 1-10. (in Chinese)
[15] Coenders J.L., editor. (2008).Reader of the course 'CIE5251 - Structural Design - Special Structures'. Delft: Delft University of Technology.
[16] Motro R., editor. (2009). An Anthology of Structural Morphology. World Scientific, London.
[17] Motro R., editor. (2009). Structural Morphology and Configuration Processing of Space Structures. Multi-Science Publishing Co. Ltd, Brentwood.
[18] https://en.wikipedia.org/wiki/Battle_of_Luding_Bridge
[19] https://iam.tugraz.at/workshop14s/2014/05/04/tanzbrunnen-tent-in-cologne-by-bodo-rasch/
[20] https://www.stylepark.com/en/news/fabric-makes-home
[21] Adriaenssens S., Block P., Veenendaal D., Williams C., editors. (2014). Shell structures for architecture: Form-Finding and optimisation. London: Routledge Taylor and Francis.
[22] Engel, H. (1997) Structure Systems, 3rd edition. Gerd Hatje Publishers: Ostfildern, Germany.
[23] Dong S. (2009). The development history, innovation, classification and practical application of spatial structures. Spatial Structures. 15(3): 22-43.
[24] https://structurae.net/structures/deitingen-service-station
[25] https://hiveminer.com/Tags/gifu%2Ckitagata/Recent
[26] Shen S., Wu Y. (2014). Structural morphology and modern space structures. Journal of Building Structures. 35z(4): 1-10. (in Chinese)
[27] Veenendaal D., Block P. (2012). An overview and comparison of structural form finding methods for general networks, International Journal of Solids and Structures. 49(26): 3741-3753.
[28] Veenendaal D. (2017). Design and form finding of flexibly formed shell structures: including a comparison of form finding methods. PhD thesis, ETH Zurich, Zurich.
[29] Yao J., Lu Z. (2011). Vector Form Intrinsic Finite Element-overview, recent progress and future developments. 2011 International Conference on Multimedia Technology, Hangzhou, China.
[30] Block P., Lachauer L. (2014). Three-dimensional Funicular Analysis of Masonry Vaults. Mechanics Research Communications, 56: 53-60.
[31] Pottmann H., Eigensatz M., Vaxman A., Wallner J. (2015). Architectural geometry. Computers & Graphics. Graph. 47: 145-164.
[32] Kilian A. (2007). The Steering of Form. Journal of the International Association for Shell and Spatial Structures. 48 (4): 17-21.
[33] Li Q. (2013). Numerical simulation and applications of the inverse hanging method. MSc thesis, Harbin Institute of Technology. (in Chinese)
[34] Wu Y., Li Q., Shen S. (2014). Computational morphogenesis method for space structures based on principle of inverse hanging experiment. Journal of Building Structures, 35(4): 41-48. (in Chinese)
[35] Li Q., Wu Y., Shen S. (2014). Computational generation of freeform shells based on the inverse hanging experiment. Proceedings of the IASS-SLTE 2014 Symposium, Brasilia, Brazil.
[36] Ramm E., Wall W.A. (2004). Shell structures - a sensitive interrelation between physics and numeric. International Journal for Numerical Methods in Engineering, 60: 381-427.
[37] Tomás A., Martí P. (2010). Shape and size optimisation of concrete shells. Engineering Structures, 32: 1650-1658.

PART 2 Theoretical Framework for Structural Morphology

TOC

TOC

2 Theoretical Framework for Structural Morphology

§ 2.1 Introduction

During the IASS Copenhagen Symposium in 1991, the IASS Working Group NO.15 SMG was founded by the 'gang of four': Ture Wester, Pieter Huybers, Jean-François Gabriel, and René Motro [45][46]. Since then, relevant research has been one of the focus points in the field of structural engineering, especially for shell and spatial structures. However, 'Structural Morphology' is not a new discipline born with the SMG working group. Over many years, many scholars, designers, and engineers have taken the relationship between form and force as one of the key issues to be investigated [46]. Due to its extensive research content, diversified research approaches, and a characteristic of multi-subject intersection, the term 'Structural Morphology' has not gained a clear definition from the SMG since 1991, or even a basic theoretical system. Many scholars provided their own definitions or understandings for this term, but everybody has his or her personal version. For example, Wester [47] described Structural Morphology as 'the study of interaction between geometrical form and structural behaviour'. Ramm [48] described it as the 'study of the interaction between form and structures'. Further discussions can be found from serious of SMG Newsletters [38][39], and some other references [40][41][42][43][44]. Specifically, two typical viewpoints from different perspectives are introduced in detail as follows.

Motro gave a parametric approach to Structural Morphology in several of his papers [49][50][51]. Any design process for a proposed system has to deal with multi-parametric problems, and it could identify the main parameters and then classify them in four categories: forms, forces, material, and structure, shown in Figure 2.1. The position of 'Structural Morphology' in this system is at the interface between the parameters of 'form' and 'structure'; it is the direct relation between the study of form and structure extended to cover the relational sense. This relation is affected by the behaviour of the material and by the need to ensure the static (and sometimes dynamic) equilibrium of the system S being designed.

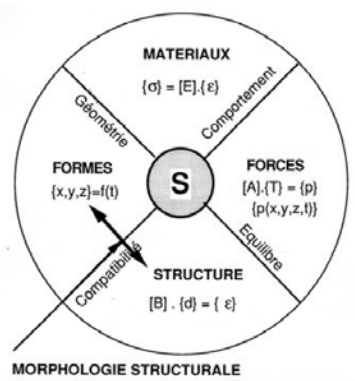


FIGURE 2.1 Conceptual model of Motro [51].

Shen and Wu suggested a preliminary definition of 'Structural Morphology'[52], defining it as a discipline that studies the interaction between the structural form and its mechanical behaviour from an integral perspective, aiming to realize the rationality and efficiency of the structures. This definition is generalised from some achievements in research and practice by our research team, as well as a comprehensive literature review.

The former viewpoint from Motro is based on the parametric analysis of the structural system, and presents an appropriate position of the 'Structural Morphology'. The latter one from Shen and Wu seems a bit abstract, but it does define the objective and essence of most research within the field of Structural Morphology. However, both viewpoints based on their own understandings are the crystallisation of their research and practice.

Nowadays, 'geometry', 'form-force relationship', 'form-mobility relationship', 'technology transfer', 'computation' and 'prototyping' become the research focus of Structural Morphology [53][54], and new challenges are continually emerging. With the development of computer technology, the numerical technique has become the most important means for research in the field of structural engineering, which can design, analyse, and optimize structures by handling a large number of parameters. On this basis, many numerical analysis methods have been gradually developed and played an important role in modern research for 'Form-Finding' [54][55] and 'structural optimisation'[54][55][56], which are the two main means and aspects of the research on Structural Morphology in the authors' view.

Against this background, this chapter concludes a common conceptual model for numerical analysis methods, which would cover the whole analysis process from the

initial structural system to the final equilibrium structure. Subsequently, based on the definition given by Professor Shen and Professor Wu, a theoretical framework of 'Structural Morphology' (including one conceptual model and one conceptual formula) is proposed.

§ 2.2 Numerical Analysis Methods for Structural Systems

As mentioned in **Chapter 1**, structural systems can be divided into two categories: 'Force-Active' structural systems and 'Force-Passive' structural systems. In this section, a common conceptual model for numerical analysis methods of both categories of structural systems is generalized. Subsequently, one numerical analysis example of a Force-Active structural system and one of a Force-Passive structural system are shown to validate the rationality of the summarized conceptual model.

§ 2.2.1 Conceptual model of numerical analysis methods

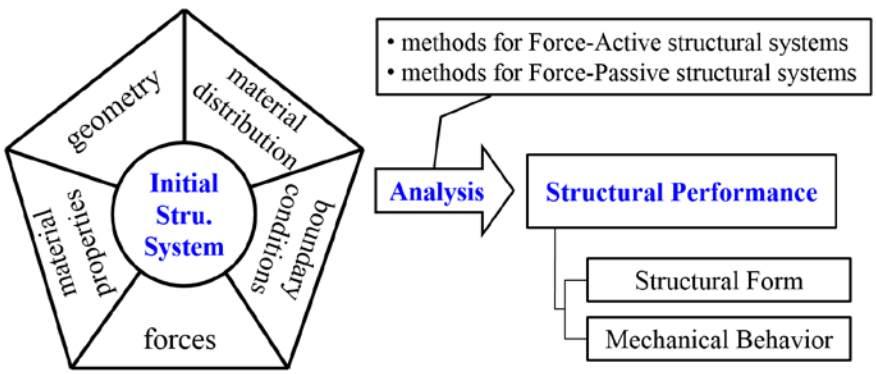


FIGURE 2.2 Conceptual model of the numerical analysis methods.

In the last few decades, many numerical analysis methods have been developed and are being developed for design, analysis, and optimisation of structural systems. Almost all of them have a similar analysis procedure. They handle the parameters that can be used to describe the initial structural system by numerical methods, and through analysis they can obtain the parameters that can be used to describe the final

structural performance, including the final structural form after complete deformation and its mechanical behaviour. Inspired by a finite element analysis process or even the lecture notes from some mechanical courses, one conceptual model of numerical analysis methods can be raised here, shown in Figure 2.2.

This conceptual model can be divided into three parts as follows:

1 The initial structural system

In numerical analysis methods, the initial structural system can be defined and described using necessary parameters, and these parameters can be divided into the following five categories:

- The parameters of **geometry**, which are used to define the initial shape and space of the initial structural system.
- The parameters of **material distribution**, which are used to define the topology and the cross sections of the initial structural system.
- The parameters of **material properties**, which are used to define the constitutive models of all building materials in the initial structural system.
- The parameters of **boundary conditions**, which are used to define the mechanical features for the supports, boundaries, and joints in the initial structural system.
- The parameters of **forces**, which are used to define all the external loads and internal forces (pre-stresses for example) that are applied to the initial structural system.

However, it should be mentioned that not all the five categories of parameters are necessary needed in one numerical analysis method. For instance, parameters of material properties are not needed in the Force Density Method [57].

2 Numerical analysis methods

From the first part, it can be observed that an initial structural system can be totally defined and described with the five categories of parameters. Then the next problem occurs: how to handle the five categories of parameters.

Nowadays, many numerical methods have been developed or are still being developed. A simple introduction of two sophisticated numerical analysis methods for two categories of structural systems are given.

- For a 'Force-Active' structural system, such as a piece of cable or membrane, it cannot develop the equilibrium equations for the current position of the initial structural system. The basic and critical step to analyse this system is to find its state of equilibrium under certain loads and boundary conditions, which is a strongly nonlinear problem, and after some dispose to keep stable it can be used as a structure. The Dynamic Relaxation (DR, for short) method [58] is one relatively mature numerical analysis method to solve these problems, in which the system oscillates about the equilibrium position by an iterative process with each iteration based on an update of the geometry.

- For a 'Force-Passive' structural system, such as a common concrete or steel structure, it is possible to analyse it with equilibrium conditions, or with additional equations if it is an indeterminate structure. The Finite Element Method (FEM) [59] is one of the most sophisticated numerical analysis methods to handle the five categories of parameters of the initial structural system by generating mesh, developing element stiffness equations, and recombining all the element equations into a global system of equations for the final calculation. On this basis, the Nonlinear Finite Element Method was developed to solve nonlinear questions in which the deformation cannot be neglected.

3 Structural performance

After numerical analysis, the final equilibrium structure with complete deformation under certain loads and constrain conditions can be obtained. The structural performance of the final equilibrium structure can also be described using parameters. These parameters are derived from the five categories of parameters of the initial structural system, and can be divided into the following two groups:

- The external structural performance - **structural form**, which refers to the final equilibrium structural form after complete deformation under certain loads and constrain conditions. It is the final appearance of the structure, including its geometry (or shape), topology and cross sections. It equals the difference between the initial form and displacement, and each of the five categories of parameters may have influence on it. For Force-Passive structural systems, under the action of the loads, the system should still maintain its shape and

remain within its location. For Force-Active structural systems, the final equilibrium form may be completely different from the initial one.

– The internal structural performance - **mechanical behaviour**, which refers to the mechanical behaviour of the final structure under certain loads and constrain conditions. It includes the internal force, stress, strain, strain energy, and other parameters. It can design the structure or evaluate its mechanical property using distinct kinds of the mechanical behaviour. The rationality of the mechanical property of the structure, which pursues efficient use of structural materials and optimal performance under multiple working conditions, is of crucial importance to structural ensure safety and to conserve building materials.

In addition, to determine whether the final system can be used as a structure, the four following properties of the mechanical behaviour of a structure are as follows:

– **Equilibrium**, which is the most basic property of the structure and provides the basic equations for structural analysis.

– **Strength**, which is an important indicator of the limit states of the ultimate bearing capacity.

– **Stiffness**, which is an important indicator of the limit states of the serviceability of a building.

– **Stability**, which is an important indicator of the design process for columns, beams, plates and shells.

§ 2.2.2 Numerical examples

In this part, two simple examples are shown to verify the rationality of the former context, and process of the numerical analysis would follow the conceptual model in Figure 2.2.

1 Equilibrium form of a 10-link mechanism

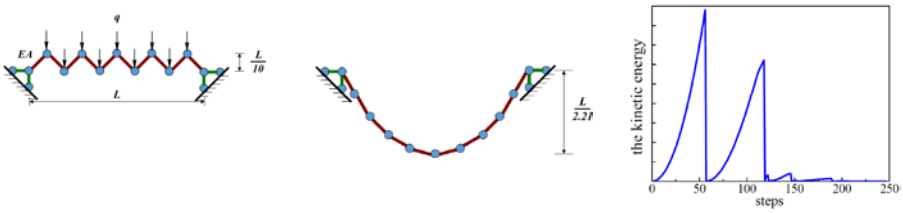
In this example (*Example 2.1*), we would like to obtain the final equilibrium shape of the 10-link mechanism with two bearings in the ends, in which all the masses are

focused on the joints with the value of q. This 10-link mechanism is a typical Force-Active structural system. The links have no weight and cannot be stretched, and known conditions are shown in Figure 2.3(a).

First, it shows the five categories of the initial system as follows:

- The parameters of geometry -- L, which refers to the span of the mechanism; $L/10$, which refers to the coordinates of some joints.
- The parameters of material distribution -- A, which refers to the section area of the cross-section.
- The parameters of material properties -- E, which refers to the elastic modulus of the material; in this example, the value is very large to ensure a very small elongation of the links.
- The parameters of the boundary conditions -- both supports are fixed hinge bearings. All joints are articulated which cannot bear the bending moments.
- The parameters of loads -- q, which refers to the mass in each joint.

Second, we analyse the former five categories of parameters using the DR method to get the structural performance. In this example, to ensure the constant length of the links, some special sets are done in the analysis process: 1) the link can only be stretched with a negligible deformation by setting a very large elastic modulus; 2) the axial force of the link is set to zero when it is in compression.



(a) Initial mechanism. *(b) Equilibrium shape.* *(c) Evolution curve.*

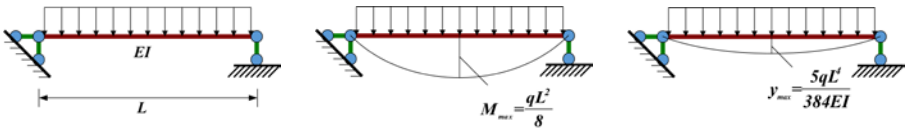
FIGURE 2.3 *Example 2.1.*

After analysis, we obtain the final equilibrium shape of the 10-link mechanism shown in Figure 2.3(b) and the evolution curve of the kinetic energy by steps shown in Figure

2.3(c). We can also attain the distribution of internal force or other behaviour of the equilibrium mechanism, which are not covered here.

2 Simple beam under distributed load

In *Example 2.2*, we would like to create the bending moment diagram and deformation diagram of one simple beam under uniformly distributed loads, and the known conditions are shown in Figure 2.4(a). This simple beam is a typical Force-Passive structural system.



(a) Initial structure *(b) Bending moment diagram* *(c) Deformation diagram*

FIGURE 2.4 *Example 2.2*.

First, it shows the five categories of the initial system as follows:

- The parameters of geometry -- *L*, which refers to the span of the beam.
- The parameters of material distribution -- *I*, which refers to the section inertia of the cross section.
- The parameters of material properties -- *E*, which refers to the elastic modulus of the material.
- The parameters of the boundary conditions -- the left support is a fixed hinge bearing and the right one is a sliding bearing.
- The parameters of loads -- *q*, which refers to the distributed load.

Secondly, we analyse the former five categories of parameters using the equations of static equilibrium and the method of sections, which is one of the most basic methods in structural mechanics and is not covered here, to obtain the structural behaviour. It should be noted that the bending rigidity *EI* of this beam is large enough in this problem to obey the small deformation assumption.

After analysis, we gain the bending moment diagram shown in Figure 2.4(b) and the deformation diagram shown in Figure 2.4(c), and both the value of the bending moment and the deformation are expressed by some of the five categories of parameters.

From the former two simple numerical examples, the classification of the parameters for the initial structural system is reasonable. After numerical analysis, it is also reasonable to divide the parameters of structural performance into two categories, which would be considered in different degrees based on the requirements in the design, analysis, and optimisation process. Moreover, both aspects of the structural performance are obtained from the analysis of the five categories of parameters of the initial structural system. They exist simultaneously and interdependently. In this case, each of the five categories of the parameters of the initial structural system have an influence on the structural performance.

In conclusion, parameters play a key role in the analysis process from the initial structural system to the final equilibrium structure. Therefore, rational classification, disposal, and analysis for those parameters become some of the most important works needed in the process of structural design, analysis, or optimisation.

§ 2.3 Theoretical Framework for Structural Morphology

Since a very early age, people prefer to build buildings with novel forms to meet their increasing requirements and with optimal mechanical behaviour to reduce costs or ensure safety. Meanwhile, the coordination between the structural form and its mechanical behaviour has been taken as a research focus in the field of structural engineering, particularly for shell and space structures, which always have novel structural forms and use their shape to bear loads.

With recent economic and social development, more novel and diverse structural forms are emerging to meet people's visual enjoyment and spiritual needs. Due to the growing power of the computer function and structural construction technology, it seems that 'anything can be carried out as long as you want to' has become the key characteristic of the modern structural technique, and the rationality of the mechanical behaviour has been placed in a relatively minor position. Therefore, new methods, techniques, and structural system innovations are needed to coordinate the relationship between structural form and its mechanical behaviour. In this case, related research on Structural Morphology shows its increasing significance.

To embody and develop the preliminary definition of 'Structural Morphology' proposed by Shen and Wu [52], this thesis tries to develop one theoretical framework of Structural Morphology on the basis of the conceptual model presented in Figure 2.2. A conceptual model and a conceptual formula of 'Structural Morphology' are proposed in this research.

Figure 2.5 shows the conceptual model of 'Structural Morphology'. Different from Figure 2.2, requirements of 'Structural Form' and 'Mechanical Behaviour' are added to present the goal of Structural Morphology. A component of 'Optimise' with a dotted arrow is included in Figure 2.5, this means that an optimisation process may be needed to improve the structural performance.

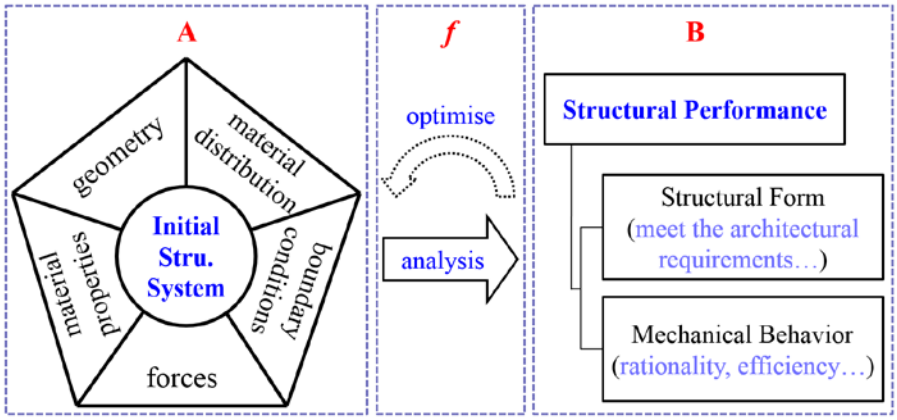


FIGURE 2.5 Conceptual model of the Structural Morphology.

Based on this, a conceptual formula of 'Structural Morphology' can be described as follows:

$$B = f(A) \qquad \text{Equation 2.1}$$

which indicates that: to obtain the structure with novel form and optimal mechanical behaviour subject to certain constraints, it can adjust some of the five categories of parameters of the initial structural system under certain constraint conditions using some algorithms. Here,

- *B* -- refers to the structural performance of the final equilibrium structures, which always require both optimal structural form (the external expression) and rational mechanical behaviour (the internal expression). Generally, *B* should

be subject to some required constraints. From the perspective of the structural engineer, the structural form should meet the architectural requirements due to its function, aesthetics and other factors. The mechanical behaviour should basically meet some requirements of strength, stiffness, and stability. On this foundation, the goal of 'Structural Morphology' is to pursue efficient use of building material and optimal performance under multiple working conditions.

- *A* -- refers to the initial structural system, which can be described by the five categories of parameters.

- *f* -- refers to the optimisation process to handle and adjust the five categories of parameters of the initial structural system to coordinate the two aspects of structural. Form-Finding (which may need a one-time analysis process or a cyclic analysis process) and Structural Optimisation (which is always a cycle analysis process) are the two important processes used for Force-Active structural systems and Force-Passive structural systems respectively.

In conclusion, it can be observed clearly that the above conceptual model and the conceptual formula can cover the entire process of numerical analysis, and show that the research goal of Structural Morphology is to balance the two aspects of structural performance - the structural form and its mechanical behaviour. Based on above, a theoretical framework for the Structural Morphology can be established. Some specific information of this framework and feasible methodologies of Structural Morphology will be introduced in the next chapter.

§ 2.4 Conclusions

This chapter summarises a conceptual model of the numerical analysis methods for structural systems. On this basis, a theoretical framework of Structural Morphology is presented. The main conclusions are as follows:

- Inspired by the finite element analysis process, a conceptual model of the numerical analysis process is summarised, which consists of three parts: the initial system described by the five categories of parameters, the setup of equations and solution methods, and the structural performance including the structural form as well as its mechanical behaviour. To verify the rationality and

feasibility of the conceptual model for both the Force-Active and the Force-Passive structural systems, two simple numerical examples are introduced.

– To embody and develop the preliminary definition of Structural Morphology proposed by Shen and Wu, based on the conceptual model of numerical analysis methods, a conceptual model and a conceptual formula to describe the Structural Morphology is proposed. Thus, the theoretical framework of Structural Morphology has been established. Compared with Motro's viewpoint [51], this conceptual formula of Structural Morphology is from the perspective of conducting the research. It covers the goal of Structural Morphology (to balance the structural form and its mechanical behaviour) and also presents the entire analysis process (the workflow).

– This chapter presents a theoretical framework of Structural Morphology, which facilitates a process of handling parameters. A more detailed introduction to this will be presented in the next chapter. Form-Finding and Structural Optimisation will be considered the two means to improve the structural performance, and are the two main aspects of Structural Morphology in this thesis.

– The theoretical framework presented in this chapter, which consists of various branches of knowledge, can also help to develop the discipline system of civil engineering or engineering mechanics to some extent. However, this is not an impeccable framework. Basically for instance, it does not cover the context of structural construction.

§ 2.5 References

[38] Structural Morphology Group (IASS Working Group NO.15). (2007). Newsletter N°14.
[39] Structural Morphology Group (IASS Working Group NO.15). (2008). Newsletter N°15.
[40] Motro R., editor. (2009). An Anthology of Structural Morphology. World Scientific, London.
[41] Motro R., editor. (2009). Structural Morphology and Configuration Processing of Space Structures. Multi Science Publishing Co Ltd.
[42] Coenders J.L., editor. (2008). Reader of the course 'CIE5251 - Structural Design - Special Structures'. Delft: Delft University of Technology.
[43] Mungan I., Abel J.F., editors. (2009). Fifty years of progress for shell and spatial structures. Multi-Science Publishing Co., Ltd, Essex.
[44] Stach E. (2010). Structural Morphology and Self-organization. Design and Nature V: Comparing Design in Nature with Science and Engineering, in: C. A. Brebbia, A. Carpi (Eds.), WIT Pres.
[45] Wester T. (2009). The first 13 years of Structural Morphology Group - a personal view. An Anthology of Structural Morphology, Ed. Motro R., World Scientific Publishing Company, Chapter 1: 1-14.

[46] Motro R. (2009). Structural Morphology. Fifty years of progress for shell and spatial structures. Ed. Mungan I., Abel J.F. Multi-Science Publishing Co. Ltd., Chapter 12: 451-458.
[47] Wester T. (1994). The nature of structural morphology and some interdisplinary examples. Spatial, Lattice and Tension Structures, IASS-ASCE, American Society of Civil Engineering, New York, 1000-1009.
[48] Ramm E., Bletzinger K.-U. (1993). Structural optimisation, International Association for Shell and Spatial structures (IASS) newsletter 112, 6.
[49] Motro R. (2002). Teaching of space structures with initial stresses, International Journal of Space Structures, 17(2&3):107-116.
[50] Bagneris M., Motro R., Maurin B., and Pauli N. (2008). Structural morphology issues in conceptual design of double curved systems. International Journal of Space Structures, 23(2): 79-87.
[51] Motro R. (2009). An approach to structural morphology. An Anthology of Structural Morphology, Ed. Motro R. World Scientific Publishing Company, Chapter 2:15-32.
[52] Shen S., Wu Y. (2014). Structural morphology and modern space structures. Journal of Building Structures. 35(4): 1-10. (in Chinese)
[53] http://www.iass-structures.org/index.cfm/page/TechAct/WG15.htm
[54] Borgart A. (2010). New challenges for the structural morphology group. Journal of the International Association for Shell and Spatial Structures. 51(3): 183-189.
[55] Bletzinger K.-U. (2011). Form-Finding and morphogenesis. Fifty years of progress for shell and spatial structures, Ed. Mungan I., Abel J.F., Multi-Science Publishing Co. Ltd., Chapter 12: 459-474.
[56] Ohmori H. (2011). Computational morphogenesis - its current state and possibility for the future. International Journal of Space Structures. 26(3): 269-276.
[57] Schek H.J. (1974). The force density method for form finding and computations of general networks. Computer Methods in Applied Mechanics and Engineering. 3:115-134.
[58] Day A.S. (1965). An introduction to dynamic relaxation. The Engineer. 29(2): 218-221.
[59] http://en.wikipedia.org/wiki/Finite_element_method

TOC

3 Form-Finding and Structural Optimisation

§ 3.1 Introduction

The theoretical framework of Structural Morphology proposed in the last chapter can give rise to feasible methodologies of relevant researches. Form-Finding and Structural Optimisation are considered the two primary means to generate novel and diverse structural forms with optimal mechanical behaviours, and are two aspects of Structural Morphology.

In this chapter, based on the proposed theoretical framework of Structural Morphology, methodologies of Form-Finding and Structural Optimisation are concluded, and some research achievements from the author's research team ([61], [70], [77], [78], [85]-[92]) are discussed to validate the rationality.

For Force-Active structural systems, a stable equilibrium state under given initial conditions is needed to serve as a 'structure'. As the 'form follows force' principle, internal forces of the equilibrium shape adjust themselves positively to keep equilibrium with the external loads. This means the mechanical behaviour of this equilibrium form is always rational. However, some architectural requirements of the structural forms (due to the usability, aesthetics, or other requirements), and some additional requirements of mechanical behaviour (stress level, stress distribution, etc.) may be needed. In this case, a Form-Finding process that aims to generate constrained and diverse equilibrium shapes is required.

For Force-Passive structural systems, the final structural form has little difference from the initial structural system. However, unreasonable distributions of internal forces (large bending moments, etc.) may occur in the final equilibrium form, which means the mechanical behaviour may not be rational and thus the material may not be utilised optimally. To obtain optimal mechanical behaviour, a Structural Optimisation process by adjusting some parameters (parameters of geometry or material distributions are always considered nowadays) of the initial structural system under certain constraints is required.

§ 3.2 Form-Finding of Force-Active Structural Systems

Form-Finding is a forward process in which parameters are explicitly/directly controlled to find an 'optimal' geometry of a structure that is in static equilibrium with a design load [60]. This term is always used to express the process of generating the equilibrium shape of Force-Active structural systems subject to certain constraints. However, the final equilibrium structural forms can also be used as 'Force-Passive' structural forms with some required settings, for example, inverting the hanging chain to obtain the structural efficient form of an arch. In this case, Form-Finding can also be used to describe the form generation process of 'Force-Passive' structural systems.

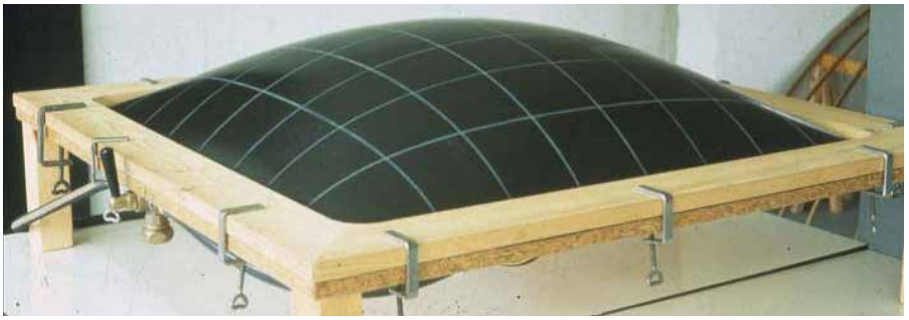
In the pre-computer age, architects and engineers used physical models to conduct the Form-Finding process. Shown in Figure 3.1, these physical models can be divided into three groups according to their manufacturing methods: hanging models that represent an equilibrium state of Force-Active structural system under gravity, tension models that represent an equilibrium state with internal stresses, and pneumatic models that represent an equilibrium state under pressure loads [61].



(a) Hanging model of Heinz Isler [66].



(b)Tension model of Frei Otto [67].



(c) Pneumatic model of Heinz Isler [68].

FIGURE 3.1 Three types of physical models.

With the development of computational techniques, most of the Form-Finding processes nowadays are carried out by numerical methods. Many numerical methods have been developed and are being developed nowadays. Adopted from Veenendaal and Block [62], these numerical analysis methods can be categorised into three main families: stiffness matrix methods, geometric stiffness methods, and dynamic equilibrium methods. The Non-linear Finite Element method [63], the Force Density method [64], and the DR method [65] are the typical example of each category.

For this kind of problem, the final equilibrium structural form always has a very close relationship with the mechanical behaviour. For instance, in tension structures, the equilibrium structural form provides the structure with geometric stiffness to withstand loads. It is acceptable for most engineers that the mechanical behaviour is reasonable after the process of Form-Finding, and what a concern to them is to find the structural form under other constraints from architectural or mechanical requirements.

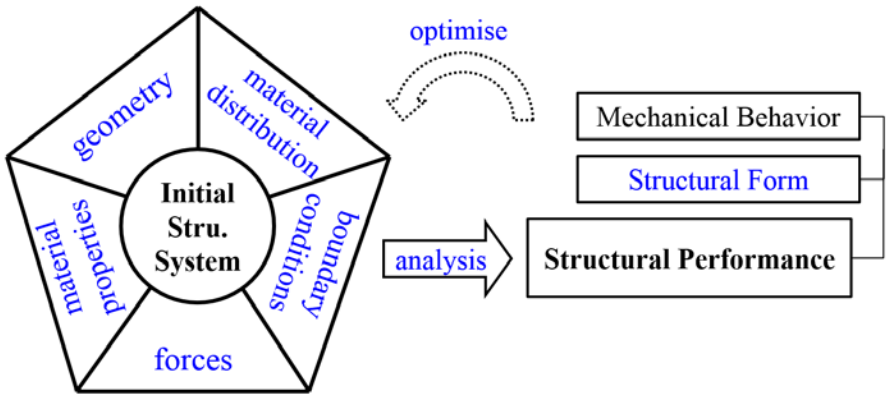


FIGURE 3.2 Conceptual model of Form-Finding: a) All the five categories of parameters of the initial structural system are in blue, indicating that all the categories can be used as variables during the Form-Finding process, b) 'Structural Form' is in blue, indicating that the main goal of Form-Finding is to generate structural forms with architectural constraints, c) 'optimize' is in blue and the arrow is dotted, indicating that an optimisation process may be needed during the Form-Finding process, but may not be needed when a one-time analysis can meet the requirements.

Figure 3.2 shows the conceptual model of the numerical Form-Finding processes. For most of these problems, after analysing the five categories of parameters of the initial structural system by numerical method, the equilibrium structural form can be obtained. To obtain the structural form with other required architectural or mechanical constraints, it also needs some adjustment of the initial structural system. In this case,

some optimisation algorithms can be introduced to deal with these during the Form-Finding process.

To validate the rationality and feasibility of the conceptual model in Figure 3.2, some research achievements in Form-Finding of Force-Active structural systems are introduced based on the above classification of physical models.

§ 3.2.1 Form-Finding of hanging structural systems

Hanging models represent a type of equilibrium state for flexible materials under their self-weight with certain constraint conditions and with stress states in pure tension. In this section, two relatively new research achievements of hanging structural systems are discussed.

In the author's master thesis [69] and several papers[70][71][72], the nonlinear FEM is used to simulate the hanging model experiment. Using the bisection method to adjust the elastic modulus of the initial structural system, the shape of the inverted structure with certain control points is obtained. Moreover, diverse structural forms of the inverted structures are obtained by adjusting parameters of the initial structural system using the methodology of the conceptual model proposed in Figure 3.2. Figure 3.3 shows some diverse numerical models changed from the same initial model.



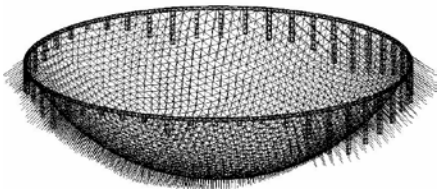
FIGURE 3.3 Diverse numerical structural models [70].

In this presented research, the VFIFE method is introduced to generate equilibrium shapes of hanging structural systems. The Newton-Raphson method and the inverse iteration method are applied to control the equilibrium structural forms with target heights. By adjusting the parameters of the initial structural system, diverse structural forms of form-found shells can be obtained. All these works will follow the presented methodology of Form-Finding shown in Figure 3.2. Detailed information will be introduced in the coming chapters.

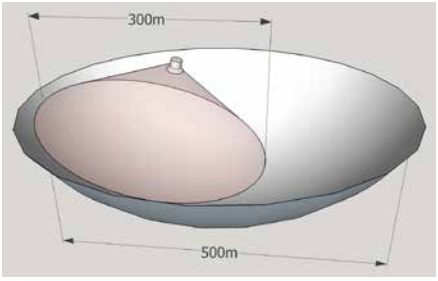
§ 3.2.2 Form-Finding of tension structural systems

Tension models are typical 'self-stressing' structural systems, with their stiffness resulting from a system of internal stresses in static equilibrium, and with their stress conditions also being pure tension. Form-Finding of tension structural systems is a relatively mature area. Many numerical methods have been put into practice over the years.

The active reflector of the FAST project is supported by spherical main cable-mesh and control cables acting on its joints, shown in Figure 3.4 (a). The nonlinear FEM is used to generate the equilibrium state of this integral cable-net structure. The inverse iteration method is used to ensure that all the joints are in a spherical surface with a radius of 318.5 m, and that part of the joints are in a parabolic reflector with an aperture of 300 m when it is working shown in Figure 3.4 (b). Moreover, several additional adjustments (cross-section optimisation, etc.) are included to determine the required stress level of the cable elements.



(a) Integral cable-net structure of FAST [73].



(b) One working condition of FAST [74].

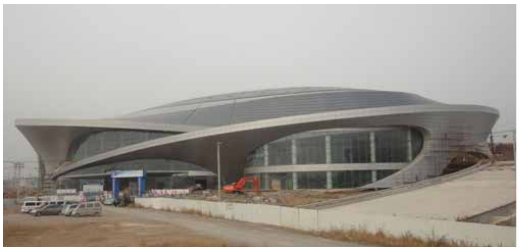
FIGURE 3.4 The FAST project.

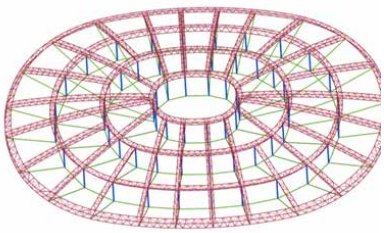
In this field, some engineering practices have been carried out by the author's research group. For example, Figure 3.5 shows the tensioned membrane structure of

Weihai Stadium designed by Wu et al. [75] and the Dalian Centre Gymnasium with a suspended dome designed by Cao et al. [77]. Both structures are form-found by using the nonlinear FEM. Among them, the inverse iteration method is also used to determine a structural form with a high-level fitness with the architectural design for the latter structure.



(a) Weihai Stadium [76].





(b) Dalian Centre Gymnasium [77].

FIGURE 3.5 Two engineering practices.

Moreover, the VFIFE method can also be used to generate the equilibrium structural form of tension structural systems, which will be introduced in Chapter 4. All these works mentioned above can support the methodology of Form-Finding shown in Figure 3.2.

§ 3.2.3 Form-Finding of pneumatic structural systems

Pneumatic models represent a type of equilibrium state of flexible materials under air pressure and certain constraint conditions, where stress states are in pure tension.

Borgart [78] introduced and developed an approximate calculation method for air-inflated cushion structures for design purposes. In this method, the complicated

geometric nonlinear behaviour of deformations of membranes has been solved by relatively simple analytical formulas. It is found that parameters of material properties are not included in these formulas, but the methodology of Form-Finding shown in Figure 3.2 is also suitable to this work. Figure 3.6 shows a numeric simulation of an air cushion.

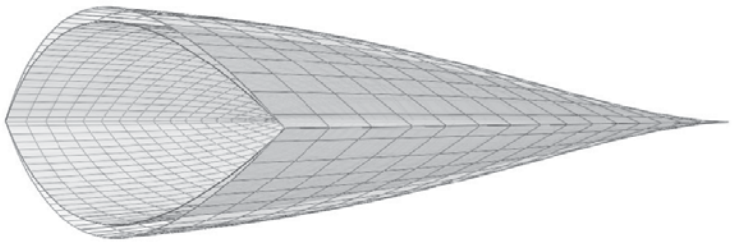
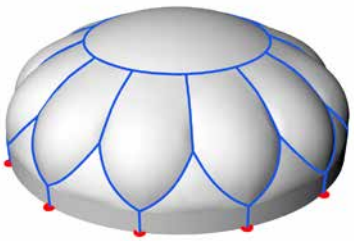


FIGURE 3.6 Numeric simulation of an air cushion [78].

The VFIFE method is also used to generate structural equilibrium forms of pneumatic structural systems, which will be introduced in Chapter 4. Based on this, the Newton-Raphson method is used to generate the pneumatic structural equilibrium form with target heights. The research results are applied to perform Form-Finding of the inflatable formwork of the ice composite dome built in the winter of 2016 [79]. Figure 3.7 shows the inflatable formwork and the construction result of the ice dome.



(a) Form-Finding result of the inflatable formwork.



(b) Ice dome after construction.

FIGURE 3.7 Ice dome.

In summary, the above research achievements obtained by the author's research group can support the proposed methodology of Figure 3.2. As the mentioned research achievements are relatively comprehensive, it can be expected that this methodology

is rational and feasible for all kinds of Form-Finding research, which can also be demonstrated in the literature review for the Form-Finding research on shell structures in Chapter 4. Based on this, systematic research on Form-Finding of shell structures is carried out in the following chapters.

§ 3.3 Structural Optimisation of Force-Passive Structural Systems

Structural Optimisation problems are formulated to improve structural properties under certain specified constraints. A Force-Passive structural system would not have excessive deformation after analysis. In this case, parameters of geometry and material distribution can almost determine the final equilibrium structural form. Then, what it concerns most is the rationality of the mechanical behaviour of the structural system. Therefore, most researches today focuses on generating optimal mechanical behaviour by adjusting the parameters of geometry or material distribution.

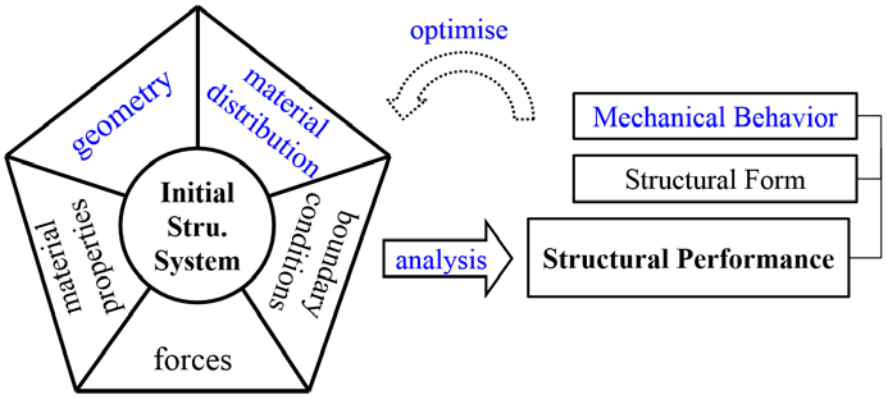


FIGURE 3.8 Conceptual model of Structural Optimisation: a) 'geometry' and 'material distribution' of the initial structural system are in blue, indicating that these two categories are always used as variables during the Structural Optimisation process, b) 'Mechanical Behaviour' is in blue means, indicating the main goal of Structural Optimisation is to improve the mechanical behaviour of the structural system, c) 'optimize' is in blue and the arrow is dotted, indicating that an optimisation process may be needed during the Structural Optimisation process, but may not be needed when a one-time analysis can meet the requirements.

Figure 3.8 shows the conceptual model of Structural Optimisation. The mechanical behaviour of the structure (strength, rigidity, stability, or their combination) acts as the optimisation objective. Each category of the parameters of the initial structural system

can act as the optimisation variable (most are the parameters of geometry or material distribution). Moreover, the objective function would be founded to link the objective with the variable. Subsequently, one suitable optimisation algorithm would be selected to conduct the optimisation process by adjusting the optimisation variables under certain constraint conditions.

Structural Optimisation is usually categorised into three categories [80]: topology, shape, and size optimisation, shown in Figure 3.9. Based on the conceptual model above, this thesis covers two categories: optimisation of geometry and optimisation of material distribution. Many achievements have been obtained by scholars in this area (see [80], [81], [82], [83], etc.). As for the optimisation algorithms, many algorithms have been developed and are being developed nowadays [84]. However, as the goal of this section is to demonstrate the conceptual model of Structural Optimisation shown in Figure 3.8, these algorithms are not introduced in detail here.

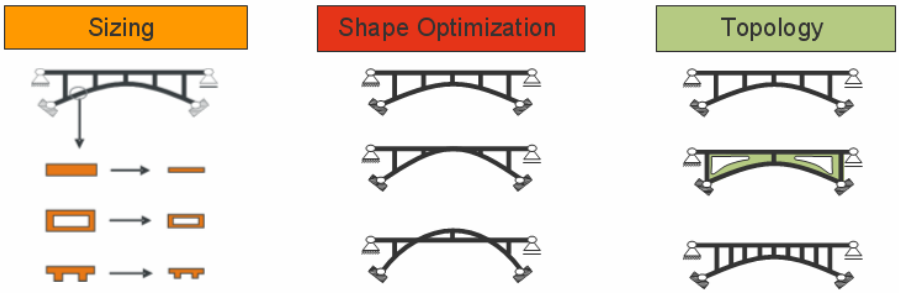


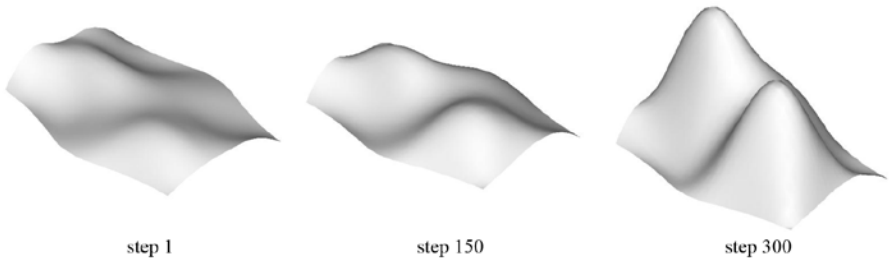
FIGURE 3.9 Different branches of Structural Optimisation [81].

In this section, to validate the rationality and feasibility of the presented methodology of Structural Optimisation shown in Figure 3.8, contributions by the author and other members of the research team are introduced in the following three sections.

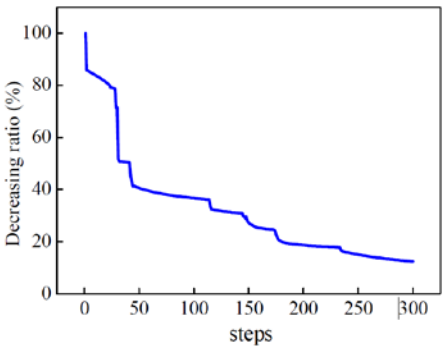
§ 3.3.1 Optimisation of geometry

This area can also be called 'shape optimisation of structures'. Parameters of geometry of the initial structural system are considered the optimisation variables. Two examples carried out by the author's research team are shown in this section. One relates to freeform shells, and the other one to freeform reticulated shells.

Li et al. [85] presented a method of shape optimisation for freeform shells: the NURBS-GM method. This method uses the NURBS technique to describe the geometry of the initial structure. It takes minimum structural strain energy (the smaller the value, the better the mechanical behaviour) as the objective goal. Additionally, it takes the FEM as the structural analysis method, and uses the gradient method (GM) to adjust the control points and the weights of the numerical function of the NURBS surface. By using this method, the structural form can be modified to obtain an optimal mechanical behaviour. Figure 3.10 shows the evolution of one surface and the strain energy of one freeform shell using this method.



(a) Evolution of the structural form.

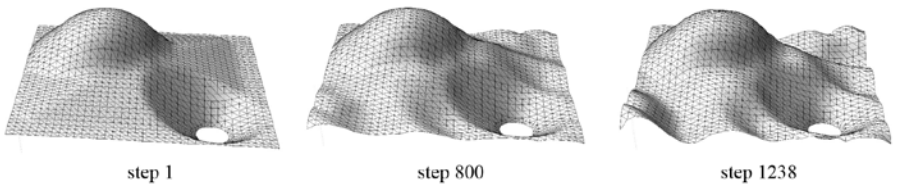


(b) Evolution of strain energy.

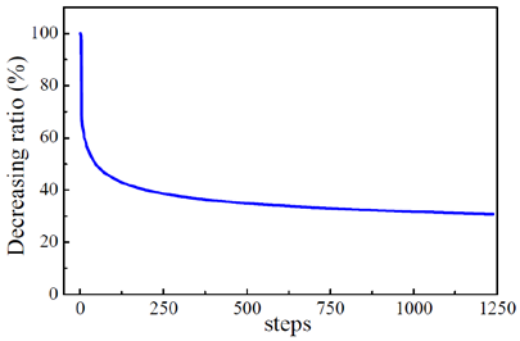
FIGURE 3.10 Example of freeform shells [85].

Cui et al. [86] presented a method of shape optimisation for freeform reticulated shells. This method takes minimum structural strain energy as the objective goal, takes the FEM as the structural analysis method, and uses differential geometric methods to describe the geometry of the initial structure. Based on the relationship between structural strain energy and its nodal coordinates, the method adjusts the nodal coordinates to achieve a reasonable structural form with minimum structural strain energy. The GM is the selected

optimisation algorithm. Figure 3.11 shows the evolution of the surface and the strain energy of a freeform reticulated shell using this method.



(a) Evolution of the structural form.



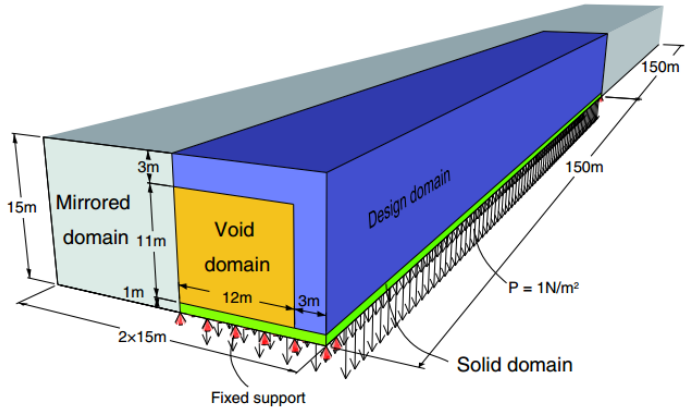
(b) Evolution of strain energy.

FIGURE 3.11 Example of freeform reticulated shells [86].

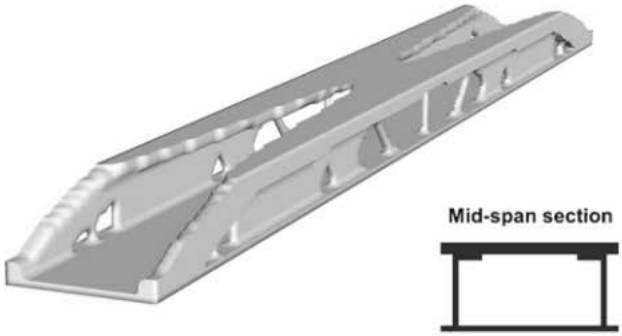
§ 3.3.2 Optimisation of material distribution

Optimisation problems of material distribution can include both the 'topology optimisation' and the 'size optimisation' from Figure 3.9. Parameters of material distribution are seen as the optimisation variables. This section shows two examples. The first one is about continuum structures, and the second is about discrete structures.

Chang et al. [87] presented a structural topology optimisation algorithm using the direct gradient projection method with a transformation of variables technique. This is an efficient and reliable topology optimisation method for continuum structures. The method takes the compliance of the structure as the optimisation objective, takes the FEM as the structural analysis method, and adjusts the parameters of material distribution. Figure 3.12 shows a numerical example of this method.



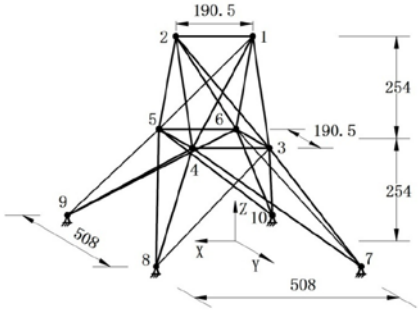
(a) Initial structure.

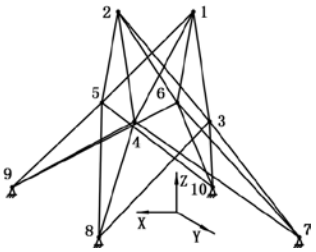


(b) Final structure.

FIGURE 3.12 Example of continuum structure [87].

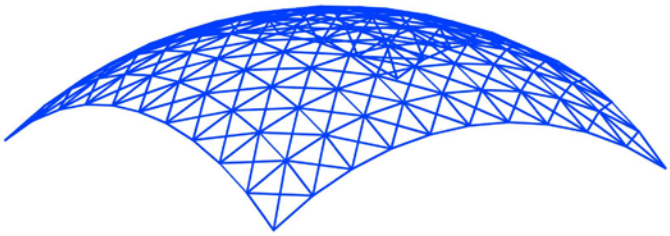
Wu et al. [88][89] introduced and improved the Firefly Algorithm to conduct the size and topology optimisation for trusses with discrete design variables. Cross section variables which are capable of including topology variables are considered optimisation variables in this method. Minimum self-weight of the structure or its combination with structural energy is taken as the optimisation goal. Shown in Figure 3.13, a benchmark example of size and topology optimisation of one 25-bar spatial truss structure was carried out using the proposed method. Shown in Figure 3.14, the size and topology optimisation of a four-corner-supported spherical grid shell with two different optimisation goals was carried out using this method.



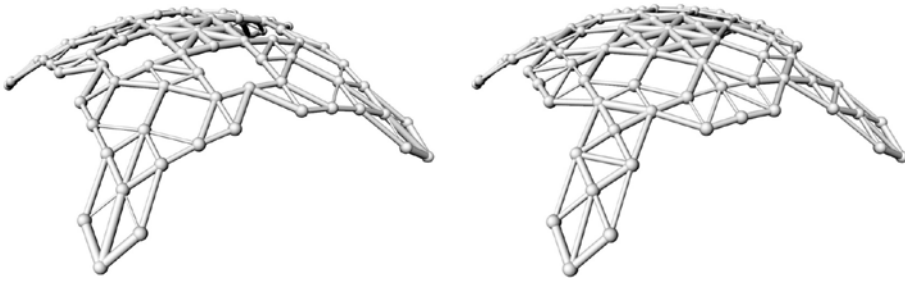


(a) Initial structure *(b) Optimised structure*

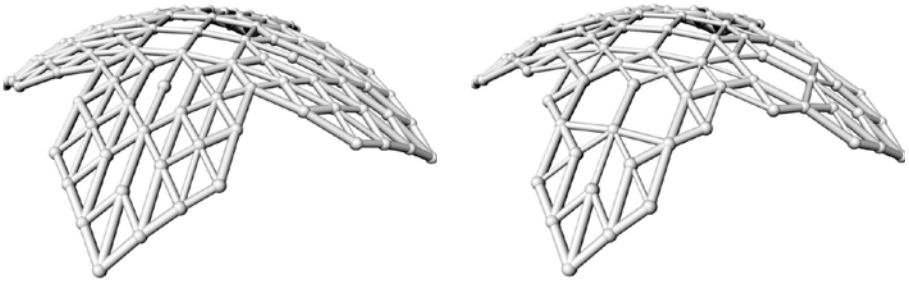
FIGURE 3.13 Size and topology optimisation of the 25-bar spatial truss structure [88].



(a) Initial structure.



(b) Two optimized structures with optimisation goal of minimum self-weight.



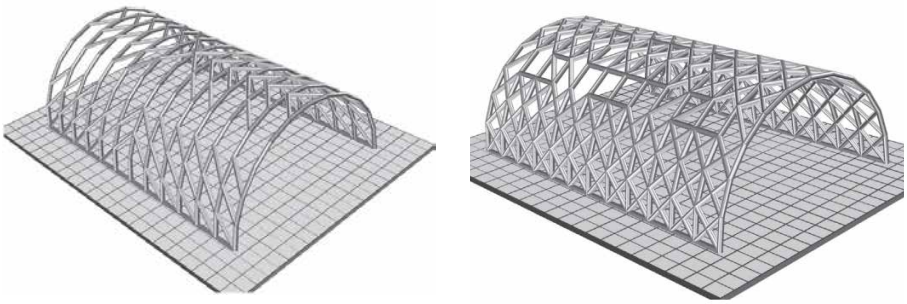
(c) Two optimized structures with optimisation goal of minimum product of self-weight and strain energy

FIGURE 3.14 Size and topology optimisation of a four-corner-supported spherical grid shell [89].

§ 3.3.3 Optimisation of combined parameters

Moreover, optimisation of the combined parameters is also a research focus. In most cases, combined parameters of 'geometry' and 'material distribution' are considered optimisation variables. Two examples carried out by the author' research team are shown here.

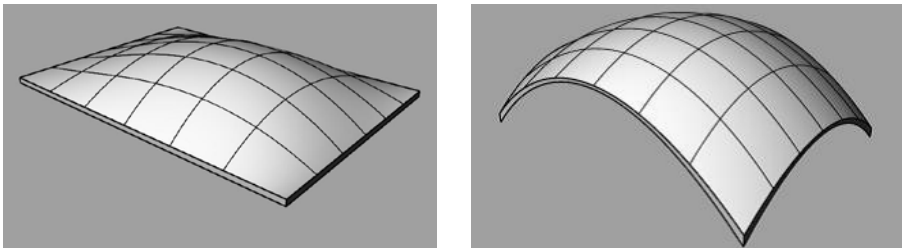
Cui and Jiang [90] presented an optimisation method for the topology and shape optimisation of framed structures subject to spatial constraints. This method is based on the elemental and nodal sensitivity information to generate or modify the structural topology. It adjusts the nodal positions to achieve a structural form with minimum strain energy. This method combines direct elemental addition or elimination, free nodal shift, and restricted nodal shift related to the structural geometry. FEM is the structural analysis method during this work, and GM is the selected optimisation algorithm. Figure 3.15 shows a numerical example optimising a single-layer cylinder reticulated shell.



(a) Initial structure. *(b) Final structure.*

FIGURE 3.15 Example of discrete structure [90].

Wu et al. [91][92] proposed a structural optimisation method using the hybrid optimisation method and the NURBS entity technique. In this method, minimal strain energy and self-weight are taken as optimisation objectives, control points of the NURBS entity function are taken as optimisation variables to determine the shape and thickness of the freeform shell, FEM is used to do structural analysis, and the hybrid optimisation method is used as the optimisation method. Figure 3.16 shows a numerical example of shape and thickness optimisation of a four-corner-supported shell.



(a) Initial structure *(b) Final structure*

FIGURE 3.16 Example of optimisation of combined parameters [92].

All the research achievements mentioned above can clearly support the conceptual model and thus the methodology of structural optimisation shown in Figure 3.8. Guided by this, three key issues are included in the ongoing research from the author's research team.

- More optimisation variables must be considered. Each of the five categories of parameters of the initial system and their combination can be seen as optimisation variables. For example, taking the parameters of material properties as optimisation variables, a more efficient structure may be generated by replacing the tensile members with cables in a truss structure.

- More realistic situations need to be considered. More constraints due to the architectural or mechanical requirements should be considered in the optimisation process. Moreover, the optimisation for different load combinations should be developed in addition to the single load case.

- New construction techniques need to be developed. The results of the structural optimisation often have very complex shapes and cross sections, which would impose difficulties and new challenges to the construction. In this case, new tasks are ahead regarding the practice of the structural optimisation methods for scholars, architects, and engineers.

§ 3.4 Conclusions

In this chapter, the two main means to improve structural performance and two fundamental research aspects of Structural Morphology (Form-Finding of Force-Active

structural systems and Structural Optimisation of Force-Passive structural systems) are discussed. The main conclusions are as follows:

- Based on the theoretical framework of structural morphology, a conceptual model and thus the methodology for Form-Finding are presented. Several research achievements gained from the author or members of the research team are introduced to support the presented conceptual model and thus the methodology of Form-Finding. On this basis, systematic Form-Finding research on shell structures, including equilibrium problems of Force-Active structural systems, controlling form-found shells with target heights, and generation of diverse structural forms of form-found shells, will be performed in the following chapters.

- Based on the theoretical framework of structural morphology, a conceptual model and thus the methodology for Structural Optimisation is presented. From the introduction of several research achievements gained from the author or members of the research team, the presented conceptual model and methodology of Structural Oprimisation are rational and feasible to guide relevant research. Based on this, relevant research on complicated Structural Optimisation problems is ongoing in the author's research groups.

§ 3.5 References

[60] Adriaenssens S., Block P., Veenendaal D. and Williams C., editors. (2014). Shell Structures for Architecture: Form Finding and Optimisation. London: Routledge Taylor and Francis.

[61] Li Q., Su Y., Wu Y., Borgart A., Rots J.G. (2017). Form-Finding of shell structures generated from physical models, International Journal of Space Structures. 32(1): 11-33.

[62] Veenendaal D., Block P. (2012). An overview and comparison of structural form finding methods for general networks, International Journal of Solids and Structures. 49(26): 3741-3753.

[63] http://en.wikipedia.org/wiki/Finite_element_method

[64] Schek H.J. (1974). The force density method for form finding and computations of general networks. Computer Methods in Applied Mechanics and Engineering. 3: 115-134.

[65] Day A.S. (1965). An introduction to dynamic relaxation. The Engineer, 29(2): 218-221.

[66] Billington D.P. (2011). Heinz Isler: From Delft to Princeton and Beyond. Journal of the International Association for Shell and Spatial Structures (J. IASS). 52(3): 135-141.

[67] https://www.pinterest.com/pin/317011261243639594/

[68] Ramm E. (2011). Heinz Isler Shells – The Priority of Form. Journal of the International Association for Shell and Spatial Structures (J. IASS). 52(3): 143-154.

[69] Li Q. (2013). Numerical simulation and applications of the inverse hanging method. MSc thesis, Harbin Institute of Technology. (in Chinese)

[70] Wu Y., Li Q. (2012). Inverted hanging method and its application on structural morphogenesis. 14th Academic Conference of Space Structures in China. Fuzhou, China, 2012. (in Chinese)

[71] Li Q., Wu Y., Shen S. (2014). Computational generation of freeform shells based on the inverse hanging experiment. Proceedings of the IASS-SLTE 2014 Symposium, Brasilia, Brazil.
[72] Wu Y., Li Q., Shen S. (2014). Computational morphogenesis method for space structures based on principle of inverse hanging experiment. Journal of Building Structures, 35(4): 41-48. (in Chinese)
[73] Qian H. (2007). Theoretical and Experimental Research on Supporting Structure of FAST Reflector. PhD thesis, Harbin Institute of Technology. (in Chinese)
[74] https://en.wikipedia.org/wiki/Five_hundred_meter_Aperture_Spherical_Telescope
[75] Wu Y., Xiang Y., Shen S. (2001). Structural wind tunnel test of the cable-membrane structure of Weihai stadium. Building Structure. 6: 66-68. (in Chinese)
[76] http://www.whnews.cn/news/2008-08/28/content_1372944_2.htm
[77] Cao Z., Wu Y., Qian H., Shen S. (2011). Design and analysis of giant grid suspen-dome of Dalian Centre Gymnasium. Steel Construction, 26(1): 37-42. (in Chinese)
[78] Borgart A. (2010). An approximate calculation method for air inflated cushion structures for design purposes. International Journal of Space Structures, 25(2): 83-91.
[79] Wu Y., Liu X., Li Q., Chen B., Luo P., Pronk A.D.C., Mergny E. (2017) . Form-Finding and construction of ice composite shell structures. Proceedings of the IASS Annual Symposium 2017, Hamburg, Germany.
[80] Christensen P. W., Klarbring A. (2009). An Introduction to Structural Optimisation. Springer.
[81] Masching H. (2016). Parameter Free Optimisation of Shape Adaptive Shell Structures. PhD thesis, Technischen Universität München.
[82] Bletzinger K.-U. (2011). Form-Finding and morphogenesis. Fifty years of progress for shell and spatial structures, Ed. Mungan I., Abel J.F. Multi-Science Publishing Co. Ltd., Chapter 12: 459-474.
[83] Ohmori H. (2011). Computational morphogenesis - its current state and possibility for the future. International Journal of Space Structures, 26(3): 269-276.
[84] Weise T. (2009). Global Optimisation Algorithms - Theory and Application. Self-Published, second edition. Online available at http://www.it-weise.de/.
[85] Li X., Wu Y., Cui C. (2011). NURBS-GM method for computational morphogenesis of free form structures. China Civil Engineering Journal, 44(10): 60-66. (in Chinese)
[86] Cui C., Wang Y., Jiang B. and Cui G. (2013). Study on the structural morphogenesis technique for single-layer reticulated shells of free-curved surface. China Civil Engineering Journal, 46(4): 57-63. (in Chinese)
[87] Chang C., Borgart A., Chen A. and Hendriks M.A.N. (2014). Direct gradient projection method with transformation of variables technique for structural topology optimisation. Structural and Multidisciplinary Optimisation, 49: 107-119.
[88] Wu Y., Li Q., Hu Q. and Borgart A. (2017). Size and Topology Optimisation for Trusses with Discrete Design Variables by Improved Firefly Algorithm. Mathematical Problems in Engineering.
[89] Hu Q. (2015). Topology optimisation analysis for framed structures based on the improved firefly algorithm. MSc thesis, Harbin Institute of Technology. (In Chinese).
[90] Cui C., Jiang B. (2014). A morphogenesis method for shape optimisation of framed structures subject to spatial constraints. Engineering Structures, 77: 109-118.
[91] Wu Y., Xia Y. and Li Q. (2015). Structural morphogenesis of freeform shells by adjusting the shape and thickness. Proceedings of the IASS Symposium, Amsterdam, the Netherlands.
[92] Xia Y. (2015). Computational morphogenesis of freeform structures based on hybrid optimisation method. MSc thesis, Harbin Institute of Technology. (In Chinese).

TOC

PART 3 Form-Finding of Shell Structures

TOC

TOC

4 Introduction to Shell Structures

§ 4.1 Introduction

The structural form of a shell is completely described by the curved shape of the middle surface and the thickness distribution of the shell. For a shell structure, the geometric shape plays a significant role in its structural efficiency. In this chapter, characteristics of the structural forms of shells are discussed first. To present the finite element results, several factors that can be used to assess the mechanical behaviour of shell structures for the conceptual design phase are introduced. Finally, a detailed introduction of Form-Finding research on shells is provided.

§ 4.2 Structural Forms of Shells

There are many ways to study the structural forms of shells: according to whether the surface is developable, according to the geometrical generation methods of surfaces, and other methods. When considering the structural efficiency of one surface, the curvatures of the surface are crucial factors, as they play important roles in the classical theory of shell structures [93].

Surfaces can be described in a global Cartesian coordinate system ($\bar{x}$, $\bar{y}$, $\bar{z}$). Local properties of surfaces can also be described by a local coordinate system (x, y, z) , shown in Figure 4.1. In the local coordinate system, the z-direction is perpendicular to the surface and the x- and y-directions are tangent to the surface.

Curvatures can be defined for surfaces. Figure 4.2 shows a point on the surface and the vector $\boldsymbol{z}$ of this point which is normal to the surface. Any plane can be drawn through this normal vector. This normal plane intersects the surface in a curved line. In this point of the curved line, there is a best approximating circle that touches the curve. The curvature of this line is referred to as the 'normal section curvature' k, which equals the reciprocal of the radius of the circle. If the circle lies in the positive side of the $\boldsymbol{z}$ axis, k is

positive. If the circle lies in the negative side of the *z* axis, *k* is negative. The direction of the *z* axis can be chosen freely (pointing inward or outward).

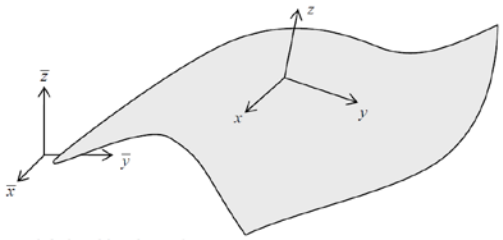


FIGURE 4.1 Global and local coordinate systems [94].

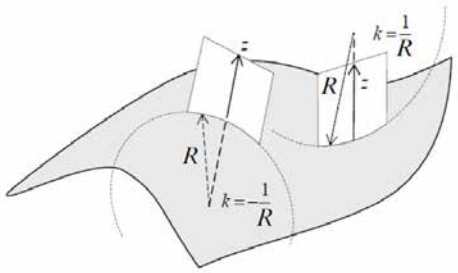


FIGURE 4.2 Curvatures on surface [94].

In the local coordinate system, curvatures in the *x*- and *y*-direction are as follows,

$$k_{xx}=\frac{\partial^2 z}{\partial x^2}, k_{yy}=\frac{\partial^2 z}{\partial y^2} \qquad \text{Equation 4.1}$$

The twist of the surface is as follows,

$$k_{xy}=\frac{\partial^2 z}{\partial x \partial y} \qquad \text{Equation 4.2}$$

In the global coordinate system, the curvatures become the following,

$$k_{\bar{x}\bar{x}}=\frac{\frac{\partial^2 \bar{z}}{\partial \bar{x}^2}}{(1+(\frac{\partial \bar{z}}{\partial \bar{x}})^2)^{3/2}}, k_{\bar{y}\bar{y}}=\frac{\frac{\partial^2 \bar{z}}{\partial \bar{y}^2}}{(1+(\frac{\partial \bar{z}}{\partial \bar{y}})^2)^{3/2}} \qquad \text{Equation 4.3}$$

Among these numerous curvatures of this point, there will be a minimum value k_2 and maximum value k_1, which are called the principal curvatures and are given by the following formulas:

$$k_1 = \frac{1}{2}(k_{xx} + k_{yy}) + \sqrt{[\frac{1}{2}(k_{xx} - k_{yy})]^2 + k_{xy}^2} \quad \text{Equation 4.4}$$

$$k_2 = \frac{1}{2}(k_{xx} + k_{yy}) - \sqrt{[\frac{1}{2}(k_{xx} - k_{yy})]^2 + k_{xy}^2} \quad \text{Equation 4.5}$$

The curvatures of the surface at one point can also be presented in the Mohr's circle for curvatures, shown in Figure 4.3.

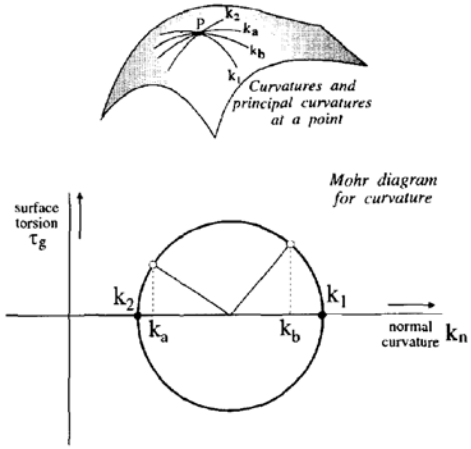


FIGURE 4.3 Mohr's circle for curvatures [95].

The Gaussian curvature and the mean curvature are two important characteristics of one structural surface. The product of the two principal curvatures, Equation 4.6, is called the Gaussian curvature of the surface at this point:

$$k_G = k_1 k_2 \quad \text{Equation 4.6}$$

The Gaussian curvature can be positive, negative, or zero, see Figure 4.4 [96]. k_G = 0 describes no curvature or 'single curvature' like cylinders, cones, or barrel shells. 'Double curvature' is sub-categorized to $k_G > 0$, leading to 'synclastic' shapes with curvature radii on one side, like paraboloids or domes; and $k_G < 0$, leading to 'anticlastic' shapes with curvature radii located on opposite sides, like saddles and hyperbolic paraboloid.

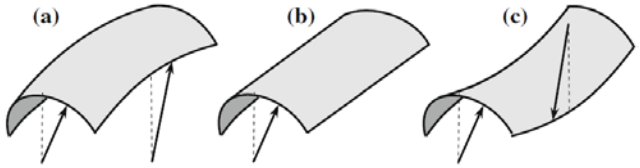
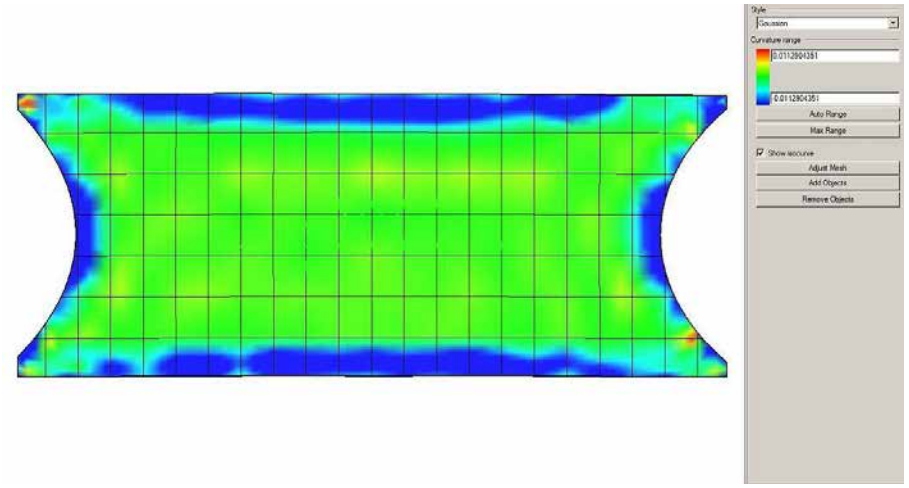
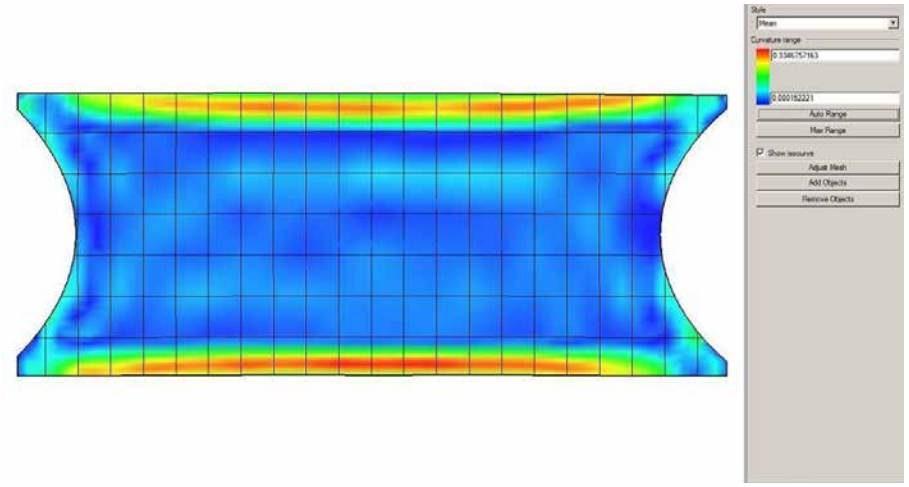


FIGURE 4.4 Types of Gaussian curvature: a) Positive, b) Zero, and c) Negative [96].



(a) The Gaussian curvature.



(b) The mean curvature.

FIGURE 4.5 Curvature analysis of roof structure of the sports hall of Heinz Isler ([97]).

The average of the two principal curvatures is called the mean curvature of the surface at this point. Surfaces with zero mean curvature everywhere are minimal surfaces. It is useful for finding areas of abrupt change in the surface curvature.

Curvature analysis of one surface can be easily conducted in Rhino software, even for freeform shapes. Figure 4.5 shows the contour plots of the Gaussian curvature and the mean curvature of a shell design that Heinz Isler made for sports halls [97]. The freeform surfaces have a complicated distribution of Gaussian curvatures and mean curvatures, which is their typical geometrical feature.

§ 4.3 Mechanical Behaviour of Shells

Nowadays, the FEM is commonly and easily used in many computer programs to analyse the mechanical behaviour of shell structures. Although the Finite Element Analysis provides good insight into the quantitative behaviour of shell structures during loading, it provides very little qualitative insight into their structural behaviour. How to assess the mechanical behaviour of shell structures in the conceptual design phase is discussed in this section.

§ 4.3.1 Mechanical behaviour assessment of shells in the conceptual design phase

In the conceptual design phase of shell structures, it is important to know whether the shell performs as a shell or a slab, and to know its buckling behaviour under certain load conditions. For a shell structure, primarily its self-weight and similarly distributed loadings should be considered, which are also considered by most of the Form-Finding or Structural Optimisation techniques. However, the weakness of a shell is always its behaviour under other loadings, such as the half-side loads. Therefore, linear static analysis and buckling analysis under two different loadings can be enough to assess their mechanical behaviour in the conceptual design phase.

A mechanical behaviour assessment strategy (Figure 4.6) for the conceptual design phase can be proposed. This assessment strategy is used in **Chapter 8** to compare the mechanical behaviour of form-found shells with different support shapes. However, Chapter 8 requires a detailed comparison of the structural efficiency of these form-found shells; thus, nonlinear analyses for these are also included.

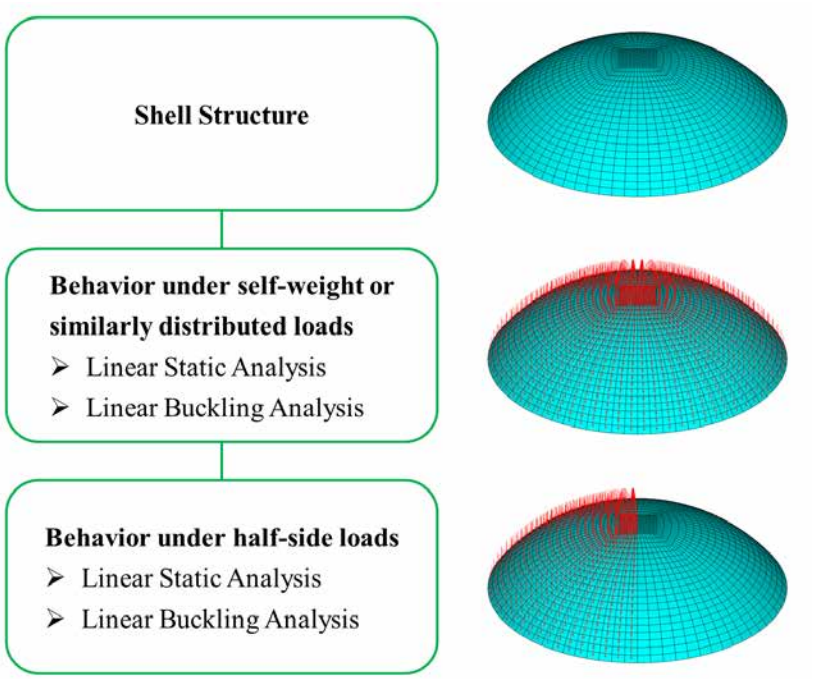


FIGURE 4.6 Mechanical behaviour assessment strategy.

Among the two structural analysis typologies mentioned above, linear buckling analysis is used to calculate the buckling loads and determine the buckling mode shape. This information can be easily and directly obtained from a finite element analysis program.

As for the linear static analysis, a finite element analysis program can compute and display the displacements, strains, stresses, reaction forces, and other quantities in a shell structure due to a prescribed load or displacement. However, shell structures have a unique way of remitting the loads to the supports, which makes it hard to assess the mechanical behaviour of the shell structure solely based on quantities such as displacements and stresses. In this research, two types of factors have been computed and researched that are introduced in detail in the following section.

§ 4.3.2 Factors to represent linear static analysis results of shells

Displacements, strains, stresses, reaction forces and some other quantities can be obtained and displayed directly from a finite element analysis program. In the following

chapters, the directions and magnitudes of principal stresses at the middle surface of a shell are observed to partly study the mechanical behaviour of a form-found shell, such as the characteristics of the distribution of its normal forces in this shell. However, to comprehensively study the mechanical behaviour of a shell structure where membrane action may or may not be dominant in this shell, some additional factors are needed.

Figure 4.7 shows all stress resultants and displacement ***w*** of a shell element under positive pressure loading ***p***, where N_x, N_{xy}, N_{yx}, N_y indicate the in-plane internal forces (membrane forces) per unit length, Q_x, Q_y denote the transversal shear forces per unit length, M_x, M_y are the bending moments per unit length, and M_{xy}, M_{yx} denote the twisting moments per unit length. Correspondingly, some quantities of deformation are mentioned here, where $\varepsilon_{xx}, \gamma_{xy}, \varepsilon_{yy}$ indicate in-plane strains of the middle surface, $\kappa_{xx}, \rho_{xy}, \kappa_{yy}, \gamma_{xz}, \gamma_{yz}$ denote the curvature deformations of the middle surface, and γ_{xz}, γ_{yz} are the transversal strains.

Based on these above-mentioned quantities which can be directly output from a finite element analysis program, two types of factors are computed and displayed. These factors are aimed at increasing the insight in the qualitative aspect of the mechanical behaviour of shell structures in a conceptual structural design phase.

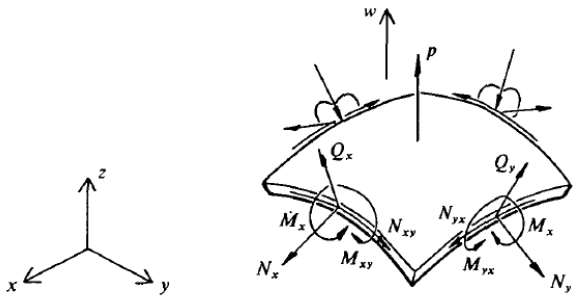


FIGURE 4.7 Shell element under positive pressure loading, all stress resultants, and displacement *w* [98].

1 Stress ratios

The ratios between the normal stress and the total stress caused by bending moments and normal forces in the directions of the principal normal forces are considered here. These ratios can be used to assess whether a shell carries its load efficiently. The magnitudes of principal normal forces can be calculated using Equation 4.7 ~ Equation 4.11, and their directions coincide with those of the two in-plane principal stresses at the middle surface:

$$a = \frac{N_x + N_y}{2}$$ Equation 4.7

$$b = \frac{N_x - N_y}{2}$$ Equation 4.8

$$r = \sqrt{b^2 + N_{xy}{}^2}$$ Equation 4.9

$$N_1 = a + r$$ Equation 4.10

$$N_2 = a - r$$ Equation 4.11

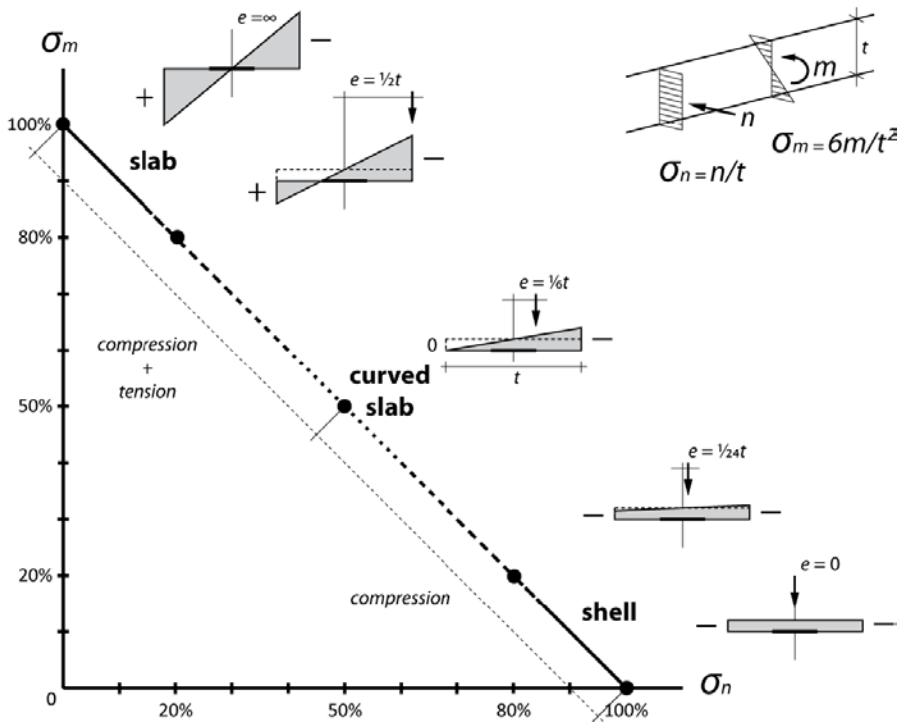


FIGURE 4.8 Shell assessment based on the ratio of normal stress and the sum of bending and normal stresses [99].

Shown in Figure 4.8, if the ratio approaches 100% it indicates more shell like behaviour while a ratio closer to 0% indicates more plate like bending behaviour. With a simple derivation, shown in Equation 4.12 and Equation 4.13, R_1 denotes the ratio in the direction of the first normal forces, and R_2 denotes that in the direction of the second normal forces:

TOC

$$R_1 = \frac{N_1}{\frac{6M(\alpha_0)}{t} + N_1} \times 100\%$$ Equation 4.12

$$R_2 = \frac{N_2}{\frac{6M(\alpha_0 + \pi/2)}{t} + N_2} \times 100\%$$ Equation 4.13

where, N_1 and N_2 indicate the first and second principal normal forces of the shell element, $M(\alpha_0)$ and $M(\alpha_0+\pi/2)$ denote its bending moments in the directions of the two normal forces, α_0 is the angle between the direction of the first normal force and the ***x***-axis of the element coordinate system, and *t* means the thickness of the element.

2 Strain-energy ratio

Strain energy is the energy that is stored in a structure when it deforms due to a load. With the aid of strain energy, it is possible to show whether a shell structure displays shell or plate behaviour. The ratio of the difference between bending strain energy and normal strain energy to the total strain energy [94] is considered. It should be mentioned that strain energy combines forces and deformations in all directions, resulting in a single display of analysis results to asess a shell structure.

The strain-energy ratio can be calculated as follows.

For a shell element, the membrane strain energy is calculated as follows:

$$E_{sm} = \frac{1}{2} N_x \varepsilon_{xx} + \frac{1}{2} N_{xy} \gamma_{xy} + \frac{1}{2} N_y \varepsilon_{yy}$$ Equation 4.14

The bending strain energy is calculated as follows

$$E_{sb} = \frac{1}{2} M_x \kappa_{xx} + \frac{1}{2} M_{xy} \rho_{xy} + \frac{1}{2} M_y \kappa_{yy} + \frac{1}{2} Q_x \gamma_{xz} + \frac{1}{2} Q_y \gamma_{yz}$$ Equation 4.15

The strain-energy ratio α can be defined as follows

$$\alpha = \frac{E_{sm} - E_{sb}}{E_{sm} + E_{sb}}$$ Equation 4.16

When $0 < \alpha < 100\%$, it means membrane action is dominant in this shell element, and when $-100\% < \alpha < 0$, bending action is dominant.

3 Example

To demonstrate these two types of factors, a dome is modelled and analysed in ANSYS software. Dimensions of this dome are the same as those of an example in the master's

thesis by Schuddeboom [100]. Figure 4.9 shows the finite element model of the dome. Its height is 10.0 m, its span is 40.0 m, and its thickness is 0.10 m. The Young's modulus of the material used is 3.6E11 N/m^2, and the Poisson ratio is 0.2. This dome is pinned around its bottom edge; thus, all translations are equal to zero, and all rotations are undetermined.

Linear static analysis of this dome under its self-weight is carried out in ANSYS. After analysis, contour plots of the three principal stresses at the middle surface of the dome are shown in Figure 4.10 ~ Figure 4.12, and vectorial representation of the principal stresses is shown in Figure 4.13. It can be observed clearly that the principal stresses occur only in the compression state, with the principal directions observed in Figure 4.13. In the perpendicular directions of the dome, principal stress S_1 is very small, in comparison to both of the other perpendicular principal directions in the plane tangent of the shell with S_2 and S_3 (only compression stress states). Principal stresses in the radial direction (S_3) are larger than those in the hoop direction (S_2). However, these cannot assist to determine whether membrane action is dominant in this dome.

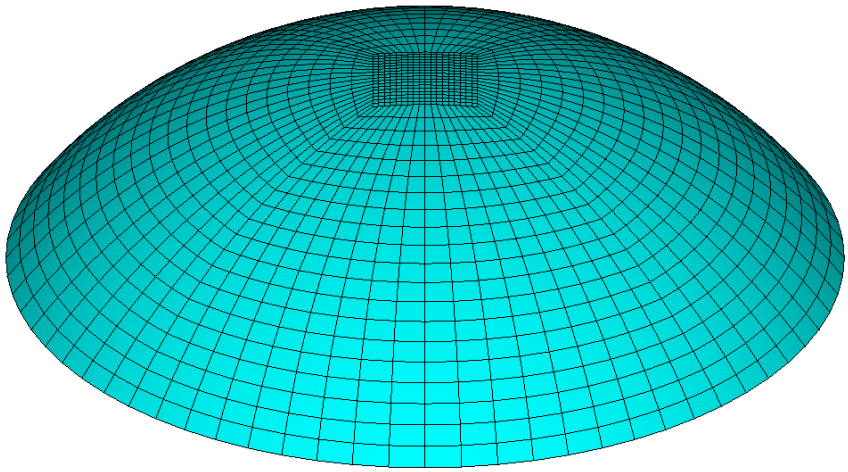


FIGURE 4.9 Finite element model of the dome.

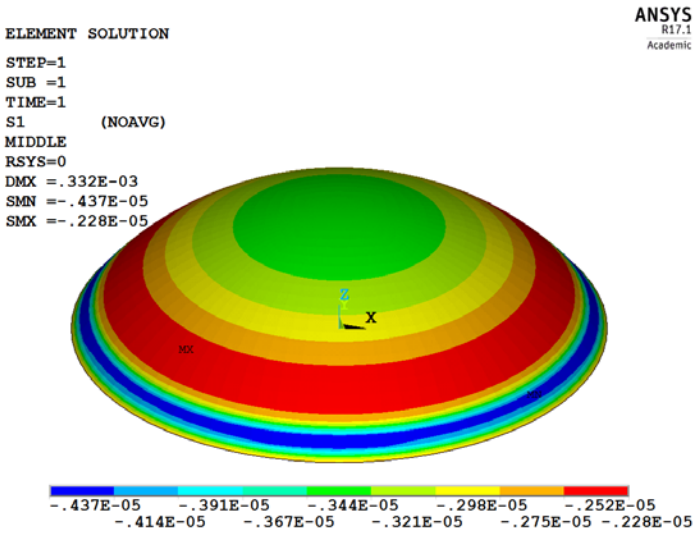


FIGURE 4.10 Principal stress S_1 at the middle surface of the dome (Pa).

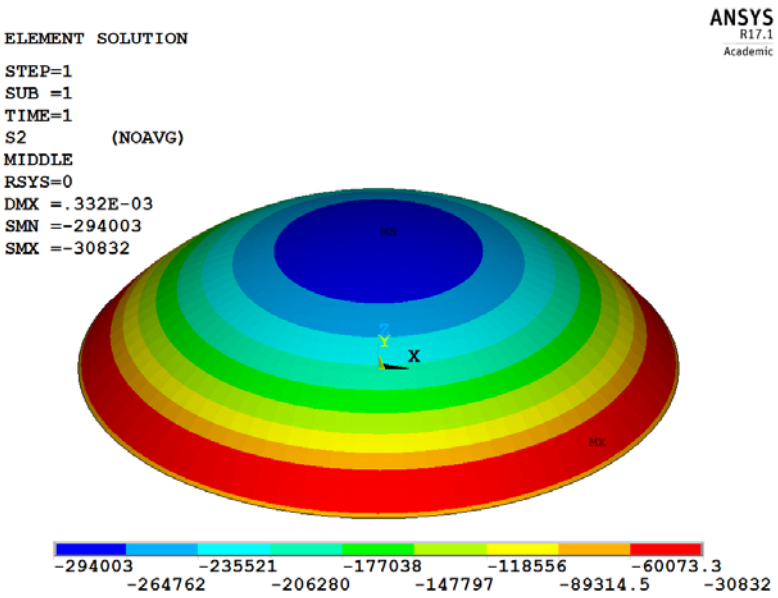


FIGURE 4.11 Principal stress S_2 at the middle surface of the dome (Pa).

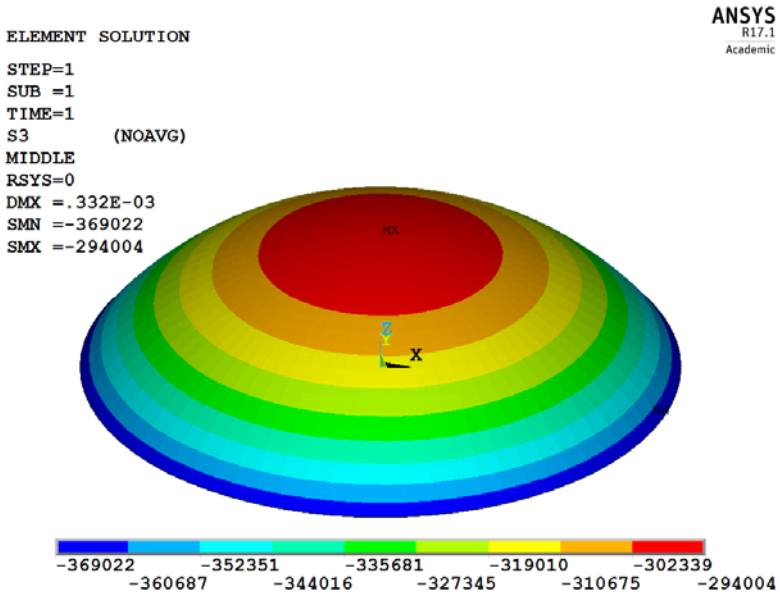


FIGURE 4.12 Principal stress S_3 at the middle surface of the dome (Pa).

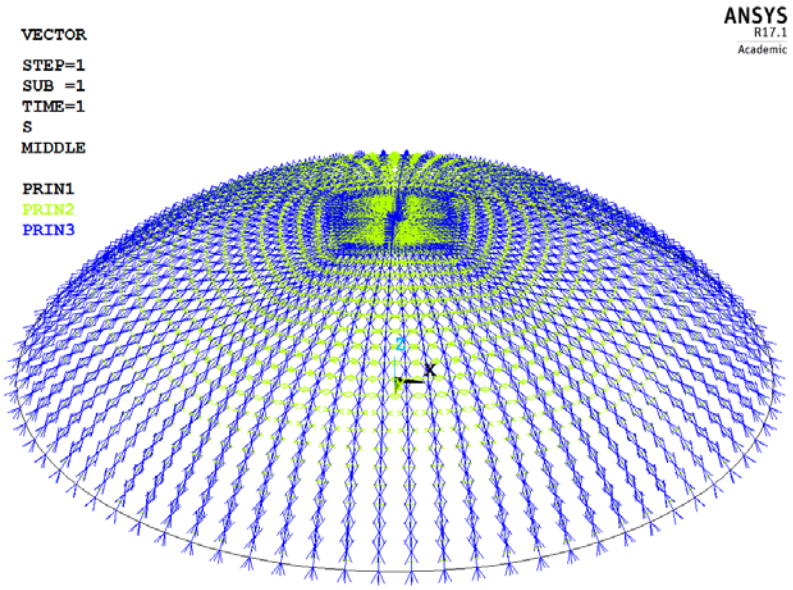


FIGURE 4.13 Vectorial representation of the principal stresses of the dome.

TOC

Subsequently, by a secondary development of the analysis results from ANSYS, two stress ratios in the directions of the two principal normal forces of this dome are shown in Figure 4.14 and Figure 4.15. The direction of the first (second) principal normal force of the dome coincides with that of the second (third) principal stress at its middle surface shown in Figure 4.13. It can be observed clearly that optimal shell behaviour occurs in both the directions of the principal normal forces. Some small bending moments occur near the supports because of the edge disturbance.

The strain-energy ratio of this dome is computed and displayed in Figure 4.16. It can also be observed clearly that membrane action is dominant in this dome. The edge disturbance can also be recognised near the supports. However, the strain-energy ratio is a combined quantity of forces and deformations in all directions; thus, some information related to different directions cannot be observed. Therefore, the above two stress ratios are recommended for most cases, while the strain-energy ratio is recommended when the two directions of principal normal forces cannot be easily distinguished or when an overall assessment is needed.

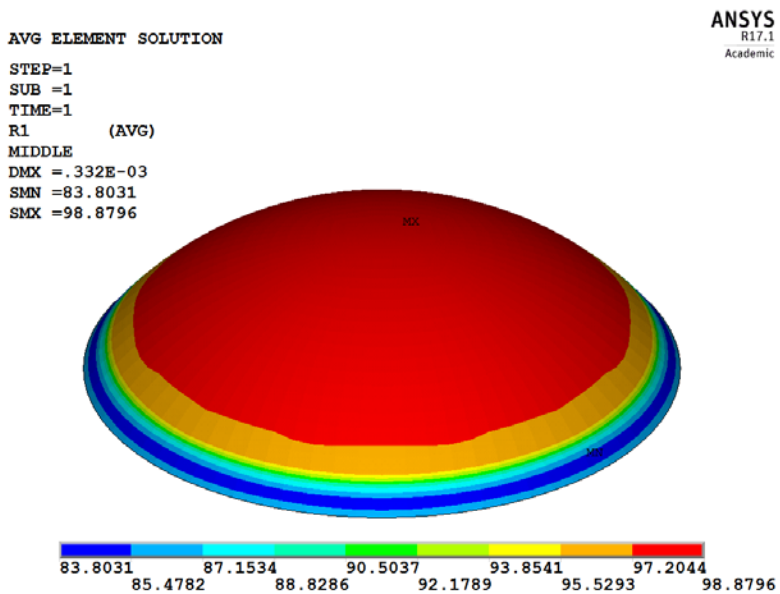


FIGURE 4.14 Stress ratio R_1 of the dome (%).

TOC

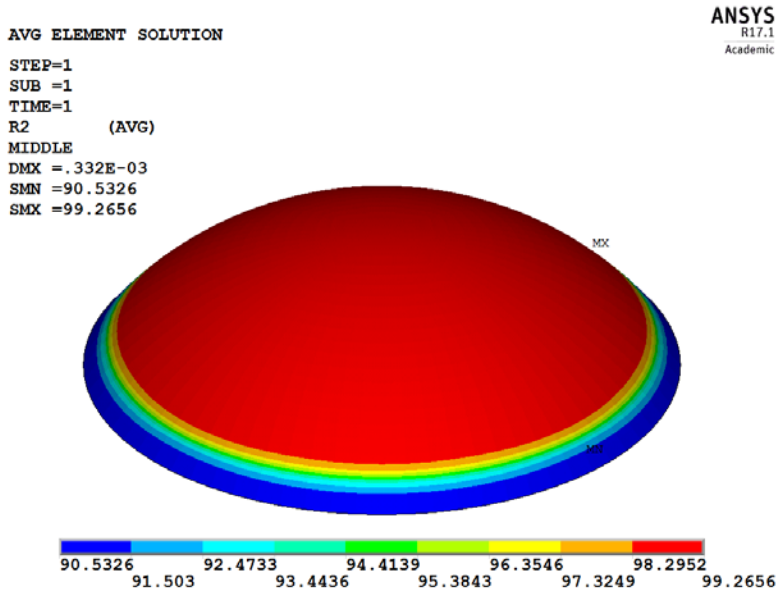


FIGURE 4.15 Stress ratio R_2 of the dome (%).

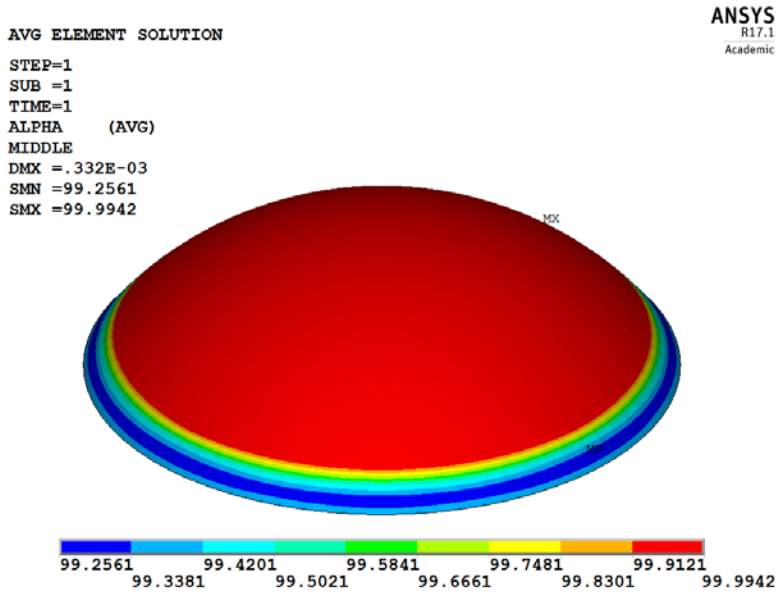


FIGURE 4.16 Strain-energy ratio α of the dome (%).

TOC

In the following chapters, the direct output principal stresses at the middle surface, the two stress ratios, and the strain-energy ratio are used to assess the shell behaviour of the form-found shell structures. It should be mentioned that not all the three types of quantities are used at the same time.

§ 4.4 Form-Finding of Shells

The stress state occurring in a shell depends strongly on its 3D shape, and the ideal stress state for shells is pure compression. Therefore, to obtain a structurally efficient shell, its shape should depend on the flow of forces, and vice versa; its design requires a process of Form-Finding. It is acknowledged that Form-Finding of shell structures is an established area. In this section, a comprehensive literature review of this area is presented.

§ 4.4.1 Physical Form-Finding methods

In the pre-computer age, physical models based on the 'form follows force' principle were widely used to design or construct shells. Nowadays, in most cases, physical models are still being used in teaching activities to reveal the mechanical principles, and in the construction process as moulds. As methods of Form-Finding, physical models are made of small pieces of flexible membranes or fabrics subject to certain loads and boundary conditions, and after evaluating and scaling them, efficient shapes of shells can be obtained. As moulds for construction, referring to pneumatic physical models in this research, they are also made of flexible membranes but with full sizes, and afterwards, they are covered with building materials. Based on their different manufacturing methods, these physical models can be divided into three groups.

1 Hanging models

Based on its structural principle, the hanging model is self-forming and capable of transferring its self-weight and area load solely by means of tension, and when it is turned upside down a pure compression model arises. Heinz Isler (1926–2009) [101] [102] developed a number of hanging models to determine suitable shapes of concrete shells, and Figure 4.17 shows one case with such a structure. Additionally, Frei Otto

(1925-2015) [103] used hanging chain models for designing grid shells, and one example is the roof for the Multihalle in Mannheim shown in Figure 4.18.



FIGURE 4.17 Deitingen Service Station, Switzerland, 1968 [104].



FIGURE 4.18 Figure 4.18: Roof for Multihalle in Mannheim, Germany, 1975 [105].

2 Tension models



FIGURE 4.19 Figure 4.19: Suspension model for Form-Finding of the new train station in Stuttgart, Germany, 2000 [107].



FIGURE 4.20 Figure 4.20: Basento Viaduct in Potenza, Italy, 1974 [108].

These models, which are made of soap film or gauze, aim to find the equilibrium shape of a minimal surface between pre-set boundaries. They represent a highly significant tool for exploring the shapes of tent constructions. However, tension models were also used for Form-Finding of shells. Frei Otto [103] applied this kind of model in the design of the Stuttgart train station, demonstrating the formal and structural novelty, which is derived from experiments with minimal surfaces. Figure 4.19 shows the suspension model for Form-Finding of the arches for this project. In addition, Sergio Musmeci

(1926-1981) [106] designed the shell-supported slabs using physical models. Figure 4.20 shows the Basento Viaduct in Potenza.

3 Pneumatic models

For these models, the soap film or a piece of membrane (air tight or allowing very little air through) is blown in a certain shape possibly with a closed pre-set boundary, and the overpressure inside forms an equilibrium shape. Pneumatic models can be adopted to determine the efficient shape of shells, and they can also be used as moulds for construction [109]. Pneumatic models were also favoured by Heinz Isler [101][102] to design concrete shells, and one example with such a structure is shown in Figure 4.22. As moulds for construction, pneumatic models were extensively used by Bini [110] to design and construct reinforced concrete thin shells (Figure 4.21), and were also applied by Kokawa [112] to design and construct ice shells (Figure 4.23).

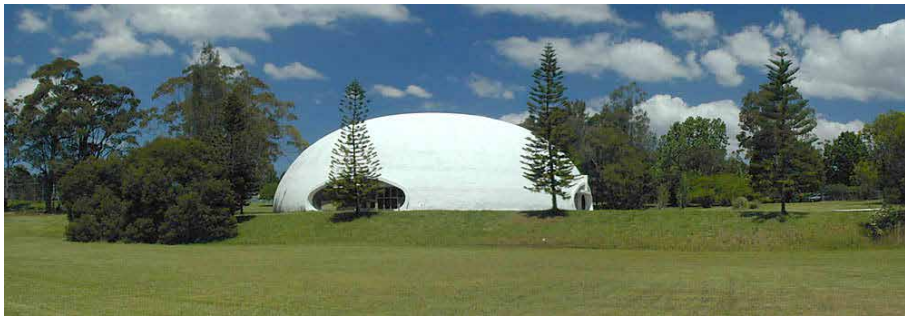


FIGURE 4.21 One Binishell in Ku-ring-gai High School [111].



FIGURE 4.22 COOP Storage and Distribution Centre, Wangen, Switzerland, 1960 [102].



FIGURE 4.23 An ice dome at Tomamu in Hokkaido, Japan, 2001 [112].

From the above introduction, it can be observed that each group of physical models represents a typical type of static force equilibrium that obeys the 'form follows force' principle. However, all three of these groups of physical models maintain a pure tension state subject to certain loads and boundary conditions. When they are used as shapes of shells after some required measures (e.g., inversion, scaling proportionally, section design, and et al.) and construction, the shells will maintain a high structural efficiency.

However, many architectural requirements for the structural forms should be met in the design process. For example, the structural form should fit some requirements of net height, span, space, etc. Then, changes or modifications should be conducted to the physical models to meet these requirements, which is called 'Form-Control' in this thesis. For instance, to precisely control the shape of his models, Gaudi changed variables such as string lengths and weight distributions to modify and steer the shape according to his design intent [113]. However, it is relatively tedious and time-consuming to make these changes to the physical models, and it is overall impractical for more complex structures.

§ 4.4.2 Numerical Form-Finding methods

1 Numerical analysis methods for Force-Active structural systems

Since the 1960s, with the development of analysis theories and computer techniques, numerical methods have become the most important means to generate structural forms for Force-Active structural systems and thus for shells. These methods generate ideal shapes that are the results of stable force equilibrium. Among these, many numerical methods, such as the DR method [114], the Force Density method [115] [116], the finite element based methods [117], the structural optimisation based methods[118], and the Thrust Network Analysis method [119], can be used to solve Form-Finding problems for cable or membrane structures and thus for shells. To know more about these numerical methods, Vizotto [120] gave a more detailed summary of various Form-Finding methods and their applications. Veenendaal and Block [121] conducted a comprehensive technical comparison of various Form-Finding methods. An extensive overview of various Form-Finding techniques for shells is given in the book '*Shell Structures for Architecture: Form-Finding and Structural Optimisation*' edited by Adriaenssens et al. [122].

During the work of literature review, it is found that the VFIFE method is a relatively new numerical analysis method. It was proposed by Ting et al.[123][124] and Shih et al.[125] in 2014. Different from the traditional numerical analysis methods based on continuum mechanics and variational principles, the VFIFE method is based on point value description and the vector mechanics theory. With the description of point values and path units, the VFIFE method describes the structural system composed of particles whose motions are determined by Newton's second law. During the calculation procedure, there is no need to integrate the structural stiffness matrix, and it can increase (or decrease) elements or change any property of the structural system. Therefore, the VFIFE method has a remarkable predominance in nonlinear problems and complex behaviours of structures compared with the traditional numerical analysis methods. Many scholars (e.g., [126][127][128][129][130] [131], etc.) conducted their research using the VFIFE method in the field of complicated behaviour analysis of structures, including geometric nonlinearity, material nonlinearity, mechanism motion, dynamic responses, buckling or wrinkle failure, and so forth.

At the beginning of this research, few studies of Form-Finding of shell structures using the VFIFE method were found in the literature. Based on this situation, and motivated by the advantages of the VFIFE method in nonlinear problems and for the complex behaviour analyses of structures, the VFIFE method was selected to generate equilibrium structural forms of Force-Active structural systems.

2 Form-Control of structural forms

After obtaining the equilibrium forms of Force-Active structural systems, some architectural requirements of the structural forms based on usability, aesthetics or other factors; and some additional requirements of the mechanical behaviour (stress level, stress distribution, etc.) may be necessary. In this case, a Form-Control process, which aims to generate the specific equilibrium shape under such constraints, is required.

As mentioned in Section 4.4.1, Form-Control during a physical Form-Finding process is tedious and time-consuming. Different from these physical processes, the numerical technique brings a much more convenient way to control the structural form.

Many scholars have conducted these Form-Control problems of shells generated from hanging models to meet the given requirements. Among others, Brew and Lewis [132] dealt with approaches to constrain hanging models to a single target height. Block and Lachauer [133][134] presented an efficient optimisation routine to find the best-fit thrust networks for a target surface with multiple height constraints. Van Mele et al. [135] presented a comprehensive framework to find a thrust network that best fits a

given target surface for a given set of loads. Many other papers from the book '*Shell Structures for Architecture: Form-Finding and Structural Optimisation*' [122] address relevant issues. It can be observed that for Form-Control problems with fewer target points, the proposed Form-Control strategies can solve these problems efficiently. For those with multiple target points, some optimisation methods are always introduced that are relatively complicated and time-consuming.

During the research in the author's MSc thesis, the author [136][137][138] proposed a much simpler strategy to solve the Form-Control problem. The bisection method was used to adjust Young's modulus of the initial model to generate structural forms with a single target and multiple target points in the Form-Finding process by ANSYS. The initial model was a finite element model composed of membrane elements with isotropous material properties. However, the former work still has many shortcomings. For example, it requires two initial structural models and its capacity to handle the Form-Control problem with multiple target points is limited. Therefore, in this research, simpler and more effective Form-Control strategies need to be researched.

§ 4.5 Conclusions

In this chapter, an overview of the structural form and mechanical behaviour of shell structures is introduced. Subsequently, a comprehensive review of Form-Finding methods of shell structures is provided in detail. The main conclusions are as follows:

- To study the structural form of a shell structure, the curvature analysis can be displayed. This will be used in Chapter 8 to compare the structural forms of form-found shells with different support shapes.

- To assess the mechanical behaviour of a shell structure in the conceptual structural design phase, an assessment strategy is proposed. This strategy will be used in Chapter 8 to compare the structural forms of form-found shells with different support shapes.

- For the linear static analysis of shell structures, two stress ratios in the directions of two principal normal forces and the strain-energy ratio are used to assess whether the membrane action is dominant in a shell structure. These ratios are computed based on combinations of basic quantities that are directly obtained from a finite element analysis program. Stress ratios are recommended in most cases, while the strain-energy ratio is recommended when the directions of

the principal normal forces cannot be easily distinguished or when an overall assessment is needed.

– Based on the overview of numerical analysis methods for Force-Active structural systems, and motivated by the advantages of the VFIFE method in nonlinear problems and complex behaviour analyses of structures, the VFIFE method was selected to generate equilibrium structural forms of Force-Active structural systems at the beginning of this research. According to the research status of Form-Control problems of shell structures, simpler and more effective Form-Control strategies need to be researched.

§ 4.6 References

[93] Calladine C.R. (1983). Theory of Shell Structures. Cambridge University Press, New York.
[94] Hoogenboom P.C.J. (2017). Notes on Shell Structures, reader of the course ' CIE4143 Shell Analysis, Theory and Application'. Delft: Delft University of Technology.
[95] Lisle R.J., Robinson J.M. (1995). The Mohr circle for curvature and its application to fold description. Journal of Structural Geology, 17(5): 739-750.
[96] Blaauwendraad J., Hoefakker J.H. (2014). Structural Shell Analysis: Understanding and Application. Springer, Dordrecht.
[97] Borgart A., Eigenraam P. (2012). Scanning in 3D and analysing the models of Heinz Isler, the preliminary results. Proceedings IASS-APCS, Seoul, Korea.
[98] Calladine C.R. (1977). The static–geometric analogy in the equations of thin shell structures. Mathematical Proceedings of the Cambridge Philosophical Society, 82: 335-351.
[99] Borgart A. (2017). Lecture notes of the course 'CIE5251-09 Structural Design, Special Structures'. Delft: Delft University of Technology.
[100] Schuddeboom P. (2014). New Ways of Representing Finite Element Results of Shell Structures. MSc thesis, Delft University of Technology.
[101] Chilton J. (2000). The Engineer's contribution to contemporary architecture: Heinz Isler. Thomas Telford Publishing, London.
[102] Ramm E. (2011). Heinz Isler Shells - The Priority of Form. Journal of the International Association for Shell and Spatial Structures, 52 (3): 143-154.
[103] Nerdinger W., With I.C., Meissner I., Möller E., Grdanjski M., Architecture Museum of Technical University Munich, editors. (2010). Frei Otto complete works: lightweight construction, natural Design. China Architecture & Building Press, Beijing.
[104] https://structurae.net/structures/deitingen-service-station
[105] https://www.pinterest.com/pin/457045062154696404/
[106] Nicoletti M. (1999). Sergio Musmeci, Organicità di forme e forze nello spazio. Testo & Immagine, Turin.
[107] https://www.pinterest.com/pin/317011261243639594/
[108] https://www.pinterest.com/pin/481111172670145006/
[109] Kromoser B., Patrick Huber P. (2016). Pneumatic Formwork Systems in Structural Engineering. Advances in Materials Science and Engineering.
[110] Bini D. (2014). Building With Air. Biblioteque McLean, London.
[111] http://www.khs82.com/dbpage.php?pg=khsphotos
[112] Kokawa T. (2012). Building Techniques for Ice Shell as Temporary Structure. Proceedings of IASS-APCS 2012, Seoul, Korea.

[113] Rippmann M. (2016). Funicular Shell Design: Geometric approaches to form finding and fabrication of discrete funicular structures. PhD thesis, ETH Zurich.
[114] Day A.S. (1965). An introduction to dynamic relaxation. The Engineer, 29(2): 218-221.
[115] Linkwitz, K., Schek, H.J. (1971). Einige Bemerkungen zur Berechnung von vorgespannten Seilnetzkonstruktionen. Ingenieur Archiv, 40: 145-158.
[116] Schek H.J. (1974). The force density method for Form-Finding and computations of general networks. Computer Methods in Applied Mechanics and Engineering, 3: 115-134.
[117] Haug E., Powell G.H. (1972). Finite element analysis of nonlinear membrane structures. IASS Pacific Symposium Part II: on Tension Structures and Space Frames, Tokyo and Kyoto, Japan. p. 93-102.
[118] Bletzinger K.-U., Ramm E. (1993). Form finding of shells by structural optimisation. Engineering with Computers, 9: 27-35.
[119] Block P., Ochsendorf J. (2007). Thrust network analysis: a new methodology for three dimensional equilibrium. Journal of the International Association for Shell and Spatial Structures, 48 (3): 167 - 173.
[120] Vizotto I. (2010). Computational generation of freeform shells in architectural design and civil engineering. Automation in Construction, 19: 1087 - 1105.
[121] Veenendaal D., Block P. (2012). An overview and comparison of structural form finding methods for general networks. International Journal of Solids and Structures, 49(26): 3741-3753.
[122] Adriaenssens S., Block P., Veenendaal D., Williams C., editors. (2014). Shell structures for architecture: Form-Finding and optimisation. Routledge Taylor and Francis, London.
[123] Ting E.C., Shih C., Wang Y.K. (2004). Fundamentals of a vector form intrinsic finite element: Part I. Basic procedure and a plane frame element. Journal of Mechanics, 20(2): 113-122.
[124] Ting E.C., Shih C., Wang Y.K. (2004). Fundamentals of a vector form intrinsic finite element; Part II. Plane solid elements. Journal of Mechanics, 20(2); 123-132.
[125] Shih C., Wang Y.K., Ting E.C. (2004). Fundamentals of a vector form intrinsic finite element: Part III. Convected material frame and examples. Journal of Mechanics, 20(2): 133-143.
[126] Wu T.Y., Ting E. C. (2008). Large deflection analysis of 3D membrane structures by a 4-particle quadrilateral intrinsic element. Thin-Walled Structures, 46: 261-275.
[127] Lien K.H., Chiou Y.J., Wang R.Z., Hsiao P.A. (2010). Vector Form Intrinsic Finite Element analysis of nonlinear behaviour of steel structures exposed to fire. Engineering Structures, 32: 80-92.
[128] Wang R.Z., Tsai K.C., Lin B.Z. (2011). Extremely large displacement dynamic analysis of elastic-plastic plane frames. Earthquake Engineering and Structural Dynamics, 40:1515–1533.
[129] Wang Z. (2013). Theory and application of thin shell element based on the Vector Form Intrinsic Finite Element method. Ph.D. Thesis, Zhejiang University, Hangzhou, China.
[130] Wu T.Y. (2013). Dynamic nonlinear analysis of shell structures using a Vector form Intrinsic Finite Element. Engineering Structures, 56: 2028-2040.
[131] Zhao Y., Wang Z., Peng T. (2015). Membrane element based on Vector Form Intrinsic Finite Element and its application in wrinkling analysis of membrane structures. Journal of Building Structures, 36(1): 127-135. (in Chinese)
[132] Brew J.S., Lewis W.J. (2007). Free hanging membrane model for shell structures. International Journal for Numerical Methods in Engineering, 71:1513–1533.
[133] Block P., Lachauer L. (2011). Closest-Fit, Compression-Only Solutions for Free Form Shells. Proceedings of the IABSE-IASS Symposium 2011,London, UK.
[134] Block P., Lachauer L. (2014). Three-dimensional Funicular Analysis of Masonry Vaults. Mechanics Research Communications, 56: 53-60.
[135] Van Mele T., Panozzo D., Sorkine-Hornung O., Block P. (2014). Best-fit thrust network analysis: rationalization of freeform meshes. In Shell Structures for Architecture: Form Finding and Optimisation, 157–168.
[136] Li Q. (2013). Numerical simulation and applications of the inverse hanging method. MSc thesis, Harbin Institute of Technology. (in Chinese)
[137] Wu Y., Li Q., Shen S. (2014). Computational morphogenesis method for space structures based on principle of inverse hanging experiment. Journal of Building Structures, 35(4): 41-48. (in Chinese)
[138] Li Q., Wu Y., Shen S. (2014). Computational generation of freeform shells based on the inverse hanging experiment. Proceedings of the IASS-SLTE 2014 Symposium, Brasilia, Brazil.

5 VFIFE for Generating Equilibrium Structural Forms of Force-Active Structural Systems

§ 5.1 Introduction

As mentioned in **Chapter 4**, the VFIFE method is introduced to carry out equilibrium problems of Force-Active structural systems in this research.

In this chapter, taking the cable-link element as an example, the framework of the VFIFE method is explained first. Then, a constant strain triangle element is introduced, and the relevant required equations are deduced. Based on these works, a MATLAB script was programmed by the author. Subsequently, the VFIFE method is successfully applied to solve the equilibrium problems of three categories of Force-Active structural systems (hanging structural systems, tension structural systems and pneumatic structural systems). In addition, to validate the accuracy and robustness of the VFIFE method, the DR method is introduced to make a comparison, and the resulting geometries are used as shells and analysed by FEM to demonstrate the form-found shell performs with optimal shell behavior.

§ 5.2 The VFIFE Method

§ 5.2.1 Basic concepts of the VFIFE method

The VFIFE method discretises the structural system into particles, describes the deformation of the structural system by observing the motion of the particles based on Newton's second law, and separates the pure deformation from the rigid body motions by introducing the concept of 'reverse rigid body motion'. In this part, three basic

concepts of the VFIFE method are demonstrated, including the point description, path unit and reverse rigid body motion of the element.

1 Point description

The point description can be regarded as a body composed of spatial particles linked by a set of elements. The motion and configuration of the body are determined by the particles. The elements are deformed following the moving particles, where internal forces arise. The body configuration depends on the choice of interpolation functions. Therefore, the point description approximates real structure. Figure 5.1 illustrates that the motion and configuration (including the geometry and the spatial position) of a piece of cable can be described by discrete particles (*a, b, c, d,* and *e*), and each set of two adjacent particles are connected by one cable-link element.

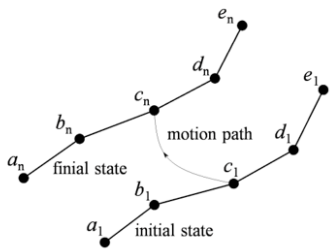


FIGURE 5.1 Discretion of the structural system.

2 Path unit

To simplify the motion process of the particles, the VFIFE method disperses the continuous and complicated motion trajectory of particles into several simple motion processes, each of which is called one path unit. Shown in Figure 5.2, using particle *c* from Figure 5.1 as an example, it has a motion path moving from the initial state c_1 to the finial state c_n, and disperses the entire period into finite time instants $t_1, t_2 \ldots t_n$. During this process, the motion process between each set of two time instants can be considered a path unit, as required. It should be noted that the motion of the particle is continuous in one path unit and obeys the governing equations based on Newton's second law.

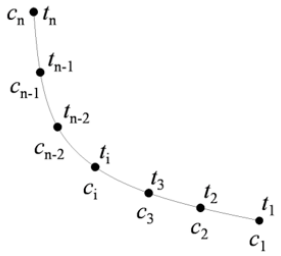


FIGURE 5.2 Schematic diagram of the path unit.

3 Reverse rigid body motion of the element

There is a complicated coupling relationship between the rigid body motion and the pure deformation of the element, and how to obtain the pure deformation is always the core of the calculation of internal forces. The VFIFE method estimates the rigid body motion which satisfies the required precision, and obtains the pure deformation of the element by deducting the rigid body motion from the whole displacement with the concept of reverse rigid body motion. Shown in Figure 5.3, taking element ab in Figure 5.1 as an example, the pure deformation of it in time t_i can be obtained in the following steps. First, translate and rotate the element a_ib_i reversely to $a_{i-1}b_{i2}$ in time t_{i-1}, and then get the value of the pure deformation of the element easily.

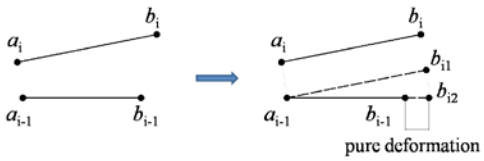


FIGURE 5.3 Schematic diagram of the pure deformation.

§ 5.2.2 Basic procedure of the VFIFE method

With the above three concepts, the VFIFE method is different from the conventional FEM, which is based on continuum mechanics and variational principles. The VFIFE method models the structural system to be composed of finite particles, and Newton's second law is applied to describe each particle's motion. Therefore, the calculation of the VFIFE method evolves into a process of solving a set of uncoupled vector-form

equations, and the calculation procedure of this method is a step-by-step and particle-by-particle cycling computation.

1 Workflow of the VFIFE method

Figure 5.4 shows the flowchart of the VFIFE method. It can be described with the following steps.

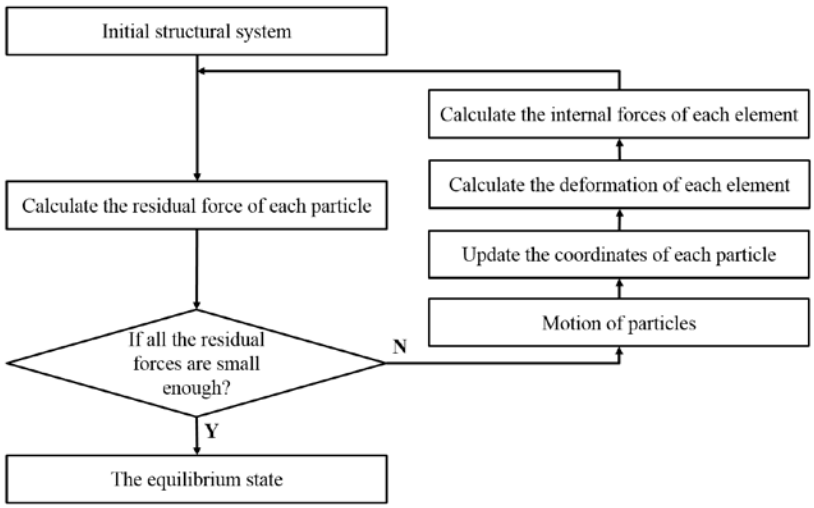


FIGURE 5.4 Flowchart of the VFIFE method.

1 The initial structural system is modelled with a set of particles, and adjacent particles are linked with elements.
2 The residual force of each particle, which is the sum of all the internal forces acting on a particle from the elements connected to it and to the applied loads, is calculated.
3 The largest residual force of all the particles is checked to determine whether it is smaller than the allowable error which will determine the precision of the calculation. If so, it can be assumed that the equilibrium state of the structural system is generated. Otherwise, the process continues with the steps below.
4 By calculating the motion of particles using the Störmer-Verlet integration based on Newton's second law, the displacement of each particle can be obtained.
5 The coordinates of each particle are updated.
6 The deformation of each element is calculated by introducing the concept of reverse rigid body motion.
7 The internal forces of each element are calculated, returning to Step 2 to enter a new calculation looping.

8 The looping continues until the required precision is achieved, which means the equilibrium state of the Force-Active structural system that meets the allowable error of residual force can be obtained.

In the above flowchart, each looping can be considered one path unit. In each path unit, the motion of each particle is continuous and obeys the governing equations based on Newton's second law. To explain the VFIFE method more clearly, two key steps are illustrated as follows, including the calculation of the residual force of each particle and the governing equations of the VFIFE method.

2 Calculation of the residual force of each particle

The residual force of each particle is the sum of all the forces acting on a particle from the elements connected to it and the applied loads. The internal force of the element obeys Hooke's Law in the iteration process introducing the concept of reverse rigid body motion to determine the pure deformation of the element. Taking element ***ab*** in Figure 5.3 as an example, the internal force increment of the element ΔF_n in step ***n*** can be calculated by Equation 5.1:

$$\Delta F_n = \frac{EAd_{pure}}{l_{n-1}} \qquad \text{Equation 5.1}$$

where ***EA*** represents the tensile stiffness of the element, d_{pure} represents the pure deformation of the element in step n, and l_{n-1} represents the length of the element in step (***n-1***).

After obtaining the force increment, the internal force of element ab in step n can be calculated by Equation 5.2:

$$F_n = \Delta F_n + F_{n-1} \qquad \text{Equation 5.2}$$

where F_{n-1} is the internal force in step (***n-1***).

After collecting the internal forces of all the elements, the residual force of each particle can be calculated by the vectorial sum of all the forces acting on the particle. Shown in Figure 5.5, taking the particle ***c*** from Figure 5.1 as an example, the residual force F_c in step *n* can be calculated by Equation 5.3:

$$\boldsymbol{F_c = F_{bc} + F_{cd} + P_c} \qquad \text{Equation 5.3}$$

where F_{bc} and F_{cd} represent the internal forces of elements ***bc*** and ***cd***, and P_c represents the applied loading on particle ***c***.

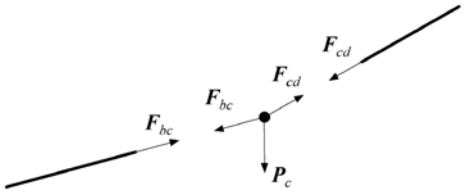


FIGURE 5.5 Residual force of particle c.

3 Governing equations of the VFIFE method

Governing equations of the VFIFE method are based on a central difference expression of Newton's second law. To introduce the governing equations clearly, taking the motion of one particle in the *x*-direction as an example, the iteration equations of the displacement of the particle can be deduced by the following steps.

According to Newton's second law, there exists the following equation:

$$\boldsymbol{F}_n = m\boldsymbol{a}_n \qquad \text{Equation 5.4}$$

The acceleration of the particle can be described using a central difference expression:

$$\boldsymbol{a}_n = \frac{\boldsymbol{v}_{n+1/2} - \boldsymbol{v}_{n-1/2}}{h} \qquad \text{Equation 5.5}$$

and the velocities of the particle with a central difference expression are:

$$\boldsymbol{v}_{n+1/2} = \frac{\boldsymbol{x}_{n+1} - \boldsymbol{x}_n}{h} \qquad \text{Equation 5.6}$$

$$\boldsymbol{v}_{n-1/2} = \frac{\boldsymbol{x}_n - \boldsymbol{x}_{n-1}}{h} \qquad \text{Equation 5.7}$$

Inserting Equation 5.6 and Equation 5.7 into Equation 5.5, and then into Equation 5.4, the iteration equation of the displacement of the particle can be described as follows:

$$\boldsymbol{x}_{n+1} = \frac{h^2}{m}\boldsymbol{F}_n + 2\boldsymbol{x}_n - \boldsymbol{x}_{n-1} \qquad \text{Equation 5.8}$$

However, when $n=1$, x_0 appeared in equation (8) does not exist. However, with the following:

$$\boldsymbol{v}_1 = \frac{1}{2h}(\boldsymbol{x}_2 - \boldsymbol{x}_0) \qquad \text{Equation 5.9}$$

x_0 can be described in another way. Finally, the iteration equations of the VFIFE method can be obtained, which is a Störmer-Verlet integration, as follows:

$$\begin{cases} \boldsymbol{x}_2 = \dfrac{h^2}{2m}\boldsymbol{F}_1 + \boldsymbol{x}_1 + h\boldsymbol{v}_1 & n = 1 \\ \boldsymbol{x}_{n+1} = \dfrac{h^2}{m}\boldsymbol{F}_n + 2\boldsymbol{x}_n - \boldsymbol{x}_{n-1} & n \geq 2 \end{cases}$$

Equation 5.10

When damping exists in the structural system, and assuming that the damping force is proportional to the velocity and mass of the particle, we know that:

$$\boldsymbol{F}_n - \xi m\boldsymbol{v}_n = m\boldsymbol{a}_n$$

Equation 5.11

where ξ is the damping-mass factor of the particle, which satisfies:

$$\xi = \frac{C}{m}$$

Equation 5.12

where C is the traditional structural damping factor in structural dynamics. However, in the VFIFE method, C need not be the real damping factor of the structure, and Wang [129] suggested that ξ satisfies the following:

$$\xi \leq \frac{C_{cr}}{m}$$

Equation 5.13

where C_{cr} is the critical damping factor of the structure.

With some deductions as above, finally, the iteration equations of the VFIFE method with viscous damping can be obtained, as follows:

$$\begin{cases} \boldsymbol{x}_2 = \dfrac{h^2}{2m}\boldsymbol{F}_1 + \boldsymbol{x}_1 + C_2 h\boldsymbol{v}_1 & n = 1 \\ \boldsymbol{x}_{n+1} = \dfrac{C_1 h^2}{m}\boldsymbol{F}_n + 2C_1\boldsymbol{x}_n - C_1 C_2\boldsymbol{x}_{n-1} & n \geq 2 \end{cases}$$

Equation 5.14

$$C_1 = \frac{1}{1 + 0.5\xi h}, \quad C_2 = 1 - 0.5\xi h$$

Equation 5.15

where m represents the mass of the particle, F represents the residual force of the x-direction acting on it, v represents the velocity of it in the x-direction, x represents the coordinate of it in the x-direction, n represents the step, and h represents the step length.

Equation 5.14 is clearly an explicit equation, which can obtain the unknowns from the known quantities. In the VFIFE method, if the initial coordinates and initial velocities of the particles are known, it can describe the motion paths of the particles by stepwise derivation using Equation 5.14.

When considering the structural behaviour under dead loads, in Form-Finding problems for instance, two strategies could be applied. One is taking the dead load as a very slowly increased living load (e.g., using an incremental loading method), and the other is adding virtual damping into the equations, which aims to eliminate the dynamic effect. Moreover, to ensure a better convergence of the VFIFE method, there are some limits of the step length and damping-mass factor adopted from Wang [129], which will not be covered here.

§ 5.2.3 Numerical example of a hanging cable net

Example 5.1 of a hanging cable net is shown here to illustrate the validity of the VFIFE method in generating equilibrium structural forms of the cable-net. *Figure 5.6* shows the initial conditions of ***Example 5.1***. A rectangular grid mesh with 30 squares in each direction is restrained at four nodes near each corner. All the nodes are in one plane and applied with a vertical force of 1.0 N, and the distance of two adjacent points is 1.00 m. All the cable elements have the same cross-sectional area of 1.0E-04 m^2, the same elastic modulus of 1.0E10 N/m^2, and no pre-stress. Each support is located five squares from the nearest edge.

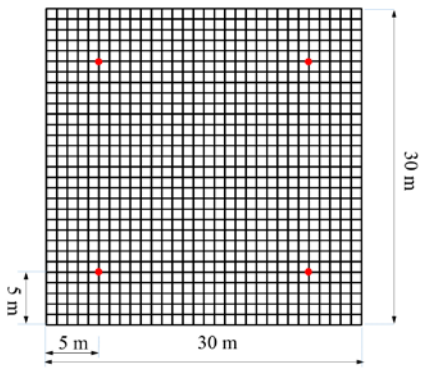


FIGURE 5.6 Initial conditions of ***Example 5.1*** (red points represent the fixed points).

With a tolerance of the residual force of 0.001 N, using the VFIFE method and the DR method, two equilibrium hanging network can be obtained, shown in Figure 5.7. By a detailed comparison between the two equilibrium forms, they have very little difference between each other. The biggest error between them is from the highest point of the

equilibrium shape, at 0.007% (the height of the highest point of the Form-Finding result of the VFIFE method is 13.8753 m, while that of the DR method is 13.8743 m).

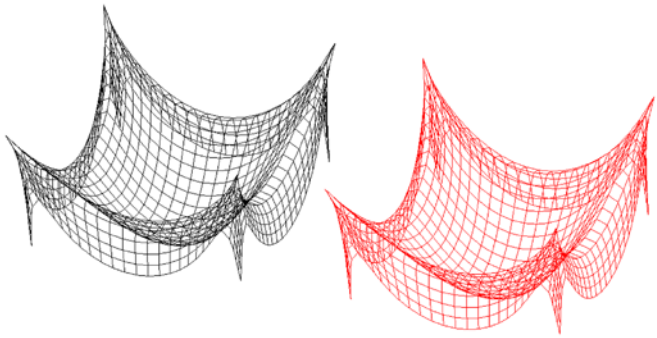


FIGURE 5.7 Equilibrium hanging networks obtained by the VFIFE method (in black) and the DR method (in red) of *Example 5.1*.

During the calculation process of the VFIFE method, the step length h is set to 1.0E-02, and the damping-mass factor ξ is set to 0.55. Figure 5.8 shows the evolution curve of the biggest residual force of the particles by steps, in which the straight line represents that the load is using an incremental loading method in this static equilibrium problem. During the calculation process of the DR method, the step length is set to1.0E-02. Figure 5.9 shows its evolution curve of the kinetic energy by steps.

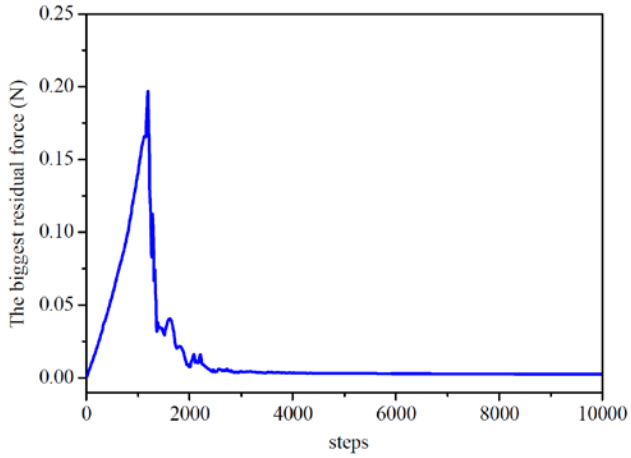


FIGURE 5.8 Evolution curve of the VFIFE method of *Example 5.1*.

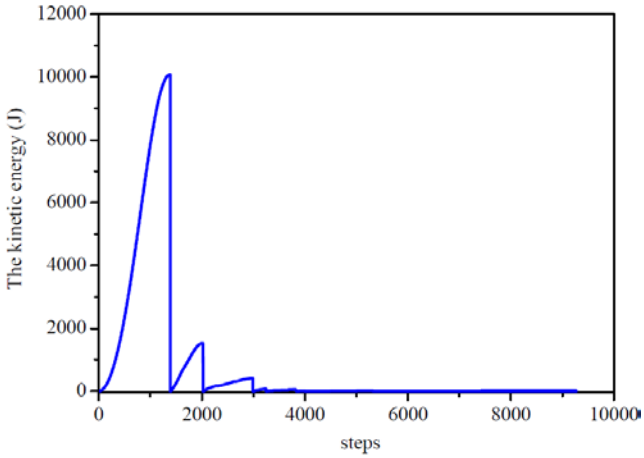


FIGURE 5.9 Evolution curve of the DR method of ***Example 5.1***.

As there are different parameters between the VFIFE method and the DR method, it cannot compare the efficiency between them. However, the accuracy and robustness of the VFIFE method for generating equilibrium structural forms of cable nets can be validated by comparing the analysis results using the DR method.

§ 5.3 The Constant Strain Triangle Element

Considering the equilibrium problems of membrane structures and thus shell structures, a constant strain triangle element based on the VFIFE method is developed. According to the framework above, the key point of developing a new element type based on the VFIFE method is the calculation of the internal force of the element. For the triangular membrane element, two steps are introduced here to calculate its internal force, including the calculation of pure deformation of the element using the concept of reverse rigid body motion, and the calculation of the internal force increment using its pure deformation.

§ 5.3.1 Calculation of pure deformation of the triangular membrane element

The pure deformation of the triangular membrane element is calculated by introducing the concept of reverse rigid body motion. Shown in Figure 5.10, taking one triangular membrane element in one path unit as an example, the element ***ABC*** moves from

$A_0B_0C_0$ to $A_1B_1C_1$ but with an elastic deformation, where *A*, *B*, and *C* represent the names of the three particles. Figure 5.10 also shows the detailed process that translates and rotates the element reversely from $A_1B_1C_1$ to $A_0B_4C_4$. The pure deformation of this element can be obtained in the following steps.

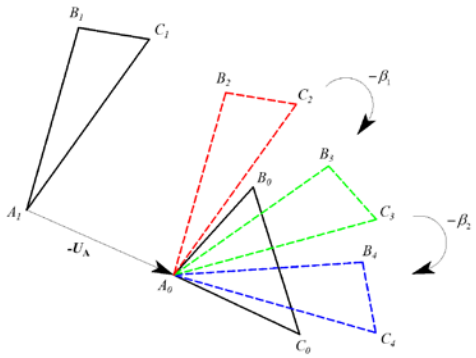


FIGURE 5.10 Process of reverse rigid body motion.

1 Taking $-U_A$ as the motion vector, reversely translate the element from $A_1B_1C_1$ to $A_0B_2C_2$, where U_A is the displacement vector of the particle *A* in the path unit. Through this process, the rigid body translation is removed from the whole displacement, and as a result, $A_0B_2C_2$ and $A_0B_0C_0$ coincide in point A_0.

2 Taking $-\beta_1$ as the motion angle, reversely rotate the element from $A_2B_2C_2$ to $A_0B_3C_3$, where β_1 is the angle between the normal vectors for $A_1B_1C_1$ and $A_0B_0C_0$. Through this process, the out-of-plane rigid body rotation is removed from the whole displacement, and $A_0B_3C_3$ and $A_0B_0C_0$ are in the same plane.

3 Taking $-\beta_2$ as the motion angle, reversely rotate the element from $A_0B_3C_3$ to $A_0B_4C_4$, where β_2 can be calculated by Equation 5.16, as follows:

$$\beta_2 = \frac{\theta_1 + \theta_2 + \theta_3}{3} \qquad \text{Equation 5.16}$$

To explain the meaning of $\theta_i (i = 1, 2, 3)$, shown in Figure 5.11, translate $A_0B_4C_4$ to coincide with the centroid of $A_0B_0C_0$ and obtain $A_5B_5C_5$, where pointx O_0 and O_5 are the centroids of $A_0B_0C_0$ and $A_5B_5C_5$ respectively, and $\theta_i (i = 1, 2, 3)$ represents the angle of relevant midlines of the two triangles. Through this process, the in-plane rigid body rotation is removed from the whole displacement.

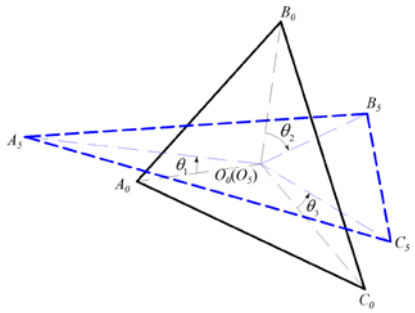


FIGURE 5.11 Calculation of β_2.

4 From above steps, all the rigid body motions are removed from the whole displacement, compare $A_4B_4C_4$ with $A_0B_0C_0$, and then the pure deformation of the element can be obtained easily, which can be described by three vectors $\boldsymbol{\eta}_A$, $\boldsymbol{\eta}_B$, and $\boldsymbol{\eta}_C$, as shown in Figure 5.12.

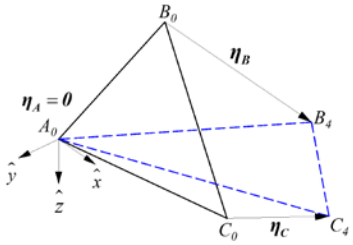


FIGURE 5.12 Calculation of the pure deformation.

§ 5.3.2 Calculation of the internal force increment of the triangular membrane element

After obtaining the pure deformation of the triangular membrane element, the VFIFE method calculates the internal force increment by introducing the deformation coordinate system which transforms the space problem to a plane problem. Taking the element and its pure deformation of one path unit in Figure 5.12 as an example, the deformation coordinate system can be set as follows:

$$\hat{\boldsymbol{e}}_1 = \frac{\boldsymbol{\eta}_B}{|\boldsymbol{\eta}_B|} \qquad \text{Equation 5.17}$$

$$\hat{\boldsymbol{e}}_2 = \boldsymbol{n}_0 \qquad \text{Equation 5.18}$$

TOC

$$\hat{\boldsymbol{e}}_2 = \hat{\boldsymbol{e}}_3 \times \hat{\boldsymbol{e}}_1$$ Equation 5.19

where $\hat{\boldsymbol{e}}_1$, $\hat{\boldsymbol{e}}_2$, and $\hat{\boldsymbol{e}}_3$ represent the unit vectors in the $\hat{x}$, $\hat{y}$, and $\hat{z}$ directions of the deformation coordinate system respectively, and the vector $\boldsymbol{n_0}$ is the normal vector of $A_0B_0C_0$.

In such deformation coordinate systems, where A_0 is the point of origin and the $\hat{x}\,\hat{y}$ plane is set at the plane of $A_0B_0C_0$ (or $A_0B_4C_4$), the displacement components and thus the force increment components in the $\hat{z}$ direction are zero. Shown in Figure 5.13, the other displacement components of the displacement vector in this coordinate system are defined as Equation 5.20, Equation 5.21 and Equation 5.22:

$$u_A = v_A = 0$$ Equation 5.20

$$u_B = |\boldsymbol{\eta_B}|, \quad v_B = 0$$ Equation 5.21

$$u_C = \boldsymbol{\eta}_C \cdot \hat{\boldsymbol{e}}_1, \quad v_C = \boldsymbol{\eta}_C \cdot \hat{\boldsymbol{e}}_2$$ Equation 5.22

where u and v represent the values in $\hat{x}$ and $\hat{y}$ directions respectively.

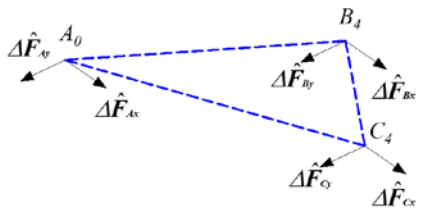


FIGURE 5.13 Force increment components and displacement components in the deformation coordinate system.

After omitting the displacements components that are zero, the displacement vector of the element can be written as in Equation 5.23:

$$\hat{\boldsymbol{u}}_e = \begin{bmatrix} u_B & u_C & v_C \end{bmatrix}^T$$ Equation 5.23

So far, the problem of calculation of the internal force increment of the triangular membrane element is quite clear. The displacement vector of the element is known, and the question is to solve the six unknown force increment components of it. To solve this problem, the principle of virtual work is applied.

From the virtual work equation, we know Equation 5.24 is as follows:

$$\sum_{i=A,B,C} \delta(\hat{\boldsymbol{u}}_i)^T \Delta\hat{\boldsymbol{F}}_i = \int_V \delta(\Delta\hat{\boldsymbol{\varepsilon}})^T \Delta\hat{\boldsymbol{\sigma}} dV$$ Equation 5.24

where $\hat{\boldsymbol{u}}_i$ and $\Delta\hat{\boldsymbol{F}}_i$ represent the displacement vector and the force increment vector of particle *i* connected to the elements, $\Delta\hat{\boldsymbol{\varepsilon}}$ and $\Delta\hat{\boldsymbol{\sigma}}$ representing the stress increment vector and the strain increment vector of the element, and *V* represents the volume of the element.

Moreover, we also understand the relationship of the stress increment and displacement increment of the element, which can be shown in Equation 5.25:

$$\Delta\hat{\boldsymbol{\sigma}} = \boldsymbol{D}\Delta\hat{\boldsymbol{\varepsilon}} = \boldsymbol{D}\boldsymbol{B}^*\hat{\boldsymbol{u}}.$$ Equation 5.25

where *D* represents the elastic matrix of the element (only isotropic material is considered), B^* represents the strain-displacement relation matrix of the triangular membrane element, and their concrete expressions are shown in Equation 5.26 and Equation 5.27 respectively:

$$\boldsymbol{D} = \frac{E}{1-\upsilon^2}\begin{bmatrix} 1 & \upsilon & 0 \\ \upsilon & 1 & 0 \\ 0 & 0 & (1-\upsilon)/2 \end{bmatrix}$$ Equation 5.26

where *E* represents the elastic modulus of this material, and υ represents the Poisson's ratio:

$$\boldsymbol{B}^* = \frac{1}{\hat{x}_B\hat{y}_C - \hat{x}_C\hat{y}_B}\begin{bmatrix} \hat{y}_C & -\hat{y}_B & 0 \\ 0 & 0 & \hat{x}_B \\ -\hat{x}_C & \hat{x}_B & -\hat{y}_B \end{bmatrix}$$ Equation 5.27

where $\hat{x}_B$, $\hat{y}_B$, $\hat{x}_C$, and $\hat{y}_C$ represent the coordinates of points B_0 and C_0 in the deformation coordinate system.

After plugging Equation 5.25 into Equation 5.24 and simplifying it, the force increment vector, which includes three force increment components of the element, can be calculated using Equation 5.28, as follows:

$$\left[\Delta\hat{F}_{Bx}\ \Delta\hat{F}_{Cx}\ \Delta\hat{F}_{Cy}\right]^T = d\left(\int_A \boldsymbol{B}^{*T}\boldsymbol{D}\boldsymbol{B}dA\right)\hat{\boldsymbol{u}}.$$ Equation 5.28

where *d* and *A* represent the thickness and area of the triangular element. Three of the six unknown force increment components have been solved so far. To solve the other three force increment components, the equilibrium equations of the element shown

in Equation 5.29, Equation 5.30 and Equation 5.31 are established, which respectively represent that the sum of the moments in point A_0, and the sum of force components in the $\hat{x}$ direction and the $\hat{y}$ direction all equal zero:

$$\sum \hat{M}_A = 0 \qquad \text{Equation 5.29}$$

$$\sum \hat{F}_x = 0 \qquad \text{Equation 5.30}$$

$$\sum \hat{F}_y = 0 \qquad \text{Equation 5.31}$$

The other three force increment components can be calculated using the following equations:

$$\Delta\hat{F}_{By} = \frac{1}{\hat{x}_B}(\Delta\hat{F}_{Bx}\hat{y}_B + \Delta\hat{F}_{Cx}\hat{y}_C - \Delta\hat{F}_{Cy}\hat{x}_C) \qquad \text{Equation 5.32}$$

$$\Delta\hat{F}_{Ax} = -(\Delta\hat{F}_{Bx} + \Delta\hat{F}_{Cx}) \qquad \text{Equation 5.33}$$

$$\Delta\hat{F}_{Ay} = -(\Delta\hat{F}_{By} + \Delta\hat{F}_{Cy}) \qquad \text{Equation 5.34}$$

However, it should be noted that the force increment components that we obtain now are described in the deformation coordinate system. When they are involved in calculating residual forces of the particles, all the force increment components should first be transformed from triangle $A_0B_4C_4$ (which is in the deformation coordinate system) to triangle $A_1B_1C_1$ (which is the end position of the path unit), and then to the global system.

In conclusion, the framework of the VFIFE method based on the cable-link element is explained first, and a constant-strain triangle element is subsequently introduced.

§ 5.4 Numerical Examples

Equilibrium problems of Force-Active structural systems are discussed using the VFIFE method in this section. Numerical examples of one hanging model, one tension model, and one pneumatic model are presented. Moreover, to verify the capability of the VFIFE method in generating optimal structural shapes for shells, structural analyses of these shells under inversed loading are conducted using these equilibrium shapes as shells' geometries.

§ 5.4.1 Equilibrium of one hanging model

Hanging models represent a type of equilibrium state of flexible materials under their self-weight and certain constraint conditions with stress states in pure tension. When these equilibrium shapes are used as the geometry of rigid structures after inverting them, they will perform with an effective structural behaviour under their self-weight or under equally distributed loading.

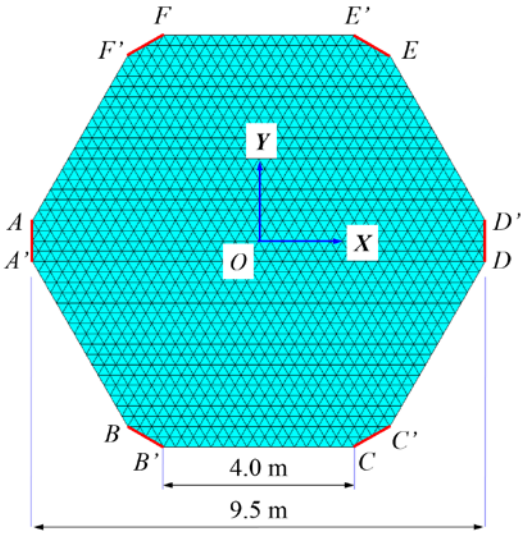


FIGURE 5.14 Initial conditions of *Example 5.2*.

Figure 5.14 shows the initial conditions of *Example 5.2*. The initial shape of this example is a hexagon in the *XY* plane with supports at the six corners, and the corners are bevelled by lines *AA'*, *BB'*, *CC'*, *DD'*, *EE'*, and *FF'*. The plane area is 64.30 m^2 (hexagon with sides of 5.0 m). The initial numerical structural model is composed of particles and triangular membrane elements. The elastic modulus of the membrane material is 5.0E05 N/m^2, the Poisson's ratio is 0.3, and the thickness of the membrane element is 0.001 m. In the VFIFE method, the mass of the structure is distributed to the particles, and in this example, masses of the internal particles are 0.1 kg and that of the boundary particles are 0.05 kg.

With the above initial conditions, the VFIFE method is used to carry out Form-Finding of this membrane structure under its self-weight. In the calculation process, the

step length *h* is set to 5.0E-03, the damping-mass factor ξ is set to 15.0, and the tolerance of the residual force is set to 0.001 N. After the calculation with 2211 steps, it approaches the equilibrium shape of the hanging membrane which meets the tolerance of the residual force in each particle. Figure 5.16 shows the inverted shape and its coordinate system. To demonstrate the calculation process, Figure 5.15 shows the evolution curve of the biggest residual force of the particles by steps, in which the straight line represents that the load is using an incremental loading method in this static equilibrium problem.

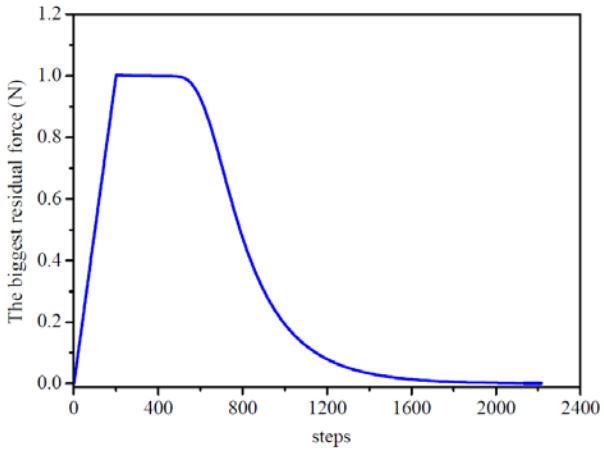
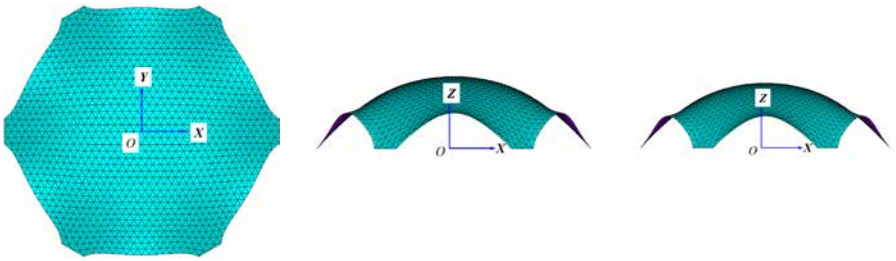


FIGURE 5.15 Evolution curve of the VFIFE method of *Example 5.2*.



(a) Top view. *(b) Front view.* *(c) Right view.*

TOC



(d) Perspective view.

FIGURE 5.16 Form-Finding result of ***Example 5.2***.

To verify the accuracy and robustness of the VFIFE method in this example, with the same initial conditions, this example is also done using the DR method, and *Figure 5.17* shows its evolution curve of the kinetic energy by steps (the step length is 0.005). Then it compares the Form-Finding results of the VFIFE method and the DR method by comparing the ***z*** coordinates of the nodes at ***x***-axis of symmetry (***y***=0) and ***y***-axis of symmetry (***x***=0), shown in *Figure 5.18* and *Figure 5.19*. From the comparison, there is a very small difference between the Form-Finding result of the VFIFE method and that of the DR method. The biggest error between them is from the highest point of the equilibrium shape at 1.60% (the height of the highest point of the Form-Finding result of the VFIFE method is 2.48 m, while that of the DR method is 2.52 m).

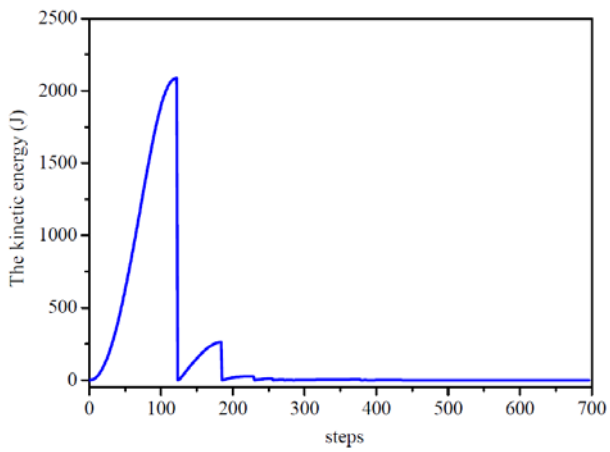


FIGURE 5.17 Evolution curve of the DR method for ***Example 5.2***.

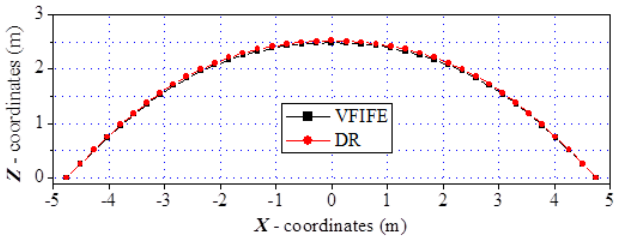


FIGURE 5.18 Comparison of the results of *Example 5.2*; *Z* coordinates of the nodes at *X*-axis of symmetry (*Y*=0).

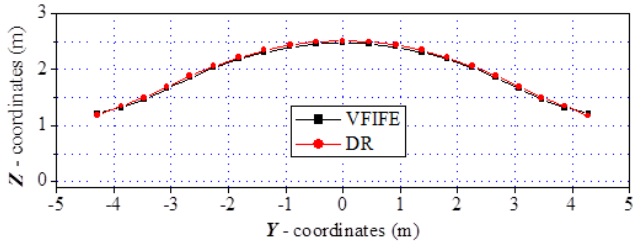


FIGURE 5.19 Comparison of the results of *Example 5.2*; *Z* coordinates of the nodes at *Y*-axis of symmetry (*X*=0).

Next, structural static analysis of this form-found shell under its self-weight is conducted using ANSYS software. The material of this shell is concrete, with an elastic modulus of 2.10E4 MPa, Poisson's ratio of 0.20, and density of 2500 kg/m^3. The thickness of this shell is 0.04 m. The acceleration of gravity is 9.80 m/s^2. The shell is simply supported at six corners.

After analysis, Figure 5.20 to Figure 5.22 present the principal stresses (S_1, S_2 and S_3) at the middle surface of the shell, and Figure 5.23 and Figure 5.24 present vectorial representations of the principal stresses. In these contour plots, principal stresses S_1, S_2, and S_3 are positive for the tension stress state, and negative for the compression stress state. In the perpendicular directions of the shell, principal stress S_1 is very small, and tension stresses occur only at a very small part, whereas, in the other two perpendicular principal directions in the plane tangent of the shell, principal stresses S_2 and S_3 are totally in compression stress states.

Figure 5.25 and Figure 5.26 show the two stress ratios of the shell under its self-weight in the directions of the two principal normal forces. The stress ratio R_1 is larger than 50% in most parts of the shell except for the parts near the supports and boundaries. This means bending behaviour occurs in the parts near the supports and boundaries in

the direction of the first principal normal forces. The stress ratio R_2 is larger than 50% in all parts of the shell. This indicates shell behaviour occurs in all parts of the shell in the direction of the second principal normal forces. However, there are still some bending moments that occur in the parts near the free edges. Figure 5.20 to Figure 5.24 show that the second principal normal forces are much larger than those of the first one. It can be concluded that this shell structure performs with a good shell behaviour. Then the strain-energy ratio of the shell under its self-weight is computed and displayed in Figure 5.27. It can be observed clearly that the strain-energy ratio is larger than zero in all parts of the shell. Similar conclusions can be obtained with the two stress ratios.

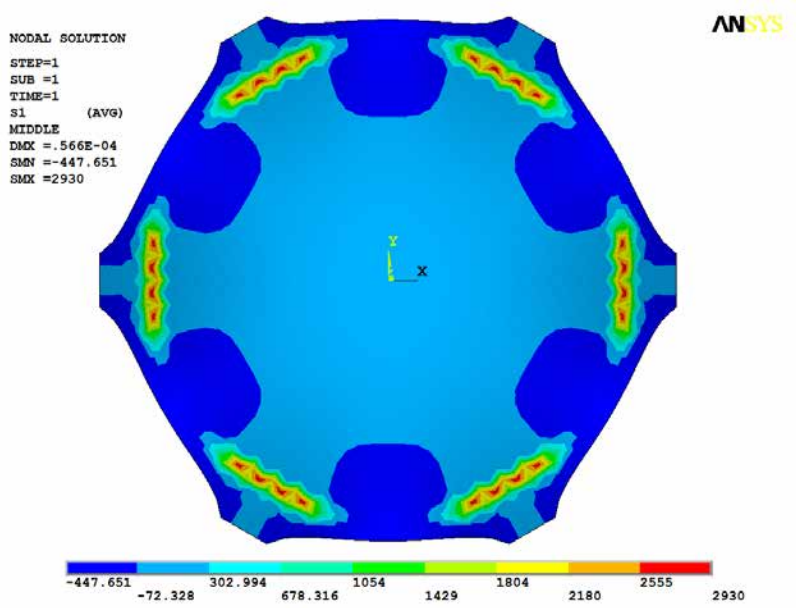


FIGURE 5.20 Principal stress S_1 at the middle surface of the shell of *Example 5.2* (Pa).

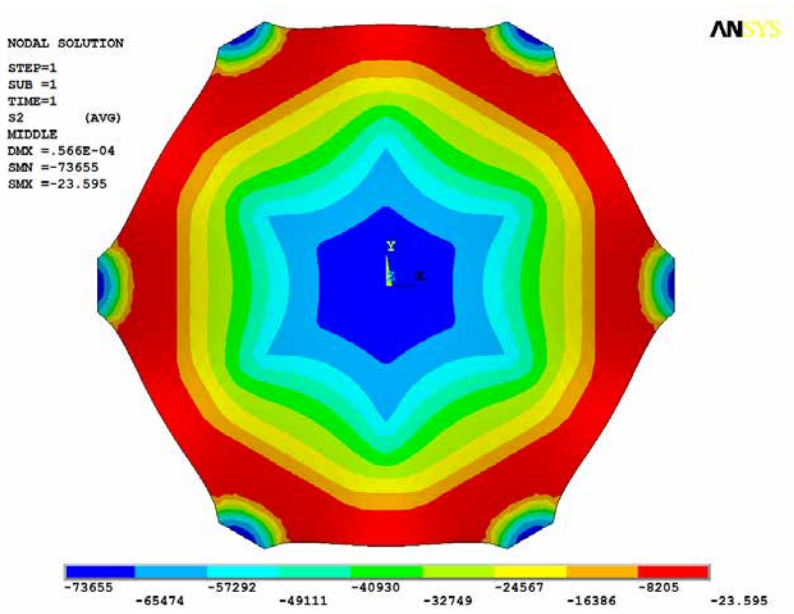


FIGURE 5.21 Principal stress S_2 at the middle surface of the shell of *Example 5.2* (Pa).

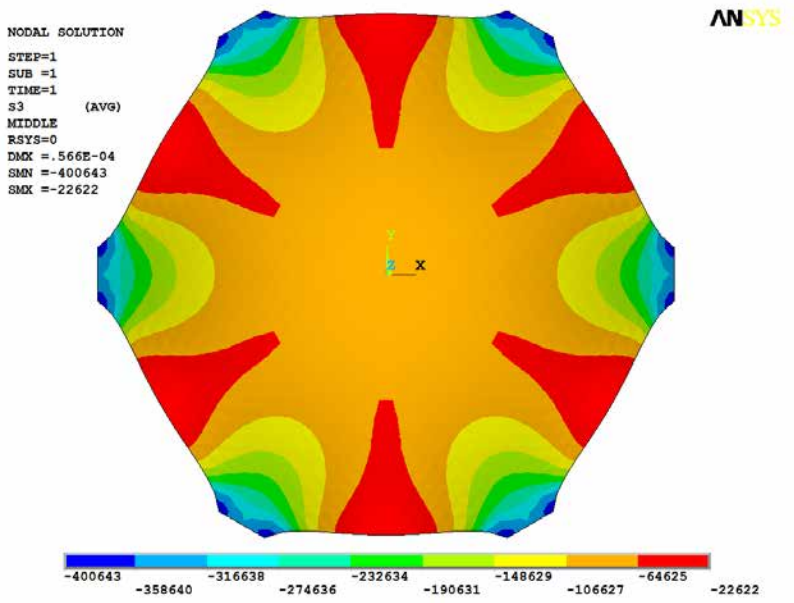


FIGURE 5.22 Principal stress S_3 at the middle surface of the shell of *Example 5.2* (Pa).

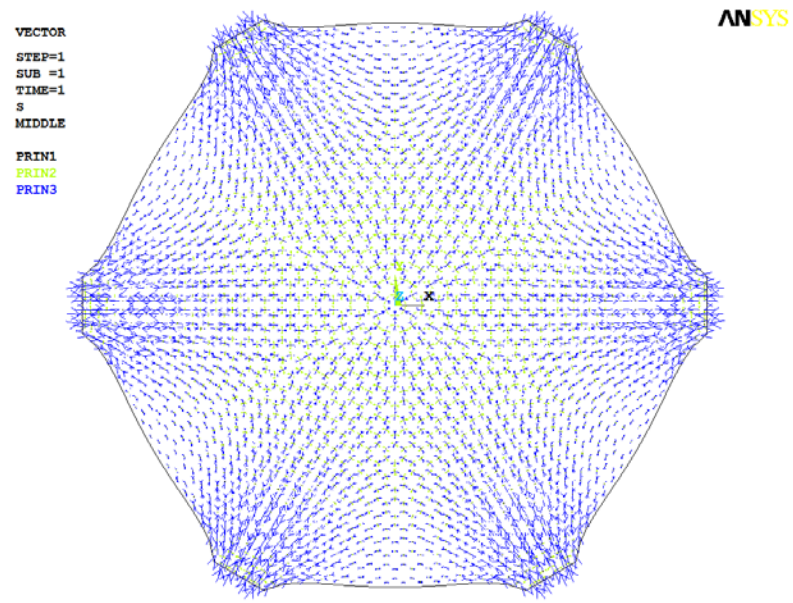


FIGURE 5.23 Vectorial representation of the principal stresses of the shell of *Example 5.2*.

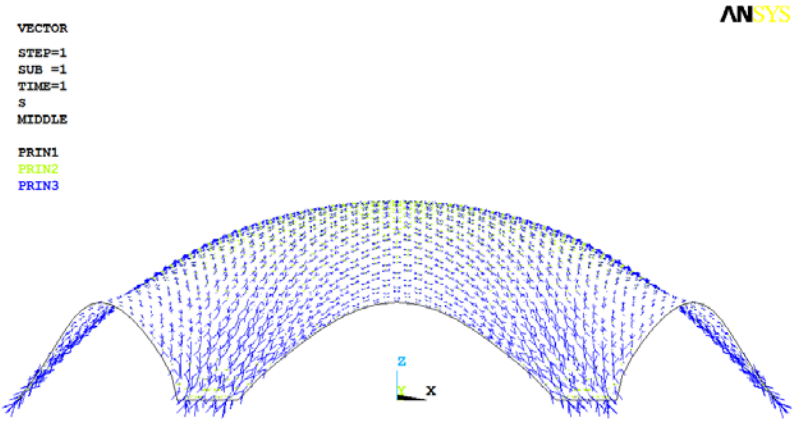


FIGURE 5.24 Vectorial representation of the principal stresses of the shell of *Example 5.2* (lateral view).

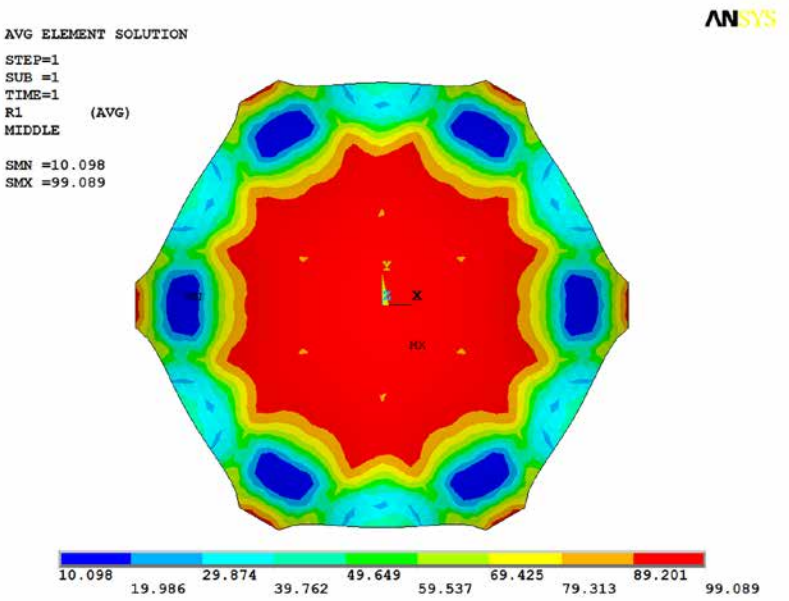


FIGURE 5.25 Stress ratio R_1 of *Example 5.2* (%).

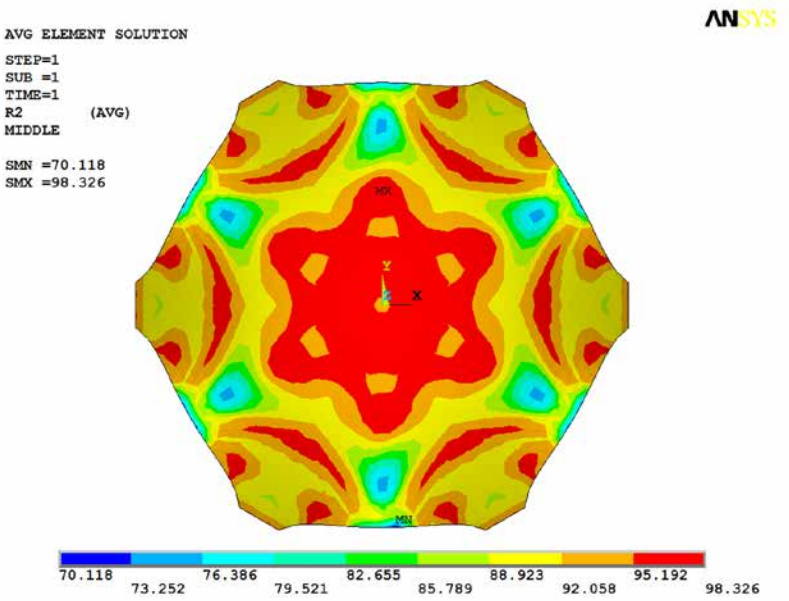


FIGURE 5.26 Stress ratio R_2 of *Example 5.2* (%).

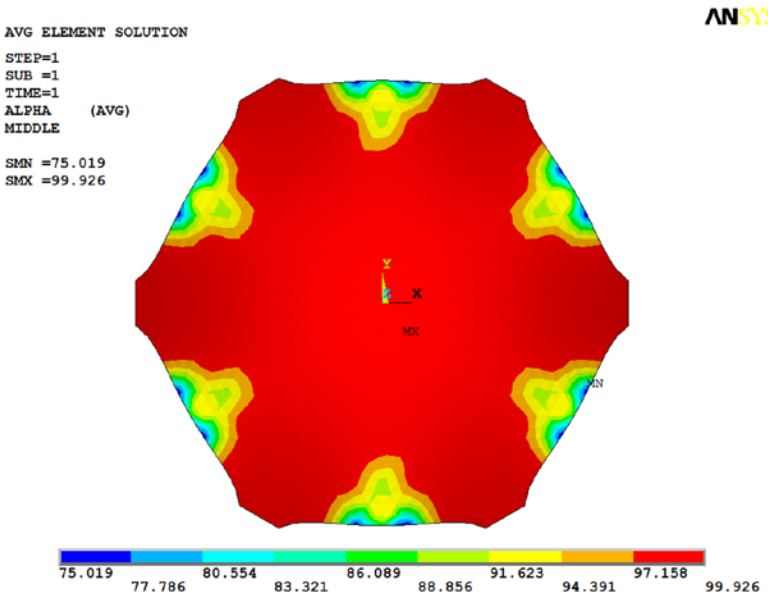


FIGURE 5.27 Strain-energy ratio α of *Example 5.2* (%).

From the former analyses, bending moments can be observed in the part near the free edges of this shell structure under its self-weight. However, it is recognised that the self-weight of this form-found shell with a uniform thickness leads to a different load distribution compared with that of the equilibrium hanging membrane. This is because the load distribution on the particles of the hanging membrane is determined by the initial membrane model shown in Figure 5.14. This load distribution does not change during the generation process of the hanging membrane using the VFIFE method. However, areas of the membrane elements of the equilibrium hanging membrane substantially change compared with those of initial plane membrane. When analysing the shell with a uniform thickness, the load distribution of this shell on the same mesh with the hanging membrane is different from that of the equilibrium hanging membrane. Structural analysis of this shell under loads with the same distribution as the hanging membrane is conducted. The resulting stress ratios and strain-energy ratio are shown in Figure 5.28, Figure 5.29 and Figure 5.30. Much better or even perfect shell behaviour is observed compared with the structural analysis results of the shell under its self-weight. Thus, when the inversed equilibrium hanging membrane serves as the structural geometry of a shell structure, the same load distribution with the equilibrium membrane can lead to an optimal shell behaviour, while a different load distribution may result in large bending moments in the shell.

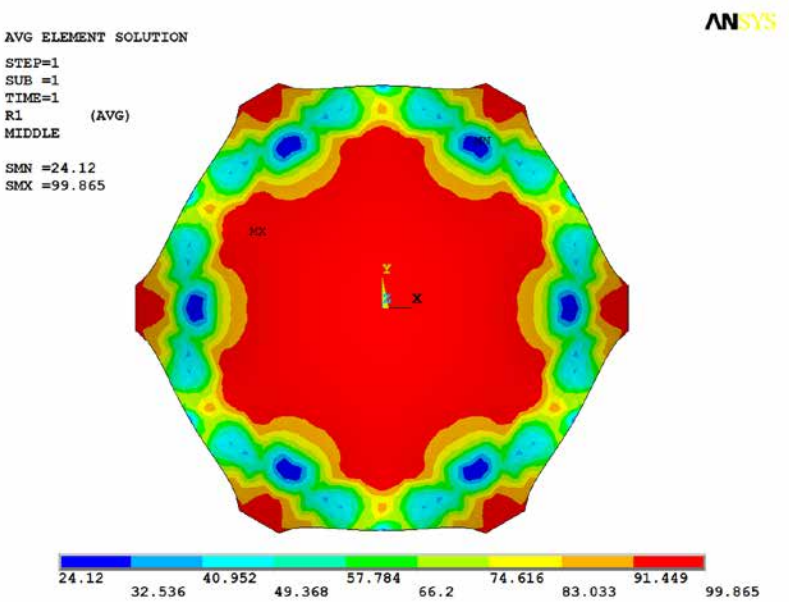


FIGURE 5.28 Stress ratio R_1 of *Example 5.2* under loads with a same distribution as the hanging membrane (%).

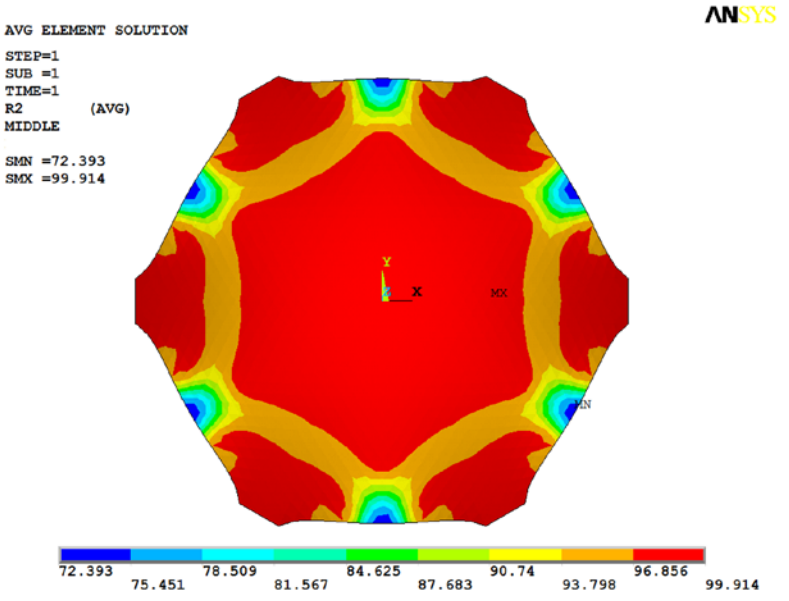


FIGURE 5.29 Stress ratio R_2 of *Example 5.2* under loads with a same distribution as the hanging membrane (%).

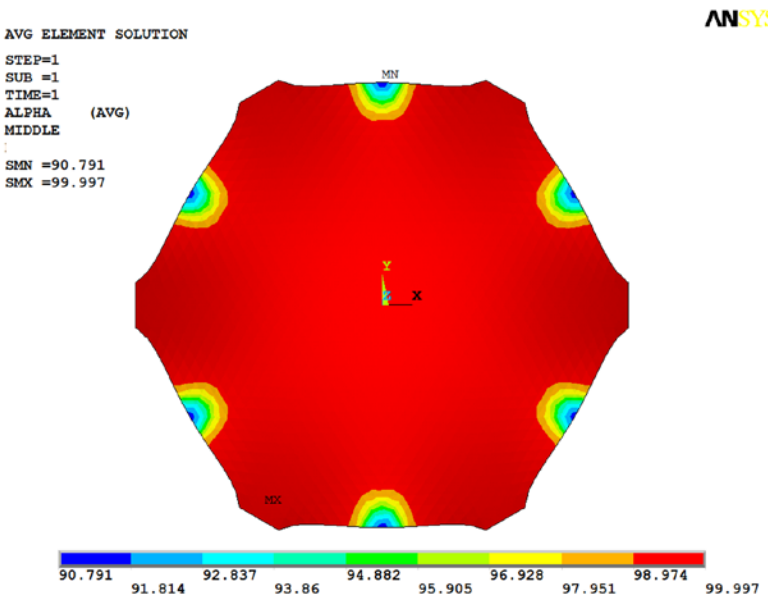


FIGURE 5.30 Strain-energy ratio α of *Example 5.2* under loads with a same distribution as the hanging membrane (%).

§ 5.4.2 Equilibrium of one tension model

Tension models are typical 'self-stressing' structural systems, with their stiffness resulting from a system of internal stresses in static equilibrium, and with their stress conditions also being pure tension. These equilibrium shapes of tension models can also be used for the development of geometries of shells.

Figure 5.31 shows the initial conditions of *Example 5.3*, most of which are same as those in *Example 5.2*. However, the gravity of each particle is not considered in this example. The membrane elements of this structural model have pre-stress of 10.0 kPa. In the centre of the initial shape, the particles in the boundary lines of the hexagon *GHIJKL* with sides of 0.75 m will be uplifted by 5.0 m. Moreover, cable elements are applied in the boundary lines *A'B*, *B'C*, *C'D*, *D'E*, *E'F*, and *F'A*, the elastic modulus of the cable is 1.0E06 N/m^2, the cross-sectional area is 0.01 m^2, and the pre-stress is 50.0 kPa.

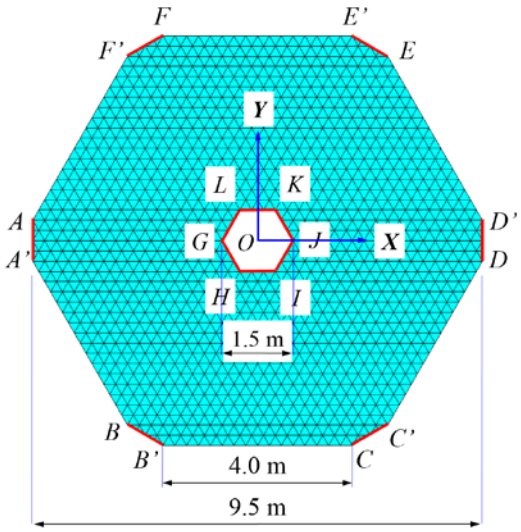


FIGURE 5.31 Initial conditions of *Example 5.3*.

In the calculation process of the VFIFE method, except that the damping-mass factor ξ is set to 10.0, other parameters match those of *Example 5.2*. After the calculation with 3336 steps, the equilibrium shape of a tent structure is approached, as shown in Figure 5.33. Figure 5.32 shows the evolution curve of the maximum value of the residual force of the particles by steps.

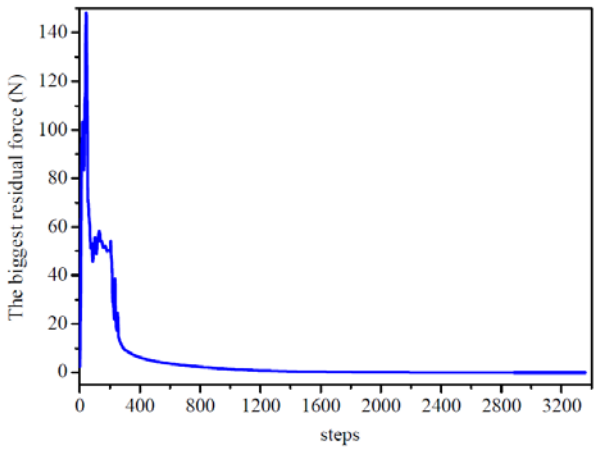
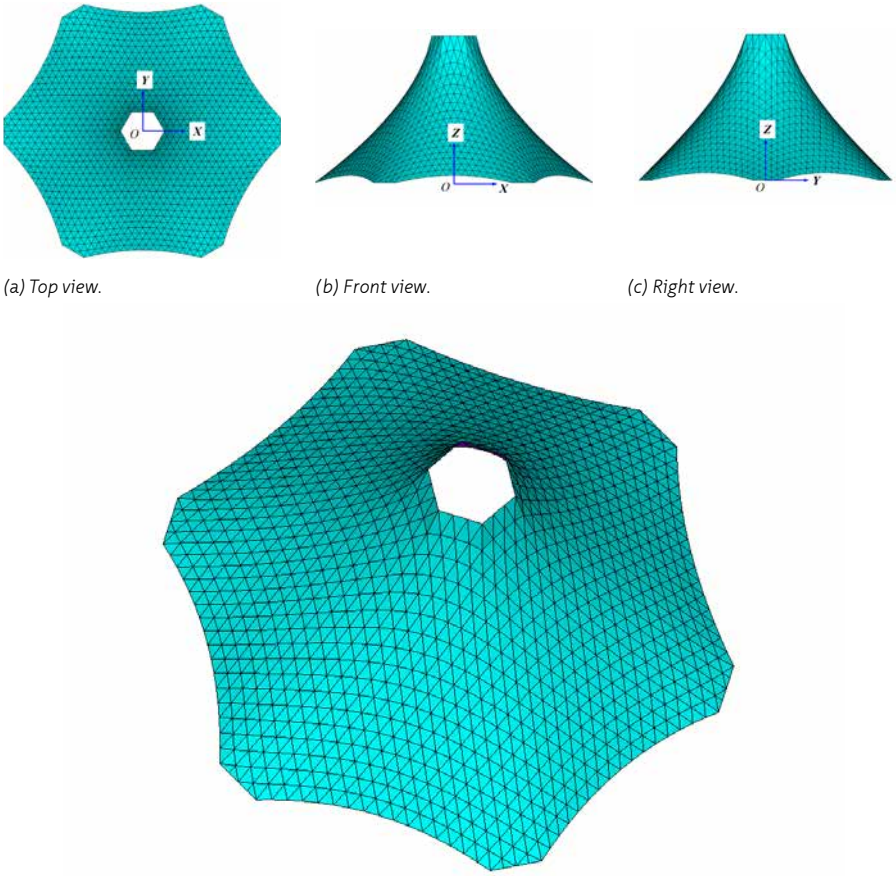


FIGURE 5.32 Evolution curve of the VFIFE method of *Example 5.3*.



(a) Top view. *(b) Front view.* *(c) Right view.*

(d) Perspective view.

FIGURE 5.33 Form-Finding result of ***Example 5.3***.

To verify the effectiveness and accuracy of the VFIFE method in this example, the DR method is also applied here to perform Form-Finding of this tent structure with same initial conditions. Figure 5.34 shows its evolution curve of the kinetic energy by steps. The comparison scheme is the same as that in ***Example 5.2***. Figure 5.35 and Figure 5.36 clearly demonstrate that the Form-Finding result of the VFIFE method is very similar to that of the DR method. The biggest error between the two Form-Finding results is 1.5% (the height of the compared point of the Form-Finding result of the VFIFE method is 3.40 m, while that of the DR method is 3.46 m).

Structural static analysis of this form-found shell under a vertical downwards load is conducted. The material and geometric parameters correlate to those in ***Example 5.2***. In this analysis, the shell is simply supported at six corners, the load of 1.00 kN acts

on the hexagon *GHIJKL*, and their lateral displacements are constrained. Moreover, the self-weight of this shell is not considered. After analysis, Figure 5.37 to Figure 5.44 present the same results as *Example 5.2*. Thus, when the equilibrium tension membrane serves as the structural geometry of a shell structure, good shell behaviour can be obtained under the loads that act in the direction opposite to that uplifting direction during the equilibrium form generation process by the VFIFE method. However, bending moments can be observed in the parts near the lower free edges, see Figure 5.44 (b).

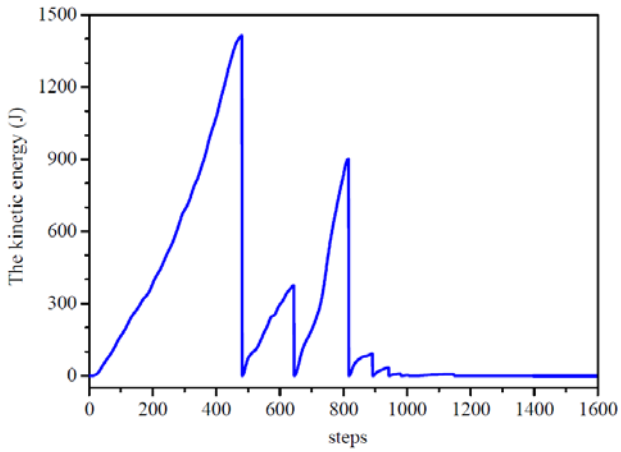


FIGURE 5.34 Evolution curve of the DR method for *Example 5.3*.

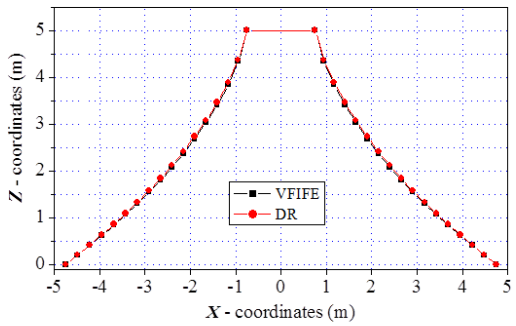


FIGURE 5.35 Comparison of the results of *Example 5.3*; *Z* coordinates of the nodes at *X*-axis of symmetry (*Y*=0).

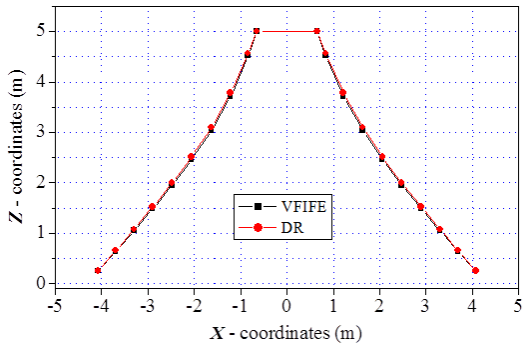


FIGURE 5.36 Comparison of the results of *Example 5.3*; *Z* coordinates of the nodes at *Y*-axis of symmetry (*X*=0).

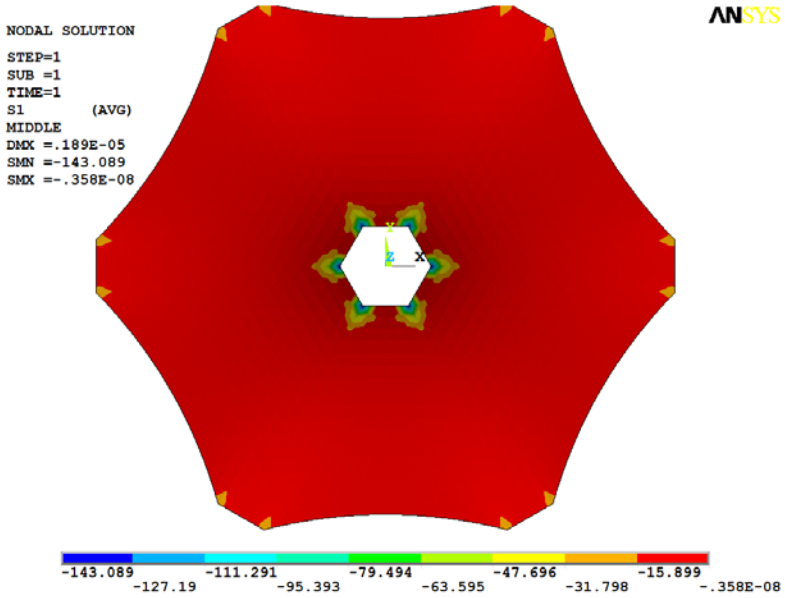


FIGURE 5.37 Principal stress S_1 at the middle surface of the shell of *Example 5.3* (Pa).

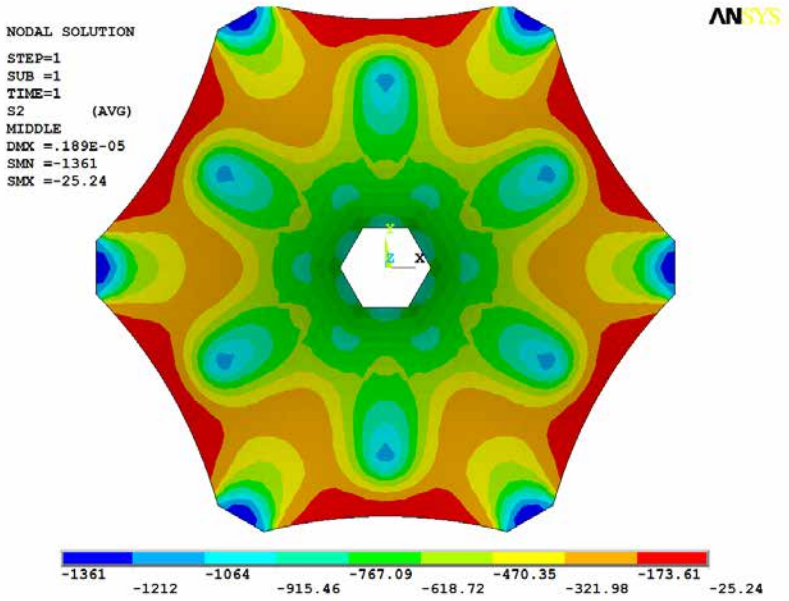


FIGURE 5.38 Principal stress S_2 at the middle surface of the shell of *Example 5.3* (Pa).

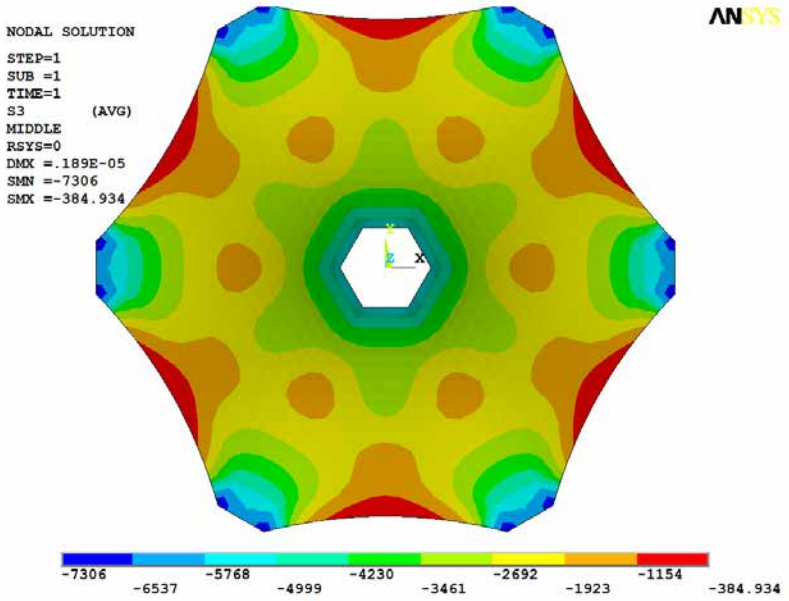


FIGURE 5.39 Principal stress S_3 at the middle surface of the shell of *Example 5.3* (Pa).

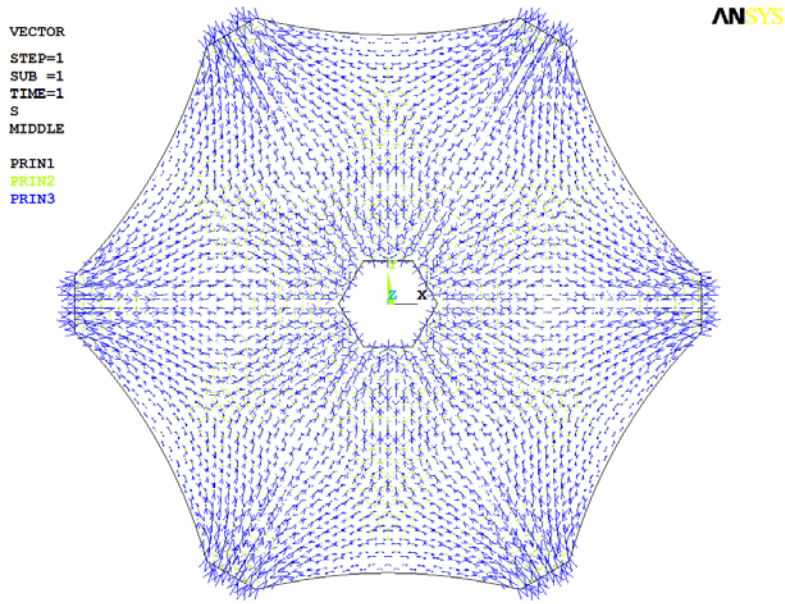


FIGURE 5.40 Vectorial representation of the principal stresses of the shell of *Example 5.3*.

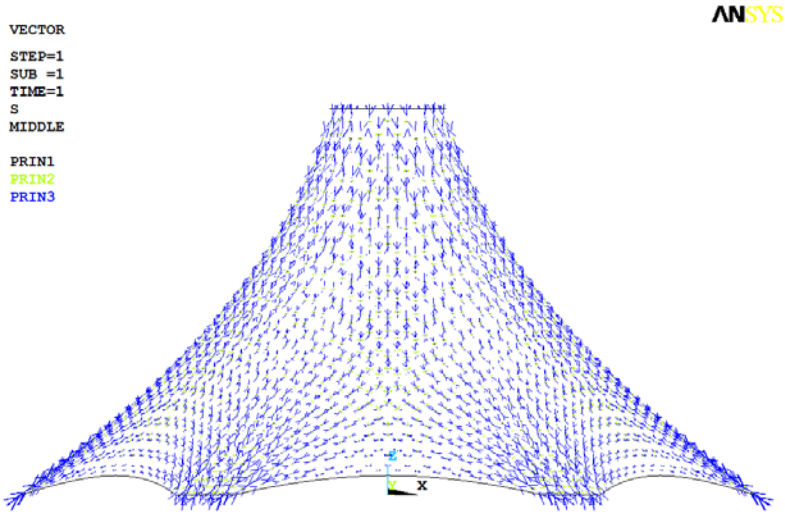


FIGURE 5.41 Vectorial representation of the principal stresses of the shell of *Example 5.3* (lateral view).

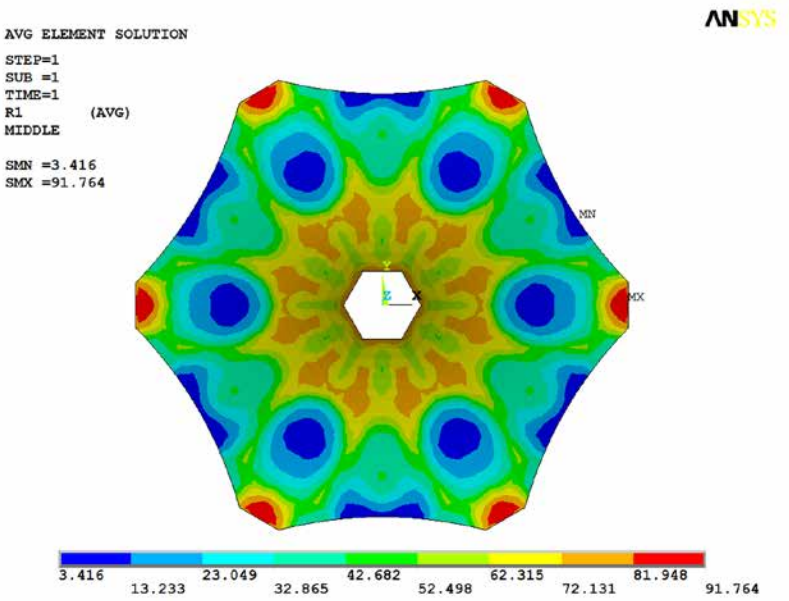


FIGURE 5.42 Stress ratio R_1 of *Example 5.3* (%).

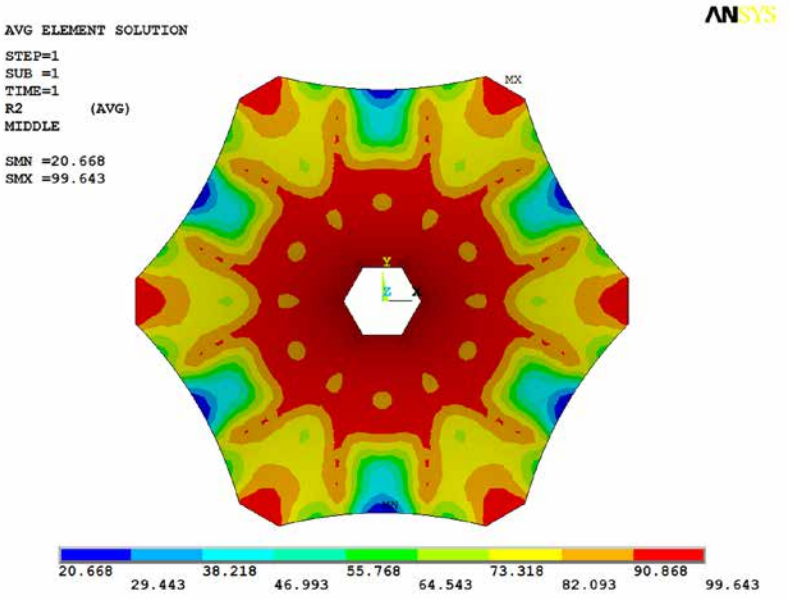
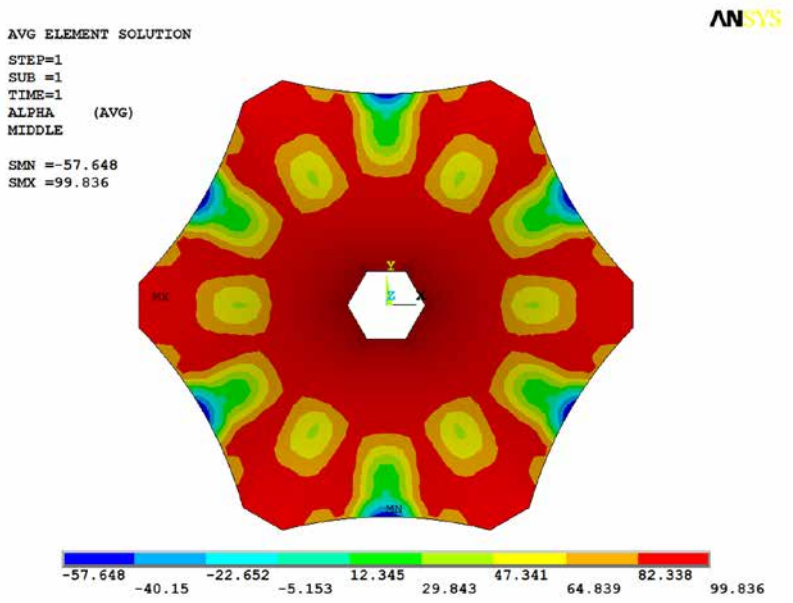
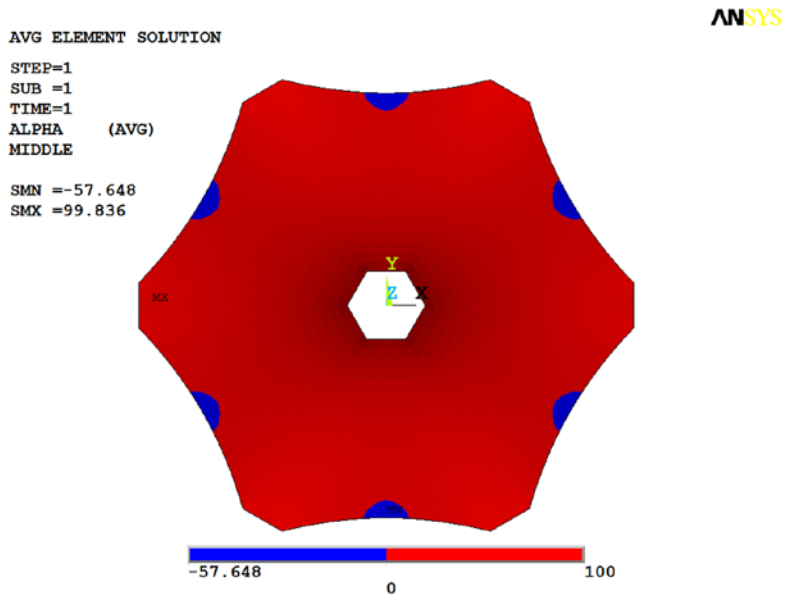


FIGURE 5.43 Stress ratio R_2 of *Example 5.3* (%).



(a) α with ten values of contours (%).



(b) α with three values of contours (%).

FIGURE 5.44 Strain-energy ratio α of ***Example 5.3*** (%).

§ 5.4.3 Equilibrium of one pneumatic model

Pneumatic models represent a type of equilibrium state of flexible materials under air pressure and certain constraint conditions, where stress states are in pure tension. These equilibrium shapes of pneumatic models can be used as the geometry of shells, and can be also adopted as moulds in the construction process.

Figure 5.45 shows the initial conditions of ***Example 5.4***, and the overall conditions are the same as those of ***Example 5.2***. However, all the boundary lines are constrained in this example. There is no pre-stress in the membrane elements. The air pressure applied to this membrane is 25.0 kPa. Like ***Example 5.2***, the gravity of each particle is not considered in this example.

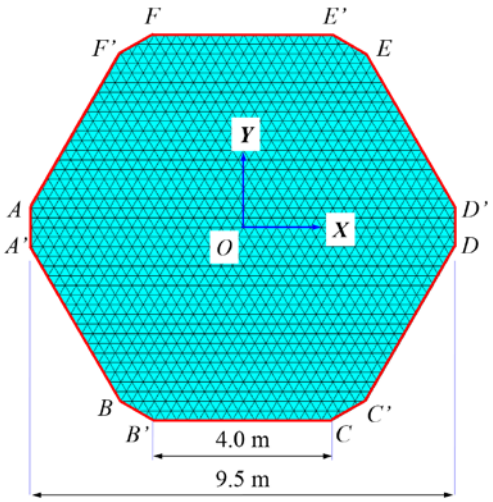


FIGURE 5.45 Initial conditions of ***Example 5.4***.

In the calculation process of the VFIFE method, all the parameters are the same as those in ***Example 5.2***. After the iteration calculation (which included 7559 steps), it finally approached the equilibrium shape of the pneumatic membrane structure shown in Figure 5.47. Figure 5.46 shows the curve of the evolution of the highest value of residual force of the particles by steps, in which the straight line represents the air pressure applied by an incremental loading method.

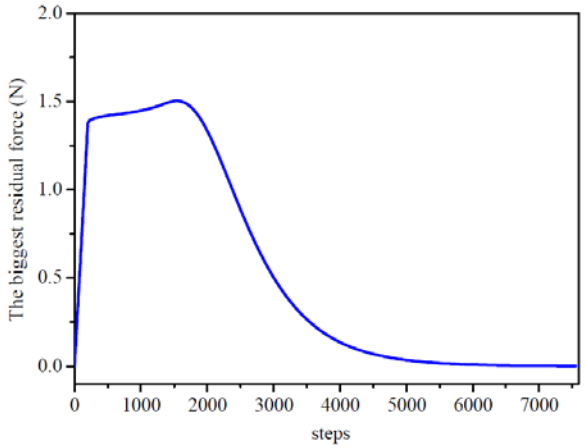
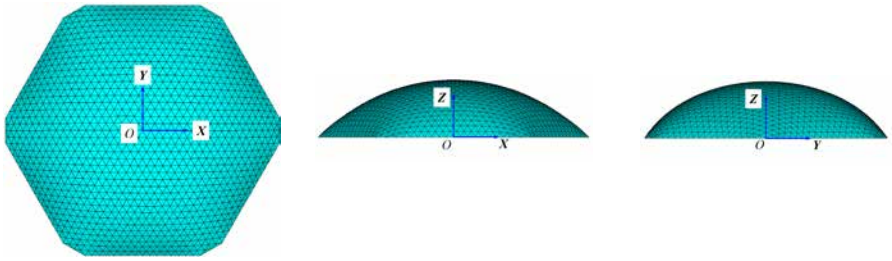
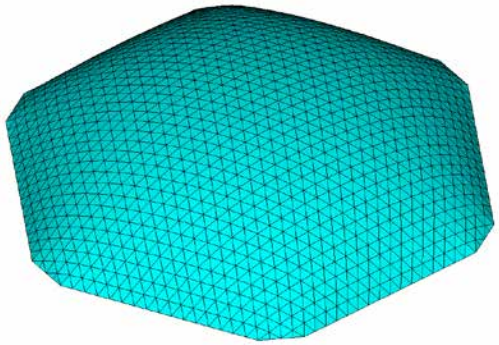


FIGURE 5.46 Evolution curve of the VFIFE method of ***Example 5.4***.



(a) Top view. *(b) Front view.* *(c) Right view.*



(d) Perspective view.

FIGURE 5.47 Form-Finding result of ***Example 5.4***.

To verify the effectiveness and accuracy of the VFIFE method in this example, the DR method is also applied here to perform Form-Finding of this pneumatic structure with the same initial conditions, and Figure 5.48 shows its evolution curve of the kinetic energy by steps (the step length is 0.01). The comparison scheme is also the same with the above two examples. Figure 5.49 and Figure 5.50 clearly illustrate that the Form-Finding result of the VFIFE method is very similar to that of the DR method. The biggest error between the two Form-Finding results, which is at the highest point, is only 0.5% (the height of the highest point of the Form-Finding result of the VFIFE method is 1.99 m, while that of the DR method is 1.98 m).

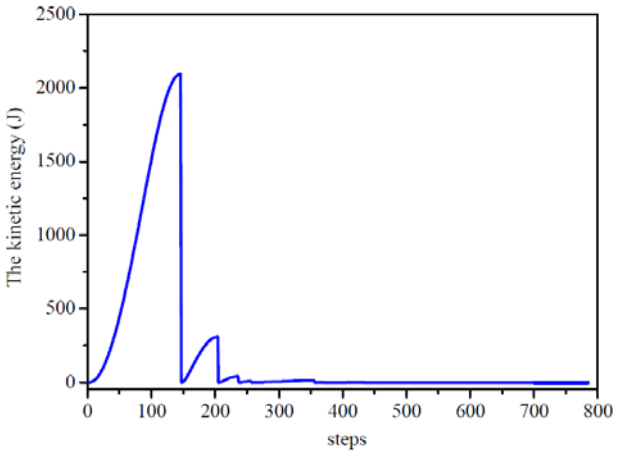


FIGURE 5.48 Evolution curve of the DR method for *Example 5.4*.

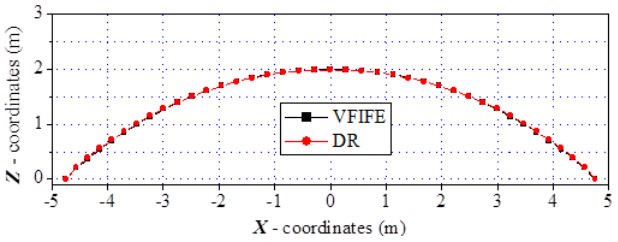


FIGURE 5.49 Comparison of the results of *Example 5.4*; *Z* coordinates of the nodes at *X*-axis of symmetry (*Y*=0).

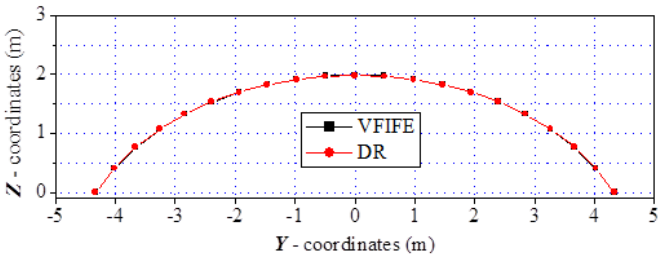


FIGURE 5.50 Comparison of the results of *Example 5.4*; *Z* coordinates of the nodes at *Y*-axis of symmetry (*X*=0).

Then, structural static analysis of this form-found shell under its self-weight is conducted. The material and geometric parameters are the same as those used in *Example 5.2*. The shell is simply supported along the edges. After analysis, Figure 5.51 to Figure 5.58 present same results with *Example 5.2*. Thus, when the equilibrium pneumatic membrane serves as the structural geometry of a shell structure, optimal shell behaviour under its self-weight can be obtained. However, it should be mentioned that distribution of gravity of the shell and that of the pressure acting on the pneumatic membrane have little difference between each other, as the shell is shallow. Structural analysis of the shell under air pressure is not covered here.

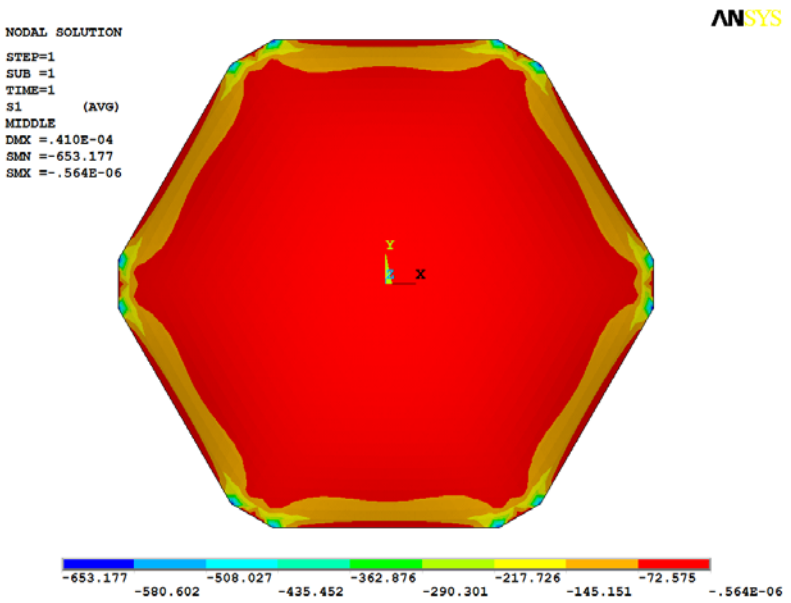


FIGURE 5.51 Principal stress S_1 at the middle surface of the shell of *Example 5.4* (Pa).

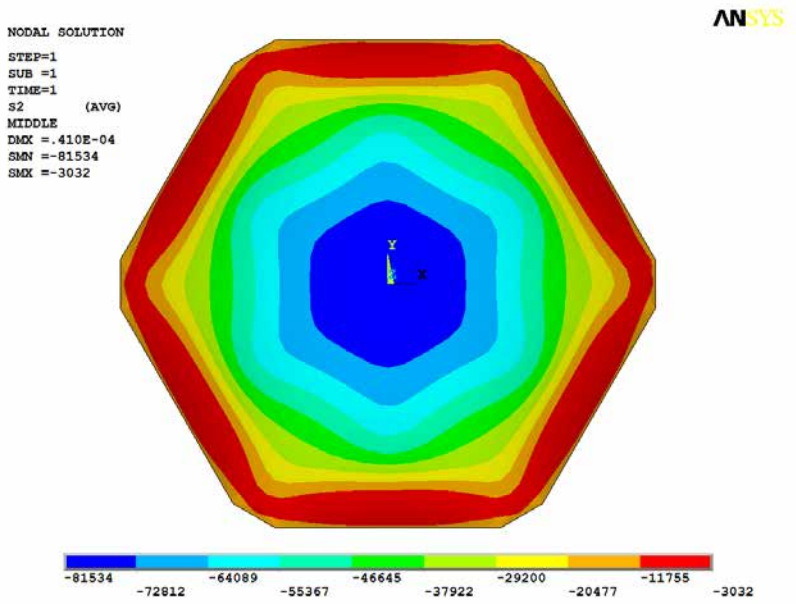


FIGURE 5.52 Principal stress S_2 at the middle surface of the shell of *Example 5.4* (Pa).

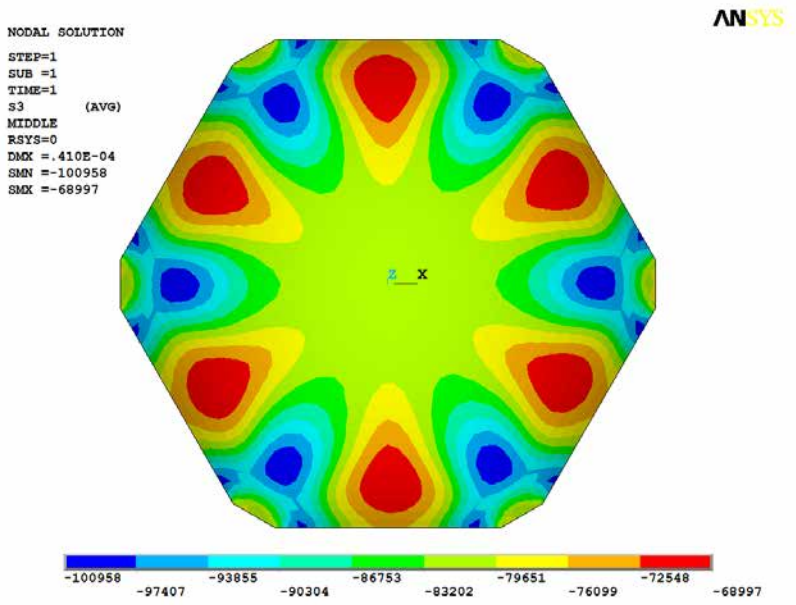


FIGURE 5.53 Principal stress S_3 at the middle surface of the shell of *Example 5.4* (Pa).

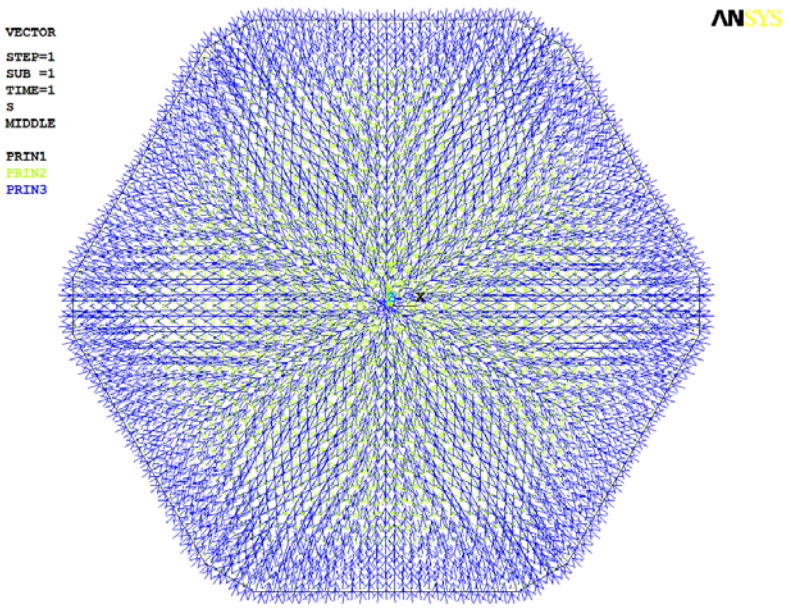


FIGURE 5.54 Vectorial representation of the principal stresses of the shell of *Example 5.4*.

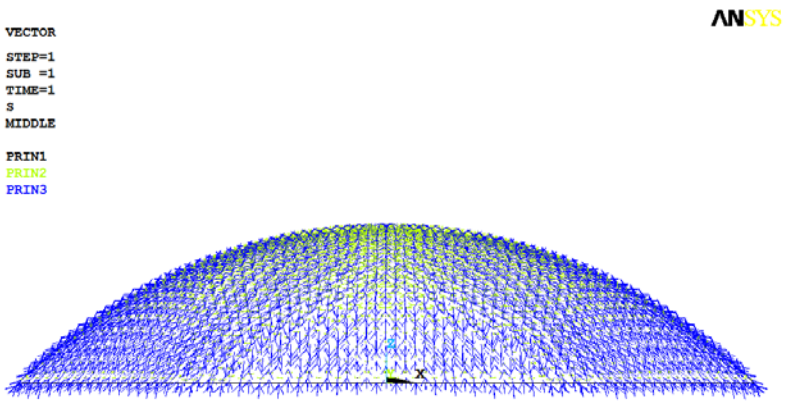


FIGURE 5.55 Vectorial representation of the principal stresses of the shell of *Example 5.4* (lateral view).

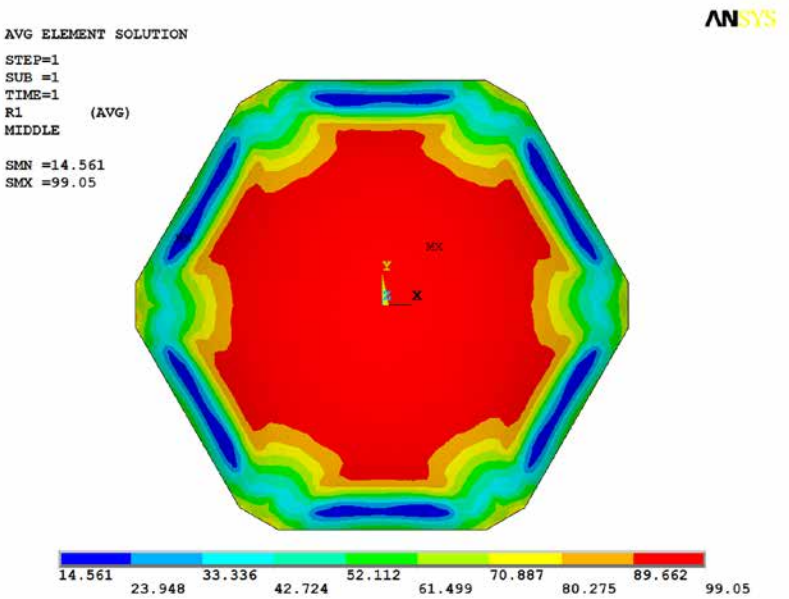


FIGURE 5.56 Stress ratio R_1 of *Example 5.4* (%).

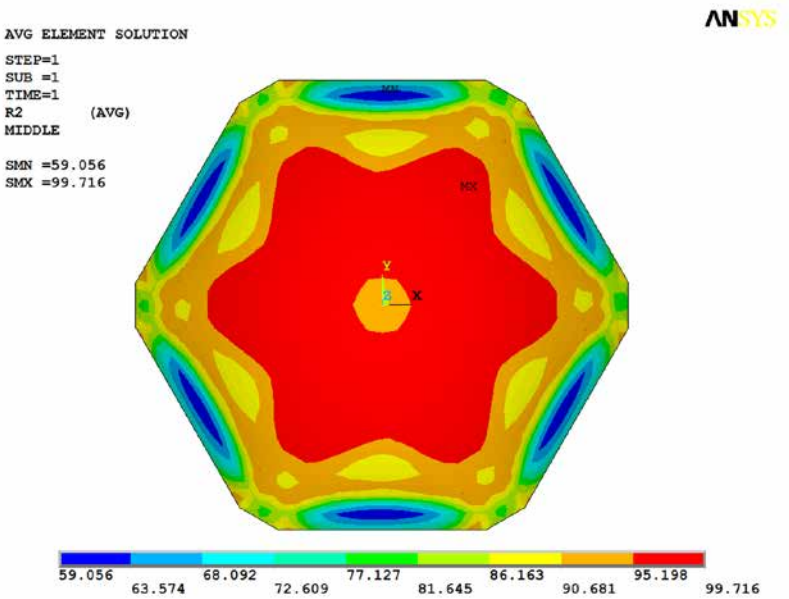


FIGURE 5.57 Stress ratio R_2 of *Example 5.4* (%).

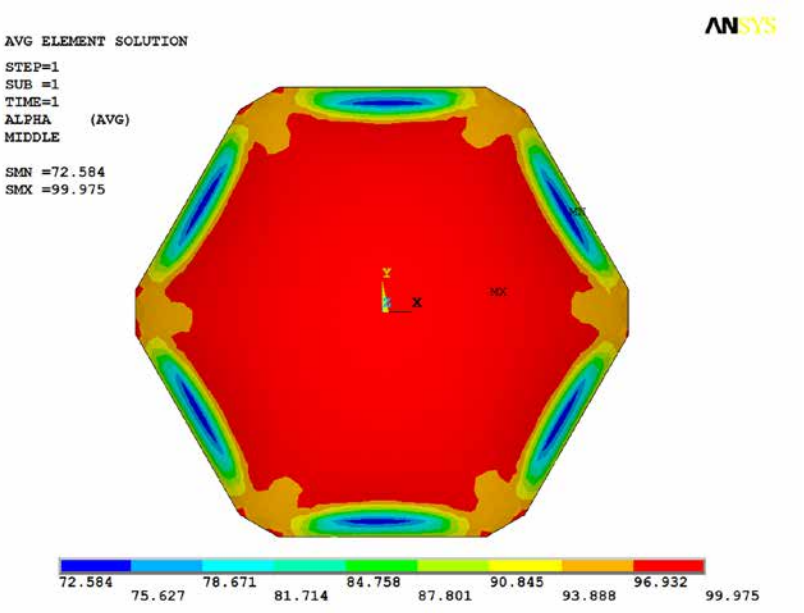
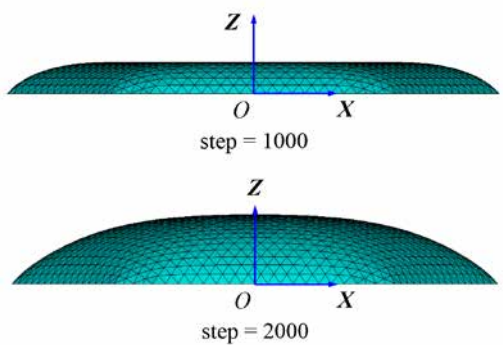


FIGURE 5.58 Strain-energy ratio α of *Example 5.4* (%).

According to its governing equations, the VFIFE method observes the structural behaviour by describing the motion of the particles. Therefore, it can reflect the real physical motion process of the structural systems. For some analysis problems that include complex structural behaviour, the complete deformation process might need to be observed. For instance, the inflation process of the pneumatic model of *Example 5.4* can be obtained, and Figure 5.59 shows some intermediate states during the calculation process.



TOC

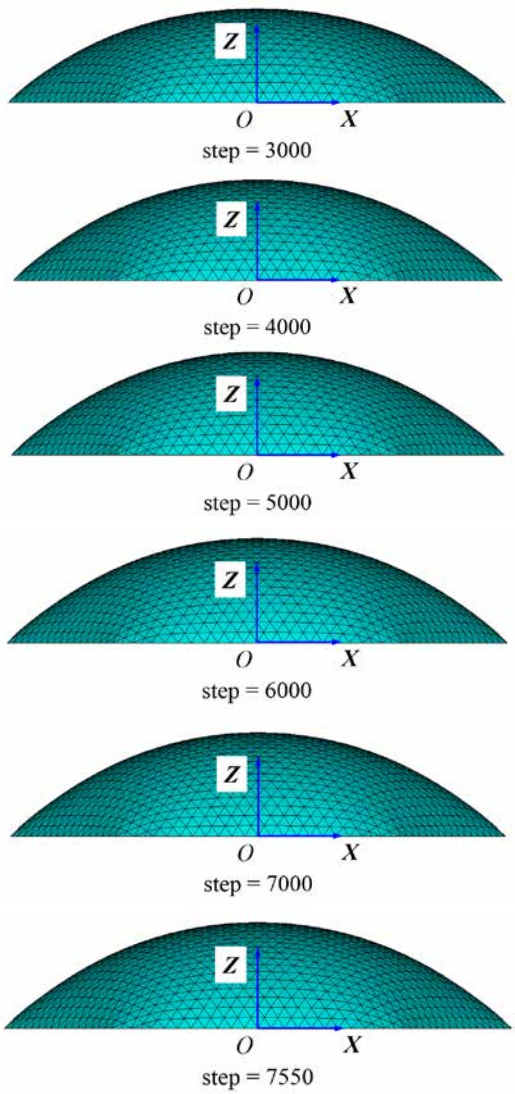


FIGURE 5.59 Inflation process of the pneumatic model of *Example 5.4*.

§ 5.5 Conclusions

This chapter introduces the VFIFE method to conduct equilibrium problems of Force-Active structural systems and thus Force-Passive structural systems. The main conclusions are as follows:

– Taking the cable-link element as example, the framework of the VFIFE method is explained with three basic concepts: the point description, path unit, and reverse rigid body motion of the element. Then, a constant-strain triangle element is introduced, and the relevant required equations are deduced. Based on this, a MATLAB script is programmed to realise this method. This script can be used to generate equilibrium structural forms of cable and membrane structures.

– Equilibrium structural forms of a hanging cable net, hanging membrane, tension membrane and pneumatic membrane are generated by both the VFIFE method and the DR method. Using a detailed comparison, very few differences between the equilibrium structural forms obtained by the two methods can be observed. The accuracy and robustness of the VFIFE method for generating equilibrium structural forms for Force-Active structural systems have been validated.

– For these examples, in the VFIFE method, there is no need to establish the stiffness matrix in the calculation process. This overcomes problems such as the stiffness matrix singularity and iterative convergence difficulty in the traditional FEM. For equilibrium problems of Force-Active structural systems, the VFIFE method can generate the equilibrium structural form from any unbalanced state with arbitrary and inaccurate specifications of geometry, which is convenient for solving such problems with strong nonlinearity.

– Equilibrium structural forms of all three types of membrane structures are used as the structural geometries of shells. Static structural analyses of these three shells are conducted. It is found that optimal shell behaviour occurs under loads with the same distribution as the equilibrium structural form of Force-Active structural systems. The capability of the VFIFE method in generating optimal structural shapes for shells has been verified. However, when the load distribution changes, bending moments occur under in these shells.

– Compared with the DR method, the governing equation of the VFIFE method uses the Störmer-Verlet integration method instead of the Leapfrog integration

method. So far, the VFIFE method has shown few advantages over the DR method. For future work, the potential value of the VFIFE method based on its new basic concepts will be explored. This work is already ongoing in the author's research group in Harbin; for example, group members are using the VFIFE method to simulate the inflation and deflation processes of inflatable moulds for ice shells.

TOC

6 Controlling Equilibrium Structural Forms with Target Heights

§ 6.1 Introduction

As mentioned in **Chapter 4**, simpler and more effective strategies are required to control the equilibrium structural form of Force-Active structural systems to meet some architectural requirements due to usability, aesthetics, or other factors.

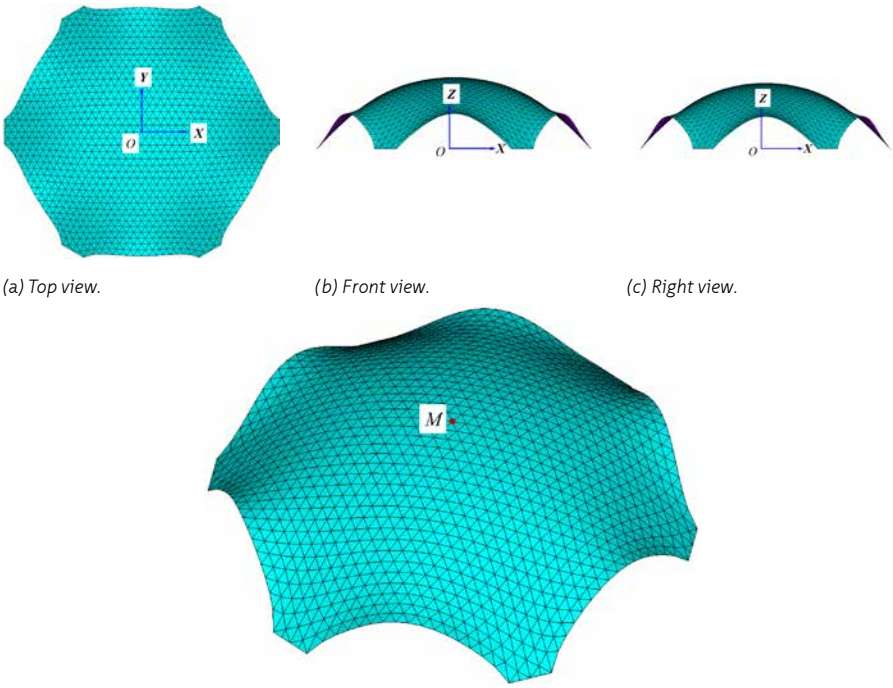
In this chapter, taking shell structures generated from the hanging models as examples, Form-Control strategies that aim to generate structural forms with single and multiple height constraints are discussed. First, by introducing the Newton-Raphson method to adjust Young's modulus of the initial structural model, a Form-Control strategy to generate the equilibrium structural form with a single target height is proposed. Subsequently, by introducing the inverse iteration method to adjust the geometry of the initial model, a Form-Control strategy to generate the equilibrium structural form with multiple target heights is proposed. To introduce these strategies more clearly, several examples are reviewed in this chapter.

§ 6.2 Form-Control of the Equilibrium Structural Form with One Target Point

§ 6.2.1 Proposal of the problem

The equilibrium form of a piece of hanging membrane can be generated by the VFIFE method presented in the last chapter. To propose the Form-Control problem with a single target point, the next example of this section (***Example 6.1***) is a secondary development of ***Example 5.2***.

Figure 6.1 presents the inverted equilibrium hanging structural form of ***Example 5.2***. As a characteristic parameter of this, the height ***h*** of the central point ***M*** is 2.48 m.



(a) Top view. *(b) Front view.* *(c) Right view.*

(d) Perspective view.

FIGURE 6.1 Form-Finding result of ***Example 5.2***.

For a piece of isotropous membrane with defined geometry and boundary conditions, during its numerical generation of the equilibrium hanging model under its self-weight, magnitudes of the density or that of Young's modulus for the hanging material will significantly influence the final equilibrium structural form. The influence of Young's modulus of the hanging material is considered in this research.

Using the VFIFE method, the equilibrium structural forms of the hanging membrane in ***Example 5.2*** are generated many times but with different Young's moduli of the initial model. The characteristic curve of the height ***h*** of point ***M*** to the Young's modulus ***E*** is shown in Figure 6.2. It can be observed clearly that the height ***h*** of point ***M*** is a function of Young's modulus ***E*** of the membrane, which can be expressed as Equation 6.1. From Figure 6.2, it can be observed clearly that this function is nonlinear and monotonically decreasing.

$$h = f(E)$$ Equation 6.1

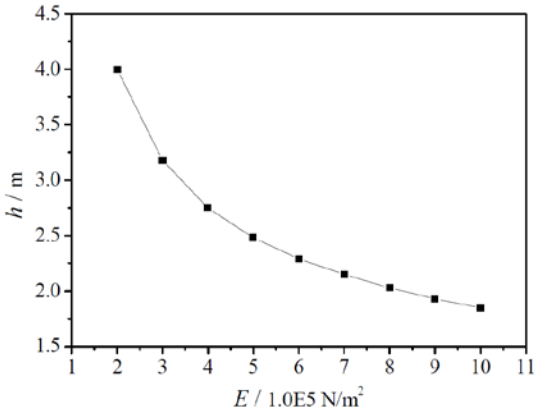


FIGURE 6.2 Curve of the height of point ***M*** to Young's modulus.

The research problem is to generate the structural form with one target height. From the above introduction, a Form-Control strategy to adjust Young's modulus for the hanging material can be researched. However, as mentioned, the relationship between the equilibrium structural form and Young's modulus of the hanging material is nonlinear. In this research, the Newton-Raphson method is introduced to solve this problem.

§ 6.2.2 Form-Control strategy based on the Newton-Raphson method

The Newton-Raphson method is a numerical method that can transform the nonlinear problem into a linear problem in the iteration process. This method uses the local linear characteristic of the function (Equation 6.1) to approach the target point, which is faster and needs just one initial value compared with the bisection method. To obtain the specific structural form with a given height h^* of point ***M***, which means to find the specific related Young's modulus, the problem can be solved using the following steps.

1 With an initial Young's modulus E_1, after numerical analysis by the VFIFE method, the height of the point ***M*** is $h_1 = f(E_1)$.

2 Using Young's modulus $(E_1+\Delta E)$ with a small difference from the initial one, after numerical analysis by the VFIFE method, the height of the point M is $h_{1+\Delta} = f(E_1+\Delta E)$.

3 Using Equation 6.2, a new Young's modulus is obtained, as follows:

$$E_2 = E_1 + \frac{\Delta E}{f(E_1+\Delta E) - f(E_1)} \times (h^* - h_1) \qquad \text{Equation 6.2}$$

where $\frac{\Delta E}{f(E_1+\Delta E) - f(E_1)}$ should represent the linear characteristic of the function $h=f(E)$ in the point $(E_1, f(E_1))$, which is the reciprocal value of the slope in the point of the function curve. Therefore, ΔE is set to a relatively smaller value.

4 With the newly obtained Young's modulus E_2, after numerical analysis using the VFIFE method, the height of the point M is $h = f(E_2)$.

5 The difference between $f(E_2)$ and the target value h^* is calculated, and when it is smaller than the allowable error ☒, the target structural form is obtained; otherwise, the following step is conducted.

6 Using the iterative Equation 6.3 to update Young's modulus, numerical analysis by the VFIFE method is conducted in each step until the allowable error ε is fitted.

$$E_2 = E_1 + \frac{\Delta E}{f(E_1+\Delta E) - f(E_1)} \times (h^* - h_1) \qquad \text{Equation 6.3}$$

With several iterations of the steps, the equilibrium structural form with one target height can be generated.

§ 6.2.3 Numerical example

To verify the effectiveness and efficiency of this Form-Control strategy, *Example 6.1* is reviewed in this section. The Form-Control of a piece of hanging membrane with one target height and the structural analysis of the form-found shell structure are demonstrated in this example.

Example 6.1 has same initial conditions as those in *Example 5.2*. Additionally, the target height of the central point M of 3.0 m is required in this example. By directly using the Form-Control procedure described in Section 3.1, the Newton-Raphson

method is applied to adjust Young's modulus of the membrane of the initial model. In this example, the allowable error for the target height is 0.001 m, and ΔE is set to 1000 N/m^2. With an iteration of four steps, the required structural form with the target height of point ***M*** is obtained. Figure 6.3 shows how Young's modulus ***E*** of the membrane and the height ***h*** of point ***M*** vary in the iterative process. The final required structural form is displayed in Figure 6.4. It can be observed clearly that the Newton-Raphson method is effective and efficient in the Form-Control process of the equilibrium structural form with a single target height.

Structural static analysis of this form-controlled shell under its self-weight is also conducted here. All the parameters are the same as those in ***Example 5.2***, such as the thickness, boundary conditions, and the material properties. After analysis, the two stress ratios and the strain-energy ratio of the shell are shown in Figure 6.5, Figure 6.6 and Figure 6.7. As explained in **Section 5.4.1**, the self-weight of this form-found shell with a uniform thickness has a different load distribution compared with that of the equilibrium hanging membrane. Compared with that of ***Example 5.2***, with a higher geometry, the difference is more significant, so that relatively larger bending moments occur in the parts near the free edges of the shell. However, it can still be concluded that the form-controlled shell has good shell behaviour under its self-weight.

Moreover, static structural analysis of this form-controlled shell under loads with the same distribution as the equilibrium hanging membrane is conducted. After analysis, the two stress ratios and the strain-energy ratio of the shell are illustrated in Figure 6.8, Figure 6.9 and Figure 6.10. An optimal shell behaviour can clearly be observed. Again, it validates the accuracy and robustness of the VFIFE method in generating equilibrium hanging membranes and thus structurally efficient geometry for shells.

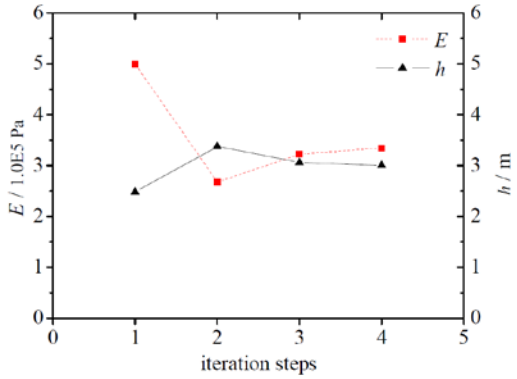
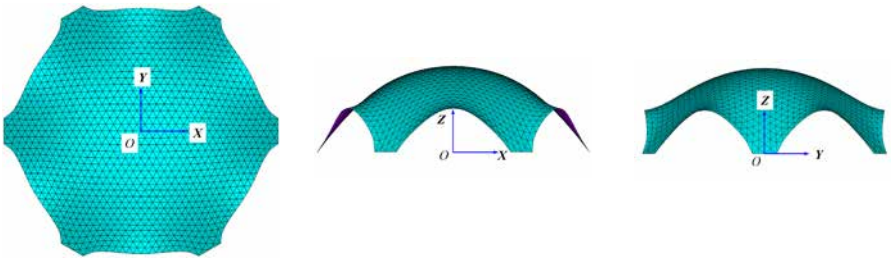
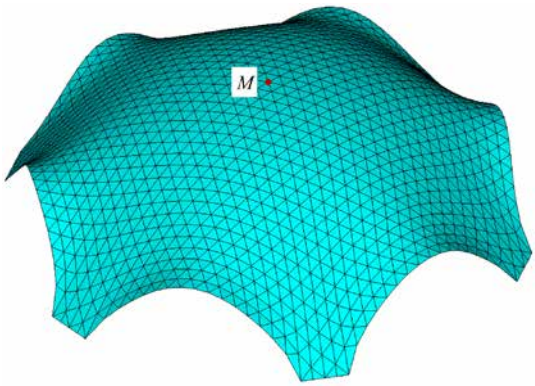


FIGURE 6.3 Iteration curve of ***Example 6.1***.



(a) Top view. *(b) Front view.* *(c) Right view.*



(d) Perspective view.

FIGURE 6.4 Form-Control result of ***Example 6.1***.

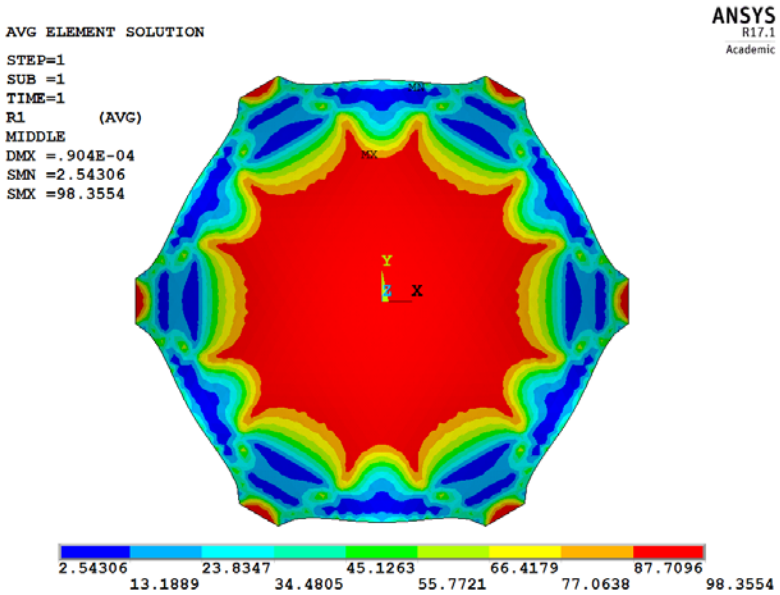


FIGURE 6.5 Stress ratio R_1 of *Example 6.1* under self-weight (%).

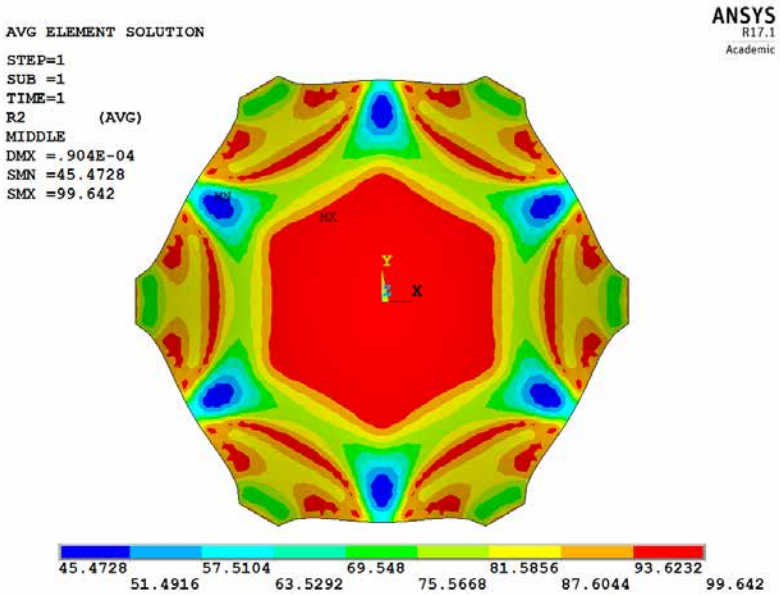


FIGURE 6.6 Stress ratio R_2 of *Example 6.1* under self-weight (%).

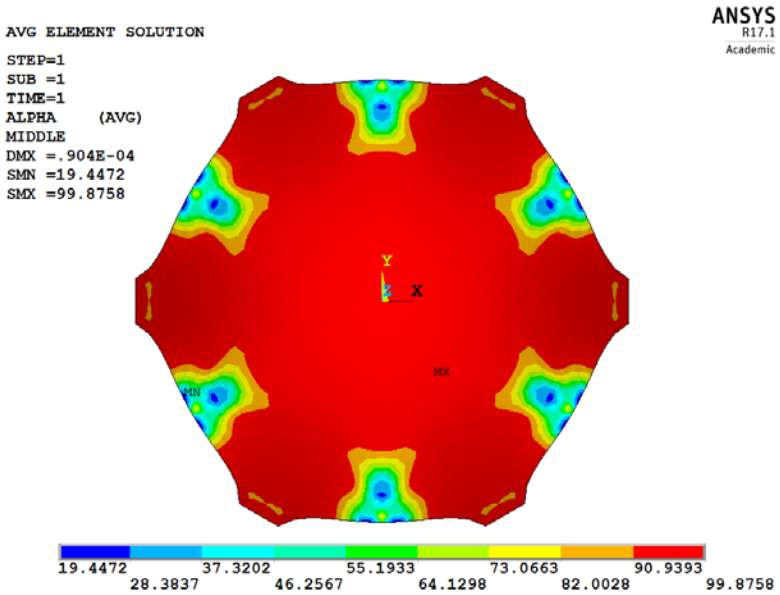


FIGURE 6.7 Strain-energy ratio α of *Example 6.1* under self-weight (%).

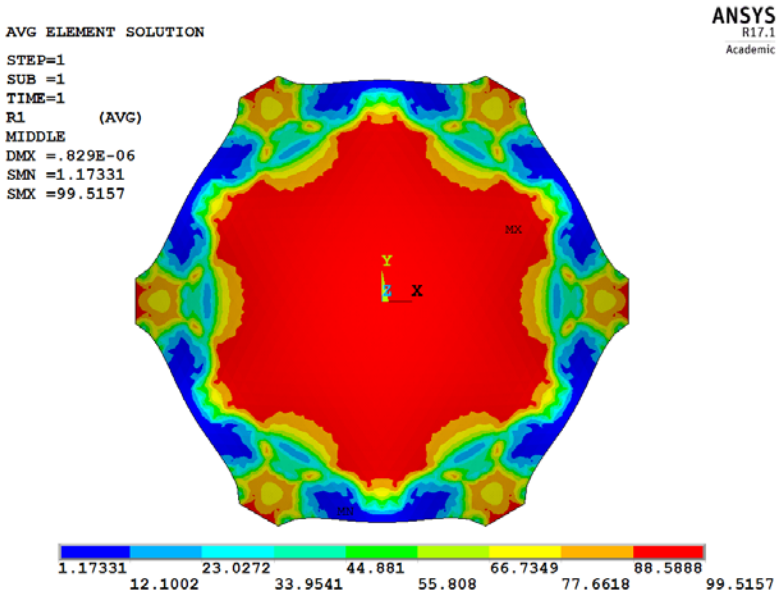


FIGURE 6.8 Stress ratio R_1 of *Example 6.1* under the same load distribution with the equilibrium hanging membrane (%).

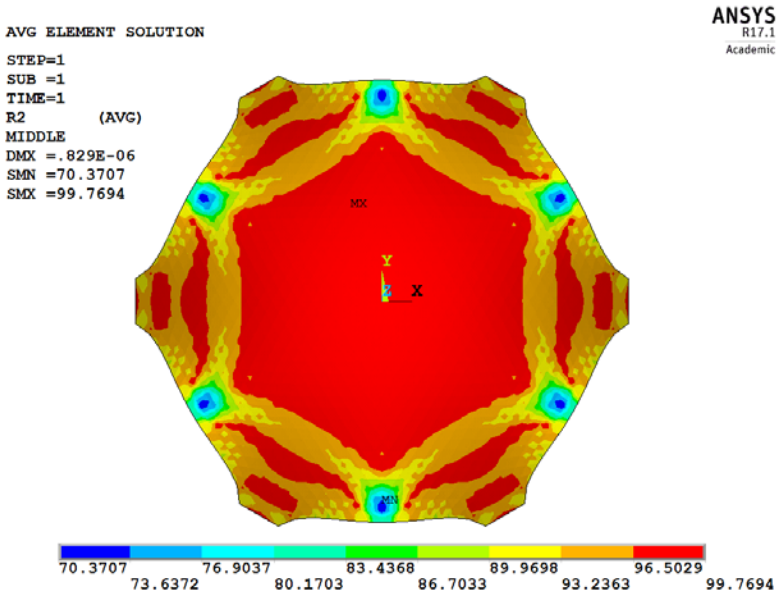


FIGURE 6.9 Stress ratio R_2 of *Example 6.1* under the same load distribution with the equilibrium hanging membrane (%).

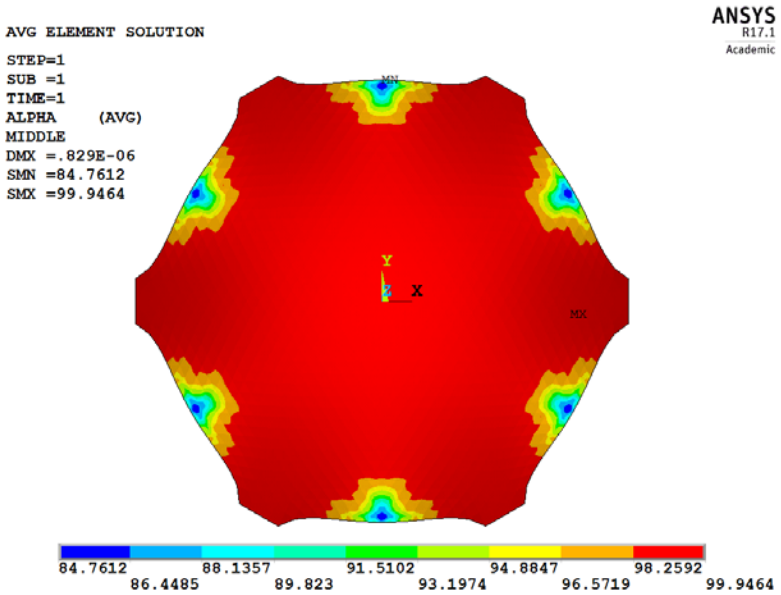


FIGURE 6.10 Strain-energy ratio α of *Example 6.1* under the same load distribution with the equilibrium hanging membrane (%).

§ 6.3 Form-Control of Equilibrium Structural Form with Multiple Target Points

§ 6.3.1 Proposal of the problem

In most cases, having only one target height is insufficient, and many more target heights are needed due to the architectural requirements in the design process. With these requirements, a structural geometry can be established using many geometric modelling methods, such as polylines, folds, or NURBS techniques. Using this geometry as the initial structural model, a corresponding equilibrium hanging structural form can be generated using the VFIFE method. Considering that the VFIFE method can attain the equilibrium structural form from any unbalanced state, a Form-Control strategy which aims to find a specific initial structural model could be researched. After numerical analysis of this specific initial structural model, the equilibrium structural form can meet the given target heights. Thus, the inverse iteration method is introduced to adjust the geometry of the initial structural model.

§ 6.3.2 Form-Control strategy based on the inverse iteration method

The inverse iteration method determines the required equilibrium structural form by iteratively adjusting the geometric parameters of the initial structural model. *Example 6.2* is shown here to illustrate that how it works. In Figure 6.11, the problem is to generate the equilibrium shape of a piece of cable under its self-weight, whose support points are *A* (0.00, 0.00) and *B* (1.00, 0.00), and the target point is point *C* (0.50, 0.35). Table 6.1 provides the first two steps of the adjustment process. The basic procedure of the Form-Control process based on the inverse iteration method is introduced as follows.

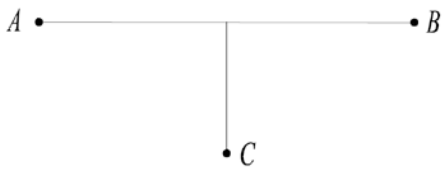


FIGURE 6.11 Problem of *Example 6.2*.

TOC

1 First, the initial structural model is established along line ***AC*** and line ***BC*** with five elements in either of them. The length of each element is the distance between the two nodes, which will change slightly by setting a relatively large Young's modulus during the numerical analysis using the VFIFE method. After that, the equilibrium structural form, which has an error of Δ_1 with the target point can be obtained.

2 Second, the point C_1 is established, which is generated from point C with a displacement of $-\Delta_1$. Then, the initial structural model along line AC_1 and line BC_1 is established with same sets as Step.1. After numerical analysis using the VFIFE method, the equilibrium structural form can be obtained, which has an error of Δ_2 for the target point, which is much smaller than Δ_1.

3 In the following steps, if the new equilibrium position is under the target height, and upward adjustment of the initial position of point C_i is implemented, the initial structural model is also updated as in Step 2, and vice versa.

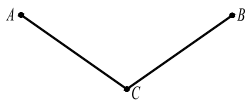
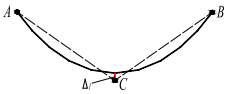
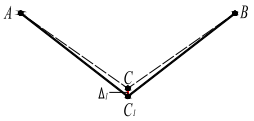
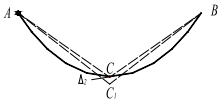
STEPS	INITIAL STRUCTURAL MODEL	EQUILIBRIUM STRUCTURAL FORM
Step 1		
Step 2		
...	...	...

TABLE 6.1 Adjusting process of ***Example 6.2***.

After just four steps, the method can generate the structural form across the target point within the allowable error. It can be observed that the inverse iteration method is efficient in the Form-Control process of the equilibrium hanging cable with a single target height. Different modelling methods, such as the quadratic NURBS curve, can be used as the initial structural model instead of just using two straight lines. While the quadratic NURBS curve is close to a catenary, the adjustment process is not as apparent as that of using two straight lines.

§ 6.3.3 Numerical example

With the additional four target heights of *Example 5.2*, *Example 6.3* is shown to verify the effectiveness and efficiency of the inverse iteration method to solve Form-Control problems with multiple target heights. This example aims to generate a form-found shell with five target heights.

Figure 6.12 illustrates the initial conditions of *Example 6.3*; it has the same boundary conditions as *Example 5.2* and *Example 6.2*. The target heights are as follows:

- the central point *M* of the structural form is 3.0 **m**,
- the middle point N_1 of the boundary *E'F* is 0.5 m,
- the middle point N_2/N_3 of the boundary *F'A*/*D'E* is 1.0 m,
- the middle point N_4/N_5 of the boundary *A'B*/*C'D* is 1.5 m, and
- the middle point N_6 of the boundary *B'C* is 2.0 m.

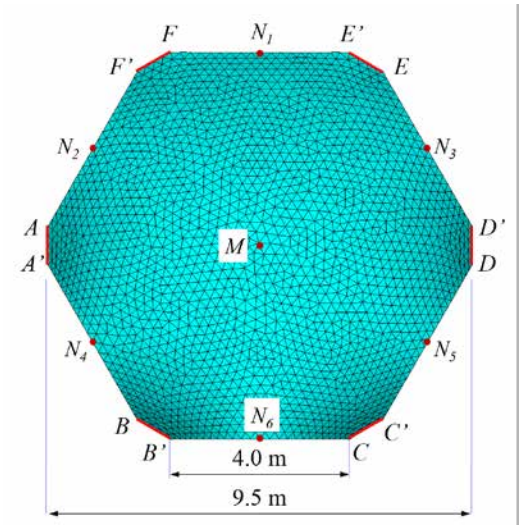


FIGURE 6.12 Initial conditions of *Example 6.3*.

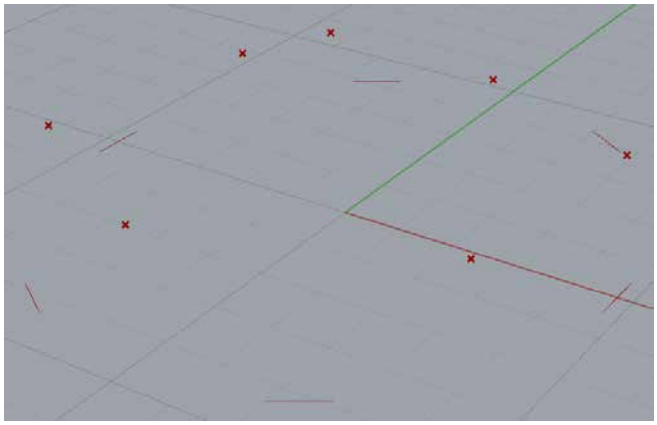
Using seven points with the required target heights and six support lines, the initial structural model can be established in Rhino-Grasshopper based on the NURBS technique. The modelling process of the initial structural model is shown in Figure 6.13, which contains three steps: modelling the seven points and six support lines, modelling six interpolated boundary curves and three interpolated curves using the 'IntCrv' command, and modelling the geometry of the initial structural model using

the 'Patch' command. Based on the NURBS technique, the 'IntCrv' command is used to create an interpolated curve through a set of points, and the 'Patch' command is used to create a patch surface through a set of points or curves. Isotropous material properties are used when establishing the initial structural model in this example. Young's modulus of the membrane is 5.0E06 **N/m**^{2}, which is 10 times of that in ***Example 5.2***. This results in a relatively smaller elastic deformation during the numerical analysis via the VFIFE method in this case. Apart from this, other parameters of the membrane and the VFIFE method are the same as in ***Example 5.2***.

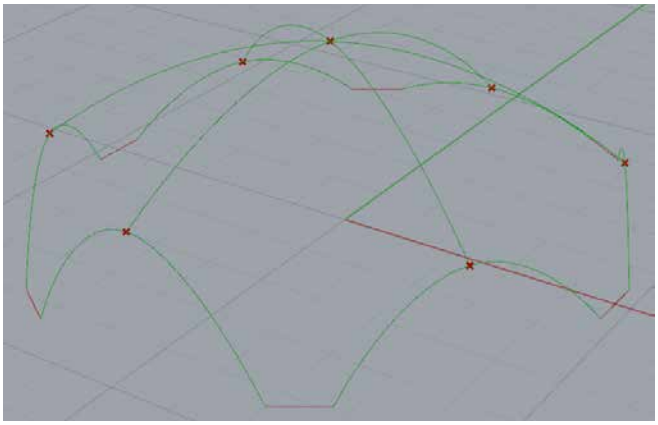
Using the inverse iteration method described above, Form-Control of the equilibrium hanging structural form with an allowable error of 0.001 **m** is conducted. In Table 6.2 and Table 6.3, the structural form with five target heights can be obtained in only four steps of adjustments. It can be observed that the inverse iteration method is effective and efficient to solve this kind of Form-Control problem with multiple target heights. It should be mentioned that the adjustments in the first two steps are much more obvious than those of the following steps, which illustrates that the initial model established by the modelling method above is relatively close to a hanging equilibrium shape. However, wrinkles occur near the supports after Form-Finding. To solve this problem, a secondary adjustment of the final equilibrium structural form should be processed.

To observe the wrinkles in the structural form more clearly, a finer mesh of the initial structural model in Step 4 is used. With this mesh, the equilibrium structural form that can meet these architectural requirements after Form-Finding, is shown in Figure 6.14. It can be seen that the wrinkles in the structural form are much pparent. Using the 'Patch' command in Rhino-Grasshopper, the wrinkles of the structural form can be eliminated, as shown in Figure 6.15.

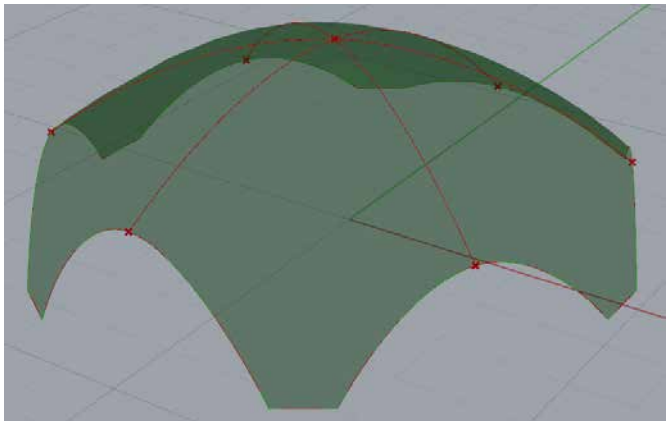
Structural static analysis of this form-controlled shell structure under its self-weight is also conducted here. In this example, the thickness, boundary conditions and material properties are same as in ***Example 5.2***. Because there are some errors when establishing the initial model of this structure in Rhino, the form-found shell is not a perfectly symmetric one. After analysis, the two stress ratios and the strain-energy ratio are presented in Figure 6.16, Figure 6.17 and Figure 6.18. Similar to ***Example 5.2*** and ***Example 6.2***, relatively large bending moments occur in small parts near the free edges. However, it can still be concluded that this Form-Controlled shell structure with five target heights has good shell behaviour, see Figure 6.18 (b).



(a) Points.



(b) Lines.



(c) Surface.

FIGURE 6.13 Figure 6.13: Modelling process of the initial structural model of ***Example 6.3***.

STEPS	HEIGHT OF *M*	HEIGHT OF *N1*	HEIGHT OF *N2/ N3*	HEIGHT OF *N4/ N5*	HEIGHT OF *N6*
Step 1	3.000	0.500	1.000	1.500	2.000
Step 2	2.755	0.317	0.863	1.362	1.874
Step 3	2.751	0.278	0.868	1.372	1.869
Step 4	2.748	0.266	0.870	1.366	1.869

TABLE 6.2 Adjustment process of ***Example 6.3*** (m).

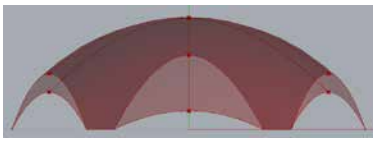
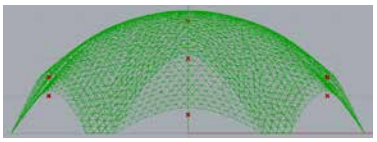
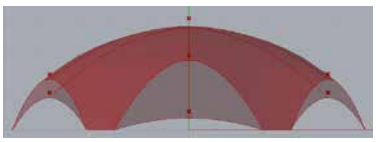
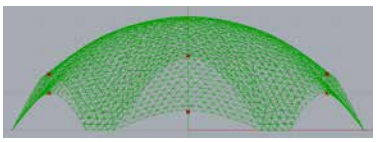
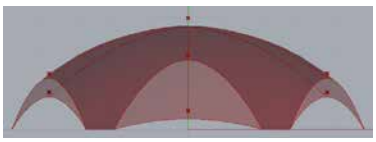
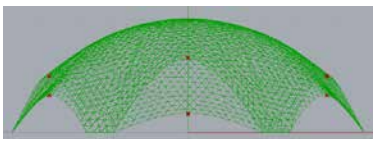
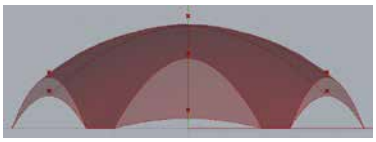
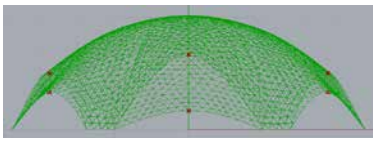
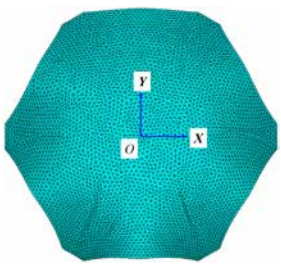
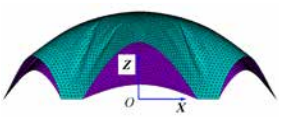
STEPS	INITIAL STRUCTURAL MODEL	EQUILIBRIUM STRUCTURAL FORM
Step 1		
Step 2		
Step 3		
Step 4		

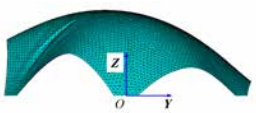
TABLE 6.3 Adjustment process of ***Example 6.3***.



(a) Top view.

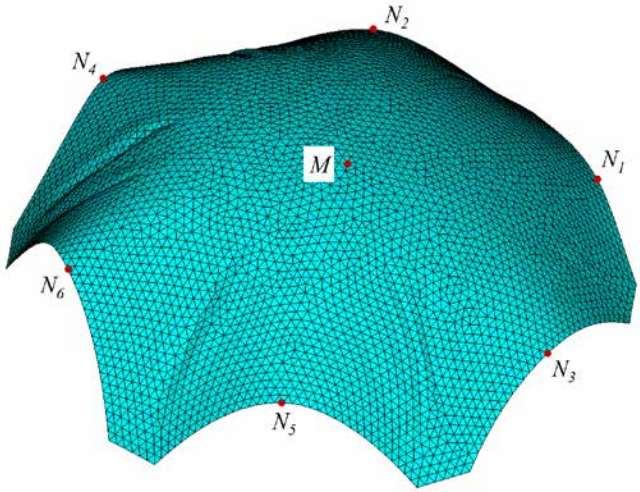


(b) Front view.



(c) Right view.

TOC



(d) Perspective view.

FIGURE 6.14 Form-Control result of ***Example 6.3*** with a finer mesh.

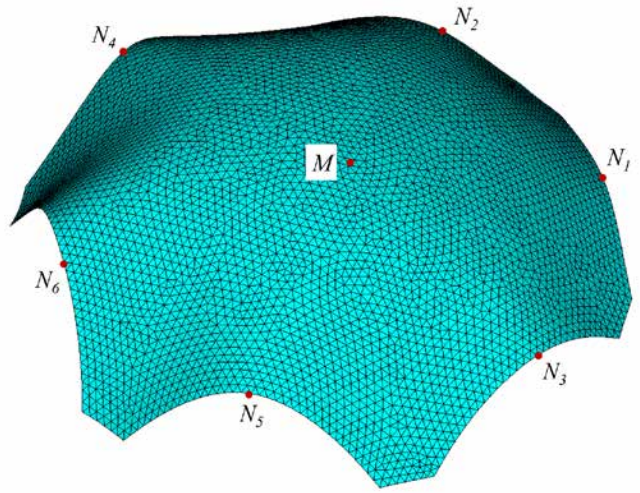


FIGURE 6.15 Smooth result of ***Example 6.3***.

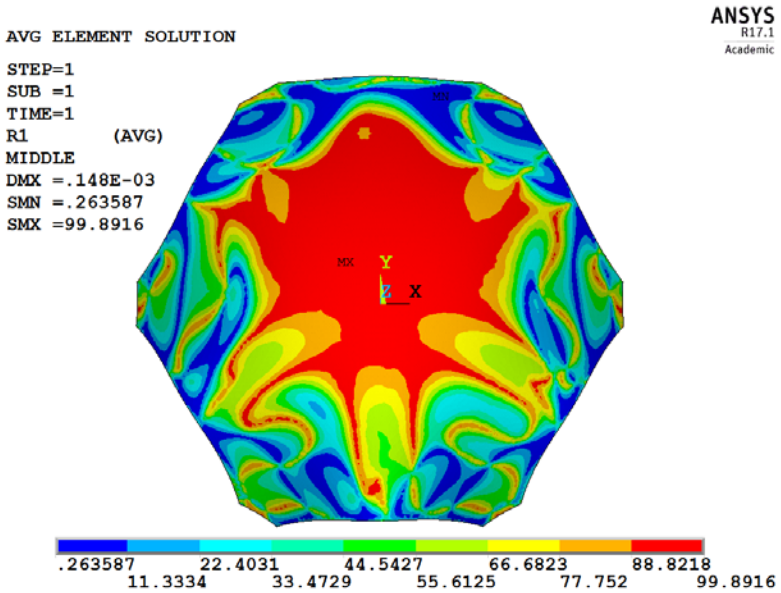


FIGURE 6.16 Stress ratio R_1 of the *Example 6.3* (%).

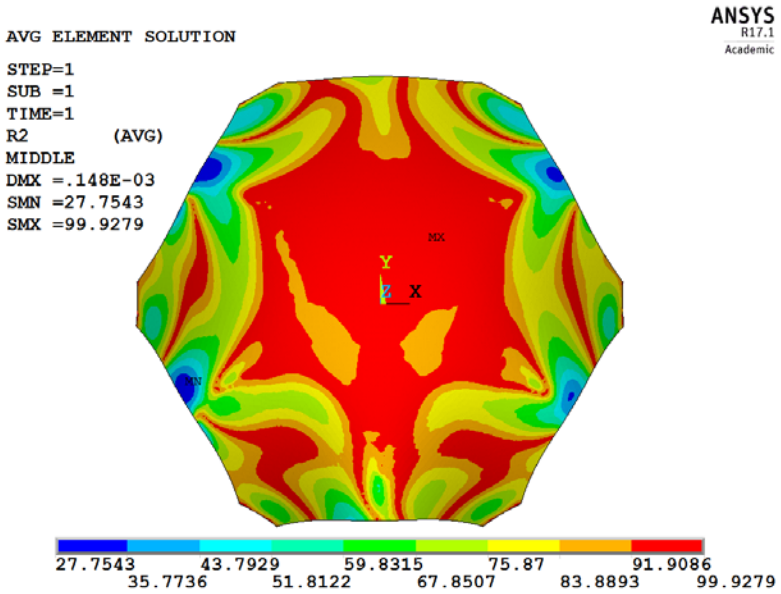
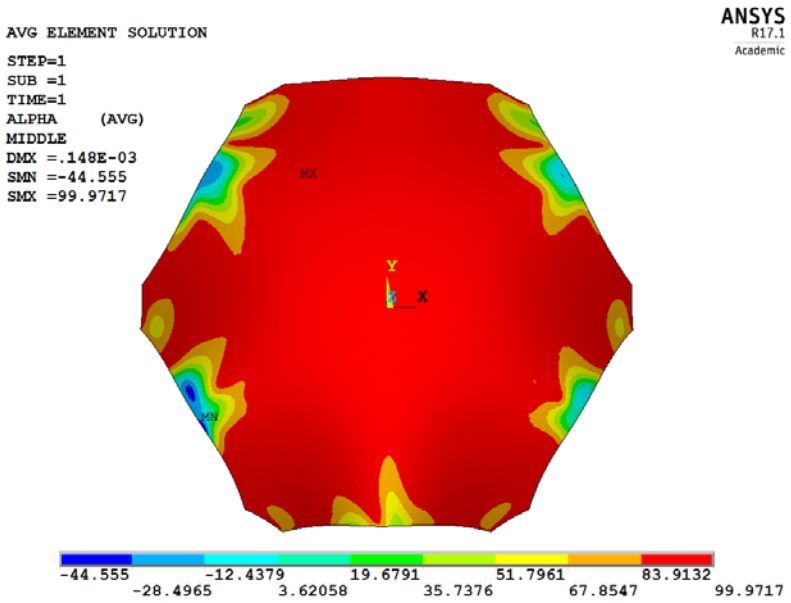
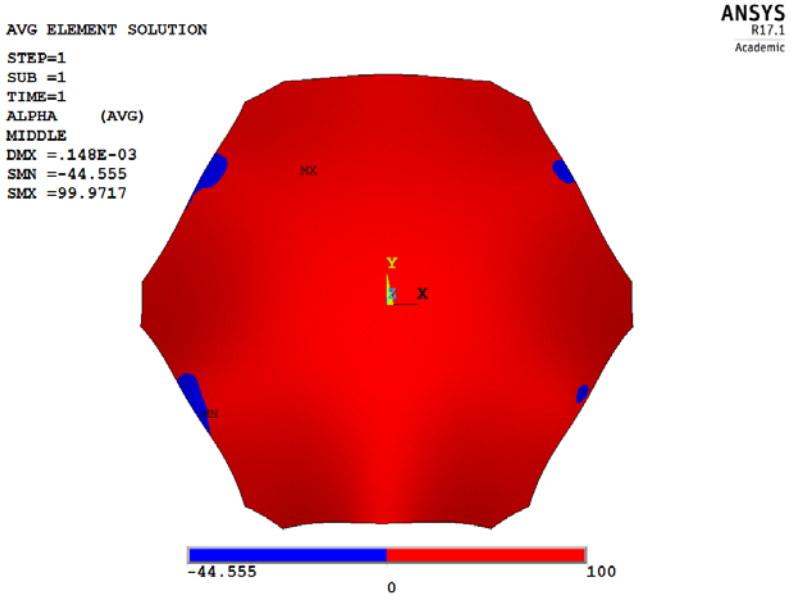


FIGURE 6.17 Stress ratio R_2 of *Example 6.3* (%).

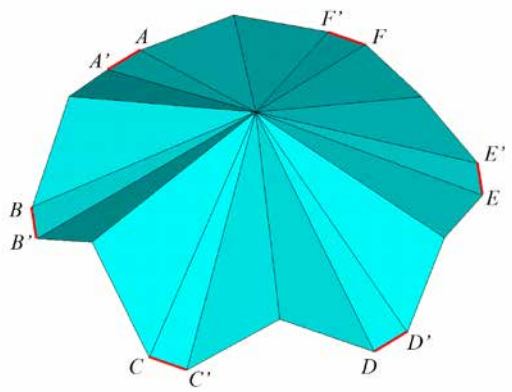


(a) α with ten values of contours (%).

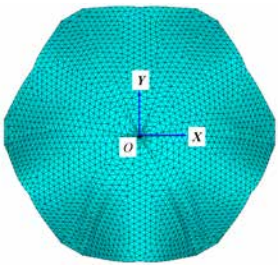


(b) α with three values of contours (%).

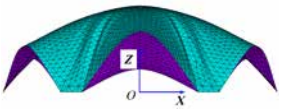
FIGURE 6.18 Strain-energy ratio α of *Example 6.3* (%).



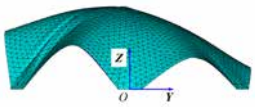
(a) Initial structural model.



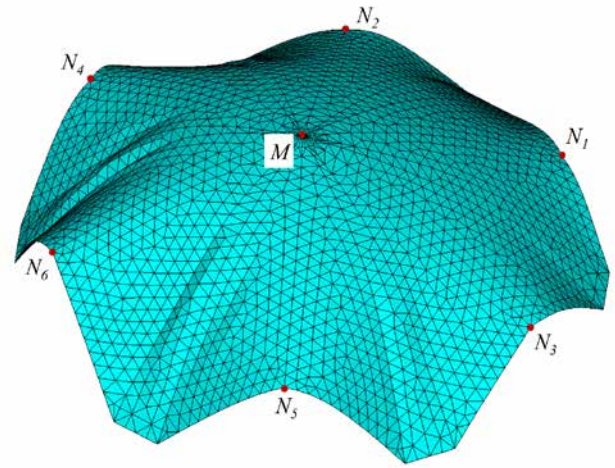
(b) Top view of the form-finding result.



(c) Front view of the form-finding result.



(d) Right view of the form-finding result.



(e) Perspective view of the form-finding result.

FIGURE 6.19 Form-Finding result of ***Example 6.3*** with a fold as the initial model.

Moreover, different modelling methods can also be applied to establish the geometry of the initial structural model in the Form-Control process. To illustrate this problem, a fold model is used in this example to conduct the same Form-Control process. The fold model is established using the seven adjusting points and the six support lines. Figure 6.19 shows the fold model as the initial structural model in the last step and its relevant equilibrium structural form. However, it can be observed that the central point *M* is a cuspidal point in the equilibrium shape when it uses the fold as the initial model. It can be observed clearly that different modelling methods for the initial model can introduce different equilibrium structural forms. In this case, other requirements can be considered to select a suitable modelling method.

§ 6.4 Form-Finding Plug-in in Rhino-Grasshopper

Based on the work from Chapter 5 and 6, a Form-Finding plug-in using C# script is developed in the Rhino-Grasshopper platform. Motivated by the conceptual model of numerical analysis methods shown in Figure 2.2 and the theoretical framework of the Structural Morphology, the plug-in contains three parts with many components:

- The first part with several components is used to deal with the parameters of the initial structural system.
- The second part with one component conducts the calculation process using the VFIFE method.
- The third part with several components is used to present the Form-Finding results.

This plug-in can be used to perform Form-Finding of cable-net structures, membrane structures, and cable-membrane structures under any initial conditions. The main calculation component for hanging membranes is shown in Figure 6.20. By inputting the required initial parameters, the calculation process is carried out in this component, and after that, several parameters of the Form-Finding result are obtained.

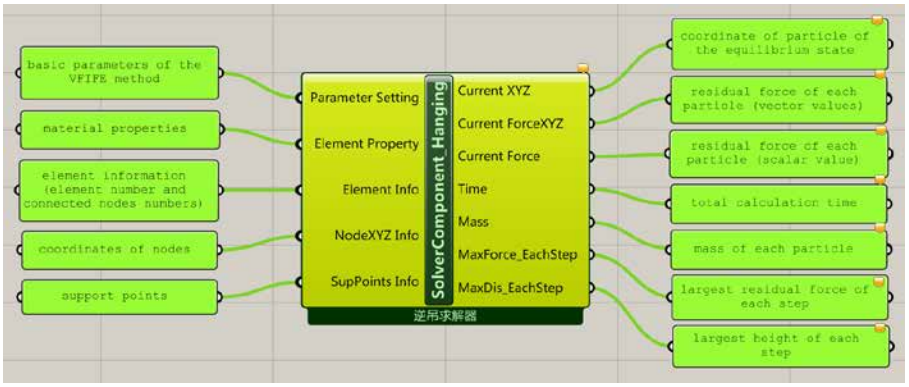


FIGURE 6.20 The calculation component of the plug-in.

Compared with the former workflow (initial modelling in Autodesk, then numerical analysis in MATLAB, and finally displaying the result in AutoDesk or ANSYS), the plug-in greatly reduces the complexity of the work, and effectively improves the efficiency of Form-Finding by reducing the time of data conversion between different software. Compared with the calculation script in MATLAB, the calculation efficiency of this plug-in is considerably improved using compiled programming language and parallel computing on the program. Moreover, a Form-Control process based on the Newton-Raphson method is also included in this plug-in. This substantially improves the work efficiency of Form-Finding. Figure 6.21 shows the assembled components of this Form-Finding tool in Rhino-Grasshopper to perform the Form-Control of ***Example 6.1***.

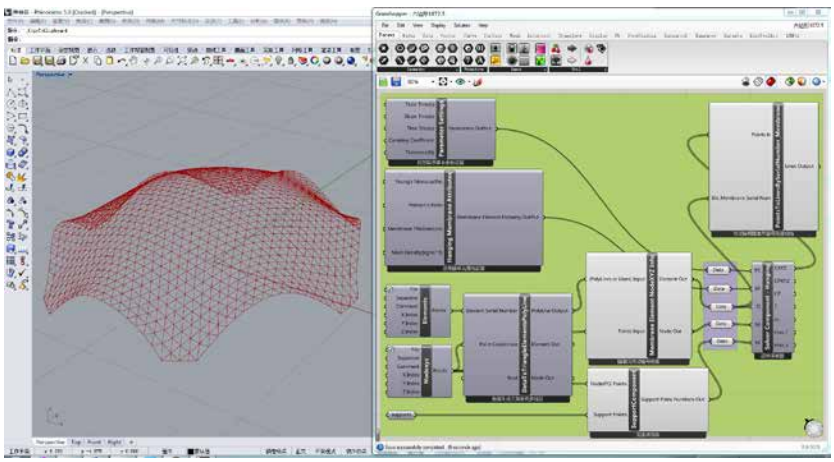


FIGURE 6.21 Assembly of components of ***Example 6.1***.

§ 6.5 Conclusions

In this chapter, From-Control problems of the equilibrium structural form with a single target height and multiple target heights are discussed, and two relevant Form-Control strategies are proposed. These strategies can help architects or engineers determine the structurally efficient geometry in the design process much more easily. The key conclusions are as follows:

- By introducing the Newton-Raphson method, a Form-Control strategy to generate the equilibrium structural form with a single target height is proposed. The principle of this strategy is using the Newton-Raphson method to select the specific Young's modulus of the initial structural model. After Form-Finding for this initial structural model, the equilibrium structural form can meet the required single target height. Compared with the Form-Control process using the bisection method, this strategy is more convenient.

- By introducing the inverse iteration method, a Form-Control strategy to generate the equilibrium structural form with multiple target heights is proposed. The principle of this strategy is using the inverse iteration method to select the specific geometry of the initial structural model. After Form-Finding for this initial structural model, the equilibrium structural form can meet the required target heights. Compared with some complicated optimisation algorithms to obtain the best-fit thrust networks for a target surface, this strategy is much easier and just needs several iterations to meet the requirements.

- Based on the work in Chapters 5 and 6, a Form-Finding plug-in using C# script is developed in the Rhino-Grasshopper platform. This plug-in performs at a much higher efficiency than the former work in MATLAB and other software.

7 Demonstration Towards Diverse Structural Forms

§ 7.1 Introduction

According to the work from **Chapters 2** and **3**, for either a force-active or force-passive structural system, the structural form and its mechanical behaviour are influenced by the five categories of parameters of its initial structural system (Figure 2.5). In this case, during the cooperating design work with architects, structural engineers can also contribute to diverse and reasonable structural forms by adjusting these parameters. As mentioned in **Chapter 4**, it is relatively tedious and time-consuming to make and adjust physical models. Compared with these physical processes, numerical Form-Finding techniques bring a more convenient and efficient approach to generate diverse structural forms with reasonable mechanical behaviour with a very high efficiency.

In this chapter, based on the theoretical framework of Structural Morphology, using these methods developed in **Chapters 5** and **6**, diverse structural forms of form-found shells can be generated.

§ 7.2 Adjusting Strategies for Diverse Structural Forms

In addition, taking shell structures generated from hanging models as research cases, considering the requirements from both architecture and structure, a series of adjusting strategies can be presented by varying the five categories of parameters of the initial structural system during the Form-Finding process. To introduce the adjusting strategies in detail, examples that are secondary developments of ***Example 5.2*** are presented. Heights of the central points for most examples are the same as that of ***Example 5.2***, which means a form-control process developed in **Section 6.2** is included in such examples.

The equilibrium form of a piece of hanging membrane can be generated by the VFIFE method described in Chapter 5. Figure 7.1 presents the initial conditions and the inverted equilibrium hanging structural form of *Example 5.2*.

§ 7.2.1 Strategy by adjusting the parameters of 'geometry'

In this section, adjusting the parameters of 'geometry' refers to modifying the plane shape of the initial structural system. Figure 7.2 presents two initial structural systems with different plane shapes and their relevant form-found shell models in *Example 7.1*. Apart from the plane shapes, other parameters are the same as those in *Example 5.1*. It can be clearly observed and easily understood that differences between the initial geometries have significant influence on the structural forms of these form-found shells. However, it should also be mentioned that it is the architect who oversees the overall shape of the structural forms.

§ 7.2.2 Strategy by adjusting the parameters of 'material properties'

From the former research, it is well known that whether the material is isotropous can significantly influence the Form-Finding results. This will not be covered here. In this work, adjusting the parameters of 'material properties' mainly refers to modifying the elastic modulus of the material used in the initial structural system. From the conclusions discussed in Chapter 6, the elastic modulus of the isotropous hanging membrane material can also influence the Form-Finding results. Figure 7.3 presents just two Form-Finding results with two different elastic moduli of the hanging membrane.

§ 7.2.3 Strategy by adjusting the parameters of 'forces'

In this section, adjusting the parameters of 'forces' refers to modifying the distribution or the typologies of the external loads of the initial structural system. From these numerical examples of Chapter 5, three types of forces clearly lead to different Form-Finding results, which will not be repeated here. Figure 7.4 presents two initial

structural systems with different distributions of the loads and the relevant Form-Finding results. It should also be mentioned that this strategy can lead to diverse structural forms of form-found shells; however, actual load distribution should be considered when structural analyses are conducted.

§ 7.2.4 Strategy by adjusting the parameters of 'material distribution'

In this section, adjusting the parameters of 'material distribution' refers to modifying the mass distribution of one material (the cross section or thickness) and the distribution of varied materials in the initial structural system. Of course, as for varied materials, the properties of each can also influence the structural forms. This can be considered a combined form-diversity strategy by adjusting different typologies of parameters, which is not covered here.

Figure 7.5 presents the initial conditions of two structural systems with different distributions of hanging material and relevant form-found shells, and the initial conditions of two structural systems with different distributions of cable elements inside the hanging material and relevant form-found shells.

§ 7.2.5 Strategy by adjusting the parameters of 'boundary conditions'

In this section, adjusting the parameters of 'boundary conditions' refers to modifying the numbers, positions, lengths, or shapes of the supports of the initial numerical structural system. Figure 7.6 presents the four initial conditions of the structural systems with different supports and the relevant Form-Finding results. Significant differences may occur when the length, number, or the position of the supports change. However, in this example, the shapes of the supports have little influence on the form-found structural forms. Then, an interesting problem appears that how the shapes of the supports influence the mechanical behaviour of the form-found shells. Their influences on the structural behaviour of these shells will be analysed in detail in the following chapters.

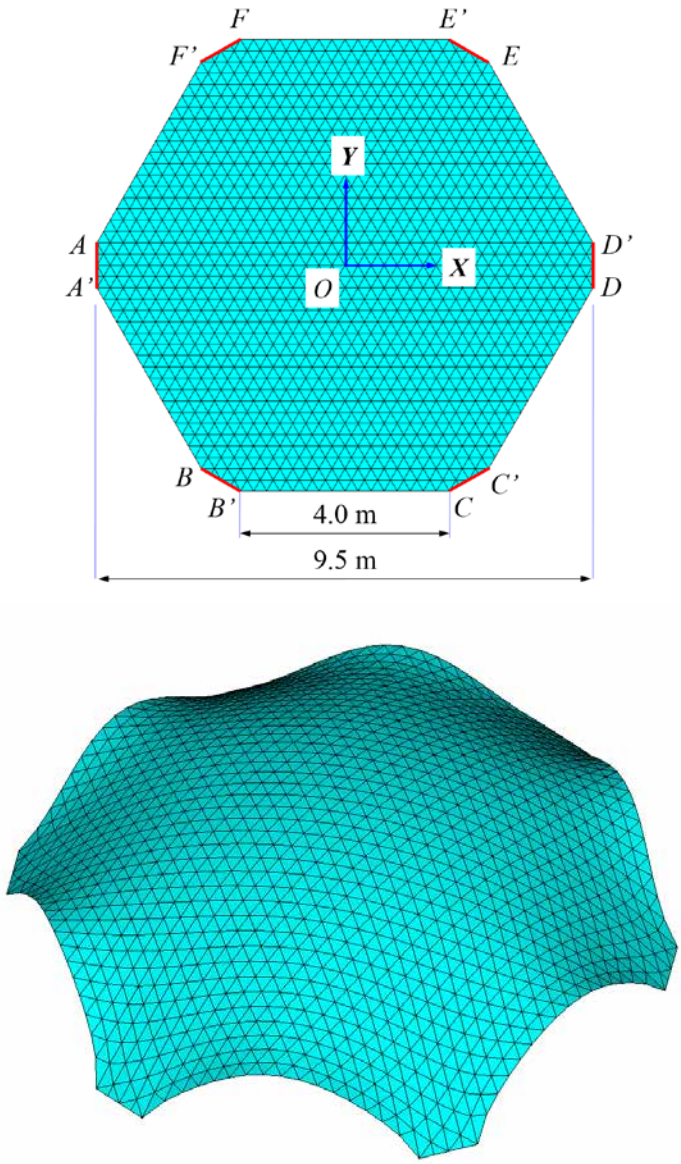
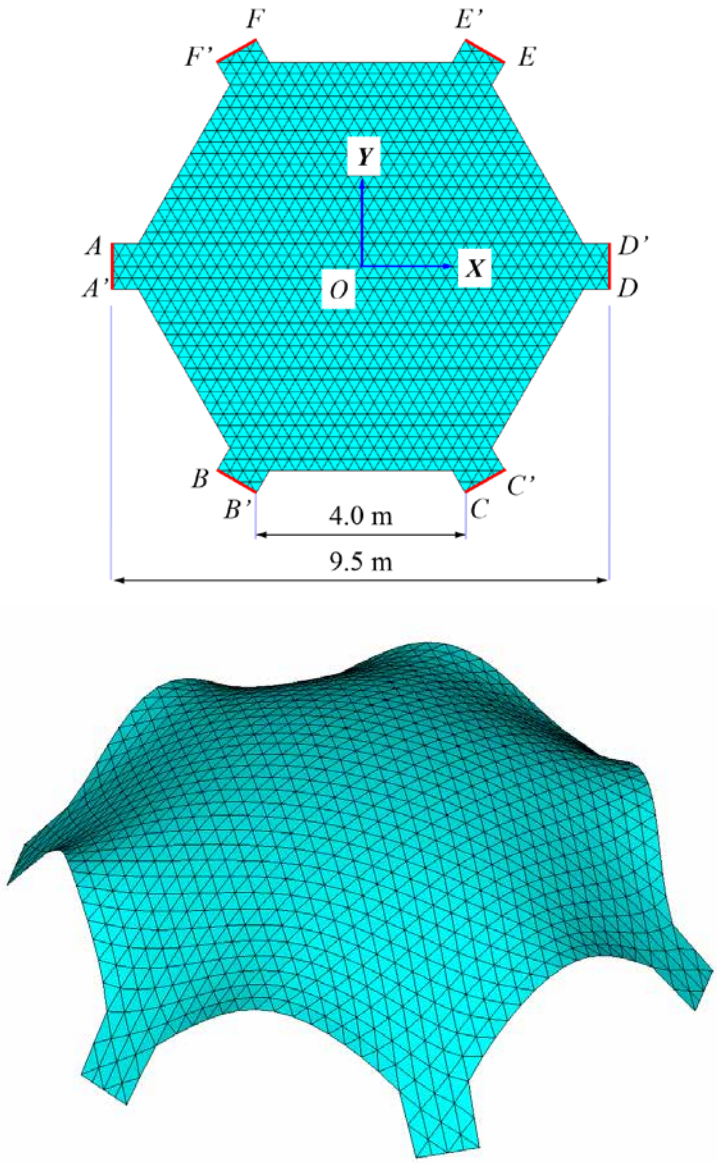
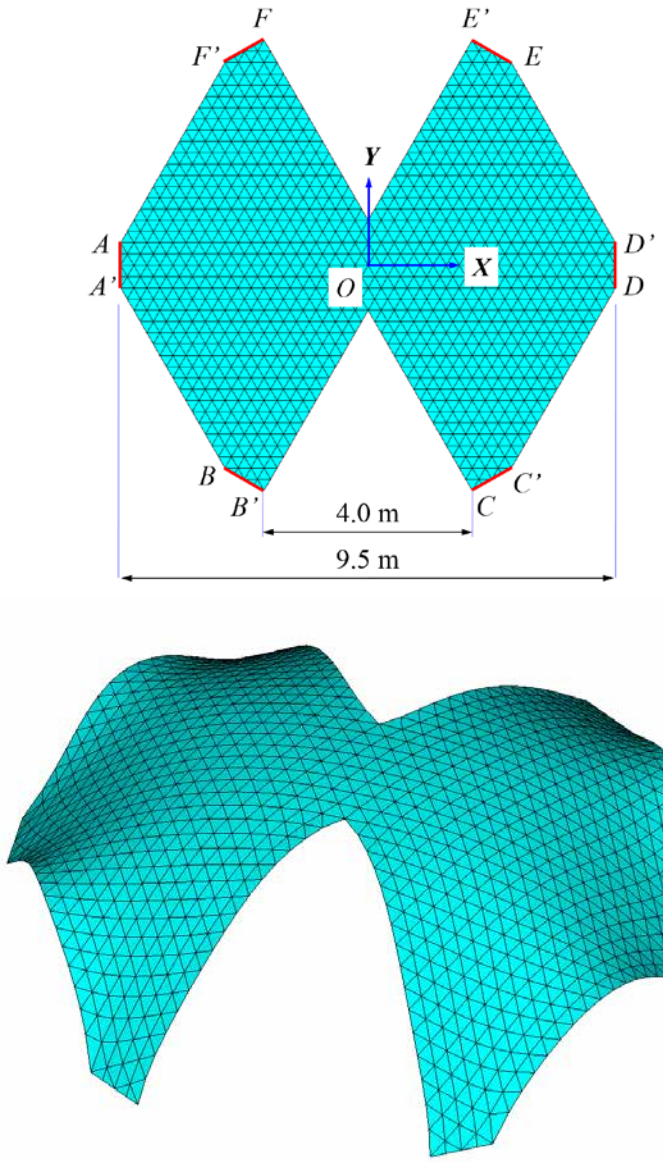


FIGURE 7.1 Initial conditions and Form-Finding result of *Example 5.2*.

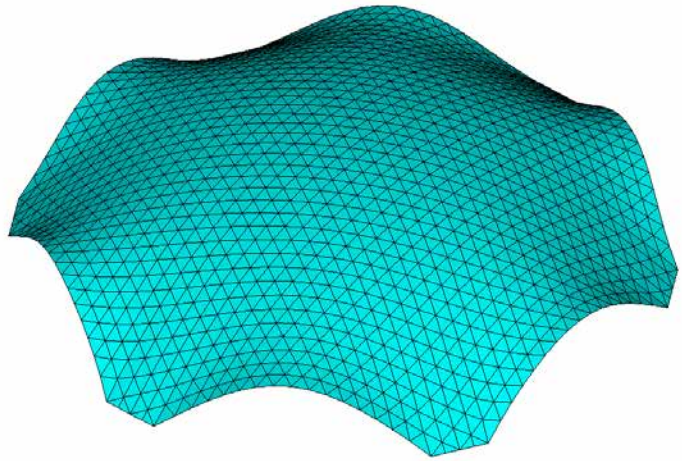


(a) First initial structural system and Form-Finding result.

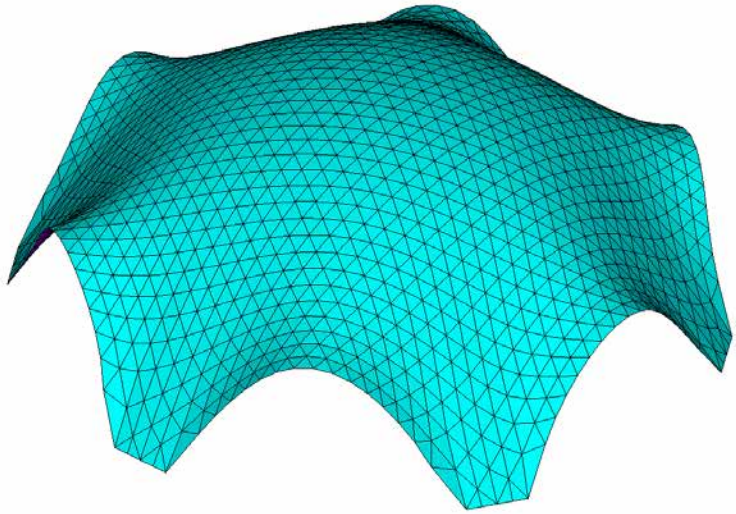


(b) Second initial structural system and Form-Finding result.

FIGURE 7.2 Two initial structural systems and Form-Finding results of ***Example 7.1***.

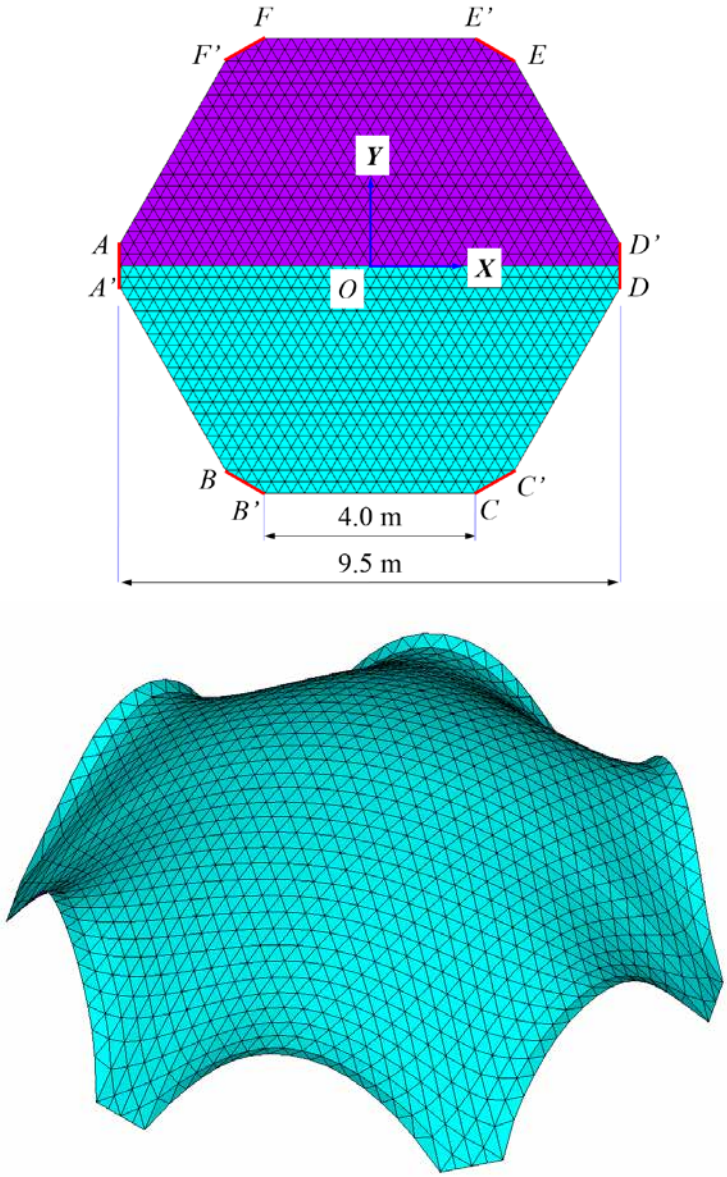


(a) First Form-Finding result with doubled elastic modulus of the hanging membrane of ***Example 5.2****.*

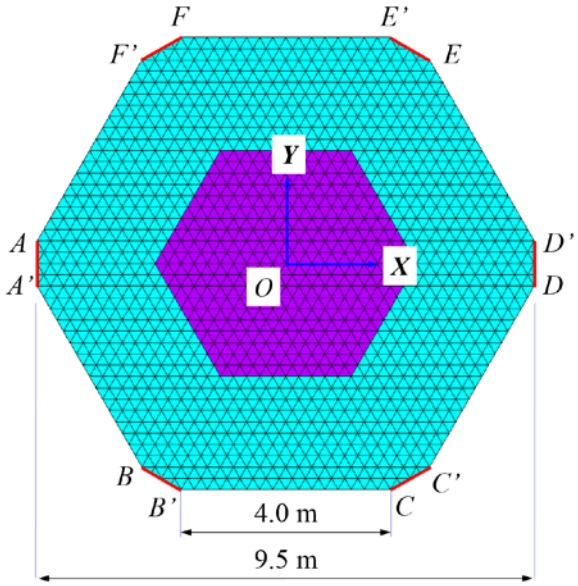


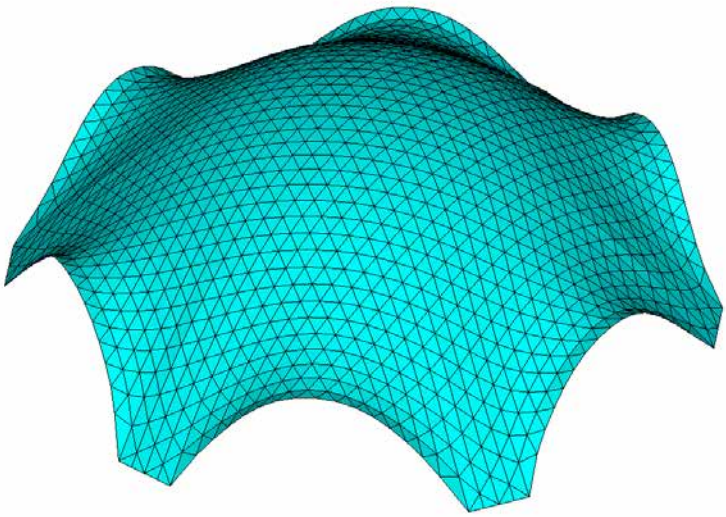
(b) Second Form-Finding result with half elastic modulus of the hanging membrane of ***Example 5.2****.*

FIGURE 7.3 Two Form-Finding results of ***Example 7.2***.



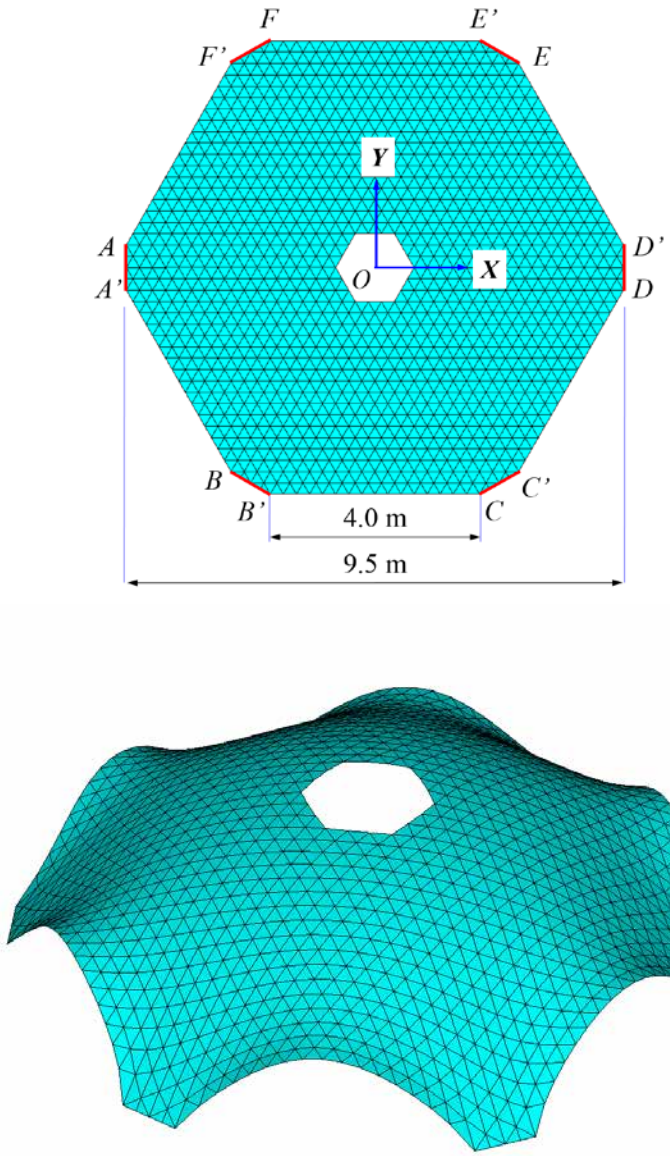
(a) First initial structural system with 2 times the loads in the upper part and its Form-Finding result.



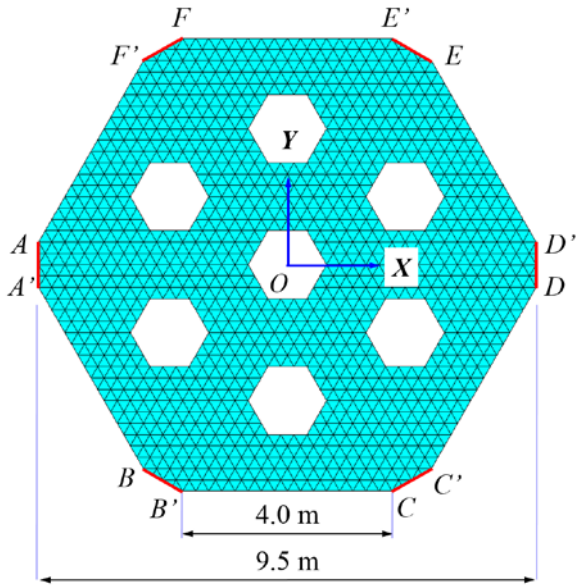


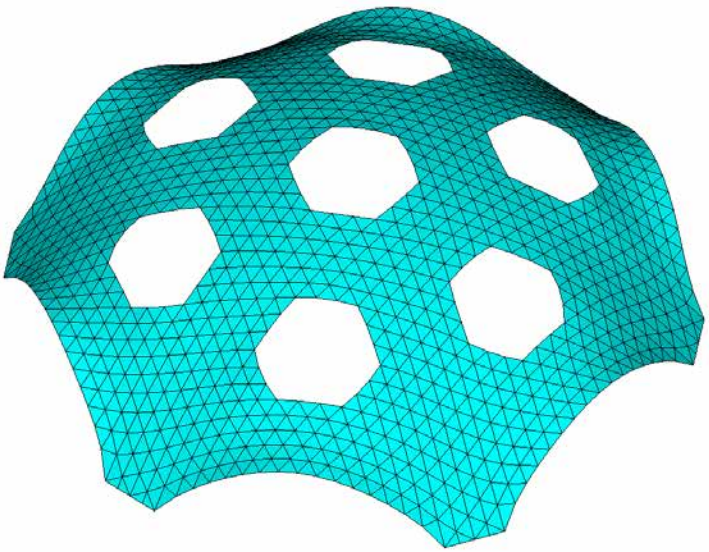
(b) Second initial structural system with 2 times the loads in the central part and its Form-Finding result.

FIGURE 7.4 Two initial structural systems and Form-Finding results of ***Example 7.3***.

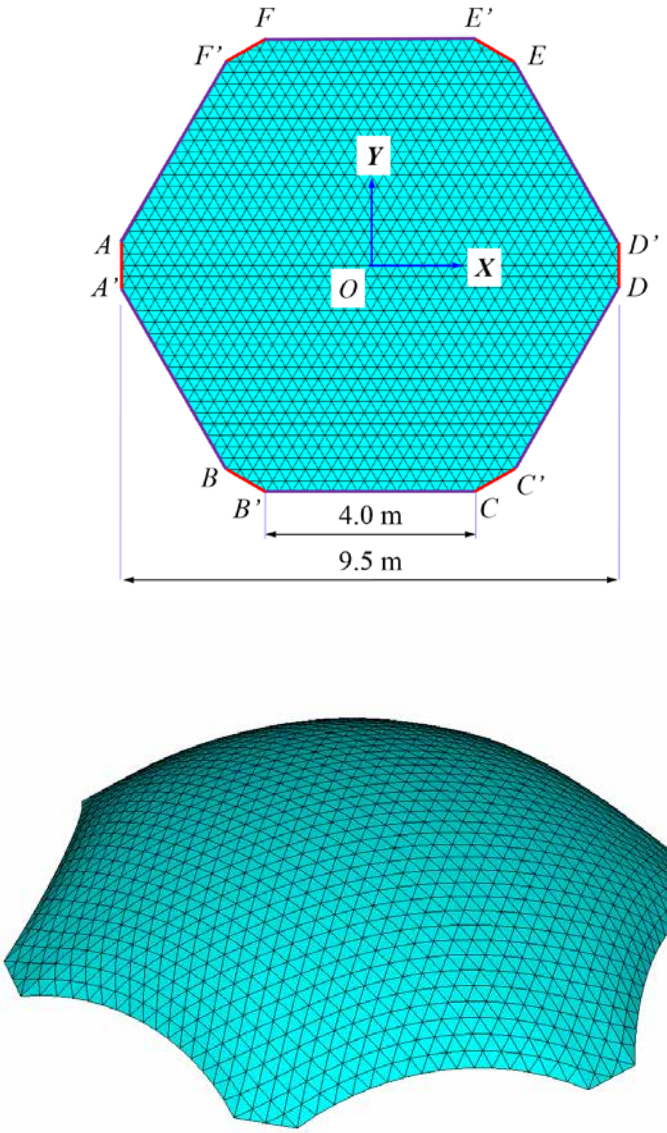


(a) Initial conditions of ***Example 5.2*** *with one hexagonal hole in the central part and the Form-Finding result.*

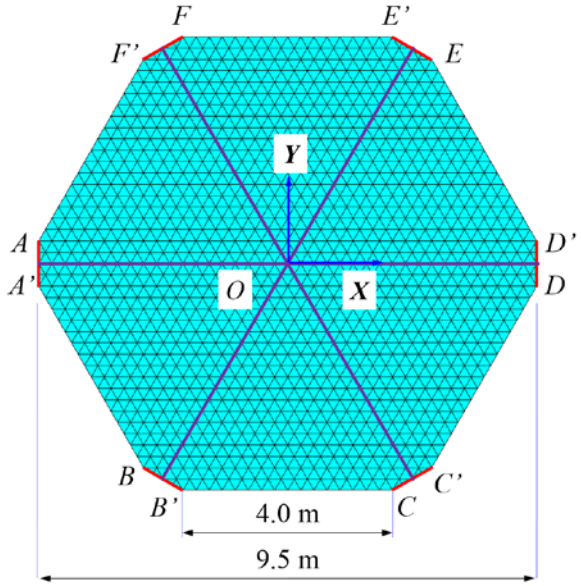


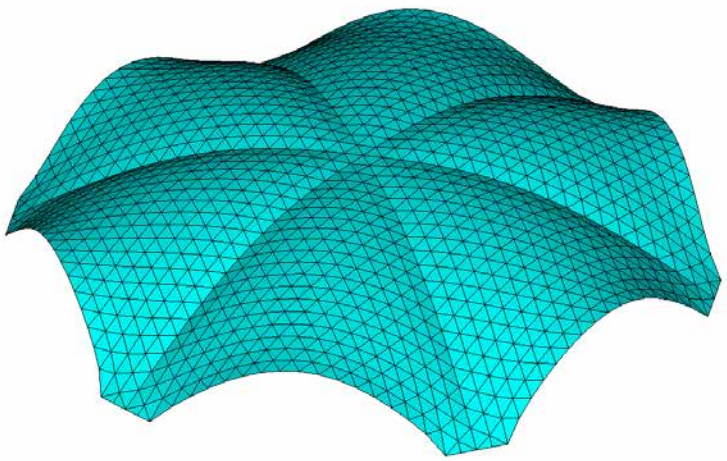


(b) Initial conditions of ***Example 5.2*** *with seven hexagonal holes symmetrically and the Form-Finding result.*



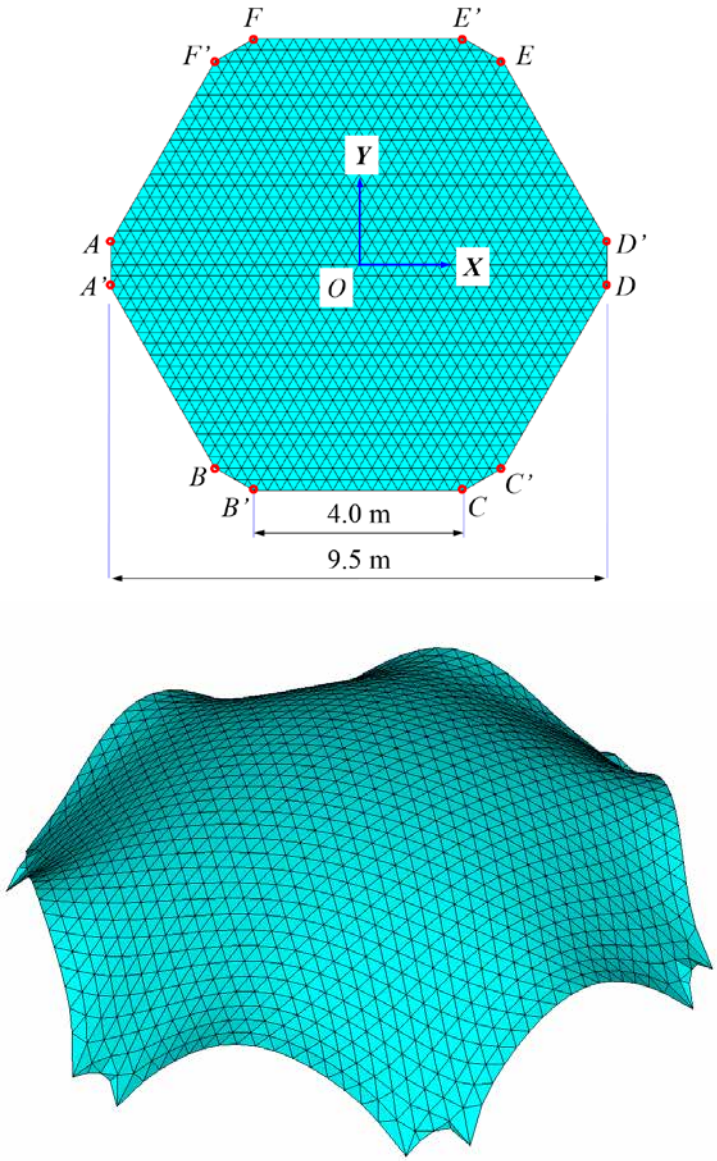
(c) Initial conditions of ***Example 5.2*** *with cable elements in the boundaries and the Form-Finding result.*



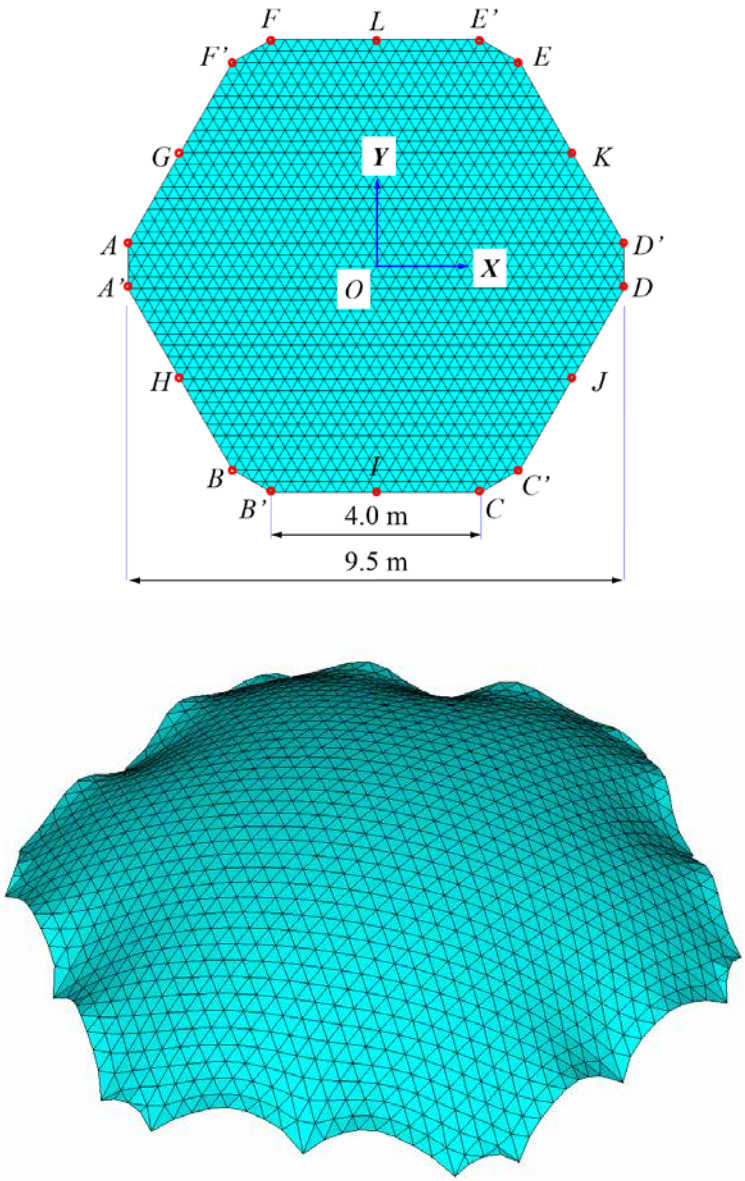


(d) Initial conditions of ***Example 5.2*** *with cable elements in the diagonals and the Form-Finding result.*

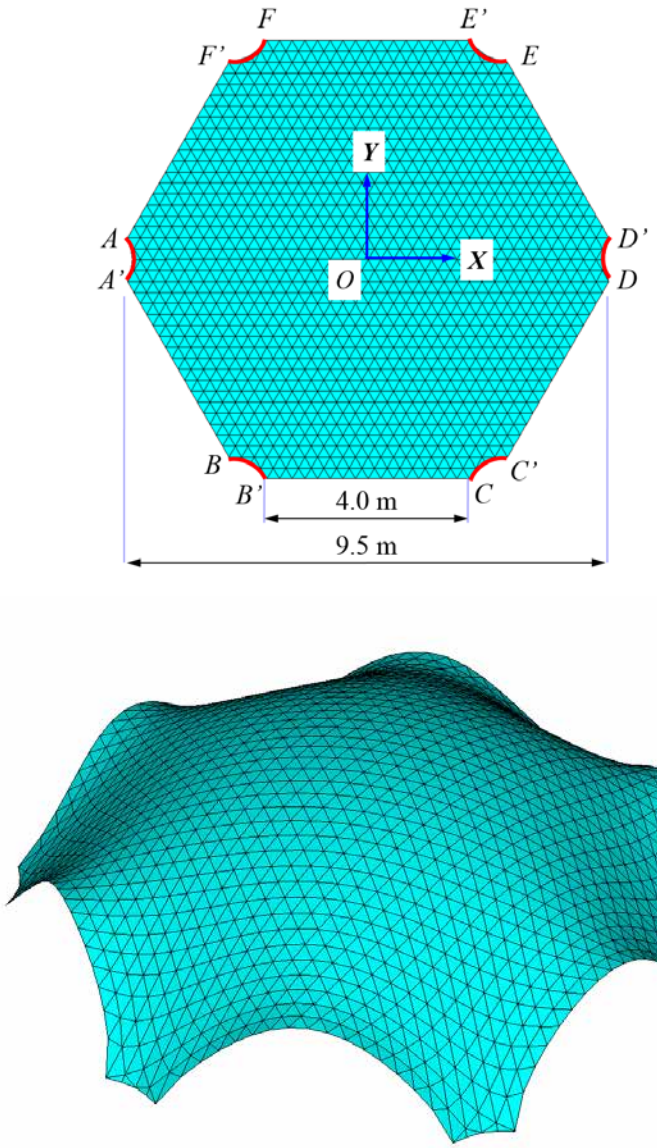
FIGURE 7.5 Four initial structural systems and Form-Finding results ***Example 7.4***.



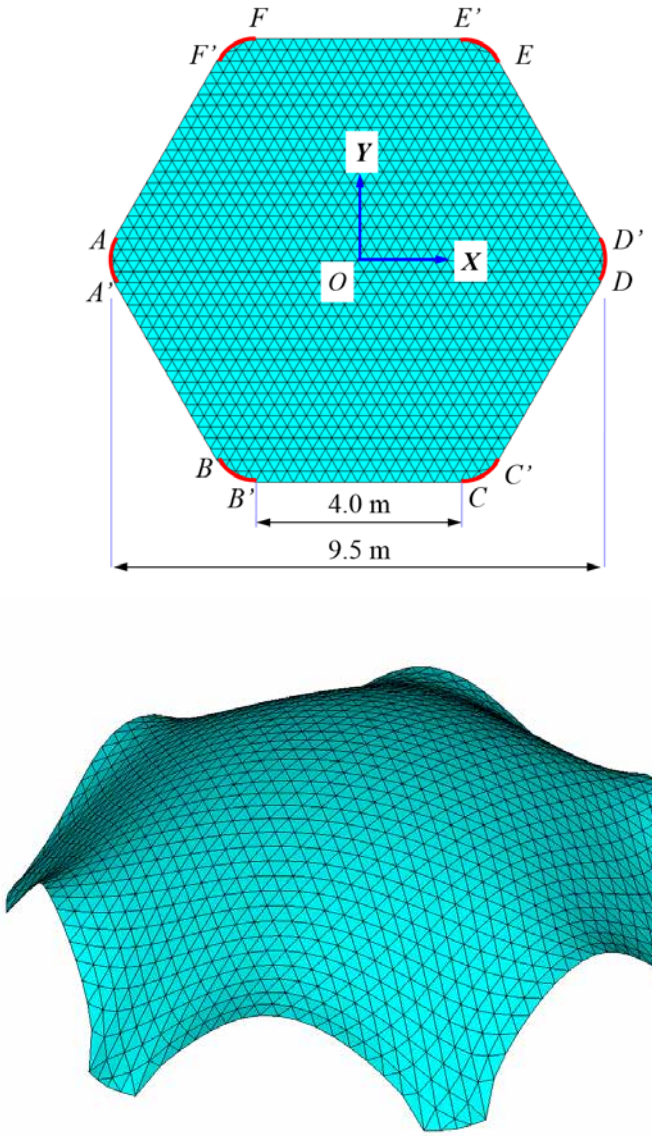
(a) Initial conditions of ***Example 5.2*** *with point supports and the Form-Finding result.*



(b) Initial conditions of ***Example 5.2*** *with more point supports and the Form-Finding result.*



(c) Initial conditions of ***Example 5.2*** *with inward-curved supports and the Form-Finding result.*



(d) Initial conditions of ***Example 5.2*** *with outward-curved supports and the Form-Finding result.*

FIGURE 7.6 Four initial structural systems and Form-Finding results of ***Example 7.5***.

§ 7.3 Conclusions

Based on the theoretical framework of Structural Morphology, clearly the different sets of these parameters of the initial structural systems will influence the eventual structural form and behaviour. Demonstration towards diverse form-found structural forms is discussed in this chapter. The primary conclusions are as follows:

- Diverse structural forms can be obtained by adjusting the five categories of parameters of the initial structural systems during the Form-Finding process. These techniques overcome many disadvantages of physical Form-Finding methods, such as their complicated model manufacturing, adjustment and recording processes. It can be expected that more diverse structural forms could be obtained from combinations of these strategies.

- During the work of this chapter, it is found that some parameters of the initial structural system may lead to structural forms with invisible differences after Form-Finding. For example, Figures 7.1, 7.6(c) and 7.6(d) illustrate that the curvatures of the supports have little influence on the structural forms of form-found shells. However, their influence on the mechanical behaviour of these form-found shells is not clear. Detailed research on this point will be discussed in the next part of the thesis.

- However, it still must be noted that the diversities of structural forms should combine with the specifications of engineering practices and should also meet architectural requirements. Therefore, the parameters cannot be optionally adjusted in the process of Form-Finding. Only in this way can the method be feasible in practical projects.

PART 4 Influence of Support Shapes on Form-found Shells

TOC

TOC

8 Influence of Support Shapes: Numerical Research

§ 8.1 Introduction

It can be concluded from Chapter 7 that different combinations of the five categories of parameters of the initial structural systems during the Form-Finding process can lead to diverse structural forms. However, small differences of some parameters may have less noticeable influences on structural forms but unclear influences on the structural behaviour of form-found shells. In this chapter, taking the parameters of boundary conditions as research cases, the influence of support shapes on the structural form and the mechanical behaviour of shells generated from hanging models is studied in detail.

It is well known that shell structures are extremely parameter sensitive; even minor changes of the initial design may drastically change the internal stress state [139]. A shell structure can be described by the curved shape of the middle surface, thickness distribution and supports. Among others, the 3D shape and thickness distribution are always emphatically considered during the design process of the shell structure. Thus, Form-Finding and Structural Optimisation techniques are commonly used to improve the structural efficiency of a shell. A lot of research has been done and is continuously being done in these fields (see [140]-[147], to mention a few). Figure 8.1 [144] illustrates a shape optimisation example finished by Bletzinger. It can be observed clearly that the load-carrying capacity for the optimised shell is substantially higher (around 250%) than the original one, but the difference between the optimised and the original shells are apparent.

As for the supports of shells, some research has been done to steer or diversify the structural forms of form-found shells by adjusting the numbers, positions, or shapes of the supports [148][149]. However, few literature studies have contemplated considering the influence of supports on the structural behaviour of shells.

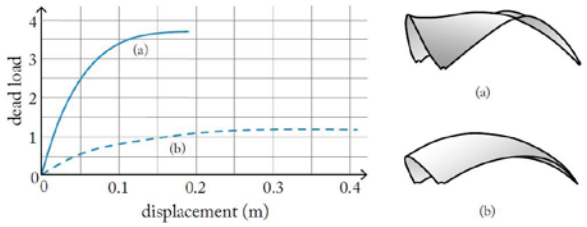


FIGURE 8.1 Nonlinear response of the Kresge Auditorium for (a) the optimised shell and (b) original shell [144].

Shells can be supported in points (Figures 8.2, 8.3 and 8.4) or over some length. Supports over some length can be straight lines (Figure 8.5), inward curves (Figures 8.6 and 8.7), or outward curves (Figure 8.7). In some shells the thickness towards a support is gradually increased (Figures 8.2, 8.3, 8.4 and 8.5). In other shells, the thickness is uniform, but the shape at the support is curved (Figures 8.6 and 8.7). These examples show that there are many ways to support a shell structure.



FIGURE 8.2 Kresge Auditorium [144].



FIGURE 8.3 BP Service Station [144].



FIGURE 8.4 Supporting shell of the Basento Viaduct in Potenza [147].



FIGURE 8.5 Aichtal Outdoor Theatre [144].



FIGURE 8.6 Prototype for the Droneport project [150].



FIGURE 8.7 Tile vault prototype at ETH Zurich [151].

In order to diversify the structural forms, Kilian [148] changed the shape of the supports to steer the structural geometries, shown in Figure 8.8. The author [149] presented a series of strategies to steer forms of shell structures generated from hanging models, including adjusting the numbers and positions of the supports, shown in Figure 8.9. It is obvious to observe the influences of numbers and positions of the supports on the form-found structural forms. Moreover, during the optimisation process of a shell roof, Veenendaal et al. [152] took the shapes of the supports as design variables, shown in Figure 8.10, but influences of the supports on structural forms and behaviour of the optimised shells were not specifically analysed.

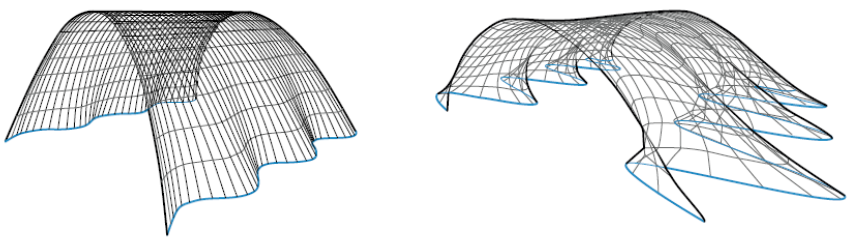


FIGURE 8.8 Structural geometries with different support constraints [144].



FIGURE 8.9 Diverse numerical inverted hanging geometry [149].

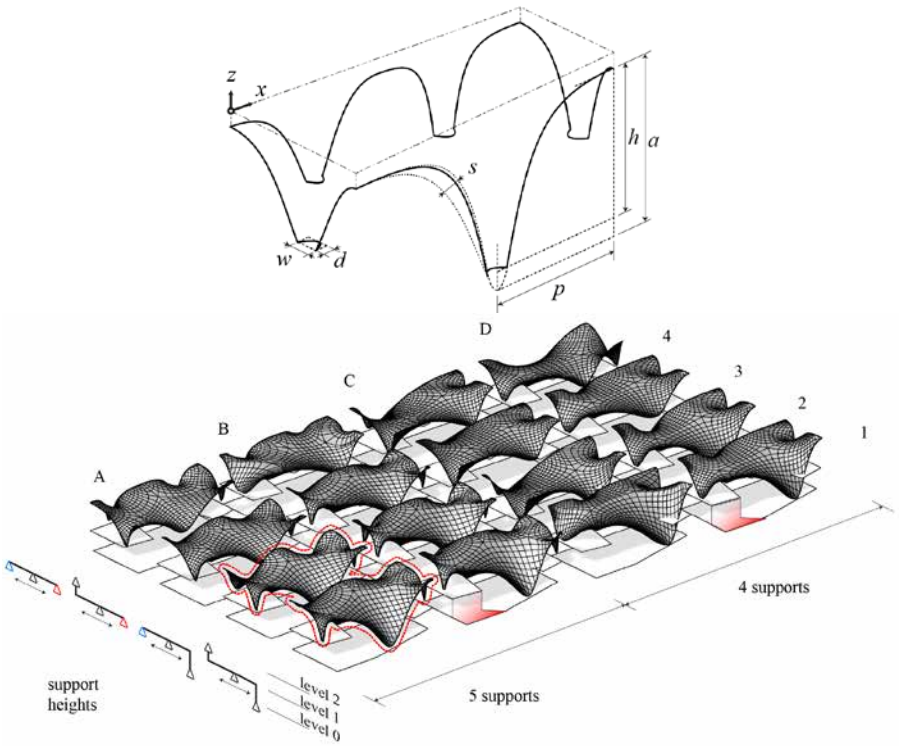


FIGURE 8.10 Design variables of supports and the optimisation results [152].

From the introduction above, individual architects and engineers clearly have qualitative preferences during the from-design process of shells. Intuitively, they remain aware of the importance of the supports. However, there is a need to quantify the consequences of designing particular shell supports. To explain and quantify the research problems, taking shell structures generated from hanging models as research cases, this chapter presents a systematic study of supports over a length with various curvatures.

It is well known that shell structures generated from hanging models have structurally efficient forms [140][147]. Apparently, these forms are influenced by the exact shape of the supports, which can also be observed from the last chapter. The structural behaviour is also influenced by the exact shape of the supports and by the support conditions (fixed or simply supported).

In this chapter, influences of slight changes of the support shapes on the structural forms and on the structural behaviour of shells generated from hanging models will be quantitatively studied. As a general example, four hexagonal shells generated from hanging models are considered. The shell behaviour assessment strategy proposed in Chapter 4 is used to compare the static and the buckling behaviours of these form-found shells. Moreover, nonlinear analyses of these shells are conducted to compare their load-carrying capacities.

§ 8.2 Comparison of Structural Forms of Form-found Shells

In this section, four hexagonal form-found shells with different support shapes but with the same target point are introduced. These shell models are inversed hanging models obtained using the VFIFE method and the Newton-Raphson method. After that, comparison of the coordinates and curvature analysis results between these models are conducted to study the influence of support shapes on the equilibrium hanging structural forms.

§ 8.2.1 Introduction of the form-found shells

The initial conditions of the four hexagonal shells are shown in Figure 8.11-8.14. Supports are at the six corners *AA'*, *BB'*, *CC'*, *DD'*, *EE'* and *FF'*. Four support shapes are considered: straight (*Model A*), outward-curved (*Model B*), inward-curved (*Model C*) and

strongly inward-curved (*Model D*). Among others, *Model A* is same with *Example 6.1* but with a finer mesh.

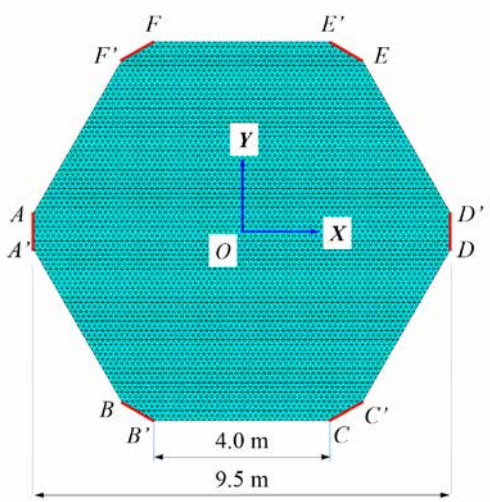


FIGURE 8.11 Initial conditions of *Model A* (shell with straight supports).

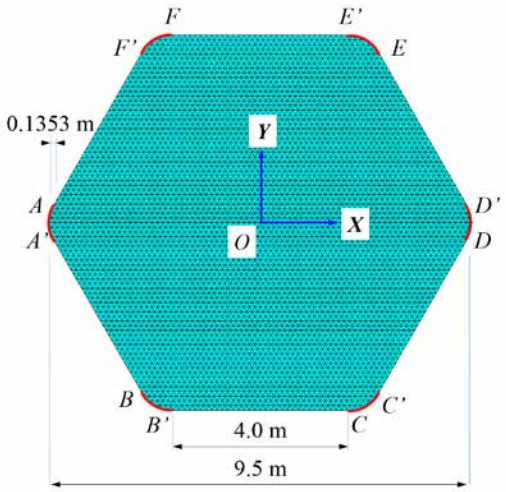


FIGURE 8.12 Initial conditions of *Model B* (shell with outward-curved supports).

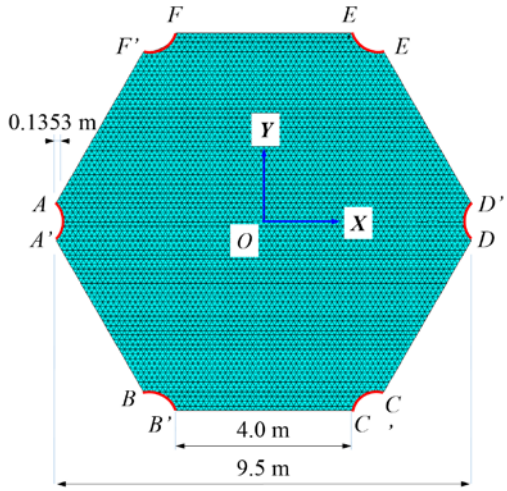


FIGURE 8.13 Initial conditions of *Model C* (shell with inward-curved supports).

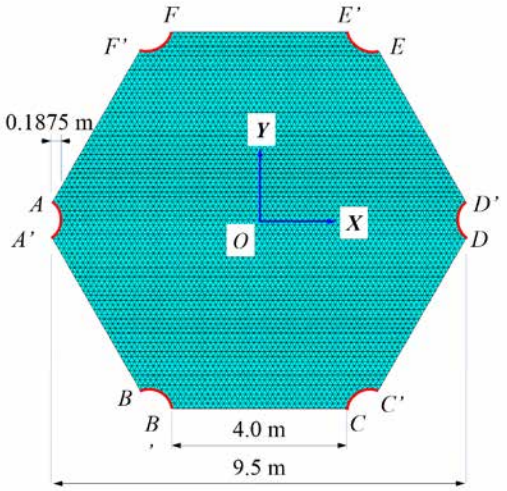
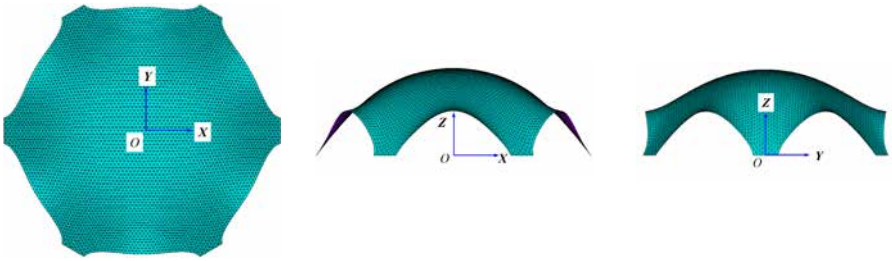


FIGURE 8.14 Initial conditions of *Model D* (shell with strongly inward-curved supports).

Using the VFIFE method and the Newton-Raphson method introduced in Chapter 6, these four inverted equilibrium hanging models can also be obtained (shown in Figures 8.15, 8.16, 8.17 and 8.18). All of them have the same coordinate system (shown in Figure 8.15) and the same target point (the height of the central point is 3.0 m) as *Model A*.



(a) Top view. *(b) Front view.* *(c) Right view.*



(d) Perspective view.

FIGURE 8.15 ***Model A*** (shell with straight supports).

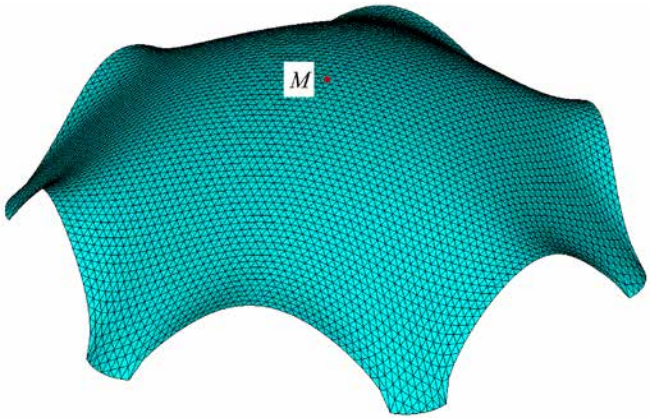


FIGURE 8.16 ***Model B*** (shell with outward-curved supports).

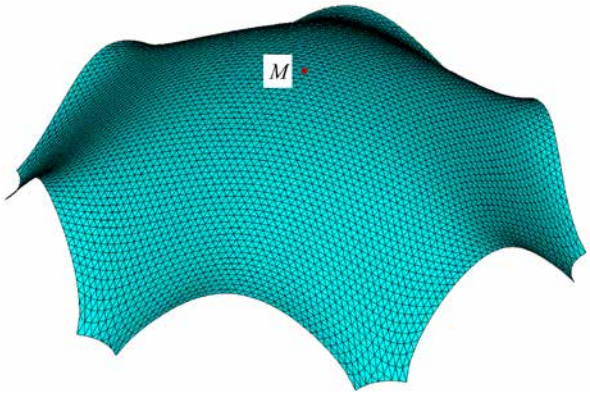


FIGURE 8.17 *Model C* (shell with inward-curved supports).

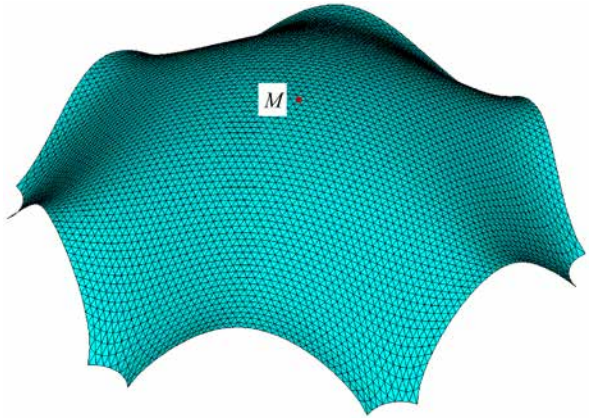


FIGURE 8.18 *Model D* (shell with strongly inward-curved supports).

§ 8.2.2 Comparison of structural forms of the form-found shells

The influence of support shapes on the above four equilibrium hanging structural forms is researched in this section. To do this, direct comparisons of the coordinates between the equilibrium hanging models are conducted, and then the curvature analysis is processed.

1 Coordinate differences between form-found shells

The final *Z*-coordinate results for the middle span section at the *X*-axis of symmetry (*Y* = 0.0) are presented in Figure 8.19. The final *Z*-coordinates for the middle span section at the *Y*-axis of symmetry (*X* = 0.0) are presented in Figure 8.20. From the two graphs, it can be observed that the four equilibrium hanging models have negligible differences in the central parts along the two axes. Because of the difference of the supports, the four equilibrium hanging models have apparent differences near the supports along the *X*-axis. However, they have relatively trivial differences in the parts near the edges along the *Y*-axis.

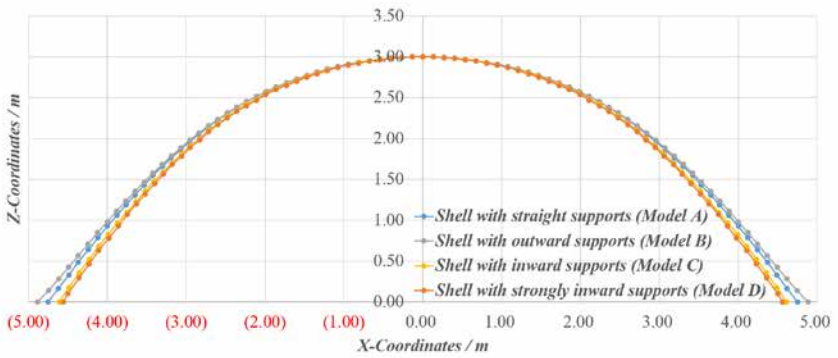


FIGURE 8.19 *Z*-coordinates at the *X*-axis of symmetry (*Y*=0).

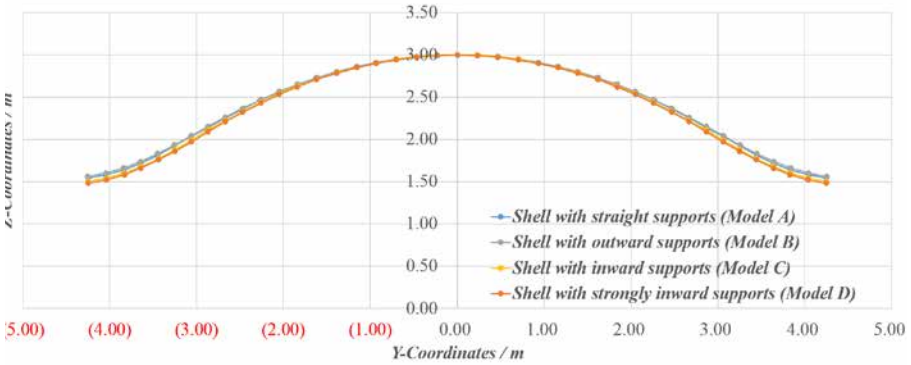


FIGURE 8.20 *Z*-coordinates at the *Y*-axis of symmetry (*X*=0).

2 Curvature analysis of form-found shells

Curvature analysis can be conducted in the Rhino software. Figure 8.21 shows the contour plot of the Gaussian curvature of the four models, where blue colour indicates a positive Gaussian curvature and red indicates a negative curvature. As the shell is symmetric, the results of 1/6 of each are shown here. This figure demonstrates that positive Gaussian curvatures occur in the central parts, while negative Gaussian curvatures occur near the boundaries and supports. The two models with inward-curved supports have a continuous negative Gaussian curvature distribution; however, the models with straight and outward-curved supports have a small portion of positive Gaussian curvature distribution near the supports.

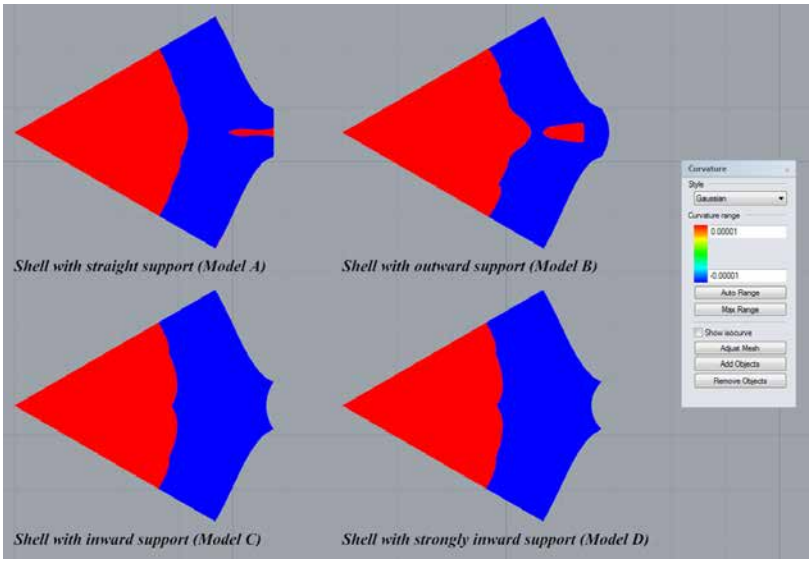


FIGURE 8.21 Gaussian curvature of the four models.

From this section, it can be concluded that the supports influence the shell shape, which is determined in a Form-Finding procedure. However, different support shapes with minor changes have negligible influence on the central parts of the equilibrium hanging models, while relatively significant differences can be observed in the parts near their supports. Specifically, during their Form-Finding processes, straight supports induce an area with zero curvature in one direction. Outward curvatures of the supports are contrary to the curvatures at free edges, and leads to changes of curvatures near the supports. Inward curvatures of the supports are suited to the chosen curvature of the free edges; thus, no flat parts are obtained during the Form-Finding process.

§ 8.3 Comparison of Structural Behaviour of Form-found Shells Under Symmetrical Loads

The shell shape at the supports also considerably influences the shell structural behaviour. In this section, the structural analysis results of these form-found shell structures symmetrically with a distributed dead load are compared in detail to study the influence of support shapes and conditions (fixed or simply supported) on the structural behaviour of the form-found shells.

NAME	MODELS
Model A_s	*Model A* (shell with straight supports) simply supported at six corners
Model A_f	*Model A* (shell with straight supports) fixed supported at six corners
Model B_s	*Model B* (shell with outward supports) simply supported at six corners
Model B_f	*Model B* (shell with outward supports) fixed supported at six corners
Model C_s	*Model C* (shell with inward supports) simply supported at six corners
Model C_f	*Model C* (shell with inward supports) fixed supported at six corners
Model D_s	*Model D* (shell with strongly inward supports) simply supported at six corners
Model D_f	*Model D* (shell with strongly inward supports) fixed supported at six corners

TABLE 8.1 Structural analysis models.

To do this, these four equilibrium hanging models are simply supported and fixed supported respectively, and three types of structural analysis (static analysis, linear buckling analysis, and non-linear analysis) for each analysis model are conducted using the ANSYS software. Eight models are analysed in this section and explained in Table 8.1. The element type SHELL181 is used to establish these eight finite element models. The material of these shell models is reinforced concrete, and all the eight shells have a uniform thickness of 0.04 m.

§ 8.3.1 Linear static analysis

Structural static analyses under a symmetrically distributed dead load of these eight shells are conducted in this part. The reinforced concrete material in this analysis is in the elastic phase with a Young's modulus of 3.36E10 N/m^2 and a Poisson's ratio of 0.20. The load added to the shell is 5.0E3 N/m^2 vertically, which has a same distribution as this hanging model.

After analysis, different types of analysis results can be output. Further, Stress Ratios in the directions of the principal normal forces with secondary treatment of the direct finite element analysis results and the results of principal stresses at the middle surface of the shell, which can be outputted directly from ANSYS, are assessed. Taking *Model A_S* (a shell with simply supported straight supports) as an example, its analysis results can be represented as follows.

1 Stress Ratios in the directions of the principal normal forces

To assess whether a shell carries its load efficiently, the relation between the membrane stresses and bending stresses in this shell can be researched. The ratios between membrane stresses and total stresses caused by the bending moments and normal forces in the directions of the principal normal forces, which were introduced in Chapter 4, are considered in this section.

By secondary programming of the analysis results from ANSYS, the two Stress Ratios of this form-found shell can be obtained as shown in Figures 8.22 and 8.23. As both the shell and loads are symmetric, the results of a 1/6 portion are shown here. These two pictures plainly illustrate the ratios R_1 and R_2 are more than 80% in the central part of the shell, which indicates optimal shell behaviour in either principal direction, while, in the parts near the boundaries and supports, relatively large bending moments occur. It can be concluded that as the shell is form-found and thus loads mainly transferred by normal forces. However, the two principal directions of normal forces cannot be identified from these two pictures. As principal stresses at the middle surface of the shell can represent the load paths of the normal forces, these results will be subsequently presented.

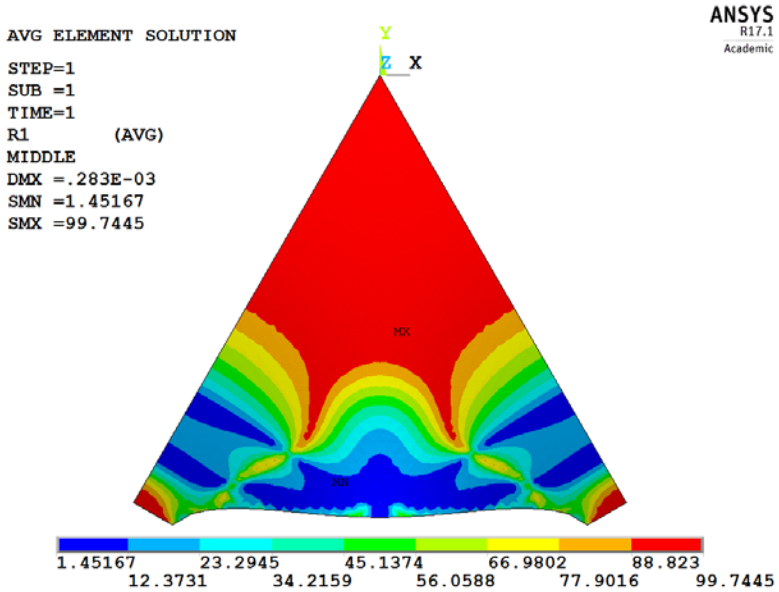


FIGURE 8.22 R_1 of Model A_5 (shell with simply supported straight supports; %).

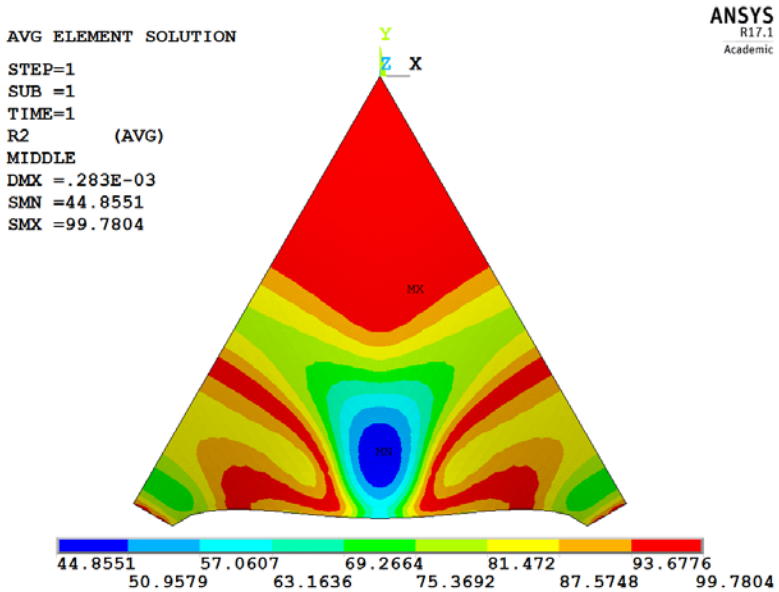


FIGURE 8.23 R_2 of Model A_5 (shell with simply supported straight supports; %).

2 Principal stresses at the middle surface of the shell

Contour plots and vectorial representations of the principal stresses (S_1, S_2, and S_3) at the middle surface of the shell can be output directly from the finite element software. Figures 8.24-8.26 are the contour plots of principal stresses S_1, S_2, and S_3, Figures 8.27 and 8.28 are their vectorial representations. In these contour plots, principal stresses are positive for the tension stress state, and negative for the compression stress state. In these vectorial plots, the directions of the arrows indicate the tension or compression stress of each element, and the size of the arrows indicates the magnitude of the principal stress. All the five pictures (Figures 8.24-8.28) demonstrate that the principal stress is negligible in the perpendicular directions of the shell, while the principal stresses are in compression stress states in the other two perpendicular principal directions in the plane tangent of the shell.

All analysis results above clearly demonstrate that the loads transfer to the supports primarily by normal in-plane compression forces, and that the shell performs good shell behaviour. As this shell is form-found, the forces are in the tangent plane at the supports. The third principal stress S_3 near the supports can represent the reaction forces of the shell. It can be seen that stress concentrations occur at the two ends of each support.

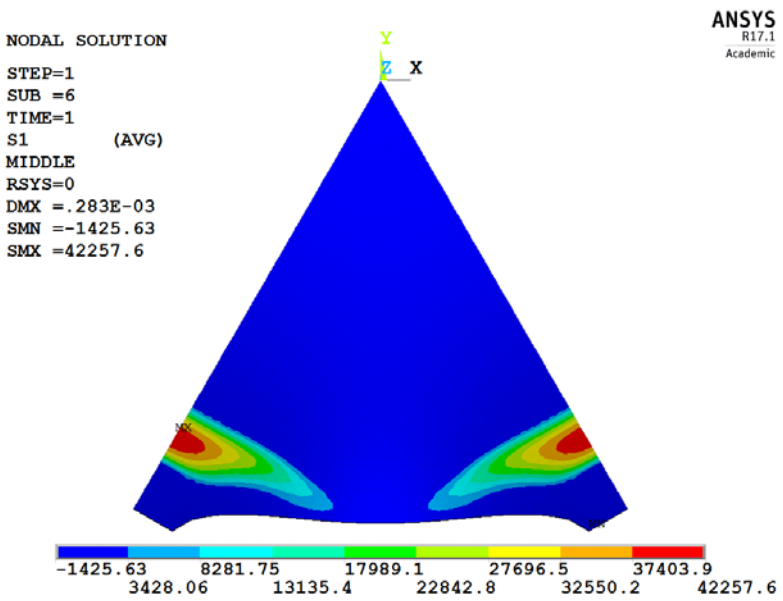


FIGURE 8.24 Principal stress S_1 at the middle surface of Model A_5 (shell with simply supported straight supports; Pa).

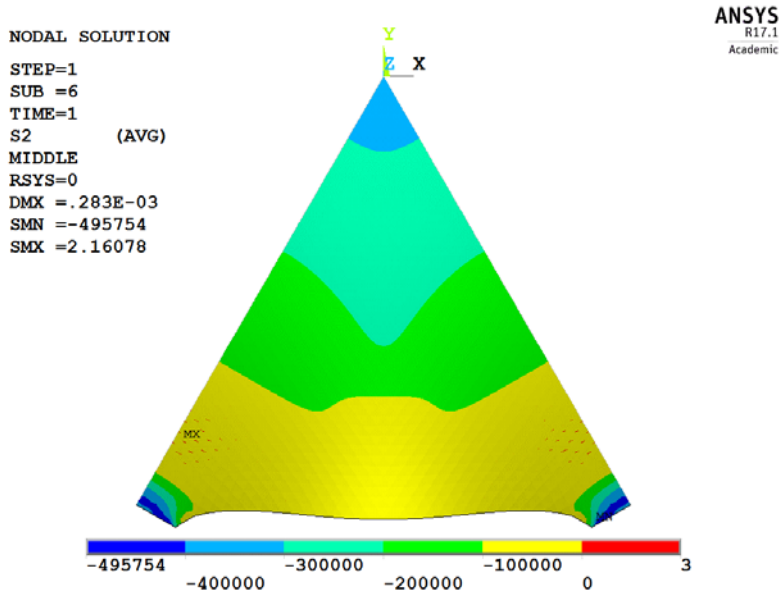


FIGURE 8.25 Principal stress S_2 at the middle surface of Model A_5 (shell with simply supported straight supports; Pa).

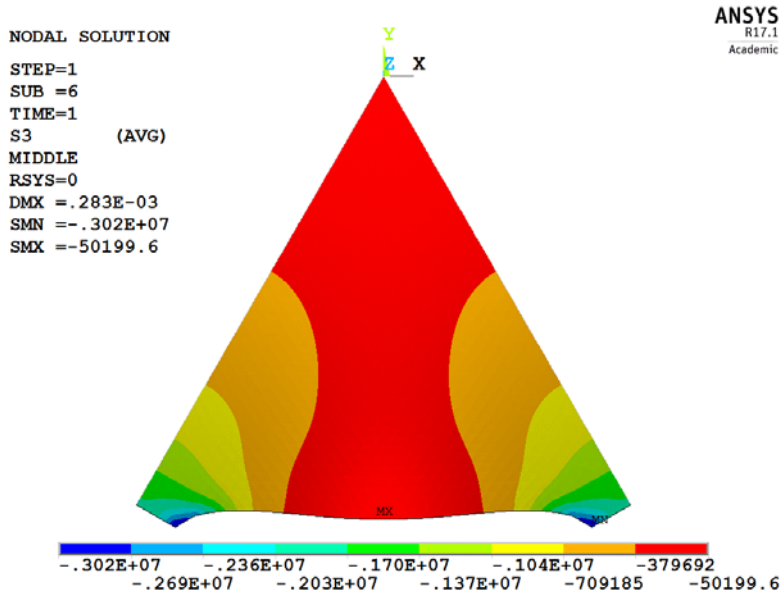


FIGURE 8.26 Principal stress S_3 at the middle surface of Model A_5 (shell with simply supported straight supports; Pa).

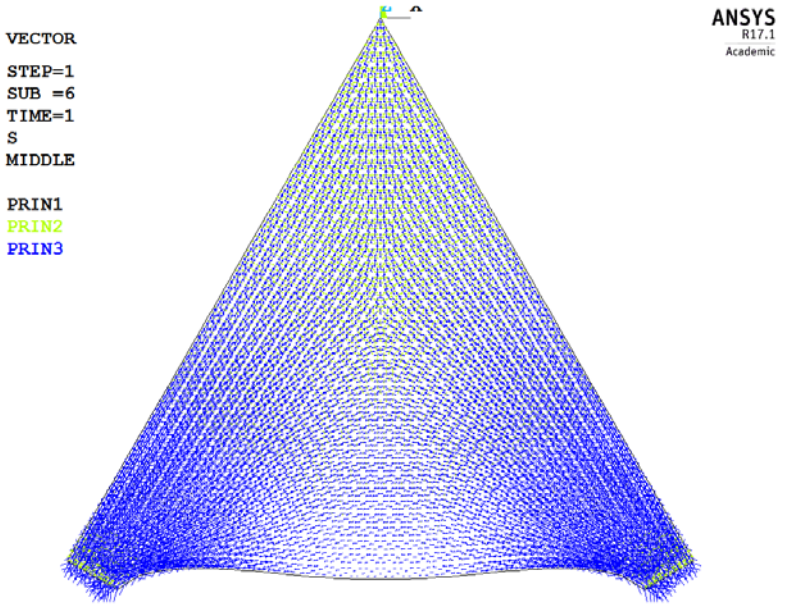


FIGURE 8.27 Vectorial representation of the principal stresses of Model A_S (shell with simply supported straight supports).

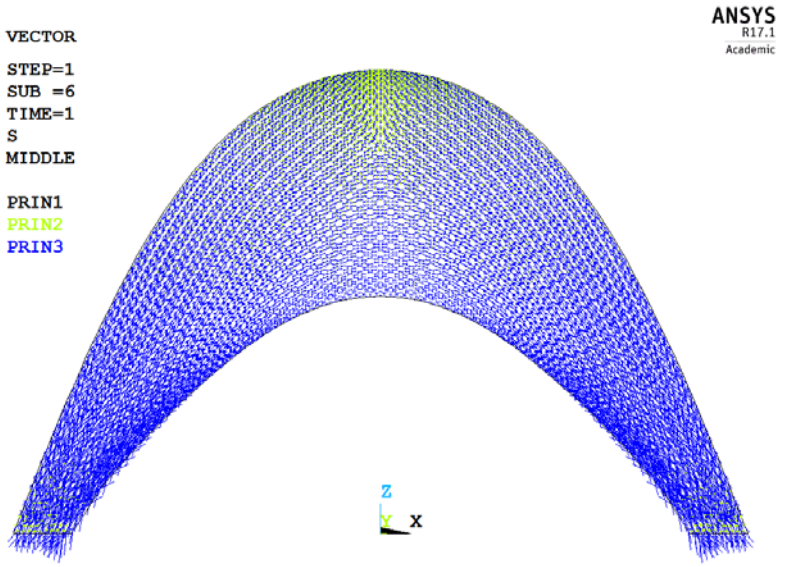


FIGURE 8.28 Vectorial representation of the principal stresses of Model A_S (shell with simply supported straight supports; lateral view).

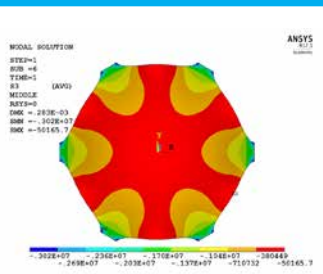
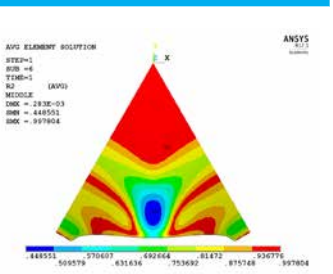
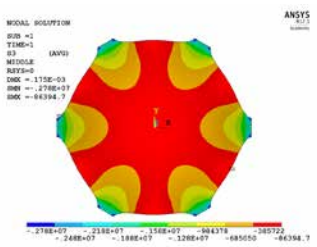
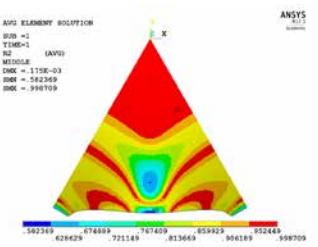
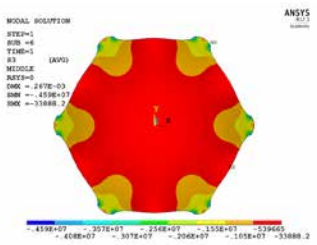
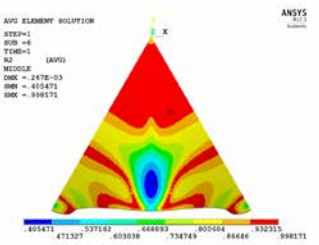
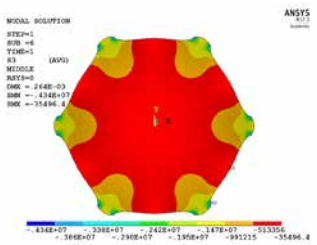
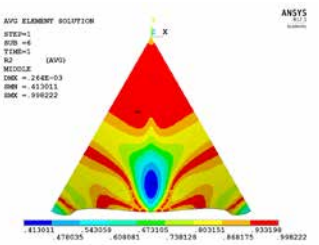
In conclusion, the central part of the shell clearly has perfect shell behaviour, while more focus should be placed on the parts near the supports and boundaries. To compare the differences in the structural behaviour near the supports, the minimum third principal stress and its distribution in each shell are listed in Table 8.2. Moreover, to consider the differences in the structural behaviour near the boundaries, the minimum R_2 (Stress Ratio in the direction of sthe econd principal normal force) and its distribution in each shell are listed.

From this table, several conclusions can be drawn.

- From the comparison of the minimum third principal stresses and their distributions, the minimum third principal stresses (blue parts in the distribution plots) of all eight shells occur in the support lines or curves. Stress concentration occurs at the two ends of each support of the shells with straight supports and outward-curved supports, while latter ones are significant and have larger values than the others. Uniform principal stresses occur along the supports of the shells with inward-curved supports, while for shells with more strongly inward-curved supports, stresses in the middle parts of the supports are relatively larger than their ends.

- The comparison of the minimum R_2 and their distributions demonstrates that bending moments (blue parts) occur in the boundary parts. Shells with inward-curved supports have much smaller bending areas than those with straight supports and outward-curved supports. For ***Model B_f***, ***Model C_s***, ***Model C_f***, ***Model D_s*** and ***Model D_f***, the minimum R_2 occurs in the middle part of the boundary lines, while for ***Model A_s***, ***Model B_s***, and ***Model B_f***, it occurs in the parts near the boundaries. Moreover, ***Model A_f***, the one with fixed straight supports, has the largest minimum R_2, which means a much better shell behaviour than the others.

- All the comparisons show that whether the supports are fixed or hinged has negligible influence on the static structural behaviour of these eight form-found shells, except for the two shells with straight supports. This is because these shells are form-found, and the forces are in the tangent plane at the supports.

MODELS	MINIMUM S_3 / PA	DISTRIBUTION OF S3 NEAR SUPPORTS	MINIMUM R_2 / %	DISTRIBUTION OF *R2* NEAR BOUNDARIES
Model A_S (shell with simply supported straight supports)	-3.02e6		44.8	
Model A_f (shell with fixed supported straight supports)	-2.78e6		58.2	
Model B_S (shell with simply supported outward-curved supports)	-4.59e6		40.5	
Model B_f (shell with fixed supported outward-curved supports)	-4.34e6		41.3	

>>>

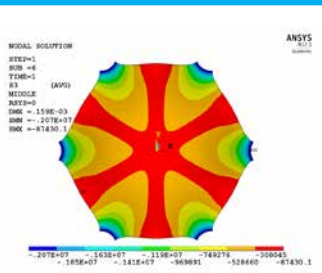
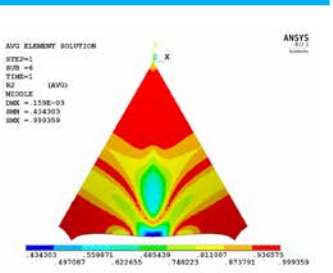
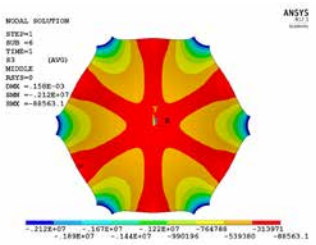
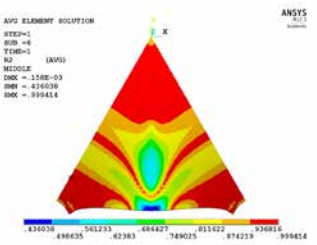
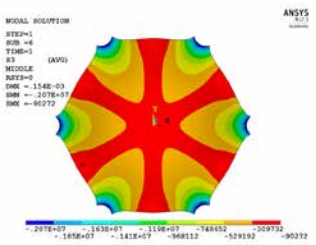
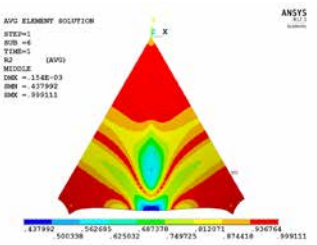
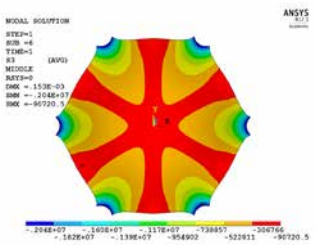
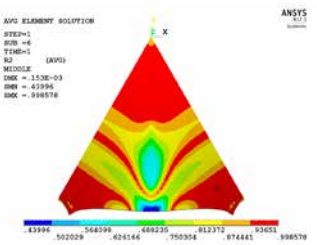
MODELS	MINIMUM S_3 / PA	DISTRIBUTION OF S3 NEAR SUPPORTS	MINIMUM R_2 / %	DISTRIBUTION OF *R2* NEAR BOUNDARIES
Model C_s (shell with simply supported inward-curved supports)	-2.07e6		43.4	
Model C_f (shell with fixed supported inward-curved supports)	-2.12e6		43.6	
Model D_s (shell with simply supported strongly inward-curved supports)	-2.07e6		43.8	
Model D_f (shell with fixed supported strongly inward-curved supports)	-2.04e6		44.0	

TABLE 8.2 Comparison of structural static analysis results.

TOC

§ 8.3.2 Linear buckling analysis

This section presents the linear buckling analyses of the eight shells that are loaded by a symmetrically distributed dead load. The material properties and loads are the same as those of the structural static analysis.

The first buckling mode and its corresponding load multiplier are shown in Table 8.3. The buckling point of each shell, which indicates the largest deformation when the shell buckles, has been considered in detail. Table 8.3 also provides the Gaussian curvature and mean curvature of the buckling point of the undeformed shell and the principal stress of this point, which is computed by the structural static analyses.

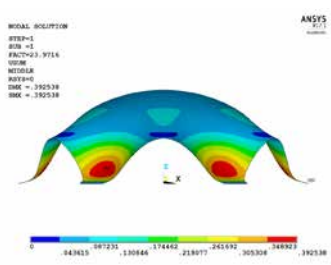
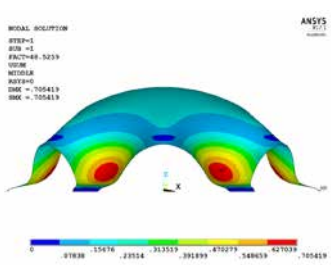
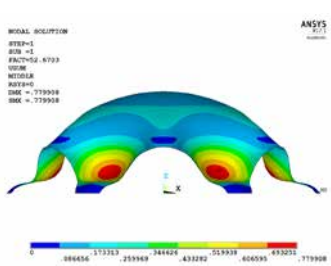
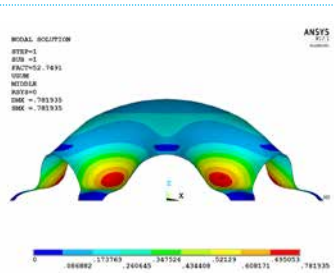
This table illustrates that the support shapes have considerable influence on the buckling behaviour of these shell structures. Several conclusions can be drawn.

- Shells that are curved at the supports have higher buckling load factors than those that are straight at the supports. Shells that are inward-curved at the supports have higher load multipliers than those that are outward-curved at the supports. The more curved the supports are, the higher the buckling load factor is.

- Fixed or hinged supports have a considerable influence on the buckling load factor of shells that are plane at the supports, but have a trivial influence on that of shells that are curved at supports. It can also be observed that for two shells with the same support shapes, the buckling mode of the simply supported shell is similar to that of the fixed supported shell.

- The larger the absolute value of the Gaussian curvature of the buckling point is, the higher the buckling load factor is, except for the two shells with outward-curved supports whose Gaussian curvature of the buckling point is positive. The mean curvature of the buckling point has an unclear apparent influence on the linear buckling behaviour of these shells. Further research should be conducted to study the relationship between the buckling behaviour and its curvature information.

- The lower the level of the principal stress of the buckling point is, the higher the buckling load factor is, except for the one with fixed straight supports.

MODELS	FIRST BUCKLING MODE	FIRST BUCKLING LOAD FACTOR	GAUSSIAN CURVATURE OF THE BUCKLING POINT	MEAN CURVATURE OF THE BUCKLING POINT	PRINCIPAL STRESS OF THE BUCKLING POINT IN STATIC ANALYSIS / PA
Model As (shell with simply supported straight supports)		23.97	-0.00557	0.01843	-1.23E+06
Model Af (shell with fixed supported straight supports)		48.51	-0.00608	0.00481	-9.54E+05
Model Bs (shell with simply supported outward-curved supports)		52.66	0.00220	0.05282	-9.57E+05
Model Bf (shell with fixed supported outward-curved supports)		52.74	0.00220	0.05282	-9.57E+05

>>>

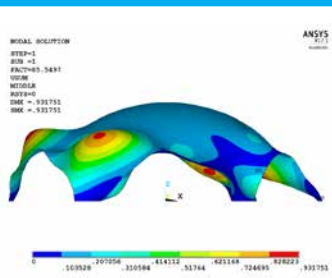
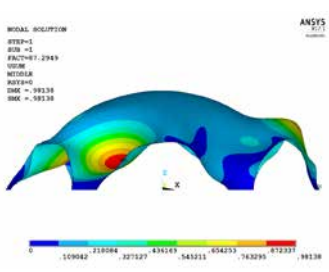
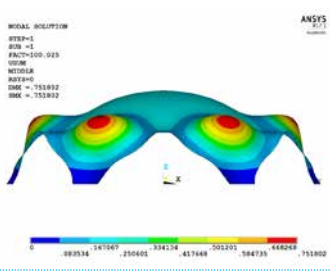
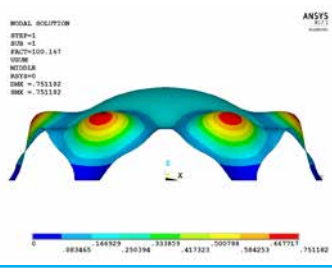
MODELS	FIRST BUCKLING MODE	FIRST BUCKLING LOAD FACTOR	GAUSSIAN CURVATURE OF THE BUCKLING POINT	MEAN CURVATURE OF THE BUCKLING POINT	PRINCIPAL STRESS OF THE BUCKLING POINT IN STATIC ANALYSIS / PA
Model Cs (shell with simply supported inward-curved supports)		85.50	-0.01221	0.00333	-6.54E+05
Model Cf (shell with fixed supported inward-curved supports)		87.27	-0.01229	0.00297	-6.53E+05
Model Ds (shell with simply supported strongly inward-curved supports)		99.99	-0.01501	0.00793	-6.31E+05
Model Df (shell with fixed supported strongly inward-curved supports)		100.13	-0.01501	0.00793	-6.31E+05

TABLE 8.3 Comparison of linear buckling analysis results.

§ 8.3.3 Nonlinear static analysis

This section presents nonlinear analyses of the eight shells that are loaded by a distributed dead load. Geometric nonlinearity, material nonlinearity, and imperfections of the shell are included. The reinforced concrete material in these analyses has two phases. In the elastic phase, Young's modulus is 3.36E10 N/m^2, and when the concrete cracks (the crack stress is 1.00E06 N/m^2) Young's modulus becomes 0.42E10 N/m^2. The load added to the shell in the first step is 5000 N/m^2 vertically and is gradually increased until the shell collapses. An imperfection with a maximum of 0.09 m is added to each shell based on the shape of the first linear buckling mode.

The load-displacement curves of the eight shells are shown in Figure 8.29. The shapes of the support conditions substantially influence the stiffness and load-carrying capacity. Shells with inward-curved supports have a larger load multiplier than those with straight and outward-curved supports; the more curved the supports are, the higher the load multiplier is. For shells with the same support shapes, shells with fixed supports have a somewhat larger load multiplier than those that are simply supported.

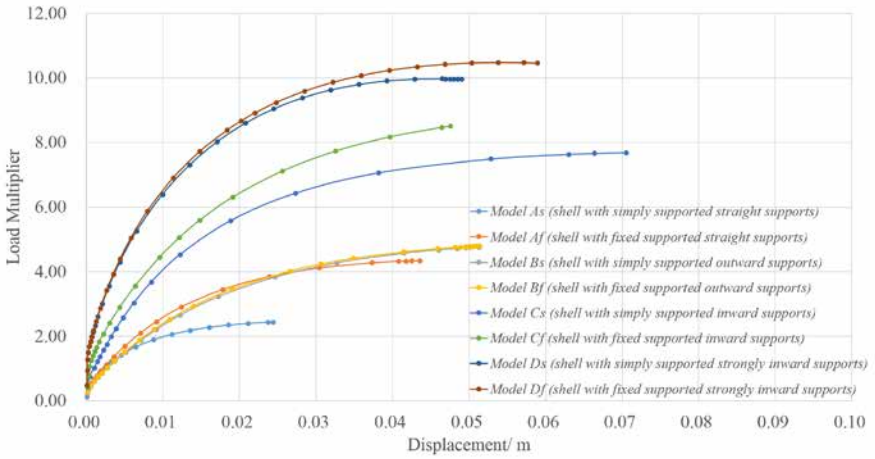


FIGURE 8.29 Load-displacement curves of all the eight shells.

In addition, taking *Model A*$_S$ as an example, two stress ratios of the shell are shown in Figures 8.30 and 8.31, compared with Figures 8.22 and 8.23, it can be observed that the central part of the shell still maintains optimal shell behaviour, while large bending moments occur in the parts near the boundaries and supports. The vectorial representations of the principal stresses (S_1, S_2 and S_3) at the middle surface of the shell are shown in Figures 8.32 and 8.33. Compared with Figures 8.27 and 8.28, it can be observed that the load paths substantially change when the shell collapses. It should be mentioned that the failure mode of *Model A*$_S$ is also symmetric so that only the results of 1/6 of it are shown.

Figure 8.1 clearly indicates that the load-carrying capacity for the optimised shell is substantially higher (around 250%) than that of the original shell. However, the structural forms of the optimised and original shells have significant differences. Compared with this example, shells with inward-curved supports perform with a much higher load-carrying capacity (from 200% to 550%) than those with straight supports, shells with outward -curved supports also perform higher load-carrying capacity (from 125% to 250%) than those with straight supports. This means slight changes of the support shapes cause a higher load-carrying capacity with slight differences in their structural forms.

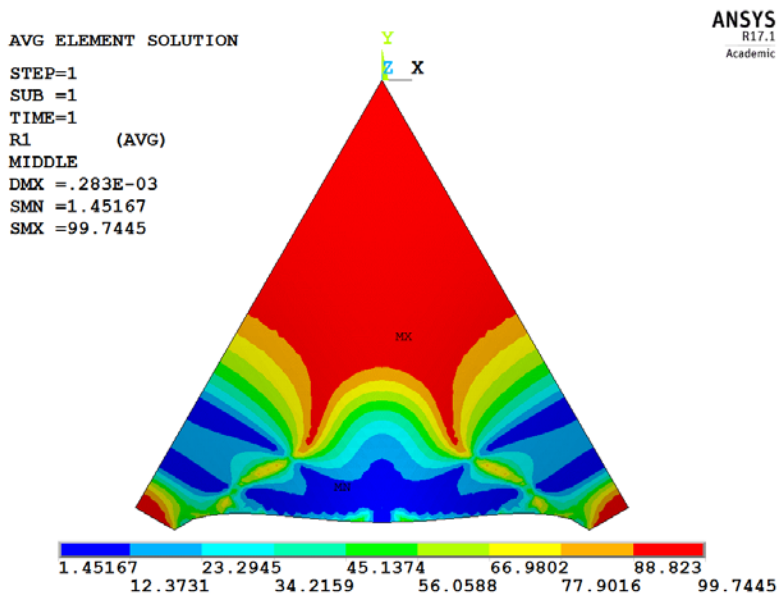


FIGURE 8.30 R_1 of Model *A*$_S$ (shell with simply supported straight supports) when the shell fails (%).

TOC

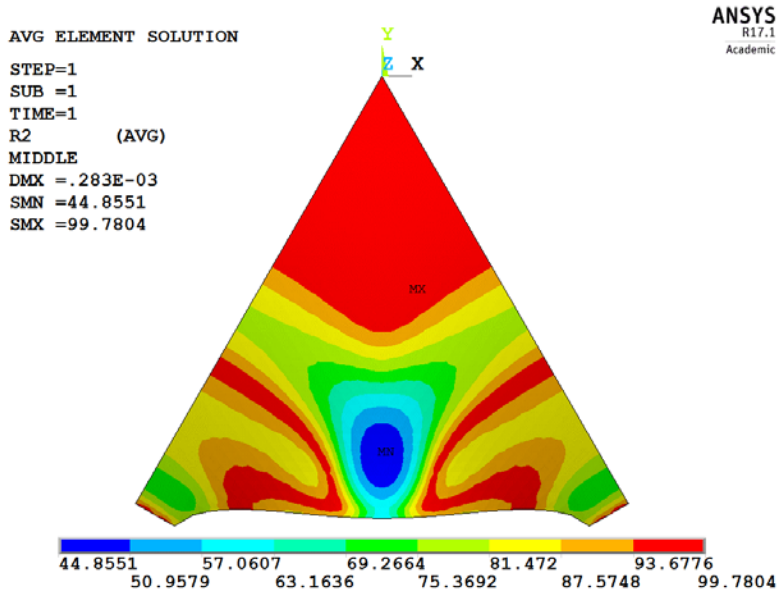


FIGURE 8.31 R_2 of Model A_S (shell with simply supported straight supports) when the shell fails (%).

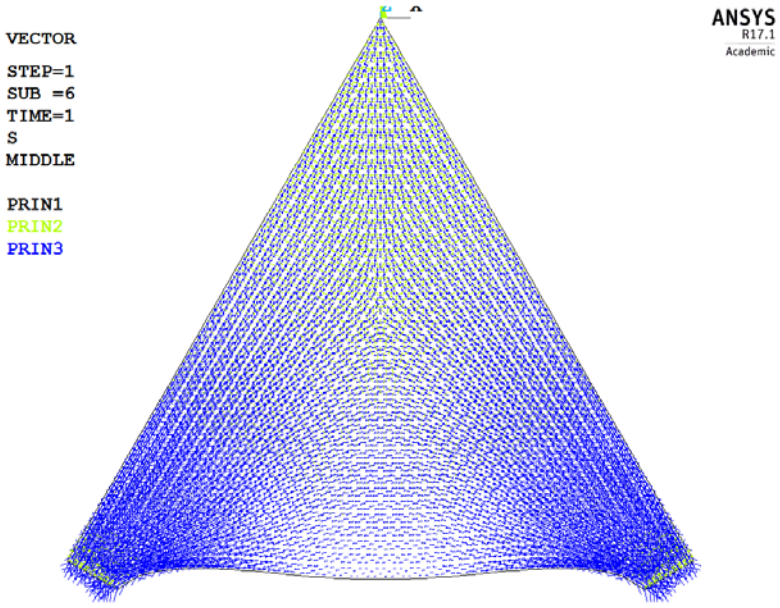


FIGURE 8.32 Vectorial representation of the principal stresses for Model A_S (shell with simply supported straight supports) when the shell fails.

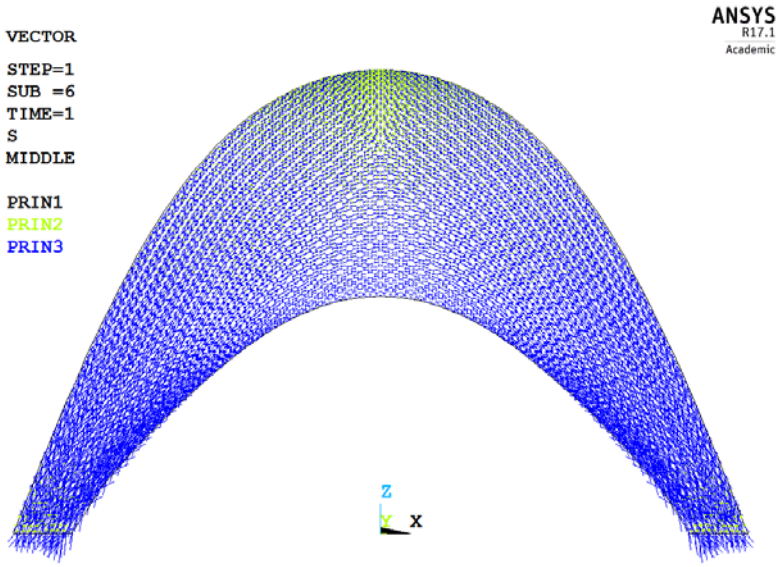


FIGURE 8.33 Vectorial representation of the principal stresses for Model A_5 (shell with simply supported straight supports) when the shell fails (lateral view).

§ 8.4 Comparison of Structural Behaviour of Form-found Shells Under Non-symmetrical Loads

The weakness of shells obtained from hanging models is their behaviour under non-symmetrical loads or thermal loads. In this section, structural analyses of these eight form-found shells under half-span loading are conducted. All the settings during the analyses are same as those of the previous section, except that the loads are added to half of the shell, as shown in Figure 8.34.

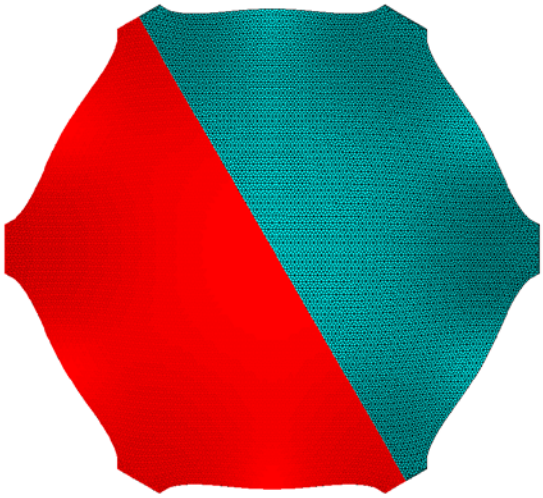


FIGURE 8.34 Half-span loading (red part).

§ 8.4.1 Linear static analysis

Taking the ***Model As*** as an example, its linear static analysis results can be presented as follows. Two stress ratios and its vectorial representation of the principal stresses at the middle surface of ***Model As*** under half-span loads are shown in Figures 8.35, 8.36 and 8.37. Tension forces and bending moments occur in this form-found shell, which indicates that it does not show good performance when the load distribution changes as well as the other shells do.

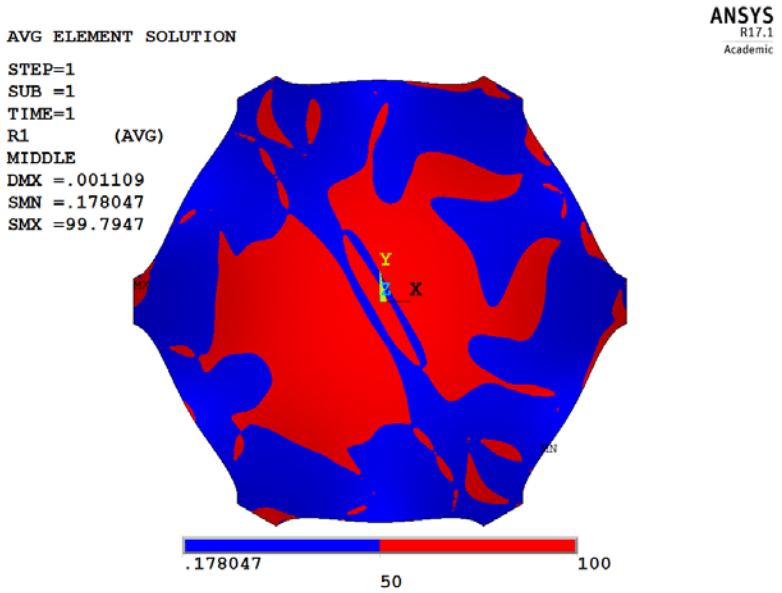


FIGURE 8.35 R_1 of Model A_s (shell with simply supported straight supports)under half-span loads.

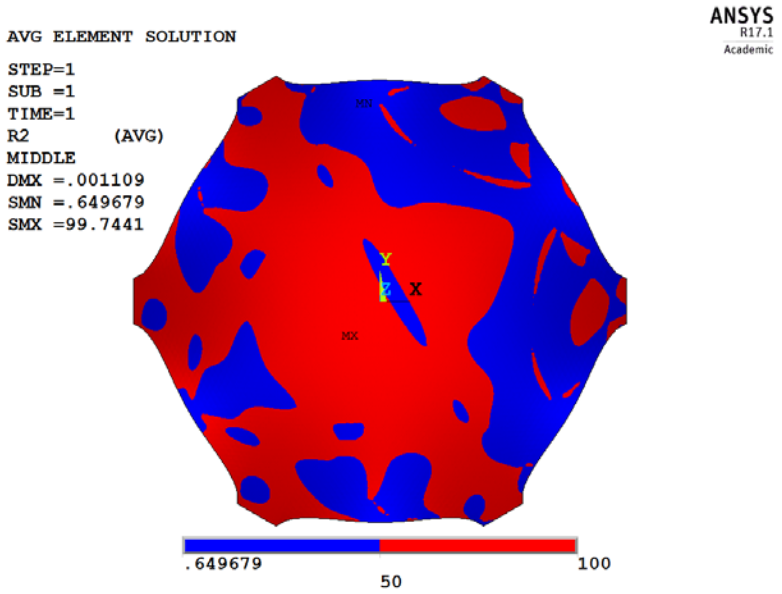


FIGURE 8.36 R_2 of Model A_s (shell with simply supported straight supports) under half-span loads.

TOC

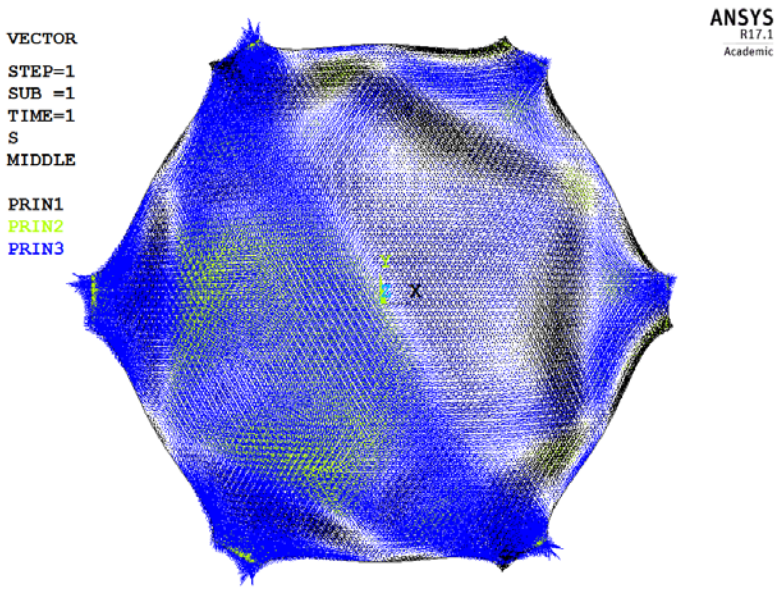
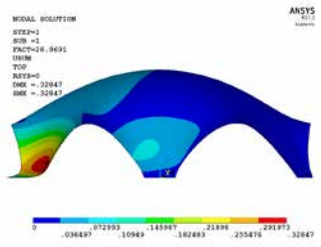
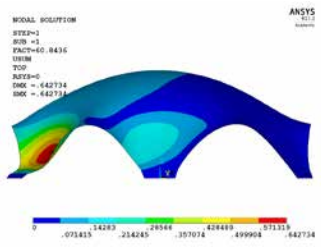
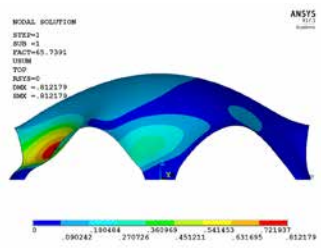
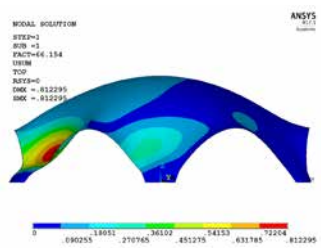


FIGURE 8.37 Vectorial representation of the principal stresses for Model A_S (shell with simply supported straight supports) under half-span loads.

§ 8.4.2 Linear buckling analysis

Linear buckling analyses under half-span loads of these form-found shells are conducted in this section. Shown in Table 8.4, it presents the first buckling mode and first buckling load factor of each form-found shell. Similar conclusions can be obtained compared with the analysis results under vertical symmetrical loads

MODELS	FIRST BUCKLING MODE	FIRST BUCKLING LOAD FACTOR
Model As (shell with simply supported straight supports)		28.97
Model Af (shell with fixed supported straight supports)		60.84
Model Bs (shell with simply supported outward-curved supports)		65.74
Model Bf (shell with fixed supported outward-curved supports)		66.15

>>>

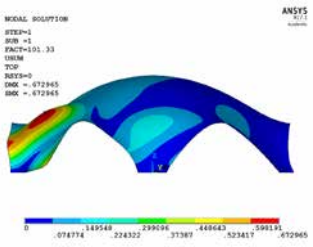
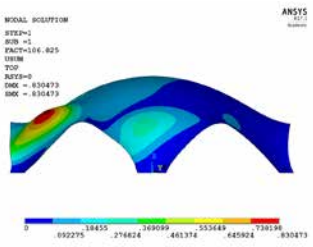
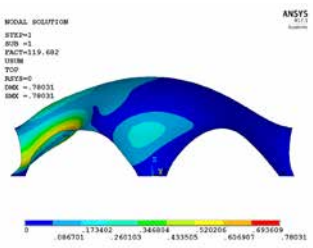
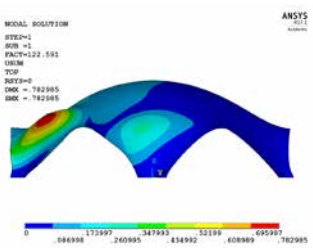
MODELS	FIRST BUCKLING MODE	FIRST BUCKLING LOAD FACTOR
Model C_s (shell with simply supported inward-curved supports)		101.33
Model C_f (shell with fixed supported inward-curved supports)		106.83
Model D_s (shell with simply supported strongly inward-curved supports)		119.68
Model D_f (shell with fixed supported strongly inward-curved supports)		122.60

TABLE 8.4 Comparison of linear buckling analysis results under half-span loads.

§ 8.4.3 Nonlinear static analysis

Like Section 8.3.3, nonlinear analyses of these form-found shells under half-span loads are conducted. Figure 8.38 presents the load-displacement curves of the eight shells. It can also be observed that similar conclusions can be obtained compared with the analysis results under vertical symmetrical load.

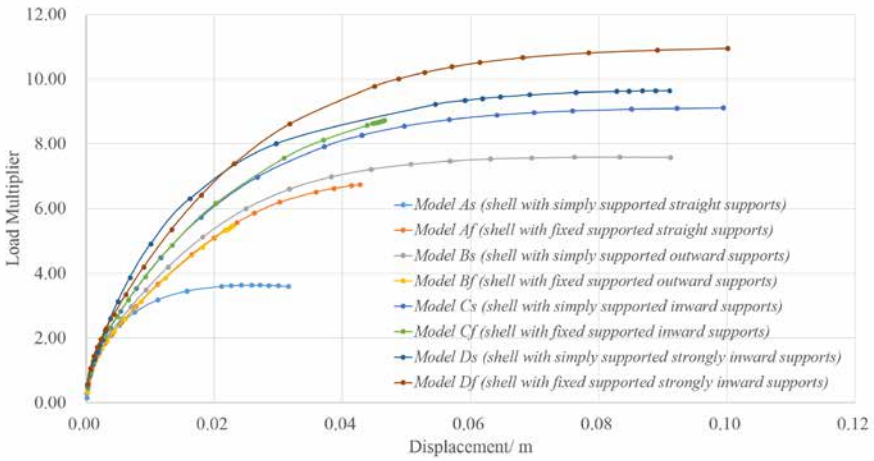


FIGURE 8.38 Load-displacement curves of all eight shells under half-span loads.

§ 8.5 Conclusions

The most important parts of a shell structure are close to the supports. In this location the stresses are largest and buckling is most likely to occur. This chapter discusses the influence of the shape of this support area on the structural forms and the structural efficiency of the form-found shells. Hexagonal shells that are shaped by hanging models are considered. The main conclusions are as follows:

– Using the Form-Control strategy proposed in Section 6.2, four hexagonal form-found shells generated from hanging models with different support shapes but with the same target point are generated. Four support shapes are considered:

straight supports, outward-curved supports, inward-curved supports and strongly inward-curved supports.

– By direct comparisons of the coordinates and curvature analysis results between the four equilibrium hanging models, the influence of support shapes on the structural forms is studied. Slight changes in the support shapes have negligible influence on the overall structural forms of these form-found shells. However, differences of curvatures can be observed in the parts near their supports. Specifically, during their Form-Finding processes, straight supports induce an area with zero curvature in one direction. Outward curvature of the supports are contrary to curvature of the free edges, and leads to changes of curvatures near the supports. Inward curvatures of the supports are suited to the chosen curvature of the free edges, thus, no flat parts are obtained during the Form-Finding process.

– The influence of support shapes and conditions on the structural behaviour of the form-found shells is studied via detailed comparisons of the structural analysis results of the shell models with different supports shapes and conditions. Static analyses, linear buckling analyses, and nonlinear analyses of these form-found shells under symmetrically and asymmetrically distributed dead load are conducted. It can be concluded that slight changes of the support shapes have a pretty large influence on structural behaviour, and these form-found shells with inward-curved supports have a relatively better structural behaviour than others. In the displayed examples of this chapter, the load-carrying capacity of the shell with strongly inward-curved supports (*Model D*) is around four times of that of the shell with straight supports (*Model A*).

§ 8.6 References

[139] Bletzinger K.-U., Ramm E. (1993). Form finding of shells by structural optimisation. Engineering with Computers, 9: 27-35.

[140] Ramm E. (2004). Shape finding of concrete shell roofs. Journal of the International Association for Shell and Spatial Structures, 45(1): 29-39.

[141] Ramm E., Wall W.A. (2004). Shell structures - a sensitive interrelation between physics and numeric. International Journal for Numerical Methods in Engineering, 60: 381-427.

[142] Ohmori, H., Kimuraa, T., Maeneb, A. (2009). Computational Morphogenesis of Free Form Shells. Proceedings of the International Association for Shell and Spatial Structures (IASS) Symposium, 28 September - 2 October 2009, Universidad Politecnica de Valencia, Spain.

[143] Tomás A., Martí P. (2010). Shape and size optimisation of concrete shells. Engineering Structures, 32: 1650-1658.

[144] Adriaenssens S., Block P., Veenendaal D., Williams C., editors. (2014). Shell structures for architecture: Form-Finding and optimisation. Routledge Taylor and Francis, London.
[145] Marino E., Salvatori L., Orlando M., Borri C. (2016). Two shape parametrizations for structural optimisation of triangular shells. Computers & Structures. 166: 1-10.
[146] Li Q., Borgart A., Wu Y. (2016). How to understand 'Structural Morphology'?. Journal of the International Association for Shell and Spatial Structures, 57(2): 145-158.
[147] Li Q., Su Y., Wu Y., Borgart A., Rots J.G. (2017). Form-Finding of shell structures generated from physical models. International Journal of Space Structures. 32(1): 11-33.
[148] Kilian A. (2007). The Steering of Form. Journal of the International Association for Shell and Spatial Structures, 48(4): 17-21.
[149] Li Q., Wu Y., Shen S. (2014). Computational generation of freeform shells based on the inverse hanging experiment. Proceedings of the IASS-SLTE 2014 Symposium, Brasilia, Brazil, 2014.
[150] Heathcote E., Ledgard J. (2016). 'A'A' Perspectives - The Droneport Project. LafargeHolcim Foundation.
[151] Block P., Rippmann M., Van Mele T., Escobedo D. (2017). The Armadillo Vault: Balancing computation and traditional craft. FABRICATE 2017, Menges A., Sheil B., Glynn R. and Skavara M. (editors): 286-293, UCL Press London.
[152] Veenendaal D., Bakker J., Block P. (2017). Structural design of the flexibly formed, mesh-reinforced concrete sandwich shell roof of NEST Hilo. Journal of the International Association of Shell and Spatial Structures, 58(1): 23-38.

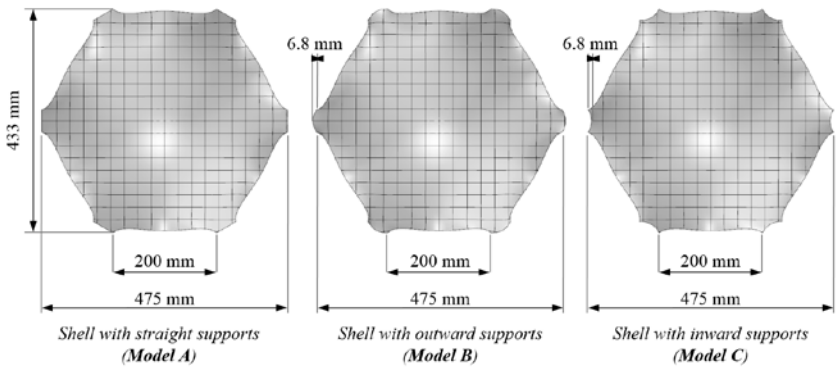
9 Influence of Support Shapes: Experimental Research

§ 9.1 Introduction

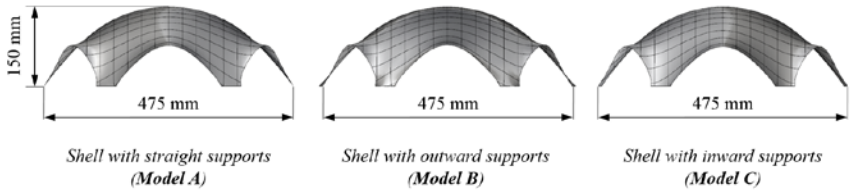
In this chapter, experimental research on the influence of supports on form-found shells is conducted. Three plastic shell models, which are scaled models from the previous chapter, are manufactured and tested. Subsequently, the test results of each shell model are explained in detail, and a qualitative comparison with the numerical analysis results is conducted. From these observations, the influences of supports on form-found shells can be studied visually and qualitatively.

§ 9.2 Manufacture of the Shell Models

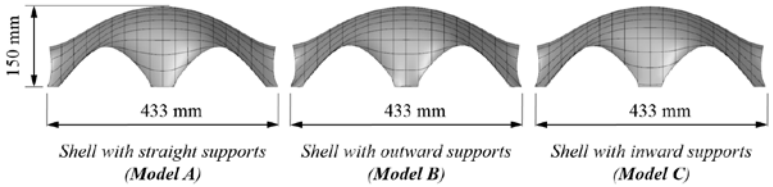
Figure 9.1 presents the dimensions of the three form-found shell models. They are scaled models of the *Model A*, *Model B* and *Model C* of the last chapter.



(a) Top view of the three shell models.



(b) Front view of the three shell models.



(c) Right view of the three shell models.

FIGURE 9.1 Dimensions of the three shell models.

A computer numerical control (CNC) milling machine was used to make the formworks of the three shell models shown in Figure 9.2. These formworks have high similarity with the designed shell models because of the high accuracy of the CNC machine.



(a) Formwork of ***Model A*** *(shell with straight supports).*



*(b) Formwork of **Model B** (shell with outward supports).*



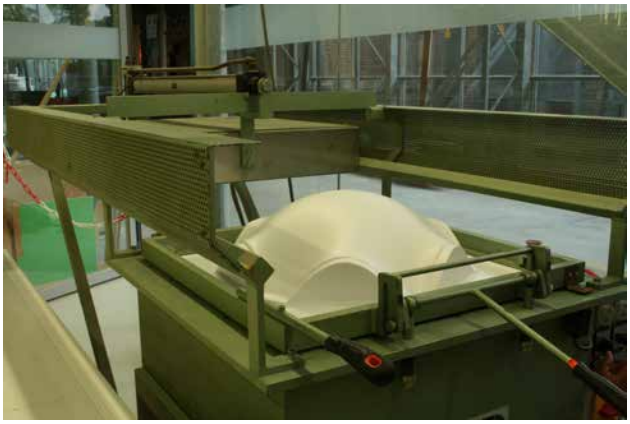
*(c) Formwork of **Model C** (shell with inward supports).*

FIGURE 9.2 Formworks of the three shell models.

Subsequently, the vacuum forming machine was used to manufacture the shell models from three pieces of polyester sheets with a thickness of 1.0 mm. The manufacturing process of one shell model is shown in Figure 9.3.







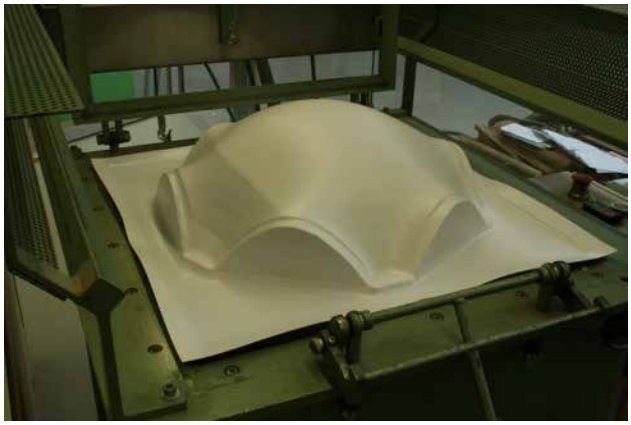


FIGURE 9.3 Manufacture of shell model using the vacuum forming machine.

Three shell models are obtained after removing the edges, shown in Figure 9.4. As the curvatures occur after manufacturing, the thickness of the shell models is no longer uniform. Figure 9.5 presents the thickness distributions of these three shell models. The average thickness of these shell models is 0.75 mm, and the ratio of the radius to the thickness is more than 300. Moreover, the thickness of the support parts is less than that of the central parts, which is different from engineering practices. Further, the thickness of the free boundary parts is thicker than that of the central parts, which could be considered a reinforcement of the free edges.

The supports of these three shell models are manufactured by gluing them to the wood plane and attaching extra reinforced wood components to clamp them, as shown in Figure 9.6. Via this method, these supports can be acknowledged as fixed supports of these shell models, which is similar to engineering practices. Then, these shell models can be tested.

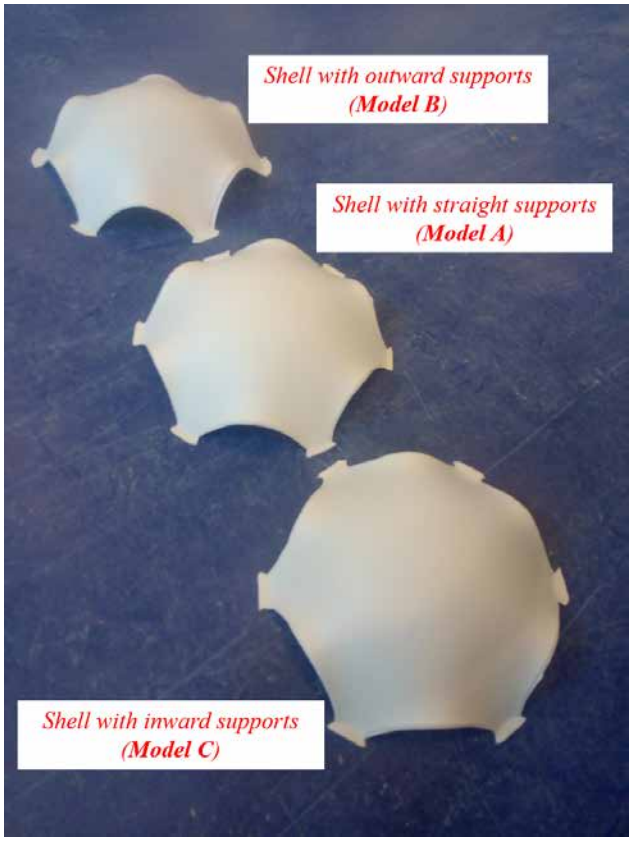


FIGURE 9.4 Three shell models.

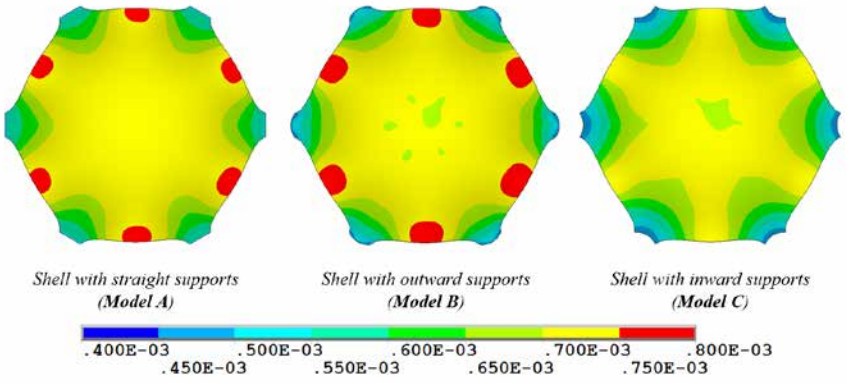


FIGURE 9.5 Thickness distributions of the three shell models (m).

TOC



FIGURE 9.6 Three plastic shell models with supports.

§ 9.3 Setup and Tests of Shell Models

Shown in Figure 9.7, it presents the design scheme of the setup of the test.

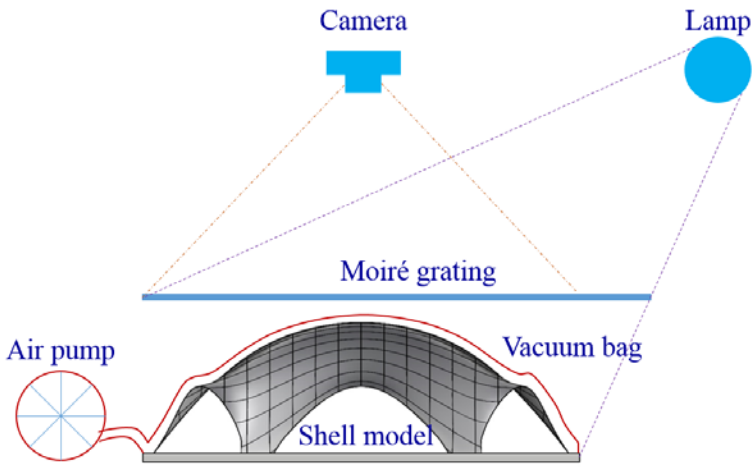
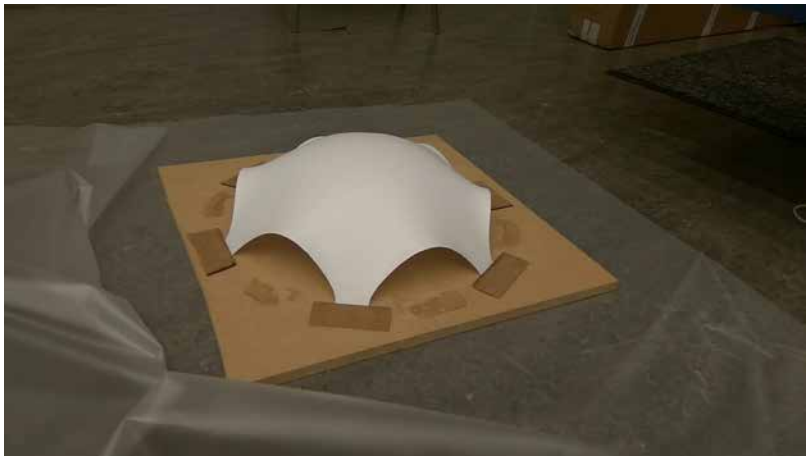


FIGURE 9.7 Design of the setup of the test.

In these tests, the shell model is subjected to air pressure on its surface by withdrawing air out of the vacuum bag using the air pump. An air-pressure sensor is used to measure the air pressure inside the vacuum bag during the test. Figure 9.8 presents the manufacturing process of the vacuum bag for ***Model A***.

To observe the buckling process of the shell model during the test, the shadow Moiré method [153] is used in this research. It is an optical noncontact method for mapping the 3D shape of objects, which can be used for defect inspection and profile measurements covering a wide range of resolutions [155]. The setup of the shadow Moiré method is very simple, it has no special requirements for light coherence or mechanical isolation. The lamp is used as the light source, and the camera is used to record the Moiré patterns during the test.

Based on this design, the setup of the test is shown in Figure 9.9. Using this setup, the three shell models are tested one by one, during which the air pressure inside the vacuum bag and the Moiré patterns are recorded.



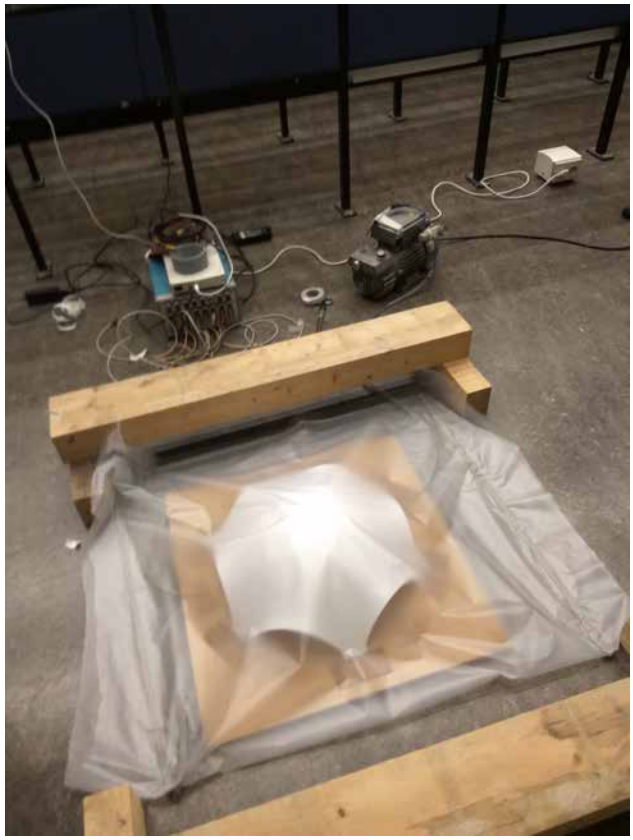


FIGURE 9.8 Manufacture of the vacuum bag.



FIGURE 9.9 Setup of the test.

§ 9.4 Analyses of the Test Results

In this section, the buckling process of each shell model under gradually increasing air pressure is analysed based on the recorded air-pressure data and Moiré patterns during the test.

In these tests, the air pressure inside the vacuum bag is recorded per second, and the Moiré pattern is recorded every 2 seconds. As the pumping speed of the air pump was not stable during these tests, 19 effective air-pressure data was recorded for ***Model A***, 23 for ***Model B*** and 35 for ***Model C***. Correspondingly, 10, 12, and 18 effective Moiré patterns are recorded for each shell model.

Figure 9.10 presents the air-pressure history curves of three shell models. It can be observed that the variation curve of *Model A* is monotonically increasing, which means its buckling process is continuous. As for *Model B* and *Model C*, some local sudden descents can be observed in their air-pressure history curves, which indicates that some local areas buckled during the buckling processes. Moreover, it should also be mentioned that the critical air pressure (or buckling point) cannot be recognised because of the inaccuracy of the air-pressure sensor and the unstable pumping speed of the air pump.

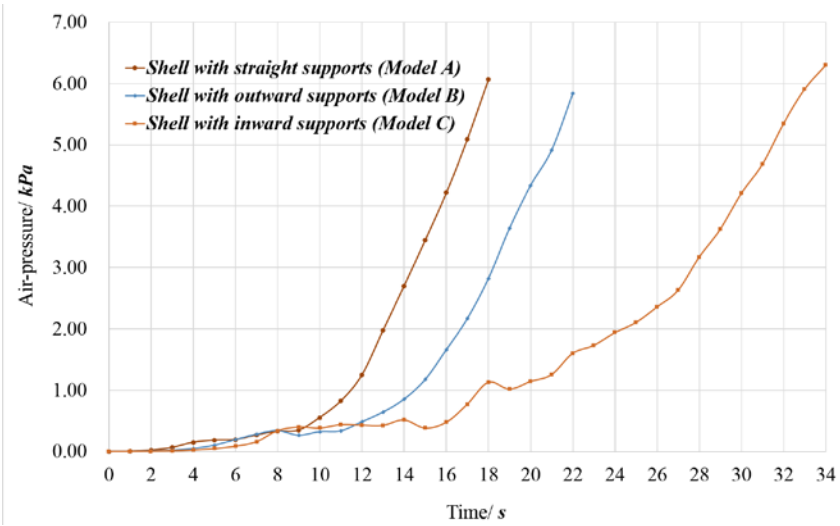


FIGURE 9.10 Changes in the air-pressure during tests of the three shell models.

From observation and comparison of the obtained Moiré patterns, the buckling process of each shell model can be analysed visually and qualitatively as follows.

Figure 9.11 presents Moiré patterns during the test of shell *Model A*. It can be observed clearly that shell *Model A* begins to buckle from the supports, and the buckling of this shell model continues to the central part. Specifically, from the initial shell model at 2 seconds, the support parts with a single curved shape where the Moiré patterns are parallel straight lines (red lines in the first two pictures), begin to buckle. At 4 seconds, the support parts begin to be attached to the wood plane and continue in the following seconds. From observation of red curved lines of the boundaries from 0 to 18 seconds, it can be observed that boundary parts are weak to buckling. Moreover, as shown in the circled parts at 2, 4, 6 and 8 seconds, it can be concluded that flat parts of the shell model are also easy to buckle. At 10 seconds, clear folds begin to occur (the red lines),

which indicate the strong parts of the shell model. These folds develop untill the last second (red lines in the picture at 18 seconds). Moreover, the buckling of shell ***Model A*** is also influenced by the thickness distribution of shell model. The early buckling parts coincide with those areas with less thickness, and folds formed during the buckling also coincide with those areas with greater thickness. A clear buckling mode can be observed from at 8 seconds at which all six legs go inward.

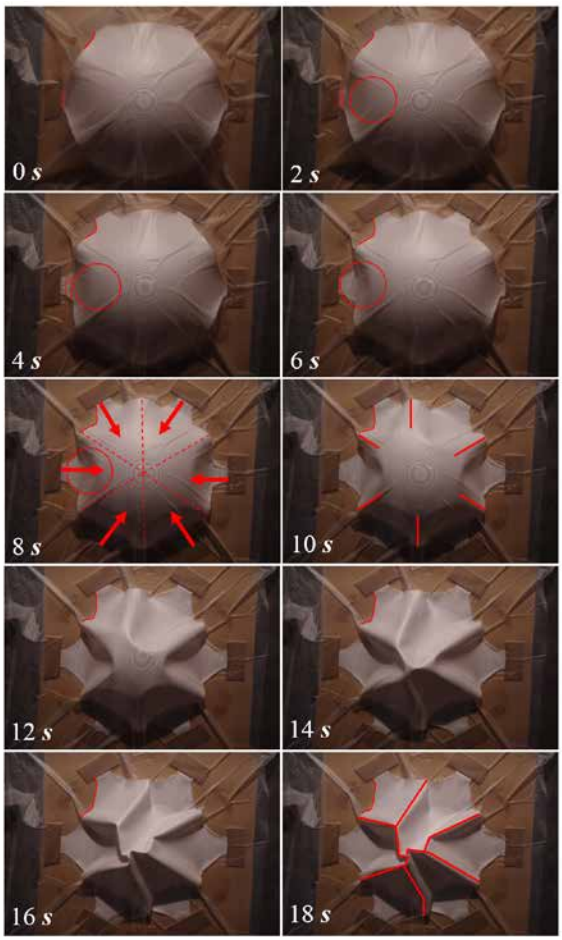


FIGURE 9.11 Moiré patterns of shell with straight supports (***Model A***).

Figure 9.12 presents Moiré patterns during the test of shell ***Model B***. Different from shell ***Model A***, the buckling of shell ***Model B*** does not start from the supports, but from an area with variational curvatures near the supports, which can be observed from the red curves in the pictures of the initial shell model at 2 and 4 seconds. In these parts,

the curvature of the lower area in the horizontal direction is contrary to that of the free edges, while the curvature of the upper area coincides with that of the free edges. After the local buckling of these areas, flat parts occur and buckling develops in these parts, as shown in the circled parts in the pictures at 6, 8 and 10 seconds. Then, clear folds occur starting from at 12 seconds (shown in the red lines in the picture at 12 seconds), and develop until the last second (shown in the red lines in the picture at 22 seconds). However, supports of shell ***Model B*** still maintain certain stiffness, as the support parts are not attached to the wood plane, as shown in the picture at 22 seconds. Similar to shell ***Model A***, the boundaries of shell ***Model B*** are also easy to buckle, and the thickness distribution of the shell model also influences its buckling process, which is not repeated here. A clear buckling mode can be observed at 10 seconds that all the six legs go inward, which are similar to that of ***Model A***.

Figure 9.13 presents Moiré patterns during the test of shell ***Model C***. Significantly different from shell ***Model A*** and shell ***Model B***, the buckling process of shell ***Model C*** starts from a relatively flat and thin area near one support, as shown in Figure 9.5 and the red curves in the pictures at 6 and 8 seconds of Figure 9.13. Figure 9.10 shows that the shell ***Model C*** starts to buckle with a higher air pressure (0.40 kPa at 8 seconds). This is also different from the former two shell models whose critical buckling loads cannot be recognised. The buckling continues at 8 seconds near this same support. Then, the areas near the two adjacent supports begin to buckle at 12 seconds. At the 14 seconds, the areas near the other support buckle, and then the areas near the last two supports buckle at 16 seconds. All mentioned supports are marked in corresponding pictures by ovals shown in Figure 9.13. Subsequently, the development of buckling of the shell model is based on similar rules mentioned for the other two shell models. Clear folds begin to form at 22 seconds, and continue to develop untill the last second. These folds are completely different from those of shell ***Model A*** and shell ***Model B***, which also indicates that these folds do not coincide with thicker areas of the shell model. A clear buckling mode can be observed at 18 seconds, at which the interval three legs go inward and the other three go outward, which are completely different with the results of ***Model A*** and ***Model B***.

To observe the differences between each model, the buckling modes of all three shell models are shown in Figure 9.14. From the observation and comparison of these data and Moiré patterns, shell structures take their stiffness from curvature, flat or single curved parts should be avoided during the generation of the structural geometry of shells, and free boundaries should be considered carefully. Moreover, the thickness distribution of the shell should not be neglected. Specifically, straight supports induce an area with zero curvature in one direction, in a place where stresses concentrate. This drastically reduces the capacity of the shell. Outward curvatures of the supports are contrary to curvatures of the free edges, and induce therefore again flat areas near the

supports, which also reduce the capacity of the shell. Inward curvatures of the supports are suited to the chosen curvature of the free edge; thus, no flat parts are obtained after Form-Finding; and therefore, shell ***Model C*** performs much better than the other two shell models.

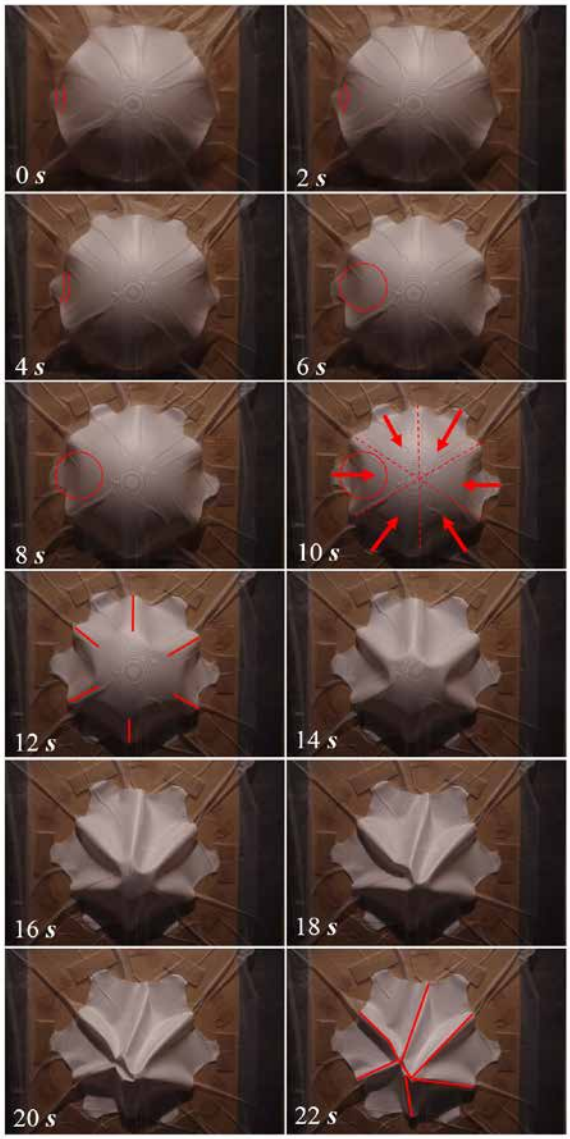


FIGURE 9.12 Moiré patterns of shell with outward supports (*Model B*).

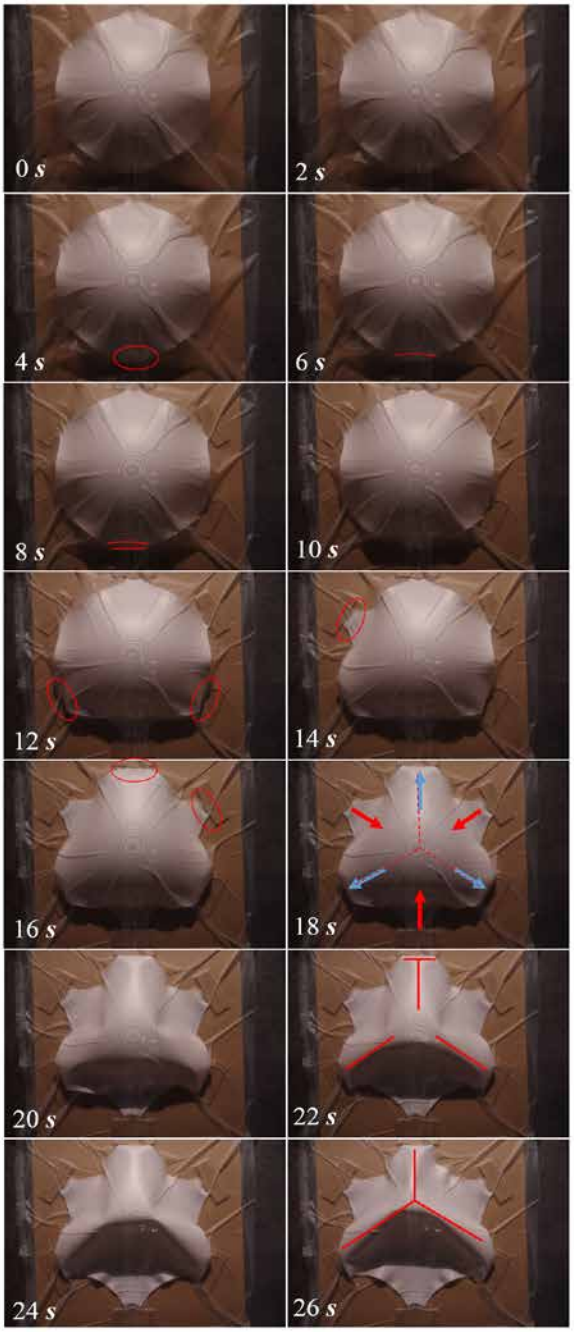
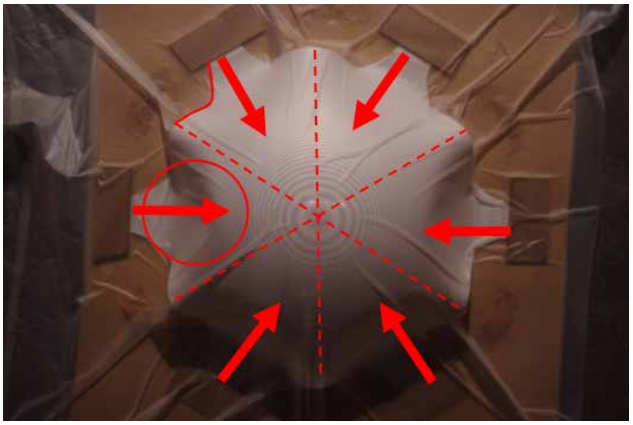
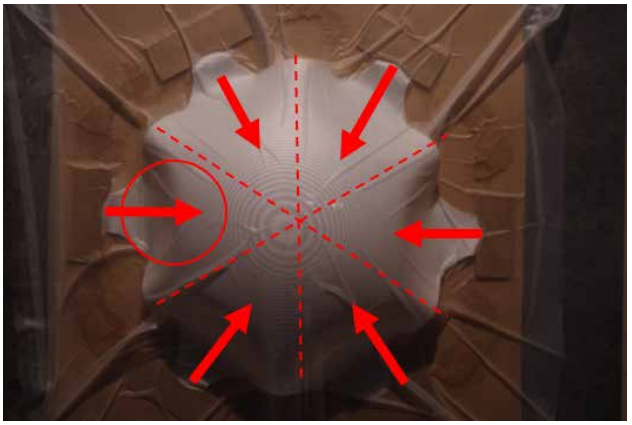


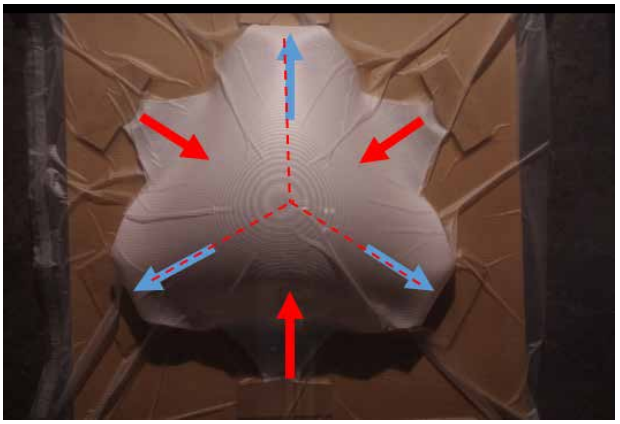
FIGURE 9.13 Moiré patterns of shell with inward supports (*Model C*).



*(a) Buckling mode of **Model A** (shell with straight support).*



*(b) Buckling mode of **Model B** (shell with outward-curved support).*



*(c) Buckling mode of **Model C** (shell with inward-curved support).*

FIGURE 9.14 Buckling modes of the three shell models.

§ 9.5 Buckling Analysis of the Shell Models

Finite element models of the three physical shell models are established in the ANSYS software. Element type SHELL63 is used for these three finite element models, and nonuniform thickness distribution is considered and simulated. Young's modulus of the plastic material is 2020 MPa, and Passion's ratio and the density are neglected. The initial air pressure loaded on the shell surface is 1 Pa. Linear buckling analysis of the three shell models under the effects of air pressure are subsequently conducted. Figures 9.15, 9.16 and 9.17 show the first six buckling modes under air-pressure of *Model A* (shell with straight supports), *Model B* (shell with outward-curved supports) and *Model C* (shell with inward-curved supports) respectively.

Compared with the buckling modes of the three physical shell models shown in Figure 9.14, buckling modes of the physical shell models are different from the numerical results. The main reason is that the loading processes of the physical shell models cannot be simulated accurately in the numerical analysis models.

Specifically, during the tests, the vacuum bag induces unknown extra loads on the free edges of the shell models. Additionally, the speed of the air pump cannot be controlled, and the accuracy of relevant measuring tools (the air-pressure sensor and the camera) of the setup is not sufficient enough.

For simulating real loads on the shell model, two improvement measures can be considered as follows:

- The first measure is to eliminate the effects of the extra loads by adding by adding baffles next to the free edges
- The second measure is to establish the numerical model of the vacuum bag attached to the shell models, which indicates that the vacuum bag should be precisely tailored.

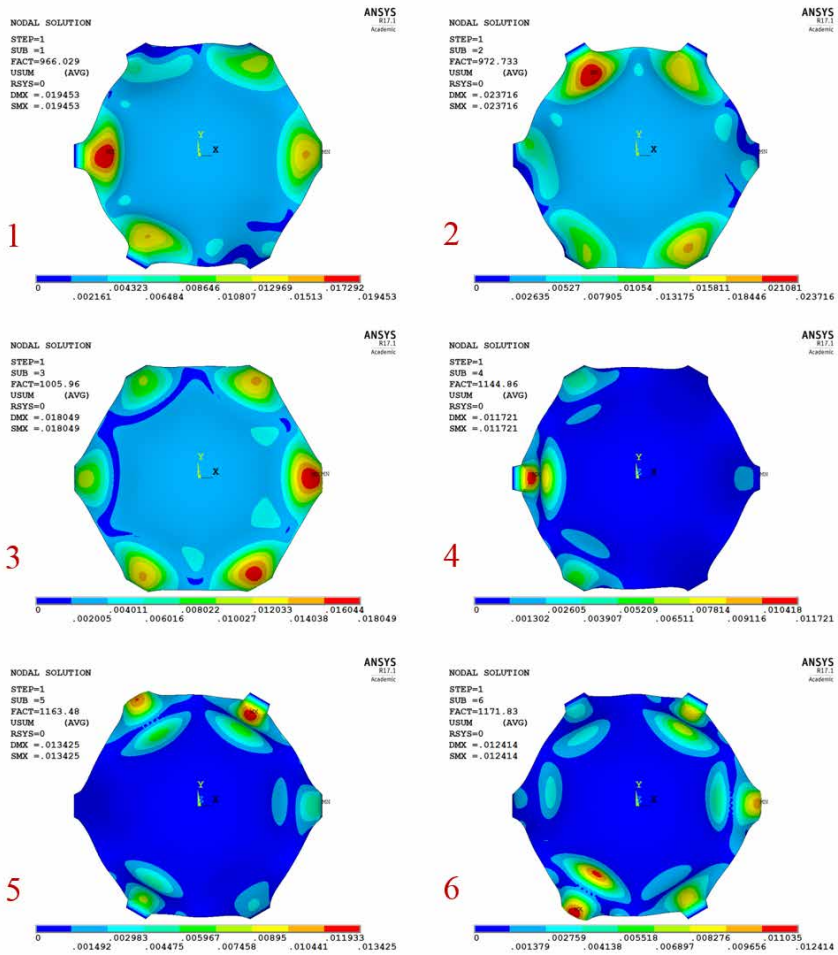


FIGURE 9.15 First six buckling modes of *Model A* (shell with straight supports).

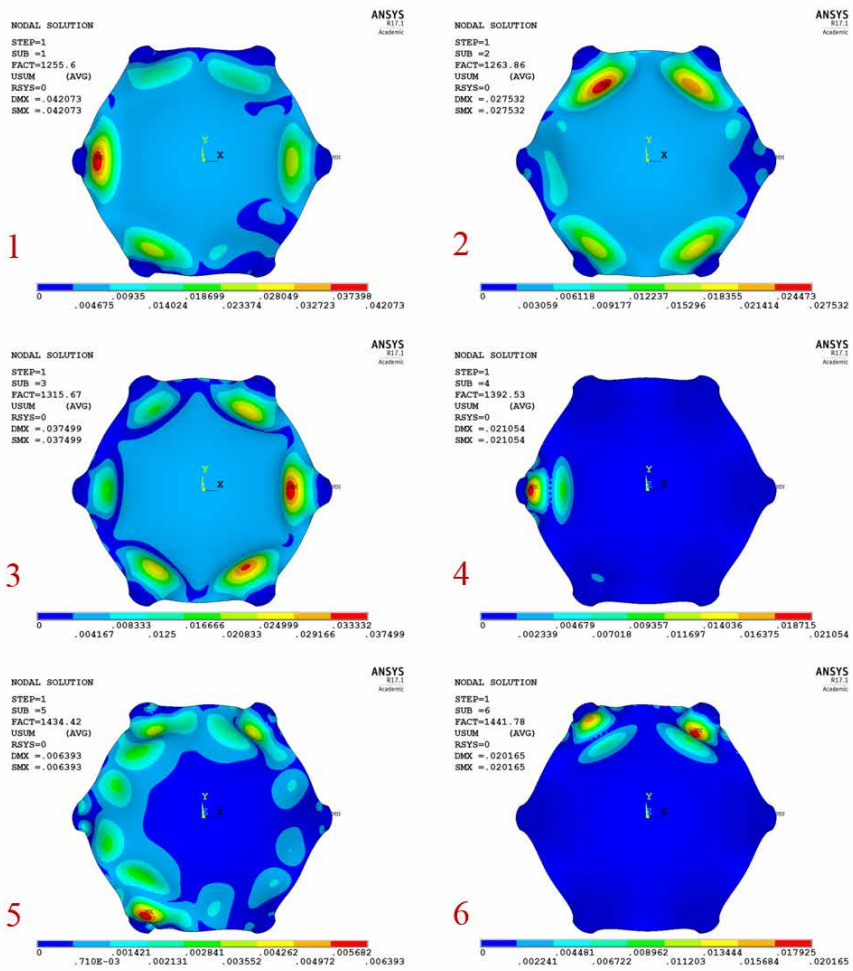


FIGURE 9.16 First six buckling modes of ***Model B*** (shell with outward-curved supports).

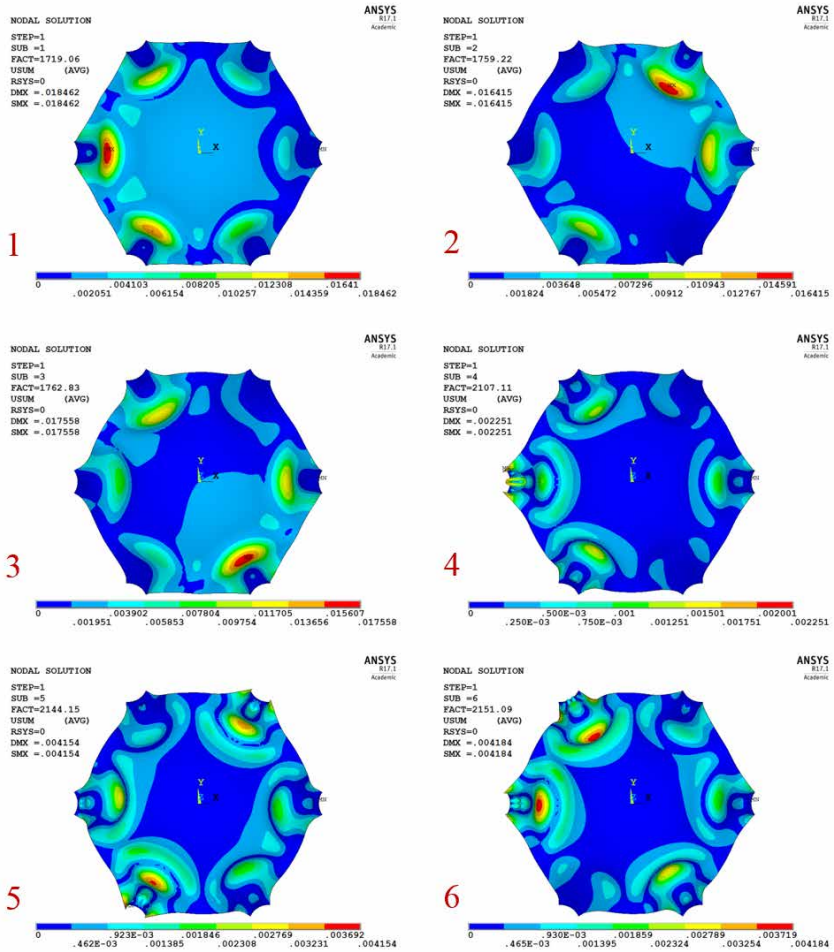


FIGURE 9.17 First six buckling modes of *Model C* (shell with inward-curved supports).

§ 9.6 Conclusions

Experimental research on the influence of support shapes on mechanical behaviour of form-found shells is conducted. The influence of supports on mechanical behaviour of form-found shells is studied visually and qualitatively. The main conclusions are as follows:

- Three plastic shell models, which are the scaled model of ***Model A*** (Figure 8.15), ***Model B*** (Figure 8.16), and ***Model C*** (Figure 8.17), are manufactured by a vacuum machine. Therefore, thicknesses of these shell models are not uniform.

- From the observation of buckling modes of the three shells shown in Figure 9.14, shells with straight supports (***Model A***) and with outward-curved supports (***Model B***) perform with similar buckling modes where all six legs deform inward under the effects of air pressure. However, a very different buckling mode occurs in the shell model with inward-curved supports (***Model C***), where three legs deform inward and the other three deform outward. Qualitatively, this is predominantly due to the differences of curvature distributions in the support parts of these three shell models. In addition, the thickness distributions of these three shell models can also lead to differences in the shell buckling modes.

- The applied setup of the tests is very simple. For example, the vacuum bag induces unknown extra loads on the free edges of the shell models. Additionally, the speed of the air pump cannot be controlled, and the accuracy of the relevant measuring tools (the air-pressure sensor and the camera) of the setup is not high enough. The Moiré patterns for the areas far from the Moiré grating are also not clear enough. All these issues lead considerable uncertainties during the tests.

- Shell structures take their stiffness from curvature, flat or single curved parts should be avoided during the generation of the structural geometry of shells, and free boundaries should be considered carefully. Moreover, the thickness distribution of the shell should not be neglected.

§ 9.7 References

[153] Theocaris P.S. (1969). Moiré fringes in strain analysis. Elmsford: Pergamonpress.
[154] Sciammarella C.A. (1983). The Moiré method-a review. Experimental Mechanics, 23(4): 446-449.
[155] Kafri O., Glatt I. (1990). The Physics of Moiré Metrology. John Wiley & Sons, New York.

TOC

PART 5 Conclusions

TOC

TOC

10 Conclusions

This thesis focuses on the research problem of how to generate structural forms with high structural efficiency, subject to architectural space constraints from the perspective of a structural engineer. This work attempts to solve the above problem through the development of a theoretical framework of Structural Morphology and Form-Finding research on shell structures. This final chapter presents the conclusions of this thesis. In addition, the limitations of the work are presented, and final remarks are provided.

§ 10.1 Conclusions Related to the Theoretical Framework of Structural Morphology

The first research objective of this thesis is developing a theoretical framework for Structural Morphology based on the definition given by Shen and Wu (Section 1.4.2). The conclusions are as follows:

- A theoretical framework for Structural Morphology needs to facilitate a process of handling parameters (Section 2.3).
- The best basis for the theoretical framework of Structural Morphology is two categories of structural systems: Force-Active and Force-Passive structural systems (Section 1.3.1).
- Force-Active structural systems need to be further divided into three categories: hanging, tension and pneumatic systems (Section 1.3.1).
- The proposed conceptual model for the process of computational analysis is suitable to both Force-Active and Force-Passive structural systems (Section 2.2.2). The five categories of parameters of the initial structural systems can

influence the eventual structural form and mechanical behaviour of the analysis results (Section 2.2.1).

– The proposed theoretical framework for Structural Morphology is feasible and effective to guide research on From-Finding and Structural Optimisation (Chapter 3).

§ 10.2 Conclusions Related to Form-Finding of Shells

The second research objective of this thesis is conducting systematic From-Finding research on shell structures. The first sub-objective is assessing the mechanical behaviour of the shell structure quantitatively and qualitatively in the conceptual structural design phase (Section 1.4.2). The conclusions are as follows:

– The proposed shell behaviour assessment strategy can be used to quantitatively and qualitatively assess the mechanical behaviour of shell structures in the conceptual structural design phase (Section 4.3.1).

– The proposed two stress ratios in the directions of two principal normal forces and the strain-energy ratio can be used to provide quantitative as well as qualitative insight in the force flow in shells (Section 4.3.2).

– The stress ratios are suitable in most cases, while the strain-energy ratio is suitable when the directions of principal normal forces cannot be easily distinguished or when an overall assessment is needed (Section 4.3.2).

The second sub-objective is introducing the Vector Form Intrinsic Finite Element (VFIFE) method to generate equilibrium shapes of membrane structures and thus the structural geometries of shells (Section 1.4.2). The conclusions are as follows:

– The self-programmed MATLAB script of the VFIFE method can be used to generate equilibrium structural forms of cable and membrane structures, including all three categories of Force-Active structural systems (Sections 5.2.3 and 5.4).

– The difference between the equilibrium structural forms obtained using the VFIFE method and those using the Dynamic Relaxation (DR) method can be

neglected. The VFIFE method is accurate and robust for generating equilibrium structural forms of Force-Active structural systems (Sections 5.2.3 and 5.4).

- The VFIFE method uses the Störmer-Verlet integration method in its governing equation, while the DR method uses the Leapfrog integration method. Both integration methods have control parameters, that are not known in advance, and are critical for the analysis time. Therefore, it is challenging to compare the analysis times of the VFIFE method and the DR method (Section 5.2.2)

- Equilibrium structural forms of all three types of membrane structures can be used as the structural geometries of shells. The form depends strongly on the load contribution. The shells perform optimally under the same load distribution as used in Form-Finding. However, when the load distribution changes, bending moments occur in the form-found shells (Section 5.4).

- For Force-Active structural systems, the VFIFE method can generate the equilibrium structural form for any unbalanced state with arbitrary specifications of geometry (Section 6.3).

The third sub-objective is establishing efficient and effective Form-Control strategies to generate form-found structural forms with a single and multiple target heights (Section 1.4.2). The conclusions are as follows:

- The proposed Form-Control strategy (by introducing the Newton-Raphson method to select the specific Young's modulus of the initial structural model) is more convenient to generate the equilibrium structural form with a single target height than the Form-Control process using the bisection method (former work of the author; Section 6.2).

- Based on the VFIFE method and the above Form-Control strategy, a Form-Finding plug-in using C# script is developed on the Rhino-Grasshopper platform. This plug-in performs at a much higher efficiency than the former script in MATLAB and other software (Section 6.4).

- The proposed Form-Control strategy (by introducing the inverse iteration method to select the specific geometry of the initial structural model) needs just a few iterations to generate the equilibrium structural form with multiple target heights (Section 6.3).

The fourth sub-objective is developing strategies for generating multiple form-found structural forms (Section 1.4.2). The conclusions are as follows:

– Multiple structural forms can be obtained by adjusting the five categories of parameters of the initial structural system during the Form-Finding process. It can be expected that much more diverse structural forms can be obtained by adjusting multiple parameters of the initial structural system (Section 7.2).

– These numerically developed strategies overcome many disadvantages of physical Form-Finding methods, such as complicated manufacturing and the adjustment and recording processes of physical models (Sections 4.4.1 and 7.2).

– During the Form-Finding of multiple structural forms, a slight extra curvature of the supports of the initial structural system leads to invisible differences in equilibrium structural forms. Thus, a new research problem was revealed: how can the difference in the structural forms be detected and how do the support shapes influence the mechanical behaviour of the form-found shells? (Sections 7.2.5 and 7.3).

§ 10.3 Conclusions Related to the Influence of Support Shapes on Form-found Shells

The third research objective of this thesis is quantifying the influence of support shapes on the structural form and mechanical behaviour of form-found shells (Section 1.4.2). The conclusions are as follows:

– This work results in a new technique that significantly improves the structural efficiency by slightly changing the support shapes during the Form-Finding process. This does not significantly change the structural form and thus the architect's design scheme. For example, a slight change in curvature at the supports can yield a more than 4.0 times larger load-carrying capacity (Chapters 8 and 9) while others required large geometry changes to obtain just around 2.5 times larger load-carrying capacity (Section 8.1).

– Intuitively, slight changes in the support shapes have little influence on the overall structural forms of these form-found shells. Nonetheless, differences of

curvature distributions can be observed in the parts near their supports using the curvature analysis in Rhinoceros (Section 8.2.2).

- During the Form-Finding processes, straight supports induce an area with zero curvature in one direction. Outward curving supports have curvatures contrary to those of the free edges, and induce changes in curvatures near the supports. Inward curving supports match the curvature at the free edges such that no flat parts are obtained near the supports (Section 8.2.2).

- Whether the supports are fixed or hinged has a considerable influence on the buckling load factors of shells with straight supports. Whether the supports are fixed or hinged has a negligible small influence on the buckling load factors of shells that are curved at the supports. Whether the supports are fixed or hinged does not significantly influence the buckling modes of the shells (Sections 8.3.2 and 8.4.2).

- Shells with curved supports have higher buckling load factors than shells with straight supports. Shells with inward-curved supports have higher buckling load factors than shells with outward-curved supports. The more curvature that exists at the supports, the higher the buckling load factors are (Sections 8.3.2 and 8.4.2).

- In the tests, physical shell models with straight supports and those with outward-curved supports perform with similar buckling modes such that all six legs deform inward under the effect of air pressure. However, a much different buckling mode occurs in shell models with inward-curved supports, where three of the legs deform inward and the other three deform outward. This is primarily due to the curvature differences in the support parts of these shell models. In addition, nonuniform thickness distributions of these shell models can also be a cause (Section 9.4).

§ 10.4 Limitations of the Current Work

The conclusions reached in the previous sections meet the primary objectives of this thesis to a substantial extent. However, there are still some unresolved matters. Some limitations of the present research are listed as follows:

- In the proposed theoretical framework of Structural Morphology, Form-Finding and Structural Optimisation are considered the two key aspects, of which only the former was studied in detail. Research on Structural Optimisation should also be conducted to enrich this framework.

- The scope of this thesis was limited to Form-Finding research on shell structures. The considered shells were homogeneous and smooth. More complicated Form-Finding problems of shells with beams, folds, or ribs need to be resolved. Moreover, in many chapters, only shell structures generated from hanging models are considered. The other two types of shells, which are generated from tent models and pneumatic models, should be considered in further research.

- Thus far, in Form-Finding of cable or membrane structures and thus shell structures, the VFIFE method has shown few advantages over other numerical methods, for example, the DR method. Nonetheless, the VFIFE method has new concepts, and research results achieved by other scholars have shown its better performance and potential advantages in complicated structural behavioural analyses. The scopes and advantages of the VFIFE method in Form-Finding research need to be explored. This is already ongoing in the author's research group in Harbin; for example, group members are using the VFIFE method to simulate the inflation and deflation processes of inflatable moulds for ice composite shells.

- In the Form-Control problems, some discrete height constraints were considered for the architectural requirements. However, much more complicated architectural or mechanical constraints should be considered and studied. To resolve Form-Control problems with multiple target points, the inverse iteration method is introduced successfully (Section 6.3). However, further feasibility of this method for much more complicated problems will be explored in future work.

- The five categories of parameters of the initial structural system influence not only the structural form but also the mechanical behaviour of form-found shells. In this research, only the influence of support shapes is studied in detail (Chapter 8). For future work, other influence parameters of form-found shells need to be considered, for example, the number or the length of the supports, the edge beams, etc.

- In the physical tests, Moiré patterns of the areas far from the Moiré grating cannot be recognised clearly. However, it should be possible and needs to be

studied. Moreover, it is not easy to determine the load on the free edges of the physical shell models exerted by vacuum bags. This aspect of the experiment requires careful designing, for example, by precisely tailoring the vacuum bag or by adding baffles next to the free edges.

– While numerical and experimental methods are included in this research, more analytical research should be covered in future work as well.

§ 10.5 Final Remarks

The coupling relationship between form and force has become one of the major issues in the field of spatial structures since the end of the last century. Correspondingly, the term Structural Morphology gains increasing attention in recent years. In this thesis, a theoretical framework of Structural Morphology is proposed based on the numerical analysis process of structural systems, and subsequently, systematic Form-Finding research on shell structures has been conducted. From these works, the research problem of generating multiple structural forms with high structural efficiency subject to architectural space constraints during the conceptual structural design phase is solved. However, much more complicated problems regarding the relationship between form and force could be present in engineering practices during the entire structural design process. In the future, further and deeper research will be conducted to enrich this proposed theoretical framework of Structural Morphology with the goal of designing both architecturally pleasing and structurally efficient structures.

TOC

List of Figures

1.1 Himalayas Centre Shanghai [7]. 31

1.2 Heydar Aliyev Centre [8][9]. 32

1.3 Harbin Opera House [10][11]. 32

1.4 Arnhem Centraal station [12]. 32

1.5 'Force-Active' structural systems. 35

1.6 Shell structures. 37

1.7 Logical structure of this thesis. 41

2.1 Conceptual model of Motro [51]. 48

2.2 Conceptual model of the numerical analysis methods. 49

2.3 Example 2.1. 53

2.4 Example 2.2. 54

2.5 Conceptual model of the Structural Morphology. 56

3.1 Three types of physical models. 62

3.2 Conceptual model of Form-Finding: a) All the five categories of parameters of the initial structural system are in blue, indicating that all the categories can be used as variables during the Form-Finding process, b) 'Structural Form' is in blue, indicating that the main goal of Form-Finding is to generate structural forms with architectural constraints, c) 'optimize' is in blue and the arrow is dotted, indicating that an optimisation process may be needed during the Form-Finding process, but may not be needed when a one-time analysis can meet the requirements. 63

3.3 Diverse numerical structural models [70]. 64

3.4 The FAST project. 65

3.5 Two engineering practices. 66

3.6 Numeric simulation of an air cushion [78]. 67

3.7 Ice dome. 67

3.8 Conceptual model of Structural Optimisation: a) 'geometry' and 'material distribution' of the initial structural system are in blue, indicating that these two categories are always used as variables during the Structural Optimisation process, b) 'Mechanical Behaviour' is in blue means, indicating the main goal of Structural Optimisation is to improve the mechanical behaviour of the structural system, c) 'optimize' is in blue and the arrow is dotted, indicating that an optimisation process may be needed during the Structural Optimisation process, but may not be needed when a one-time analysis can meet the requirements. 68

3.9 Different branches of Structural Optimisation [81]. 69

3.10 Example of freeform shells [85]. 70

3.11 Example of freeform reticulated shells [86]. 71

3.12 Example of continuum structure [87]. 72

3.13 Size and topology optimisation of the 25-bar spatial truss structure [88]. 73

3.14 Size and topology optimisation of a four-corner-supported spherical grid shell [89]. 73

3.15 Example of discrete structure [90]. 74

3.16 Example of optimisation of combined parameters [92]. 75

4.1 Global and local coordinate systems [94]. 82

4.2 Curvatures on surface [94]. 82

4.3 Mohr's circle for curvatures [95]. 83

4.4 Types of Gaussian curvature: a) Positive, b) Zero, and c) Negative [96]. 84

4.5 Curvature analysis of roof structure of the sports hall of Heinz Isler ([97]). 84

4.6 Mechanical behaviour assessment strategy. 86

4.7 Shell element under positive pressure loading, all stress resultants, and displacement *w* [98]. 87

4.8 Shell assessment based on the ratio of normal stress and the sum of bending and normal stresses [99]. 88

4.9 Finite element model of the dome. 90

4.10 Principal stress S_1 at the middle surface of the dome (Pa). 91

4.11 Principal stress S_2 at the middle surface of the dome (Pa). 91

4.12 Principal stress S_3 at the middle surface of the dome (Pa). 92

4.13 Vectorial representation of the principal stresses of the dome. 92

4.14 Stress ratio R_1 of the dome (%). 93

4.15 Stress ratio R_2 of the dome (%). 94

4.16 Strain-energy ratio α of the dome (%). 94

4.17 Deitingen Service Station, Switzerland, 1968 [104]. 96

4.18 Figure 4.18: Roof for Multihalle in Mannheim, Germany, 1975 [105]. 96

4.19 Figure 4.19: Suspension model for Form-Finding of the new train station in Stuttgart, Germany, 2000 [107]. 96

4.20 Figure 4.20: Basento Viaduct in Potenza, Italy, 1974 [108]. 96

4.21 One Binishell in Ku-ring-gai High School [111]. 97

4.22 COOP Storage and Distribution Centre, Wangen, Switzerland, 1960 [102]. 97

4.23 An ice dome at Tomamu in Hokkaido, Japan, 2001 [112]. 97

5.1 Discretion of the structural system. 104

5.2 Schematic diagram of the path unit. 105

5.3 Schematic diagram of the pure deformation. 105

5.4 Flowchart of the VFIFE method. 106

5.5 Residual force of particle c. 108

5.6 Initial conditions of ***Example 5.1*** (red points represent the fixed points). 110

5.7 Equilibrium hanging networks obtained by the VFIFE method (in black) and the DR method (in red) of ***Example 5.1***. 111

5.8 Evolution curve of the VFIFE method of ***Example 5.1***. 111

5.9 Evolution curve of the DR method of ***Example 5.1***. 112

5.10 Process of reverse rigid body motion. 113

5.11 Calculation of β_2. 114

5.12 Calculation of the pure deformation. 114

5.13 Force increment components and displacement components in the deformation coordinate system. 115

5.14 Initial conditions of ***Example 5.2***. 118

5.15 Evolution curve of the VFIFE method of ***Example 5.2***. 119

5.16 Form-Finding result of ***Example 5.2***. 120

5.17 Evolution curve of the DR method for ***Example 5.2***. 120

5.18 Comparison of the results of ***Example 5.2***; *Z* coordinates of the nodes at *X*-axis of symmetry (*Y*=0). 121

5.19 Comparison of the results of ***Example 5.2***; *Z* coordinates of the nodes at *Y*-axis of symmetry (*X*=0). 121

5.20 Principal stress S_1 at the middle surface of the shell of *Example 5.2* (Pa). 122

5.21 Principal stress S_2 at the middle surface of the shell of *Example 5.2* (Pa). 123

5.22 Principal stress S_3 at the middle surface of the shell of *Example 5.2* (Pa). 123

5.23 Vectorial representation of the principal stresses of the shell of *Example 5.2*. 124

5.24 Vectorial representation of the principal stresses of the shell of *Example 5.2* (lateral view). 124

5.25 Stress ratio R_1 of *Example 5.2* (%). 125

5.26 Stress ratio R_2 of *Example 5.2* (%). 125

5.27 Strain-energy ratio α of *Example 5.2* (%). 126

5.28 Stress ratio R_1 of *Example 5.2* under loads with a same distribution as the hanging membrane (%). 127

5.29 Stress ratio R_2 of *Example 5.2* under loads with a same distribution as the hanging membrane (%). 127

5.30 Strain-energy ratio α of *Example 5.2* under loads with a same distribution as the hanging membrane (%). 128

5.31 Initial conditions of *Example 5.3*. 129

5.32 Evolution curve of the VFIFE method of *Example 5.3*. 129

5.33 Form-Finding result of *Example 5.3*. 130

5.34 Evolution curve of the DR method for *Example 5.3*. 131

5.35 Comparison of the results of *Example 5.3*; *Z* coordinates of the nodes at *X*-axis of symmetry (*Y*=0). 131

5.36 Comparison of the results of *Example 5.3*; *Z* coordinates of the nodes at *Y*-axis of symmetry (*X*=0). 132

5.37 Principal stress S_1 at the middle surface of the shell of *Example 5.3* (Pa). 132

5.38 Principal stress S_2 at the middle surface of the shell of *Example 5.3* (Pa). 133

5.39 Principal stress S_3 at the middle surface of the shell of *Example 5.3* (Pa). 133

5.40 Vectorial representation of the principal stresses of the shell of *Example 5.3*. 134

5.41 Vectorial representation of the principal stresses of the shell of *Example 5.3* (lateral view). 134

5.42 Stress ratio R_1 of *Example 5.3* (%). 135

5.43 Stress ratio R_2 of *Example 5.3* (%). 135

5.44 Strain-energy ratio α of *Example 5.3* (%). 136

5.45 Initial conditions of *Example 5.4*. 137

5.46 Evolution curve of the VFIFE method of *Example 5.4*. 138

5.47 Form-Finding result of *Example 5.4*. 138

5.48 Evolution curve of the DR method for *Example 5.4*. 139

5.49 Comparison of the results of *Example 5.4*; *Z* coordinates of the nodes at *X*-axis of symmetry (*Y*=0). 139

5.50 Comparison of the results of *Example 5.4*; *Z* coordinates of the nodes at *Y*-axis of symmetry (*X*=0). 140

5.51 Principal stress S_1 at the middle surface of the shell of *Example 5.4* (Pa). 140

5.52 Principal stress S_2 at the middle surface of the shell of *Example 5.4* (Pa). 141

5.53 Principal stress S_3 at the middle surface of the shell of *Example 5.4* (Pa). 141

5.54 Vectorial representation of the principal stresses of the shell of *Example 5.4*. 142

5.55 Vectorial representation of the principal stresses of the shell of *Example 5.4* (lateral view). 142

5.56 Stress ratio R_1 of *Example 5.4* (%). 143

5.57 Stress ratio R_2 of *Example 5.4* (%). 143

5.58 Strain-energy ratio α of *Example 5.4* (%). 144

5.59 Inflation process of the pneumatic model of *Example 5.4*. 145

6.1 Form-Finding result of *Example 5.2*. 150

6.2 Curve of the height of point *M* to Young's modulus. 151

6.3 Iteration curve of *Example 6.1*. 154

6.4 Form-Control result of *Example 6.1*. 154

6.5 Stress ratio R_1 of *Example 6.1* under self-weight (%). 155

6.6 Stress ratio R_2 of *Example 6.1* under self-weight (%). 155

6.7 Strain-energy ratio α of *Example 6.1* under self-weight (%). 156

6.8 Stress ratio R_1 of *Example 6.1* under the same load distribution with the equilibrium hanging membrane (%). 156

6.9 Stress ratio R_2 of *Example 6.1* under the same load distribution with the equilibrium hanging membrane (%). 157

6.10 Strain-energy ratio α of *Example 6.1* under the same load distribution with the equilibrium hanging membrane (%). 157

6.11 Problem of *Example 6.2*. 158

6.12 Initial conditions of *Example 6.3*. 160

6.13 Figure 6.13: Modelling process of the initial structural model of *Example 6.3*. 162

6.14 Form-Control result of *Example 6.3* with a finer mesh. 164

6.15 Smooth result of *Example 6.3*. 164

6.16 Stress ratio R_1 of the *Example 6.3* (%). 165

6.17 Stress ratio R_2 of *Example 6.3* (%). 165

6.18 Strain-energy ratio α of *Example 6.3* (%). 166

6.19 Form-Finding result of *Example 6.3* with a fold as the initial model. 167

6.20 The calculation component of the plug-in. 169

6.21 Assembly of components of *Example 6.1*. 169

7.1 Initial conditions and Form-Finding result of *Example 5.2*. 174

7.2 Two initial structural systems and Form-Finding results of *Example 7.1*. 176

7.3 Two Form-Finding results of *Example 7.2*. 177

7.4 Two initial structural systems and Form-Finding results of *Example 7.3*. 179

7.5 Four initial structural systems and Form-Finding results *Example 7.4*. 183

7.6 Four initial structural systems and Form-Finding results of *Example 7.5*. 187

8.1 Nonlinear response of the Kresge Auditorium for (a) the optimised shell and (b) original shell [144]. 192

8.2 Kresge Auditorium [144]. 192

8.3 BP Service Station [144]. 192

8.4 Supporting shell of the Basento Viaduct in Potenza [147]. 193

8.5 Aichtal Outdoor Theatre [144]. 193

8.6 Prototype for the Droneport project [150]. 193

8.7 Tile vault prototype at ETH Zurich [151]. 194

8.8 Structural geometries with different support constraints [144]. 194

8.9 Diverse numerical inverted hanging geometry [149]. 195

8.10 Design variables of supports and the optimisation results [152]. 195

8.11 Initial conditions of *Model A* (shell with straight supports). 197

8.12 Initial conditions of *Model B* (shell with outward-curved supports). 197

8.13 Initial conditions of *Model C* (shell with inward-curved supports). 198

8.14 Initial conditions of *Model D* (shell with strongly inward-curved supports). 198

8.15 *Model A* (shell with straight supports). 199

8.16 *Model B* (shell with outward-curved supports). 199

8.17 *Model C* (shell with inward-curved supports). 200

8.18 *Model D* (shell with strongly inward-curved supports). 200

8.19 *Z*-coordinates at the *X*-axis of symmetry (*Y*=0). 201

8.20 *Z*-coordinates at the *Y*-axis of symmetry (*X*=0). 201

8.21 Gaussian curvature of the four models. 202

8.22 R_1 of Model A_5 (shell with simply supported straight supports; %). 205

8.23 R_2 of Model A_5 (shell with simply supported straight supports; %). 205

8.24 Principal stress S_1 at the middle surface of Model A_5 (shell with simply supported straight supports; Pa). 206

8.25 Principal stress S_2 at the middle surface of Model A_5 (shell with simply supported straight supports; Pa). 207

8.26 Principal stress S_3 at the middle surface of Model A_5 (shell with simply supported straight supports; Pa). 207

8.27 Vectorial representation of the principal stresses of Model A_5 (shell with simply supported straight supports). 208

8.28 Vectorial representation of the principal stresses of Model A_5 (shell with simply supported straight supports; lateral view). 208

8.29 Load-displacement curves of all the eight shells. 215

8.30 R_1 of Model A_5 (shell with simply supported straight supports) when the shell fails (%). 216

8.31 R_2 of Model A_5 (shell with simply supported straight supports) when the shell fails (%). 217

8.32 Vectorial representation of the principal stresses for Model A_5 (shell with simply supported straight supports) when the shell fails. 217

8.33 Vectorial representation of the principal stresses for Model A_5 (shell with simply supported straight supports) when the shell fails (lateral view). 218

8.34 Half-span loading (red part). 219

8.35 R_1 of Model A_5 (shell with simply supported straight supports)under half-span loads. 220

8.36 R_2 of Model A_5 (shell with simply supported straight supports) under half-span loads. 220

8.37 Vectorial representation of the principal stresses for Model A_5 (shell with simply supported straight supports) under half-span loads. 221

8.38 Load-displacement curves of all eight shells under half-span loads. 224

9.1 Dimensions of the three shell models. 228

9.2 Formworks of the three shell models. 229

9.3 Manufacture of shell model using the vacuum forming machine. 231

9.4 Three shell models. 232

9.5 Thickness distributions of the three shell models (m). 232

9.6 Three plastic shell models with supports. 233

9.7 Design of the setup of the test. 234

9.8 Manufacture of the vacuum bag. 235

9.9 Setup of the test. 236

9.10 Changes in the air-pressure during tests of the three shell models. 237

9.11 Moiré patterns of shell with straight supports (*Model A*). 238

9.12 Moiré patterns of shell with outward supports (*Model B*). 240

9.13 Moiré patterns of shell with inward supports (*Model C*). 241

9.14 Buckling modes of the three shell models. 242

9.15 First six buckling modes of *Model A* (shell with straight supports). 244

9.16 First six buckling modes of *Model B* (shell with outward-curved supports). 245

9.17 First six buckling modes of *Model C* (shell with inward-curved supports). 246

List of Tables

6.1 Adjusting process of ***Example 6.2***. 159

6.2 Adjustment process of ***Example 6.3*** (m). 163

6.3 Adjustment process of ***Example 6.3***. 163

8.1 Structural analysis models. 203

8.2 Comparison of structural static analysis results. 211

8.3 Comparison of linear buckling analysis results. 214

8.4 Comparison of linear buckling analysis results under half-span loads. 223

4

TOC

Acknowledgements

When I was finishing this PhD thesis, many people appeared in my life over the past few years that are appreciated from the bottom of my heart.

First and foremost, I would like to express my gratitude to my two dearest professors by telling a brief story of my life so far.

I was born in a very small and poor village of China, and had never travelled 15 kilometres away from my hometown before 2007, when I was admitted by HIT. Life changed significantly since then.

Three years later in 2010, I first contacted my dearest professor, Yue Wu, to apply for an opportunity to be his master student, and he agreed. During the following three years, he taught me how to be a good man and a good researcher. We communicated and got along with each other in a very direct way which seemed a little bit strange in our traditional Chinese culture, and trusted each other unconditionally. A very close relationship was built between us, and finally, I was lucky to become a PhD student of his in 2013.

In this very year, I contacted my second dearest professor, Andrew Borgart, to apply for an exchange PhD position at the TU Delft, and he offered his great help. During the year I worked at TU Delft (October 2014 - October 2015), he endured my poor English skills and my several 'angry emails', gave me endless support, opportunities, and guidance. With his help, I opened my eyes to a world-wide view in our research field, and I built my confidence in academic and teaching activities even in an international symposium.

In September 2015, I was lucky again that an opportunity of getting a PhD degree from TU Delft was offered by Professor Borgart. Professor Wu funded me himself just as a father would do for his son. A new life that I never expected began. It was my parents who gave me life and brought me up, and it was my two dearest professors who helped me start and build my career. I thank both of them more than I say, and I will keep in life-long touch with them.

I am equally thankful to Professor Jan Rots and Professor Shizhao Shen. As my promotor at TU Delft, Professor Rots offered me essential and timely support, and, of course, many opportunities at every step of the way. As a world-class expert in the field of space structures, Professor Shen gave me invaluable guidance during several unforgettable discussions. It was really an honour to be a student of both these respectable professors.

Their personalities, their attitudes towards education and research, and they themselves influenced me a lot and will guide me in the rest of my life.

Many colleagues and friends that I worked with and enjoyed over the years in the Netherlands have my deep appreciation: Professor Fred Veer, Professor Pierre Hoogenboom, Bo Song, Peter Eigenraam, Arno Pronk, Diederik Veenendaal, Jeroen Coenders, Gerrie Hobbelman, Roel Schipper, Kees Baardolf, Paul Vermeulen, Christian Louter, Ate Snijder, Corné Hagen, Sjef Brands, Yaron Moonen, Edwin Meulman, Giorgos Stamoulis, Aleksei Suvorov, Habiba Mukhtar, Jurek Łątka, Alejandro Prieto Hoces, Wang Pan, Yu Chen, Dadi Zhang and others. I cannot list all their names here but I do appreciate all of them.

A special thanks goes to Fred for his selfless help and support many of which I even did not know about, to Pierre for his supervision and selfless help without a thought of fame, to Bo for her suggestions about my life in the Netherlands during our conversations on many early mornings, to Peter for our numerous discussions on shell structures, to Wang for exchanging ideas during our bike-riding times, to Diederik for our common passion on structures, to Arno for our cooperation on ice composite shell structures, and to Jeroen (and Andrew) for offering me the opportunity to be a member of the organising committee and chairman of the Young Engineers Session of the IASS Symposium 2015. These years of my life in the Netherlands would not be so meaningful and colourful without the company of all these colleagues and friends. I will never forget them and the time we worked and enjoyed together.

I extend my thanks to several professors from my home university: Professor Xiaoying Sun, Professor Ying Sun, Professor Hongliang Qian, Professor Longjun Xu, Professor Huanding Wang, Professor Yaochun Zhang, Professor Zhixian Qiu, Professor Feng Fan, Professor Peng Luo, and many other professors. They taught me how to be a qualified structural engineer, how to be a good researcher, and more importantly, how to be a good man. Even during the time that I worked in the Netherlands, a lot of messages and emails from them encouraged and helped me greatly. A special thanks is given to Professor Xiaoying Sun and Professor Ying Sun for their concern not only on my research but my life.

My thanks also goes to those lovely friends and students from my home research group: Ning Su, Hong Chang, Jinyu Ye, Yong Chen, Long Chen, Yi Xia, Qingjie Hu, Yunlei Xu, Xindong Shi, Yan Su, Longrui Xue, Xiuming Liu, Boxuan Chen, Yitian Zang, Zhao Liu, Yang Yu, and others. I am really grateful to all of them for their appearance in my life and their invaluable help. It was really a pleasure to serve as the daily supervisor of some of the students above. I will never forget these days in which we grew up together. A special thanks is given to Ning Su for our numerous discussions about our research,

our lives and our research group. Here, very great thanks is given to Yan Su and Xiuming Liu for helping me to develop the numerical analysis method in this thesis, to Longrui Xue and Qingjie Hu for doing sub-research projects of mine.

Finally, my concluding thanks are dedicated to my family and friends in China, including my parents, my girlfriend, my grandparents, my little brother, my aunts, my uncles, my cousins, and all my lovely friends. Inexpressible thanks is given to my parents for giving me my life and bringing me up, and for unconditional support and endless encouragement. Very special thanks is given to my girlfriend, the love of my life. In the past years, both of us were enriching ourself during the the long waiting for each other. I promise you happiness, please trust me, and you can trust me!

TOC

Curriculum vitae



Qingpeng Li, 2017 (photo: Chenjie Yu)

03/1989

Born in Shandong, P.R. China

09/2007 - 07/2011

Bachelor of Civil Engineering from Harbin Institute of Technology, P.R. China

09/2011 - 07/2013

Master of Engineering in Architectural and Civil Engineering from Harbin Institute of Technology, P.R. China

10/2014 - 10/2015

Researcher at Faculty of Architecture and Built Environment, TU Delft, the Netherlands

08/2017 - 10/2017

Researcher at Faculty of Civil Engineering and Geosciences, TU Delft, the Netherlands

09/2013 - now

Ph.D. student at School of Civil Engineering, Harbin Institute of Technology, P.R. China

09/2015 - 03/2018

Ph.D. student at Faculty of Architecture and Built Environment, TU Delft, the Netherlands

Contact: hitssrclqp@gmail.com

List of Publications

Refereed Journal papers: (* represents the corresponding author)

1 **Qingpeng Li**, Andrew Borgart, Yue Wu*, Jan G. Rots. Influence of support shapes on structural form and behaviour of shell structures generated from hanging models. International Journal of Structural Stability and Dynamics. 2018. (under review)

2 **Qingpeng Li**, Andrew Borgart*, Peter Eigenraam, Yue Wu. Shell behavior assessment of free-form shells and its application on Heinz Isler's shells. International Journal of Architectural Heritage. 2018. (under review)

3 **Qingpeng Li**, Yue Wu*, Andrew Borgart. Structural Morphology and diversity of structural geometries. The Structural Design of Tall and Special Buildings. 2018. (under review)

4 Arno Pronk, **Qingpeng Li***, Sjef Brands, Yue Wu, Peng Luo, Elke Mergny. Structural design of the Flamenco Ice Tower. Journal of the International Association for Shell and Spatial Structures. 2018. (under review)

5 Qingjie Hu, **Qingpeng Li**, Yue Wu*. Topology optimisation of latticed shell based on the Unit Coding Method. Engineering Mechanics. 2017. (in Chinese, under review)

6 **Qingpeng Li**, Andrew Borgart, Yue Wu*, Xiuming Liu, Jan G. Rots. Form-Control of shell structures generated from hanging models. International Journal of Space Structures. 2017. (under review)

7 Yue Wu, Yunlei Xu, **Qingpeng Li***. The Effective Length Factors of Branching Structures. Journal of Building Structures. 2017. (in Chinese, accepted)

8 Yue Wu, Fang Yuan, Longrui Xue, **Qingpeng Li***. Form-Finding method for freeform shell structures with zero bending moment. Journal of Harbin Institute of Technology. 2017. (in Chinese, accepted)

9 Yue Wu, Yan Su, **Qingpeng Li***, Qingjie Hu. An Improved Numerical Inverse Hanging Method of Freeform Structure. Journal of Building Structures. 2017. (in Chinese, accepted)

10 Yue Wu, **Qingpeng Li***, Qingjie Hu, Andrew Borgart. Size and Topology Optimisation for Trusses with Discrete Design Variables by Improved Firefly Algorithm. Mathematical Problems in Engineering. 2017.

11 **Qingpeng Li**, Yan Su, Yue Wu*, Andrew Borgart, Jan G. Rots. Form-Finding of shell structures generated from physical models. International Journal of Space Structures. 2017, 32(1): 1-23.

12 **Qingpeng Li***, Andrew Borgart, Yue Wu. How to understand 'Structural Morphology'?. Journal of the International Association for Shell and Spatial Structures. 2016, 57(2): 145-158.

13 Yue Wu, Qingjie Hu, **Qingpeng Li***. Topology optimisation for truss structures based on Improved Firefly Algorithm. Journal of Building Structures. 2016, 37(6): 46-52. (in Chinese)

14 Yue Wu*, **Qingpeng Li**, Shizhao Shen. Computational morphogenesis method for space structures based on principle of inverse hanging experiment. Journal of Building Structures, 2014, 35(4): 41-48. (in Chinese)

15 Haifeng Liu*, Xiaodong Mao, **Qingpeng Li**, Zhenggang Cao, Yue Wu. Structural selection and design of gymnasium roof in URUMCHI speed-skating gymnasium. Building Structure. 2013, 43(S1): 305-310. (in Chinese)

Refereed Conference papers: (* represents the presenting author)

1 **Qingpeng Li***, Andrew Borgart, Peter Eigenraam, Yue Wu. Structural behavior assessment and load-transfer analysis of arches and curved beams. Proceedings of the IASS Annual Symposium 2018, 16-20th July, 2018, MIT, Boston, USA. (abstract accepted)

2 Andrew Borgart*****, **Qingpeng Li**, Peter Eigenraam. Manufacture and loading test of reinforced gypsum shells generated from hanging models - a workshop developed at Delft University of Technology. Proceedings of the IASS Annual Symposium 2018, 16-20th July, 2018, MIT, Boston, USA. (abstract accepted)

3 Arno Pronk*****, Yue Wu, Peng Luo, **Qingpeng Li**, Xiuming Liu, Sjef Brands, Rijk Blok, Yu Dong. Design and construct of the 30.5 meter Flamenco Ice Tower. Proceedings of the IASS Annual Symposium 2018, 16-20th July, 2018, MIT, Boston, USA. (abstract accepted)

4 Yue Wu, Xiuming Liu, **Qingpeng Li***, Boxuan Chen, Peng Luo, Arno Pronk, Elke Mergny. Form-Finding and construction of ice composite shell structures. Proceedings of the IASS Annual Symposium 2017, 25-28th September, 2017, Hamburg, Germany.

5 Arno Pronk*, Peng Luo, **Qingpeng Li**, Fred Sanders, Marjolein Overtoom, Lancelot Coar. Success factors in the realization of large ice projects in education. Proceedings of the IASS Annual Symposium 2017, 25-28th September, 2017, Hamburg, Germany.

6 **Qingpeng Li***, Andrew Borgart, Yue Wu. An approach on form-diversity of freeform shells generated from numerical hanging models. Proceedings of the IASS Annual Symposium 2016, Tokyo, Japan.

7 Yue Wu*, Yi Xia, **Qingpeng Li**. Morphogenesis of freeform shells considering multiple load conditions. Proceedings of the IASS Annual Symposium 2016, Tokyo, Japan.

8 Yue Wu*, Boxuan Chen, Xiuming Liu, **Qingpeng Li**, Arno Pronk. Developments and explorations of ice architectures and structures. 16th Academic Conference of Space Structures in China. Hangzhou, China, 2016. (in Chinese)

9 Yue Wu, Xiuming Liu*, Boxuan Chen, **Qingpeng Li**. Structural generation system of freeform structures based on the platform of Rhino-Grasshopper. 16th Academic Conference of Space Structures in China. Hangzhou, China, 2016. (in Chinese)

10 **Qingpeng Li***, Andrew Borgart, Yue Wu. The Vector Form Intrinsic Finite Element method and several other Form-Finding methods for general networks. Proceedings of the IASS Symposium, Amsterdam, the Netherlands, 2015.

11 **Qingpeng Li***, Yue Wu, Andrew Borgart. Form-Finding of gridshells generated from hanging-chain models by using the Dynamic Relaxation method and the NURBS technique. Proceedings of the IASS Symposium, Amsterdam, the Netherlands, 2015.

12 Yue Wu, Yi Xia, **Qingpeng Li***. Structural morphogenesis of freeform shells by adjusting shape and thickness. Proceedings of the IASS Symposium, Amsterdam, the Netherlands, 2015.

13 Qingjie Hu*, **Qingpeng Li**, Yue Wu. Discrete firefly algorithm in the application of topology optimisation of truss structures. Proceedings of the 11th Asian Pacific Conference on Shell and Spatial Structures - APCS 2015, Xi'an, China, 2015.

14 Yi Xia*, **Qingpeng Li**, Yue Wu. Computational morphogenesis of freeform shells based on the NURBS technique and the Hybrid Optimisation Method. Proceedings of the 11th Asian Pacific Conference on Shell and Spatial Structures - APCS 2015, Xi'an, China, 2015. (Best Paper Award)

15 **Qingpeng Li***, Yue Wu, Shizhao Shen. Computational generation of freeform shells based on the inverse hanging experiment. Proceedings of the IASS-SLTE 2014 Symposium, Brasilia, Brazil, 2014.

16 Yue Wu*, **Qingpeng Li**. Inverted hanging method and its application on structural morphogenesis. 14th Academic Conference of Space Structures in China. Fuzhou, China, 2012. (Best Paper Award, in Chinese)

TOC